Hydrido/ChloroAluminium Alkoxides and Metal (Al, Ge) Alkoxides-Synthesis, Characterization and Applications for Preparation of Novel Hydrogen Storage Nano-Materials

Dissertation

zur Erlangung des Grades
des Doktors der Naturwissenschaften
der Naturwissenschaftlich-Technischen Fakultät III
Chemie, Pharmazie, Bio- und Werkstoffwissenschaften
der Universität des Saarlandes

von

Hameed Ullah Wazir

Saarbrücken, Germany

2010

Tag des Kolloquiums:	**09.12.2010**
Dekan:	**Professor Dr.-Ing. Stefan Diebels**
Berichterstatter:	**Prof. Dr. Dr. h.c. Michael Veith**
	PD Dr. Holger Kohlmann
Vorsitz:	**Prof. Dr. Uli Kazmaier**
Akad. Mitarbeiter:	**Dr. Bernd Morgenstern**

To my Parents

(Mum Zar Bano and Dad Bakht Alam),

for their prayers, love, sacrifices and unwavering believe in me.

To my wife (Sara),

for her unconditional love, encouragement

and support during the hardships of life

I would like to extend my gratitude and thanks to my mentor/supervisor **Prof. Dr. Dr. h. c. Michael Veith** for giving me the opportunity to work under his guidance and introducing me to a novel research arena. The three and a half year Ph. D work under his supervision was a time of great opportunities for me to learn innovative ideas. I thank him for the wisdom and knowledge he has bestowed upon me during the course of my Ph. D work. His energetic and untiring working style will be a role model for me in my entire life.

I would like to extend my gratitudes to Prof. Dr. U. Kazmaier, PD Dr. H. Kohlmann and Dr. B. Morgenstern for review and assessment of my thesis.

I have worked in two different locations during the course of my Ph. D study; at Leibniz Institute of New Materials (INM) and Institute of Inorganic Chemistry, University of Saarland. Therefore, I have been helped by many people in the two institutes in different ways whenever I needed their help and support.

First of all I thank the INM administration for providing me generous facilities for conduction of my research work. I extend my cordial thanks to **Dipl. Ing. Dietmar Serwas** and his team-mates, Herbert Beerman, Uwe Magar, Michael Schneider and Werner Schneider for helping me in construction of Sievert's type apparatus and their continuous technical help during my entire working period at INM. My sincere gratitude goes to the team of microscopy and X-ray analytics at INM, Dr. Herbert Schmid, Dr. Ingrid Grobelsek, Dr. Marcus Koch and Mrs. Aude Haettich for SEM, EDX, TEM and SAED analysis. I thank the two ladies, Elke Bubel and Melanie Groh at the library of INM for their kindness and support while lending the books and other reading materials. I thank Mr. Wolfgang Türk and his team of the EDV for providing computer facilities although he did not allow me to access my social networking sites. I would like to exploit the opportunity to forward my thanks to **Dr. Oral Cenk Aktaş** for his unconditional help, support and guidance through various problems I faced during the stay at INM. I thank my colleagues at INM, Dr. Hakima Smail, Cecile Dufloux, Dr. Michael Bender, Carsten Bubel, Marina Martinez Miro, Cagri Kaan Akkan and Ju Seok Lee with whom I shared some light moments.

At the institute of Chemistry I have been helped by many persons regarding my research work. I thank **Dr. Andreas Rammo** for introducing me to the research group when I joined the group in 2007. He taught me how to work at stock apparatus under inert atmosphere and vacuum? I thank **Dr. Markus Ehses** for his valuable comments and proof reading of part of the thesis. I thank him for reading, commenting and forwarding my annual reports to DAAD. He helped me each and every time with smiling face whenever I asked.

I thank **Dr. Volker Huch** for single crystal analysis of all the compounds presented in the first part of my research work. I thank him also for powder XRD analysis of my samples presented in the second part of the thesis. A light chit-chat with him always gave me an immense

pleasure during my stay in the institute of Inorganic Chemistry. I thank **Dr. Holger Kohlmann** for helping me in DSC analysis and his highly valuable comments. I thank him from the core of my heart for giving me access to the DSC instrument in his lab facility and providing me the acquired data and software whenever I needed.

My sincere thanks go to **Dr. Michael Zimmer** for solid state ^{27}Al NMR and temperature controlled NMR analysis. The valuable discussions with him were a source of knowledge for me in the field of ^{27}Al NMR spectroscopy. I thank **Mrs. Susanne Harling** for the elemental analysis of all the compounds presented in the first part of my thesis. I would like to thank the technical staff at Institute of Chemistry, Hermann Recktenwald, Sylvia Beetz, Evelyne Altmeyer, Andreas Adolf, Günther Berlin and Armin Kempf for their support and kindness.

I thank my colleagues (**dicke Freunde)** in Lab 350, Tatjana Kirs and David Kolano. The three and half year time I spent with them will be remembered forever. The so friendly working atmosphere in our Lab was more than enough for relaxing and avoiding depressions and tensions of the workload as well as no results after experiments. I will miss them wherever I will go. I thank my research fellows in the institute, Daniela Summa, Sandra Litzenburger, Fadime Sahin, Amadou Lathyr Ndiaye and Andreas Walgenbach for their moral support, help and moving around together.

I would exploit the opportunity to thank the Pakistani crew in Saarbrücken with whom I enjoyed delicious Pakistani foods, cultural activities, get togethers and much more. It would be an unjust (Khula Tezad), if I do not mention their names; Dr. M. Abbas, Dr. Habib-u-Rehman, Dr. M. Awais Anwar, Dr. Safdar Ali, Amir F. Zahoor, M. Imran, A. waseem, M. Zeshan Afzal, R. Hamza, W. Azim, Hussain Ali, Iftekhar Ahmed, Arif Khan, Saad Ullah, Tousif Liaquat and all those whose names are not in my mind.

I would also extend my thanks to those on the other side of the world for their moral support, love and encouragement. I thank my friends in Pakistan, M. Musa Khan and Gul Wali for their friendship, moral support and prayers.

Last but not the least; I thank my parents for their patience, support, prayers. They always believed in me and extended their every sort of support, unconditionally. They raised me to the point where I am standing now. I thank my wife, **Sara** for her love, patience and

encouragement. She stood by me in every hardship of life and supported me through my tough times. I thank her for arranging my birthday parties which I never celebrated before.

Hameed Ullah Wazir

Saarbrücken, 09.12.2010

Abstract

The importance of strategy of syntheses and the characterisation of molecular precursors in the bottom-up approach of the preparation of nano-materials is now generally accepted. For the successful usage of this methodology, the knowledge of the molecular structure is decisive, since the constituents of the target products are designed at molecular level. Therefore, the purpose of this work was to synthesize molecular compounds of exactly known structures and utilize these compounds for preparation of nano-materials as thin films and powders for various uses.

In first part of this work, efforts are made to prepare structurally characterized molecular compounds of the general formulae $[H_nAl(OR)_{3-n}]_x$ (n = 2 {**1**, **2**, **5**}, 1 {**3**, **6**} or 0 {**4**, **7**}; x = 2 {**5**, **6** **7**}, 4 {**4**}, 5 {**1**} or ∞ {**2**, **3**}; R = ^{c}Hex {**1**-**4**} or ^{c}Hex*Me*-1 {**5**-**7**}), $[ClAl(H)(OR)]_2$ (R = ^{c}Hex*Me*-1 {**8**}), $[Cl_nAl(OR)_{3-n}]_2$ (n = 1 {**9**} or 2 {**10**}; R = ^{c}Hex*Me*-1 {**9**-**10**}), $[Ge(OR)_2]_2$ (R = ^{c}Hex {**11**} or ^{c}Hex*Me*-1 {**12**}, ^{i}Pr {**13**}); $[HAl(OR)(NR')]_2$ (R = ^{t}Bu {**14**}, ^{c}Hex*Me*-1 {**15**; R' = $SiMe_3$ {**14**-**15**}). The molecular compounds **1**, **2**, **4**, **5**, **7**, **8** - **12**, **14** and **15** are obtained as crystalline powders and characterized by single crystal X-ray analysis as well as ^{1}H, ^{13}C NMR and IR spectroscopy. Crystals suitable for X-ray analysis could not be grown for compound **3**, **6** and **13**. However, these compounds were characterized by NMR and IR spectroscopy. Molecular compounds containing Al as central metal atoms were also characterized by ^{27}Al NMR spectroscopy. The elemental compositions of all compounds were determined by CHN analysis as well as by other complexometric titration techniques wherever suitable.

In the second part of this thesis, the results of hydrogen adsorption studies with Al/Al_2O_3-composite nano-wires (NWs) and Ni/Al_2O_3-composite nano-powders (NPs) using a modified Sievert apparatus are presented. Al/Al_2O_3-composites were prepared as thin films by the decomposition of a molecular precursor, $[H_2Al(OR)]_2$, both upon steel as well as glass substrates in a cold wall CVD reactor. Ni/Al_2O_3-composites were prepared as powders by the decomposition of $Ni(acac)_2$ under a steady stream of $[H_2Al(OR)]_2$ in the same CVD set up, using an adapted sample holder. Both types of materials, Al/Al_2O_3 NW and Ni/Al_2O_3 NP, were characterized by XRD, SEM, TEM, EDXS, SAED and IR spectroscopy. Volumetric hydrogen storage measurements with variable temperature and pressure showed a maximum hydrogen uptake of 6.5(±0.2)wt.% with Al/Al_2O_3-composite NWs. The adsorption kinetics

was followed by DSC and IR spectroscopy. The adsorption of hydrogen at the Al/Al_2O_3-composite NWs is controlled by pure physisorption at temperatures below 100°C while above 100°C, desorption occurs as a result of increasing temperature.

Zusammenfassung

Die Bedeutung der Synthesestrategie und Charaktersierung von molekularen Vorstufen für den Bottom-Up Ansatz zur Herstellung von Nanomaterialien steht heute außer Zweifel. Für den erfolgreichen Einsatz dieser Methode ist die Kenntnis der Struktur der Vorläufermoleküle entscheidend, da die Zusammensetzung des Zielproduktes auf dem molekularen Niveau festgelegt werden soll. Somit ist es der Zweck der vorliegenden Arbeit, molekulare Verbindungen mit genau bekannter Struktur zu synthetisieren und diese Verbindungen für die Herstellung von Nanomaterialien in Form von dünnen Schichten und Pulvern für verschiedene Anwendungen zu verwenden.

Im ersten Teil der Arbeit werden Versuche zur Synthese und strukturellen Charakterisierung von molekularen Verbindungen der allgemeinen Formeln $[H_nAl(OR)_{3-n}]_x$ (n = 2 {**1**, **2**, **5**}, 1 {**3**, **6**} or 0 {**4**, **7**}; x = 2 {**5**, **6** **7**}, 4 {**4**}, 5 {**1**} or ∞ {**2**, **3**}; R = ^{c}Hex {**1**-**4**} or ^{c}Hex*Me*-1 {**5**-**7**}), $[ClAl(H)(OR)]_2$ (R = ^{c}Hex*Me*-1 {**8**}), $[Cl_nAl(OR)_{3-n}]_2$ (n = 1 {**9**} or 2 {**10**}; R = ^{c}Hex*Me*-1 {**9**-**10**}), $[Ge(OR)_2]_2$ (R = ^{c}Hex {**11**}, ^{c}Hex*Me*-1 {**12**}, ^{i}Pr {**13**}); $[HAl(OR)(NR')]_2$ (R = ^{t}Bu {**14**} or ^{c}Hex*Me*-1 {**15**; R' = $SiMe_3$ {**14**-**15**}) beschrieben. Die molekularen Verbindungen **1**, **2**, **4**, **5**, **7**, **8** - **12**, **14** und **15** werden als kristalline Pulver erhalten und durch Einkristallröntgenstrukturanalyse sowie ^{1}H, ^{13}C NMR- and IR-Spektroskopie charakterisiert. Für die Verbindungen **3**, **6** and **13** konnten keine für die Röntgenstrukturanalyse brauchbaren Einkristalle erhalten werden. Molekulare Verbindungen mit Al als Zentralatom wurden mittels ^{27}Al NMR-Spektroskopie untersucht. Diese Verbindungen wurden allerdings durch NMR- und IR Spektroskopie charakterisiert werden. Von allen Verbindungen wurden Elementaranalysen angefertigt. Wo möglich wurden komplexometrische Titrationen zur Metallgehaltsbestimmung durchgeführt.

Im zweiten Teil der Arbeit werden die Wasserstoff-Absorption von Al/Al_2O_3-kompositären Nano-Drähten (NWs) und Ni/Al_2O_3-kompositären Nano-Pulvern (NPs) mit einer modifizierten Sievert-Apparatur präsentiert. Al/Al_2O_3-Komposite wurden als dünne Schichten durch die Zersetzung einer molekularen Vorstufe, $[H_2Al(OR)]_2$, auf Stahl und Glas-Substraten in einem Kaltwand-Reaktor erzeugt. Ni/Al_2O_3-Komposite wurden als Pulver durch die Zersetzung von of $Ni(acac)_2$ unter einem stetigen Fluss von $[H_2Al(OR)]_2$ in der selben CVD-Apparatur, allerdings mit angepasstem Substrathalter gewonnen. Beide Materialtypen, , Al/Al_2O_3 NW and Ni/Al_2O_3 NP, wurden durch XRD, SEM, TEM, EDXS, SAED and IR-

Spektroskopie charakterisiert. Volumetrische Wasserstoff-Speicher Untersuchungen mit variablem Druck und variabler Temperatur zeigten eine maximae Wasserstoff-Aufnahme von 6,5(±0.2)wt.% für Al/Al_2O_3-Komposit NWs. Die Absorptions-Kinetik wurde mittels DSC und IR-Spektroskopie verfolgt. Die Waserstoof-Aufnahme der Al/Al_2O_3-Komposit NWs ist unterhalb von 100°C durch reine Physisorption bestimmt, während über 100°C aufgrund der steigenden Tempertur Desorption vorherrscht.

Acknowledgements i

Abstract v

Zusammenfassung vii

Contents ix

List of Abbreviations and symbols xv

General Introduction 1

Part 1 3

Chapter 1.1: Introduction and Objectives 5

Introduction 5

1. General Overview 5

2. Literature Review 6

2.1. Synthesis of Metal Alkoxides 6

2.2. Structural Principles of Metal Alkoxides 11

2.3. Hydride-Modified Metal Alkoxides 15

2.4. Ge(II) Alkoxides 17

Objectives 19

Chapter 1.2: Results and Discussion 21

1. $[H_nAl(O^cHex)_{3-n}]_x$ (n = 2 **1**-**2**, 1 **3** or 0 **4**; x = 4 **4**, 5 **1** or ∞ **2**-**3**) 21

1.1. Synthetic Aspects 21

1.2. Spectroscopic Characterization 22

1.3. Solid State Structures 27

2. $[H_nAl(O^cHexMe\text{-}1)_{3-n}]_2$ (n = 2 **5**, 1 **6**, 0 **7**) 40

2.1. Synthetic Aspects 40

2.2. Spectroscopic Characterization 42

2.3. Solid State Structures 47

3. $[ClAl(H)(O^cHexMe\text{-}1)]_2$ **8** and $[Cl_nAl(O^cHexMe\text{-}1)_{3-n}]_2$ (n = 1 **9** or 2 **10**) 52

3.1. Synthetic Aspects 52

3.2. Spectroscopic Characterization 53

3.3. Solid State Structures 57

4. Synthsis of $[Ge(OR)_2]_2$ (R = ^{c}Hex **11**, ^{c}Hex*Me*-1 **12** or ^{i}Pr **13**) 65

4.1. Synthetic Aspects 65

4.2. Spectroscopic Characterization 66

4.3. Solid State Structures 70

5. Reduction of $Ge\{N(SiMe_3)_2\}_2$ by $[H_2Al(OR)]_2$ (R = ^{t}Bu, ^{c}Hex*Me*-1) 78

5.1. Synthetic Aspects of the Reactions 78

5.2. Spectroscopic Characterization 79

5.3. Solid State Structures 82

6. $[M\{(OR)_{3-n}AlH_n\}_2]$ (M = Ge(II), Ni(II), Eu(II); n = 0, 1, 2) 89

6.1. Efforts for the Synthesize $[Ge\{H_nAl(OR)_{3-n}\}_2]$

(n = 0, 1 or 2; R = ^{t}Bu or ^{c}Hex*Me*-1) 90

6.2. Efforts for the Synthesize $[Ni\{H_2Al(O^tBu)\}_2]$ 95

6.3. Efforts for the Synthesis of $[Eu\{H_2Al(O^tBu)\}_2]$ 97

Summary 99

1. General 105

2. Elemental analysis 105

3. Spectroscopic Methods 105

3.1. Nuclear Magnetic Resonance (NMR) Spectroscopy 105

3.2. Infra-red spectroscopy 106

4. Single crystal determination 106

5. Synthetic Procedures 107

5.1. Synthesis of $[H_nAl(O^cHex)_{3-n}]_n$ 107

5.1.1. $[\{H_2Al(O^cHex)_2\}\{(H)_4Al_4(\mu\text{-}O)(O^cHex)_5\}]$ **1** 107

5.1.2. $[H_2Al(O^cHex)]_n$ **2** 107

5.1.3. $[HAl(O^cHex)_2]_n$ **3** 108

5.1.4. $[Al(O^cHex)_3]_4$ **4** 108

5.2. Synthesis of $[H_nAl(O^cHex\textit{Me}\text{-}1)_{3-n}]_n$ 109

5.2.1. $[H_2Al(O^cHex\textit{Me}\text{-}1)]_2$ **5** 109

5.2.2. $[HAl(O^cHex\textit{Me}\text{-}1)_2]_2$ **6** 110

5.2.3. $[Al(O^cHex\textit{Me}\text{-}1)_3]_2$ **7** 110

5.3. Synthesis of $[ClAl(H)(OR)]_2$ and $[Cl_nAl(OR)_{3-n}]_2$ 111

5.3.1. $[ClAl(H)(O^cHex\textit{Me}\text{-}1)]_2$ **8** 111

5.3.2. $[ClAl(O^cHex\textit{Me}\text{-}1)_2]_2$ **9** 111

5.3.3. $[Cl_2Al(O^cHex\textit{Me}\text{-}1)_2]$ **10** 112

5.4. Synthesis of $[Ge(OR)_2]_2$ 112

5.4.1. $[Ge(O^cHex)_2]_2$ **11** 112

5.4.2. $[Ge(O^cHex\textit{Me}\text{-}1)_2]_2$ **12** 113

5.4.3. $[Ge(O^iPr)_2]_2$ **13** 113

5.5. Synthesis of $[HAl(OR)(N\acute{R})]_2$ 114

5.5.1. $[HAl(O^tBu)(N\{SiMe_3\}_2)]_2$ **14** 114

5.5.2. $[HAl(O^cHex\textit{Me}\text{-}1)(N\{SiMe_3\}_2)]_2$ **15** 114

References 117

Part 2 127

Chapter 2.1: Introduction and Objectives 129

Introduction 129

1. General Overview 129

2. Theoretical Basis and Literature Overview 134

2.1. Compressed Hydrogen 134

2.2. Liquid Hydrogen 136

2.3. Solid Hydrogen (Material-based Hydrogen Storage) 139

2.3.1. Absorption 139

2.3.2. Adsorption 140

2.3.2.1. Physisorption 140

2.3.2.2. Chemisorption 144

2.4. Materials 145

2.4.1. Al/Al_2O_3 Composite Nano-Wires (NWs) 146

2.4.2. Ni/Al_2O_3 Composite Nano-Material 147

Objectives 149

Results 151

1. Sample Characterization 151

1.1. Al/Al_2O_3 Composite Nano-Wires (NWs) 151

1.1.1. XRD Analysis of Al/Al_2O_3 Composite Nano-Wires (NWs) 152

1.1.2. Morphology of Al/Al_2O_3 Composite Nano-Wires (NWs) 153

1.1.3. BET Analysis of Al/Al_2O_3 Composite Nano-Wires (NWs) 158

1.2. Ni/Al_2O_3 Composite Nano-Powders (NPs) 158

1.2.1. XRD Analysis of Ni/Al_2O_3 Composite NPs 159

1.2.2. Morphology and Composition of Ni/Al_2O_3 Composite NPs 159

2. Hydrogen Adsorption 162

2.1. Hydrogen Sorption Studies Using Sievert's Apparatus 162

2.1.1. Hydrogen Adsorption by Al/Al_2O_3 Composite Nano-Wires (NWs) 163

2.1.2. Hydrogen Adsorption by Ni/Al_2O_3 Composite Nano-Powders (NPs) 165

2.2. Infra-Red Spectroscopic Characterization 167

2.2.1. IR spectroscopic Analysis of Al/Al_2O_3 Composite NWs 167

2.2.2. IR spectroscopic Analysis of Ni/Al_2O_3 Composite NPs 168

2.3. Selected Area SEM Analysis of Al/Al_2O_3 Composite NWs 169

2.4. Differential Scanning Calorimetry (DSC) 172

2.4.1. DSC measurements of Hydrogen Adsorption by Al/Al_2O_3 Composite NWs 172

Discussion 176

1. Hydrogen Adsorption by Al/Al_2O_3 Composite Nano-Wires (NWs) 176

1.1. Al/Al_2O_3 Composite NWs 176

1.2. Hydrogen adsorption by Al/Al_2O_3 Composite NWs 178

1.3. Hydrogen adsorption by Ni/Al2O3 Composite NPs 181

***Chapter 2.3*: Experimental** 183

1. Materials 183

1.1. Al/Al_2O_3 Composite Nano-Wires (NWs) 183

1.1.1. Synthesis of Precursor, $[H_2Al(O^tBu)]_2$ 183

1.1.2. Deposition of Al/Al_2O_3 Composite NWs 183

1.2. Synthesis of Ni $/Al_2O_3$ Composite Nano-Powder 185

2. Methods 186

2.1. Sievert's Apparatus 186

3. Experimental Procedures 191

3.1. Sample Preparation and H_2 Adsorption using Sievert's Apparatus 191

4. Sample Preparation and H_2 Adsorption using

Differential Scanning Calorimetry (DSC) 193

Conclusion 195

References 197

Indices 201

Index I (Crystallographic Data) 203

List of Schemes 225

List of Figures 226

List of Tables 229

List of Abbreviations and Symbols

1D	one dimensional
acac	acetylacetonate or 2,4-pentanedionate
Ads.	adsorption
^{t}Bu	tertiary butyl
^{t}BuOH	tertbutanol
°C	degree centrigrade
CVD	chemical Vapour Deposition
d	lattice spacing
DOE	department of energy
DSC	differential scanning calorimetry
EDX	energy Dispersive X-ray Analysis
Eq.	equation
Et	ethyl
et. al.	and others (latin: et alii or et alteri)
HAlO	oxoaluminiumhydride
$[H_2AlO^{t}Bu]_2$	bis-(tert-butoxy)aluminium dihydride
^{c}Hex	cyclohexyl
^{c}Hex*Me*-1	1-methylcyclohexyl
HF	high frequency
HO^{c}Hex	cyclohexanol
HO^{c}Hex*Me*-1	1-methylcyclohexanol
IR	infrared
K	kelvin
M	metal
Me	methyl
MOCVD	metal-organic chemical vapor deposition
MOF	metal-organic framework
NMR	nuclear Magnetic Resonance
NPs	nano-powders
NWs	nano-wires
PDF	powder diffraction files
Ph	phenyl

ppm	parts per millions
^{i}Pr	*iso*-propyl
SAED	selected Area Electron Diffraction
SEM	scanning Electron Microscopy
TEM	transmission Electron Microscopy
T	temperature
tert	tertiary
THF	tetrahydrofuran
XRD	X-Ray Diffractometry
∞	infinity
θ	angle

General Introduction

The last two decades have seen the discovery and the subsequent enormous growth of the nanoc-scinece and nano-technology. The numbers of articles/papers containing the words nano-science, nano-technology and/or nano-materials are in thousands and are growing exponentially with time. The impact of size upon the properties of materials is now a well-known and well-proven phenomenon. By now, nano-science and nano-technology covers materials composed of metals, alloys, ceramics, composites etc. The properties of these materials are controlled at nano-level to prepare materials and/or devices for diverse applications.

The approaches used for the preparation of nano-materials could be divided into two broad categories: the top-down approach in which the nano-materials are prepared by cutting down the bulk entities into nano-level scale particles. The other approach is the bottom-up technique in which small entities work as building blocks for preparation of larger structures. This approach is a chemical way for fabrication of nano-materials. Although both the approaches have their advantages and limitations as well, but the bottom-up approach using molecular chemistry has certain advantages, for example lower expenditure of the process, high homogeneity of the resulting nano-materials, designed composition etc. Therefore the role of chemistry is vital in the bottom-up approach in the fabrications of nano-materials from molecular entities. This role pronounces more when all the necessary constituents of the resulting products are desired in a single chemical molecule called single source precursor (SSP). Therefore, the thesis aims to prepare structurally characterized molecules to be used in different processes for preparation of new and dynamic nano-materials. The resulting nano-materials may be used for different purposes. On the basis discussed above, the thesis is divided into two parts.

Part 1. In the first part of the thesis structurally characterized new molecules are prepared. A total of 15 different compounds are synthesized which are categorized into different groups based upon the nature of the metal centres and organic moieties. The first series give four compounds of the general formula, $[H_nAl(OR_{3-n})]_x$ (n = 2, 1, 0; x = 4, ∞; R = ^{c}Hex). The second series gives three compounds of the general formula, $[H_nAl(OR_{3-n})]_2$ (n = 2, 1, 0; R = ^{c}Hex*Me*-1). The third series comprises of three compounds of the general formulae, $[ClAl(H)(OR)]_2$ (R = ^{c}Hex*Me*-1) and $[Cl_nAl(OR)_{3-n}]_2$ (n= 2, 1; R = ^{c}Hex*Me*-1). The fourth

series includes Ge(II) alkoxides of the general formula, $[Ge(OR)_2]_2$ (R = ^{c}Hex, ^{c}Hex*Me*-1, ^{i}Pr). The Fifth series includes two compounds of the general formula, $[HAl(OR)(N\acute{R})]_2$ (R = ^{t}Bu, ^{c}Hex*Me*-1; $\acute{R}$ = $SiMe_3$). Efforts are also made for the preparation of hydride-modified heterometal aluminium alkoxides with Ge(II), Ni(II) and Eu(II). However, none of the reaction succeeds to give a fairly characterized compound.

Part 2. Hydride-modified aluminium *tert*-butoxide gives highly porous nano-structures upon decomposition at temperature above 450°C in a CVD chamber. The nano-structures resemble singled wall carbon nano-tubes (SWCNTs) which have been used as potential hydrogen storage material at cryogenic temperatures. Therefore, this part of the thesis is devoted to hydrogen adsorption studies upon Al/Al_2O_3 composite nano-wires (NWs) produced by the decomposition of hydride-modified aluminium *tert*-butoxide in CVD chamber at 580°C. The hydrogen adsorption studies are performed upon two different materials that are Al/Al_2O_3 composite NWs and Ni/Al_2O_3 composite nano-powders (NPs). The hydrogen uptake by the two materials is measured volumetrically using home-made Sievert's type apparatus. For comparison purposes, the hydrogen adsorption by the Al/Al_2O_3 composite NWs is also followed by differential scanning calorimetry (DSC).

Each part is further divided into three chapters. The first chapter of each part gives an introduction, and a detailed theoretical and literature overview of the subject. The second chapter includes detailed description of the results and then complete discussions in light of highly relevant literature. The third chapter of each part includes complete experimental details regarding the materials, methods and procedures. Each part is summarized and concluded at the end.

Part 1

Synthesis and Characterization of Hydrido/ChloroAluminium Alkoxides and Metal (Al, Ge) Alkoxides

Introduction

1. General Overview

Metal alkoxides, having general formula, $M^{\delta+}–^{-\delta}OR$ are under intense investigation for the last 50-60 years. However, the history of metal alkoxides dates back to the 1840 when sodium and potassium ethoxide was discovered by Liebig. In the same year the term *alkoxides* was used by Kuhlmann for the alkaline derivatives of alcohols [1]. In 1846 silicon and boron alkoxides were reported by Ebelmann [2-3]. It was only at the turn of the 19^{th} century that the catalytic activity of metal alkoxides in organic synthesis has been discovered. In 1906, Tischtschenko reported the reduction of aldehydes and Ketones using aluminium ethoxide and the process is nowadays known as Tischtschenko reaction [4]. Following the Tischtschenko reaction, the catalytic characteristics of the alkoxides were used extensively for organic synthesis by other researchers in the following years [5-7]. It was not until 1950 when D. C. Bradley started working with metal alkoxides and laid down the foundations of the modern chemistry of metal alkoxides. By now, metal alkoxides have been reported for nearly all the elements of the periodic table [8-11].

The use of metal alkoxides in material synthesis is yet another facet of metal alkoxide chemistry. It was Adkins who in 1922 observed that the hydrolysis of aluminium ethoxide gives alumina [12], which had used as catalyst for dehydration and decaboxylation reactions. However, the use of metal alkoxides in metal organic chemical vapour deposition (MOCVD) and sol-gel techniques for the preparation of modern ceramic materials stimulated the research area of this class of compounds to the extent of competition. The desired material is achieved by designing the initial metal alkoxide molecules. The composition of these starting molecules (termed “precursors”) is only limited to chemical imagination. This approach is also extended to the heterometallic alkoxides.

The first bimetalic alkoxides were reported in 1929 by Meerwein and Bersin [13-16] and thus pioneered the work of heterometal alkoxides. Many researchers have produced bimetalic alkoxides in the successive years [17-18]. However, the research in the field of heterometalic

alkoxides was based upon pure academic perspectives until very recently. The need of multimetallic advanced ceramic materials, for example $YBa_2Cu_3O_{7-\delta}$ [19], $HgBa_2CuO_4$ [20], $Bi_2Sr_2CaCuO_8$ [21] etc., to be obtained in higher purity has stimulated the research in the field of heterometal alkoxides. The molecular precursor route for the synthesis of materials allows for the production of ultra-pure products [22-25]. Besides purity better control over composition, homogeneity, microstructure etc. are possible through this methodology. However, these routes depend largely upon the availability of suitable precursors, which must be thermodynamically favourable. A large number of mono- as well as heterometallic alkoxides have been reported by M. Veith and his colleagues [25]. A very famous review article has been appeared regarding the application of these alkoxides for the preparation of nanomaterials [26].

To use metal alkoxides in MOCVD and sol-gel processes for the synthesis of versatile modern materials, certain modifications have been introduced. M. Veith [27] has pioneered hydride-modified homo [28] and heterometal alkoxides [29], which proved to be versatile single source precursors for MOCVD. High volatility, easy purification *via* crystallization, sublimation at ambient temperatures etc. are some of the characteristics of these molecular precursors. Besides lower decomposition temperature, high purity, adopted composition and microstructure are the distinguished advantages of the molecular precursor route over classical solid state production of materials.

2. Literature Review

2.1. Synthesis of Metal Alkoxides

The most common routes for the synthesis of metal alkoxides are summarized in Scheme 1.1. The simplest of the methods for the synthesis of metal alkoxides is the reaction between the metal and the corresponding alcohols (Eq. 1.1). However, this method is limited to the more electropositive metals, for example alkali metals, alkaline earth metals and lanthanides etc. For less electropositive elements a catalyst (e.g. HgI_2) is needed to prepare their alkoxides. One catalytic model focuses on cleaning the surface of the metal to facilitate initiation of the reaction. The other theory assumes that an intermediate with the metal is formed which could then react more readily with alcohol than the metal itself [11]. The reactivity increases with

increasing electropositive character of the metals and alkoxides of the alkali metals have been prepared successfully by this method [30-34]. However, the nature of the alkyl groups has profound effect upon the reaction rate. For the same metal the reaction slows down with increasing branching of the alkyl groups.

$$M + n\,HOR \longrightarrow M(OR)n + n/2\,H_2 \qquad (1.1)$$

Alkoxides of the alkaline earth metals could be produced by the direct reaction of alcohol with the metal [35-36] except for the first two members (Be and Mg), which only react in presence of a catalyst [37-40]. The reaction of alcohols with metals in presence of a catalyst was also reported for aluminium metal to prepare aluminium alkoxides [41-42]. However, the highly electropositive lanthanides have shown reactions with alcohols without using catalysts [43-44].

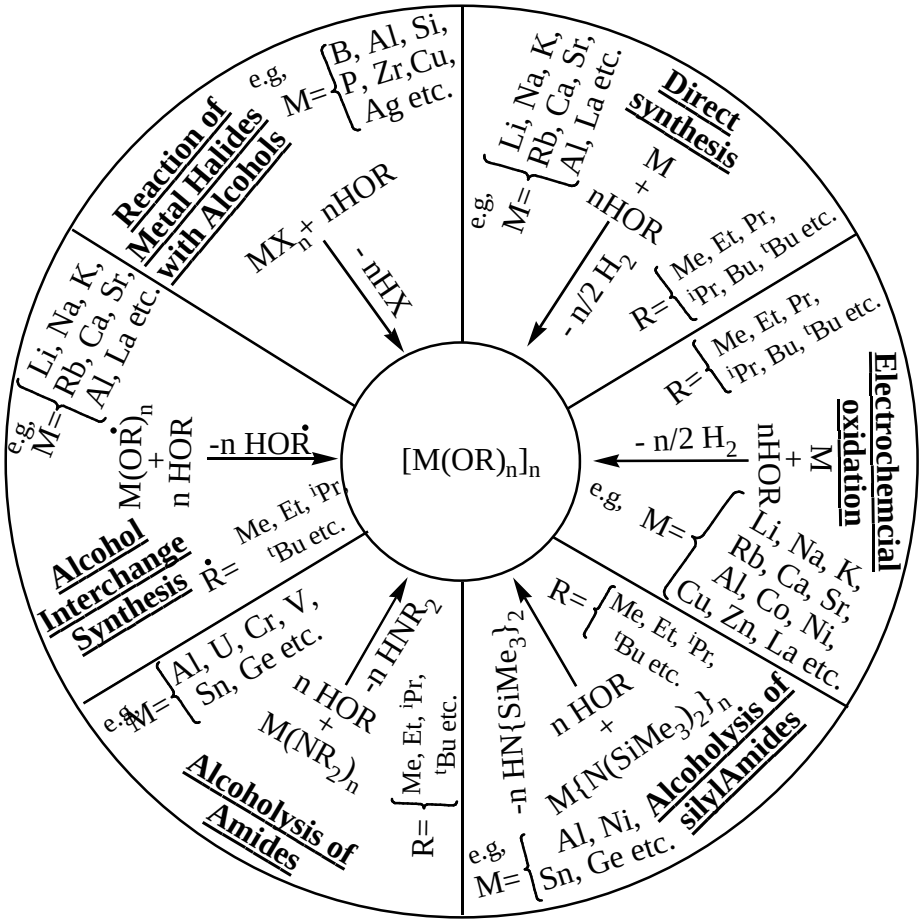

Scheme 1.1. Different reactions routes for the synthesis of metal alkoxides

The direct electrochemical synthesis of metal alkoxides is efficiently performed by the electrochemical oxidation of metals at the anode in presence of alcohols. In 1970 the first metal alkoxide (NaOMe [45]) was prepared by this method and Monsanto Chemical Co. prepared dozens of metal alkoxides by electrochemical oxidation [46]. The process depends upon the nature of the metal. Metals with high negative potential react easily [47], while the process becomes more complex for the less active metals [48-49]. The process has the advantages of simplicity, less solvent consumption, high efficiency and low-waste etc. [50-51].

Another intensively investigated method for the synthesis of metal alkoxides is the reaction of respective metal halides with alcohols. This method is quite efficient for the synthesis of alkoxides of more electronegative elements. For example in case of boron [52-53], silicon [54], and phosphorous [55] the halides are completely replaced by the alkoxy groups. However, metal halides of the more electropositive elements form solvates when isolated from solution (e.g. lanthanum [56] and thorium [57]). There are no systematic studies of the reaction mechanism known up to now. It was postulated by Sidgwick that the reaction may occur by first coordination of the alcohol to the metal centre through the oxygen followed by the elimination of HCl [58]. This postulation was supported by the lack of reaction between carbon tetrachloride and alcohols [59]. Carbon does not possess low energy vacant orbitals for accepting a lone pair of electrons from the oxygen of the alcohol and thus no pre-coordination is possible and as a result no reaction could occur. However, this postulation became ambiguous when the reaction between germanium tetrachloride and alcohols failed even at refluxing conditions [60]. Bradley *et. al.* also reported that no reaction takes place. No solvate was isolated either, which otherwise should form [61].

Metal halides have been used as starting materials for the synthesis of alkoxides in metathesis reactions with metal alkoxides. The metal alkoxides used in these reactions are usually the alkali alkoxides. These reactions are mostly carried out in alcohols and therefore, it is thought that alcoholysis of metal halogenides takes place, for example in case of $ZnCl_2$. The dissolution of $ZnCl_2$ in alcohol leads to $ZnCl_n(OR)_{2-1}$ [62]. The alcoholysis is due to the strong acidic character of metal halogenides and therefore, increases with increasing basicity of the alcohols, for example primary < secondary < tertiary. The mostly used metal alkoxides are KOR, NaOR and LiOR. The salt formed is nearly insoluble in organic solvents and thus can be removed easily by filtration. For the metals which form stronger heterometal

alkoxides, this method is not recommendable and the alkoxides are always difficult for such metals to prepare by this method. However, anhydrous ammonia is used for dechlorination of the metal to get pure metal alkoxides by this method.

Alcohol interchange synthesising methods have been used successfully for the preparation of different metal alkoxides. The general trend of increasing interchange is from tertiary to secondary to primary alcohols (depending upon the basicity and ramification). The steric demand of the alkyl part of alcohols also plays a key role in these reactions [8]. The interchange of bulky groups with less steric demanding groups could be achieved quickly. However, the replacement of less steric demanding groups with higher steric demanding groups is always slow and difficult. In this case the complete interchange is difficult to achieve and heteroleptic metal alkoxides are formed. The complete exchange may be forced by the fractionate distillation of the volatile alcohol [63]. For example the *iso*-propoxide will be replaced completely with primary and secondary butoxide by removing the more volatile *iso*-propanol. However, this is failed in case of more ramified *tert*-butanol where only two *iso*-propoxides could be replaced [63].

An interesting route for the synthesis of alkoxides is the alcoholysis of amides. The first reaction of this kind was reported for the preparation of alkoxides in liquid ammonia solution [64]. This method was used frequently for the synthesis of metal alkoxides [65-66]. The advantage is the high purity and easy isolation of the product since the only by-product is the gaseous conjugated amine which can be easily removed under low pressure. However, the formation of stable complexes of amines with alkoxides is a serious limitation of this method [67]. Besides, the amides are strong σ as well as π donors, therefore, completion of the reaction is always difficult to achieve and as a result the final product is contaminated with parent amides [68].

Replacing alkyl residue by silyl groups reduce the π donor properties. An example for a widely used amido ligand is bis-(trimethylsilyl)amide [69-70]. The bulky substituents attached to the nitrogen atom are responsible for its stabilization as monomer of metals amides. Therefore, it is very easy to remove bis-(tri-methylsilyl)amine by simple distillation from the final product. The alcoholysis of electron poor amides gives pure products in good yields for the metals having higher affinity for oxygen than for nitrogen. For example the bond enthalpy of Ge-N is lower (55 kcal/mol) than the bond enthalpy of Ge-O

(157 Kcal/mol), which is a driving force for the reaction [71]. Due to these reasons this reaction route was followed in the present work for the preparation of Ge(II) alkoxides.
In the following paragraphs a brief discussion regarding the synthetic strategies of hydride-modified aluminium alkoxides and hydride-modified heterometal alkoxides of aluminium with different metals will be presented. Aluminium alkoxides have been used for material syntheses as earlier as 1923 when alumina prepared by the hydrolysis of aluminium ethoxide was used as catalyst [72]. Aluminium containing heterometal ceramics has also found diverse applications especially when the material is in nano-meter level scale, for example $MgAl_2O_4$ spinels [73-75]. Therefore, versatile synthetic routes are important to explore. Metal hydrides were used as starting materials for the synthesis of metal alkoxides [76-78]. This route has limited choices and also limited to certain metals. However, the synthetic route for the hydride-modified aluminium alkoxides and heterometal alkoxides of aluminium with metals (especially magnesium) has matured in the last two to three decades.

Hydride-modified aluminium alkoxides were pioneered and studied in detail by H. Nöth und H. Suchy in the latter 60s [79]. The preparation is quite straightforward: AlH_3 and the corresponding alcohol are brought into reaction (Eq. 1.2). The only by-product produced is gaseous hydrogen. AlH_3 is quite unstable and can only be used *in situ* during its production from the reaction of $MAlH_4$ and $AlCl_3$ (where M = Li, Na, K). Hydride-modified aluminium alkoxides, which are structurally well characterized by single crystal X-ray diffraction analysis, have been reported only recently [28, 80].

$$\mathbf{AlH_3 + n\,HOR \longrightarrow H_{3-n}Al(OR)_n + nH_2} \qquad (1.2)$$

A revolutionary hydride-modified heterometal alkoxide of aluminium with magnesium has been reported by Veith *et. al.* [29]. This alkoxide is unique in its structure and composition. It was prepared by a two step salt elimination reaction in which two equivalents of *tert*-butanol were added to $LiAlH_4$ giving $LiAlH_2(O^tBu)_2$. Two equivalent of this complex were added to $MgCl_2$ and maintained under reflux for 8 hours (Eq. 1.3). The hydride-modified aluminium magnesium alkoxide is quite interesting and showed extra-ordinary characteristics in the MOCVD process to produce $MgAl_2O_4$ spinels [29].

$$\mathbf{LiAlH_2(OtBu)_2 + MgCl_2 \longrightarrow Mg\{H_2Al(OtBu)_2\}_2 + 2\,LiCl} \qquad (1.3)$$

This type of compounds could be of great technological interest especially for the synthesis of nano-metre level scale materials. However, the library of such compounds is yet to be established.

2.2. Structural Principles of Metal Alkoxides

Metal alkoxides have tremendous use in the preparation of modern materials especially through CVD and Sol-Gel processes. Therefore, their structural aspects are of considerable interest. In most of the cases the metal to metal composition in the final product is designed at molecular level to achieve the desired material for different applications. However, it is not a simple phenomenon to be achieved at stoichiometric considerations. Despite the molecular structure of metal alkoxides strongly depends upon two highly pronounced factors:

a. The nature of the metal atoms
b. The steric demand of the organic moiety attached to the oxygen atom of the alkoxy group

The oxygen atom of the alkoxy group has the tendency of bridging between/among different metal centres. Therefore, the coordination number of oxygen could increase from one (terminal) to two and even to three metals centres (bridging) (Figure 1.1).

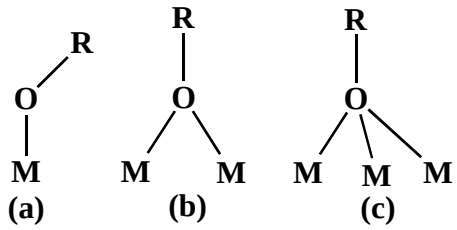

Figure 1.1. Coordination modes of oxygen in metal alkoxides

The bridging of oxygen occurs due to its strong coordination power to preclude other possible mechanisms, for example coordination of free ligand (e.g. solvent, alcohol, amine etc.) to expand the coordination sphere of the metal. However, the coordination of oxygen with more

than one metals centre in presence of donor ligands depends upon the nature of the metals. The coordination number at the metal centre depends upon its nature. However, the degree of polymerization has strict dependence upon the steric bulk of the alkyl group attached to oxygen and its ramification. In the following paragraph an overview will be presented regarding the different structural possibilities in metal alkoxides as well as heterometal alkoxides. A brief literature review regarding the structural aspects of hydride-modified aluminium alkoxides and Ge(II) alkoxides will be presented separately.

The monovalent members of the alkali metals group give mostly cubane like structures, which is also known for other metals. The first ever cubane structure was proposed by Sidgwick and Sutton [81] for thallium ethoxide which was later confirmed by single crystal X-ray diffraction analysis [82]. The thallium and oxygen atoms are occupying the corners of the cube and the ethyl groups attached to the oxygen atoms are located exohedral. Each of the thallium atoms is bonded to three oxygen atoms and each oxygen atom is coordinated to three thallium atoms. Thus the cubane structures are composed of cubes having alternating metal and oxygen atoms at the corners (Figure 1.2).

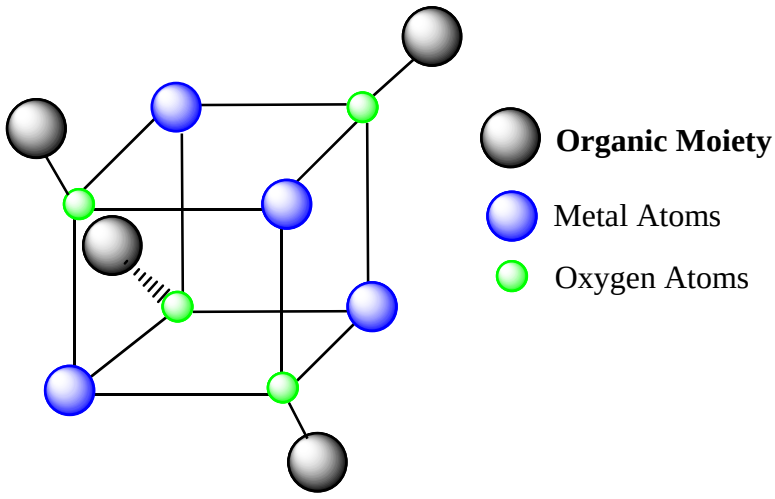

Figure 1.2. Virtually drawn cubane structure of metal alkoxides

The structures have been determined by single crystal X-ray diffraction analysis as well as spectroscopic techniques. This type of structure has been obtained for the *tert*-butoxide of K, Rb and Cs using single crystal X-ray diffraction analysis [83-86]. A cubane structure has been

proposed for the sodium perflouro *tert*-butoxide by mass spectroscopic studies [87]. Methylzinc methoxide also gave a cubane structure in solid state solved and refined by single crystal X-ray analysis [88]. Contrarily to the later members of the alkali metal groups, the light homologues, *tert*-butoxides of Li and Na have completely different structures. A hexameric structure was proposed for LiO^tBu based on mass spectroscopic data [90-91]. NaO^tBu also gives a nonameric beside a hexameric one [92-93]. The steric effect could be seen by the fact that the methoxides and ethoxides of alkali metals are all polymers.

Alkoxides having monomeric structures have been reported where the coordination number of the central metal atoms varies in a larger range (2-8). Highly bulky alkyl groups have been used to get momomeric alkoxides. The larger bulk of the alkyl group hinders the coordination ability of the oxygen atoms by shielding the central atom, the metal. The molecules are often stabilized by further donor ligands, for example ether, amine, etc. However, the ligands stabilized metal alkoxides are generally not considered as pure alkoxides. Monomeric beryllium alkoxide ($[Be(OC_6H_2{}^tBu_3\text{-}2,4,6)_2(Et_2O)$) has been reported using a sterically more demanding alkoxy group. The bulky ligand hinders the intermolecular interaction and the compound was stabilized by one ether molecule entered into the coordination sphere of berryllium [94]. However, $Be(O^tBu)_2$ is a trimer which indicates that the lowering of steric bulk directly increases the degree of polymerization. A large number of monomeric alkoxides has been reported for various metals having varying steric demand of the alkoxy groups in their coordination sphere. A few examples are $TiCl2(OC_6H_3Ph_2\text{-}2,6)_2$ [95], $Zr(O^tBu)_4$, $Hf(O^tBu)_4$ [96], $W(OC_6H_2Ph_2\text{-}2,6)_2(THF)$ [97] etc.

The most observed and reported oligomerisation degree for metal alkoxides is two. Usually, the monomers are associated through a bridging alkoxo ligand forming a central four-membered ring, $M_2(\mu\text{-}O_2)$. The bridging oxygen atoms possess a trigonal planar environment. A measure for the planar surrounding is the sum of angles, which ideally sums to 360°, being consistant with sp^2 hybridisation [98]. The most common coordination numbers at the metal centres lie within 3 to 6. The common dimeric structures adopted by metal alkoxides are summarised in the following Figure 1.3, based upon the observed coordination numbers at the metal centres. A dimeric structure without terminal substituents has been reported for indium(I) phenoxide (see Figure 1.3a) [99]. Interestingly the same sort of structure has been reported for $[Li(OC^tBu_3)]_2$ with the extremely bulky OC^tBu_3 alkoxide [100]. Dimers with metals having trigonal planar geometry (Figure 1.3b) have been reported for Cu(I), Mg(II),

Co(II) etc. [101-102]. Tetrahedral metal centres (Figure 1.3c) have been observed for Na(I) [103], Co(II) [102], Al(III) [104], La(III) [105] etc. The coordination sphere of metals in these dimers could contain neutral lingads varying among 1-3. Penta-coordinated metal centres of the general formula, $[M(OR)_nL_{4-n}]_2$ have been reported for Li [106], Cu [107], Nd [108], Ti [109] etc. The metal centres carry different bulky groups according to the requirements for stabilization of the structures. Hexa-coordinated metal centres have been reported having general formula, $[M(OR)_nL_{5-n}]_2$ in which the octahedra are usually distorted. For example $[Nb(OR)_5]_2$ (R = Me [110], ^{i}Pr [111]).

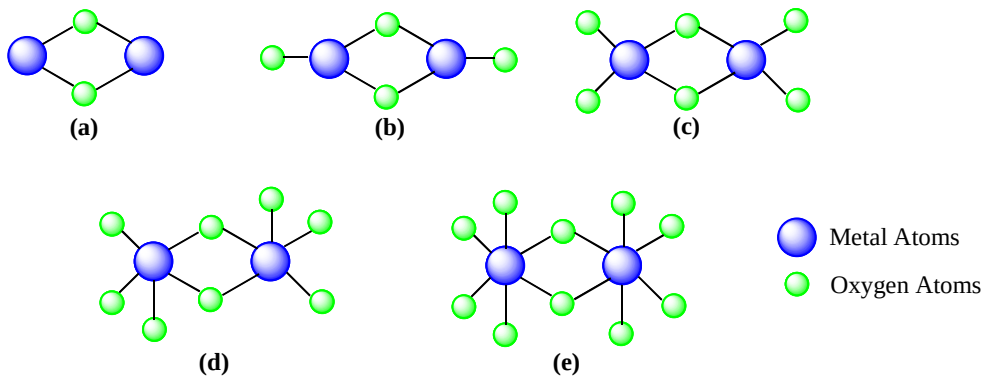

Figure 1.3. Sketches of observed structures of dimeric alkoxides

For the trimeric metal alkoxides in most of the cases linear chaines like structures have been reported. These chains can be categorised into three different forms: (a) in which no ligand is attached to the central metal atom (Figure 1.4a); such structures have been reported for e.g. $Be[(\mu\text{-}O^tBu)_2BeCl]_2$ [112], $Ni[(\mu\text{-}O^tBu)_2Al(O^tBu)_2]_2$, $Mg[(\mu\text{-}O^tBu)_2Al(O^tBu)_2]_2$ [113-114]; (b) In which the central atom carries one further ligand (Figure 1.4b), the central metal adopts trigonal bipyramidal geometry; e.g. $ClAl[(\mu\text{-}O^iPr)_2AlCl_2]_2$ [115]; (c) In which the central atom carries two ligands (Figure 1.4c), the geometry around the central atom is distorted octahedral; see e.g. $[Mg(EtOH)_2][(\mu\text{-}OEt)_2Ta(OEt)_4]_2$ [116].

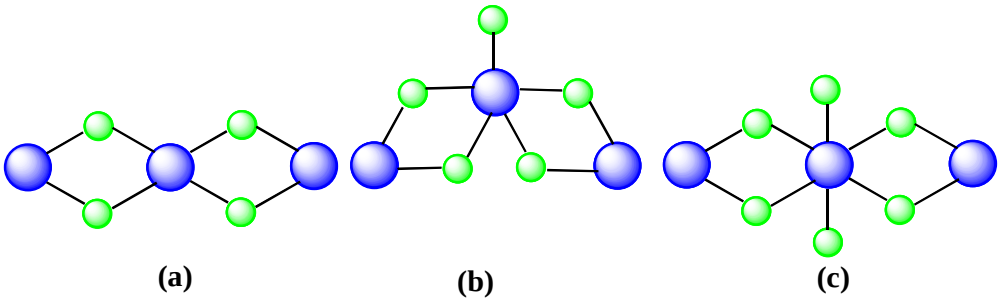

Figure 1.4. Structural possibilities in trimeric metal alkoxides

Tetramers have been reported for different metal alkoxides. The structure of $[Al(O^iPr)_3]_4$ is structurally highly interesting [117-119], because it adopts the so-called Mitsubishi motif (Figure 1.5). These types of structural motifs have been observed for other metal alkoxides too (e.g. $[Ga(O^iPr)_3]_4$ [120-121], $Er\{Al(O^iPr)_4\}_3$ [122], $Eu\{Al(OiPr)_4\}_3$ [123], $Al\{Al(OEt)_2Me\}_3$ [124], $Al\{Al(OEt)_2{}^tBu\}_3$ [125]). Other interesting structures possessing tetranuclear entities are tetrahedral, butterfly, planar cycles, linear chaines etc [98].

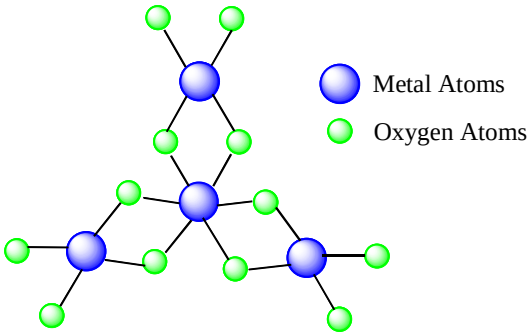

Figure 1.5. Mitsubishi motif like structure of tetrameric alkoxides

2.3. Hydride-Modified Metal Alkoxides

Hydride-modified alkoxides are mostly reported for the group 13 metals, especially Al and Ga. Therefore, the review of structural possibilities will be limited to the metals of this group. The library of hydride-modified alkoxides has yet to be established since there are very few

compounds, which are structurally characterized. The versatile *tert*-butoxyaluminium dihydride, $[H_2Al(O^tBu)]_2$ [28] reported in the group of M. Veith [27] has paved the way for research in this field. However, the small number of structurally characterized compounds limits the validity of structural diversity. As with metal alkoxides, the hydride-modified alkoxides have only been obtained as monomers applying highly bulky alkoxy groups with additional stabilisation through donor ligands. For example $H_2Al(OC_6H_2{}^tBu_2\text{-}2,6\text{-}Me\text{-}4)(NMe_3)$ is a monomer where the central aluminium metal possesses distorted tetrahedral geometry [126]. The same author also reported monomeric $ClAl(H)(OC_6H_2{}^tBu_2\text{-}2,6\text{-}Me\text{-}4)(NMe_3)$ [126].

However, due to the stronger intermolecular association, most of these compounds possess a higher degree of association. The degree of association strongly depends upon the steric demand of the alkoxy group. The intermolecular interaction is made feasible by the stronger coordinating nature of oxygen atoms of the alkoxy groups and lesser bulky hydrogen atoms attached to the metal centres. Dimers having central $M_2(\mu\text{-}O_2)$ four-membered cyclic rings are most common in these compounds. For example $[H_2Al(O^tBu)]_2$ [28] is a dimer with the Al atoms in a pseudo-tetrahedral environment. The bridges are formed by the oxygen atoms of the alkoxy groups while the hydrides remain as terminal groups (Figure 1.6). Other examples of hydride-modified metal alkoxide dimers are; $[H_2Al(OCMe^tBu_2)]_2$ [80], $[HAl(O^tBu)_2]_2$ [28], $[ClAl(H)(O^tBu)]_2$ [127], $[H_nGa(O^tBu)_{3\text{-}n}]_2$ [28], $[H_2Ga(OCH^tBu_2)]_2$ [128]. Dimeric hydride-modified aluminium alkoxides, $[HAl(\mu\text{-}H)(OC_6H_2{}^tBu_2\text{-}2,6\text{-}Me\text{-}4)(NMe_3)]_2$ have been reported where the two monomers are bridged by hydrogen atoms [126]. The coordinating ability of oxygen has been hindered by the strong steric demand of the alkyl groups.

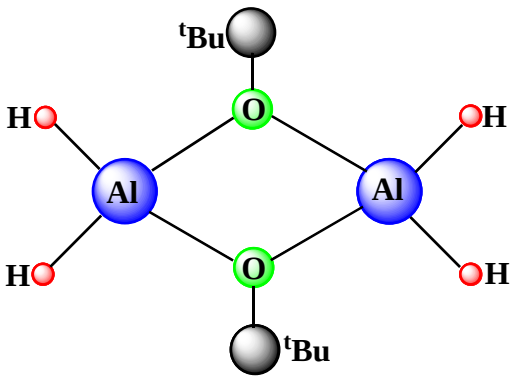

Figure 1.6. Dimeric structure of $[H_2Al(O^tBu)]$

Trimeric hydride-modified aluminum alkoxides have been reported with the central metal atom being penta-coordinated by four bridging oxygen atoms of the alkoxy groups and one hydrogen atom as terminal group [80]. Tetramers have been reported in which two dimers associate via hydride bridges. For example, $[H_2Al\{\mu\text{-}OC(Me)^tBu_2\}_2AlH(\mu\text{-}H)_2]$ [80], $[H_2Al\{\mu\text{-}OC(H)^tBu_2\}_2AlH(\mu\text{-}H)_2]$ [129] etc. In principle these molecules are dimers but due to the less bulky alkyl moiety, these are stabilized by intermolecular interaction. This intermolecular interaction takes place through hydrogen since no oxygen is available for coordination.

There are only very few examples of hydride-modified heterometal aluminium alkoxides. Most of them belong to the first group alkali metals hydridoaluminium alkoxides. However, here we will discuss the structural principles of hydride-modified alkoxide of aluminium with magnesium [29]. This is the only molecule of the type so far known apart from alkali metals hydride-modified alkoxides. Reported in Veith's group [27], the molecular structure of this compound adopts a tri-nuclear linear chain like structure. The central Mg atom is tetra-coordinated with four bridging oxygen atoms in a tetrahedral geometry. The terminal Al atoms also possess tetrahedral geometry with two bridging oxygen atoms and two terminal hydride ligands (Figure 1.7).

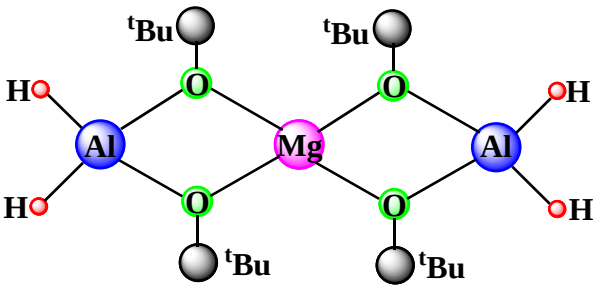

Figure 1.7. Hydride-modified heterometal alkoxide of Al with Mg

2.4. Ge(II) Alkoxides

Ge(II) ethoxide was first reported in 1979 by Silverman and Zeldin [130-131]. However, considerable contributions to that field had come from Veith's group [27] in the 1980s and

90s shown in the structural elucidation of germanium *tert*-butoxide and heterometal germanium *tert*-butoxides [132-134]. Monomeric Ge(II) alkoxides have been reported with bulky alkoxy groups [135]. Here the same tendency with respect to the influence of the steric bulk on oligomerisation degree are active: the higher the steric demand of the alkyl moiety the lower the agglomerisation, i.e the lower is the oligemerisation degree.. Examples for monomers due to high steric demand are $Ge(OC^tBu_3)_2$ [136], $Ge(OC_6H_3Ph_2\text{-}2,6)_2$ [137]. Most of the germanium alkoxides are dimers exhibiting a central Ge_2O_2 four membered ring. Contrary to the trigonal planar tri-coordinated metal centres, the tri-coordinated metal centres in group 14 metal alkoxides have pyramidal geometry. Although there is a lone pair on the metal centre but the trigonal pyramidal geometry is that of p^3 orbital [138] . $Ge(O^tBu)_2$ [131] is a dimer having tri-coordinated Ge atoms with pyramidal geometry. The terminal *tert*-butoxy groups are located at *trans*-positions to each other on the central planar four-member cycle (Figure 1.8).

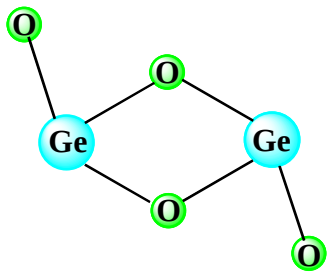

Figure 1.8. Dimeric structural motif of Ge(II) alkoxides

Apart from the two very common structural motifs of Ge(II) alkoxides, very recently Ge(II) aryloxides have been reported which adopt cluster like structures [139]. The molecular structures are either tetra-nuclear or octa-nuclear. However, these structural motifs are quite unusual.

Objectives

Hydride- modified Aluminium Alkoxides of the general formula, $[H_nAl(OR)_{3-n}]_x$ are getting attention as potential single source precursors as well as reducing agents. The use of these molecules, $[H_nAl(OR)_{3-n}]_x$ for the preparation of nano-materials has been pioneered in our research group (research group of Prof. Dr. Dr. h. c. Michael Veith). The versatilities of these compounds can be exemplified by one of their homologue, $[H_2Al(OR)]_2$ which is extensively investigated as single source precursor for preparation of nano-materials by CVD process. It gives different nano-materials at different decomposition temperatures. For example below 300°C, the compound, $[H_2Al(OR)]_2$ decomposes into glass like metastable HAlO material, at above 300-450°C it gives spherical core-shell Al/Al_2O_3 composite nano-particles while at above 450°C it gives core-shell Al/Al_2O_3 composite nano-wires. However, the library of the compounds, $[H_nAl(OR)_{3-n}]_x$ has limited number of molecules which are structurally well characterized. Therefore, the first aim of the work was to prepare hydride-modified aluminium alkoxides as well as aluminium alkoxides.

Salt elimination reactions are preferred for the synthesis of main group homo- and hetero-metal alkoxides because of simplicity of the processes and easy separation of the by-product from the product by filtration. However, structurally well characterized aluminium halides alkoxides are required to be used as reactants. Therefore, the second aim of the work was to prepare aluminium chloride alkoxides to be used as reactants in the reaction for preparation of homo- and hetero-metal alkoxides of aluminium with main groups metals, for example Ge.
The third aim of this work was to prepare Ge(II) alkoxides which are getting attention due to their use as potential single source precursor for the synthesis of Ge^0 nano-particles as well as Ge^0 nano-wires. The Ge^0 nano-particles have lower bandwidth than the bulk and thus emerging as competent semiconductor materials to silicon base materials.

It was also aimed to prepare hydride-modified homo- and hetero-metal alkoxides of aluminium with Ge(II), Ni(II) and Eu(II).

1. $[H_nAl(O^cHex)_{3-n}]_x$ (n = 2 **1**-**2**, 1 **3** or 0 **4**; **x** = 4 **4**, 5 **1** or ∞ **2**-**3**)

1.1. Synthetic Aspects

All four compounds (**1**-**4**) have been prepared utilizing salt elimination reaction pathways reported elsewhere [79]. The synthetic process is summarized in Scheme 1.2. Ethereal solutions of $AlCl_3$ and $LiAlH_4$ were mixed together in appropriate molar ratios. After stirring for one hour, *cyclo*-hexanol in ether was added into the above solution mixture very slowly according to the required stoichiometric ratios. The evolution of hydrogen was observed as soon as the alcohol started to add. A white residue precipitated out of the reaction, which was mostly LiCl salt and was removed by filtration. The volatiles were removed under vacuum which was mostly diethylether, the solvent. The four compounds have been obtained as white powders in high yields (> 85%). Colourless fine crystals of compound **4** were obtained as soon as the filtrate was condensed. Compounds **1** and **2** were crystallized by dissolving small amounts of the powders in diethylether while kept in refrigerator at +4°C. Compound **3** has been crystallized from ethereal solution in refrigerator. However, the crystal quality was too poor to resolve any suitable structure. Compounds **1** and **4** are soluble in all common organic solvents. However, compounds **2** and **3** are difficult to dissolve in organic solvents and very small amounts could be dissolved at elevated temperatures. Compound **4** is hygroscopic but chemically stable enough to be handled in open air atmosphere. Compounds **1**-**3** have shown high reactivity towards atmospheric oxygen and reacted violently with water. After exposure to the air for more than ten minutes, these compounds (**1**-**3**) decomposed completely and all the hydrides at the Al centre have been. The decomposition reactions of these compounds in open atmosphere were confirmed by IR spectroscopy.

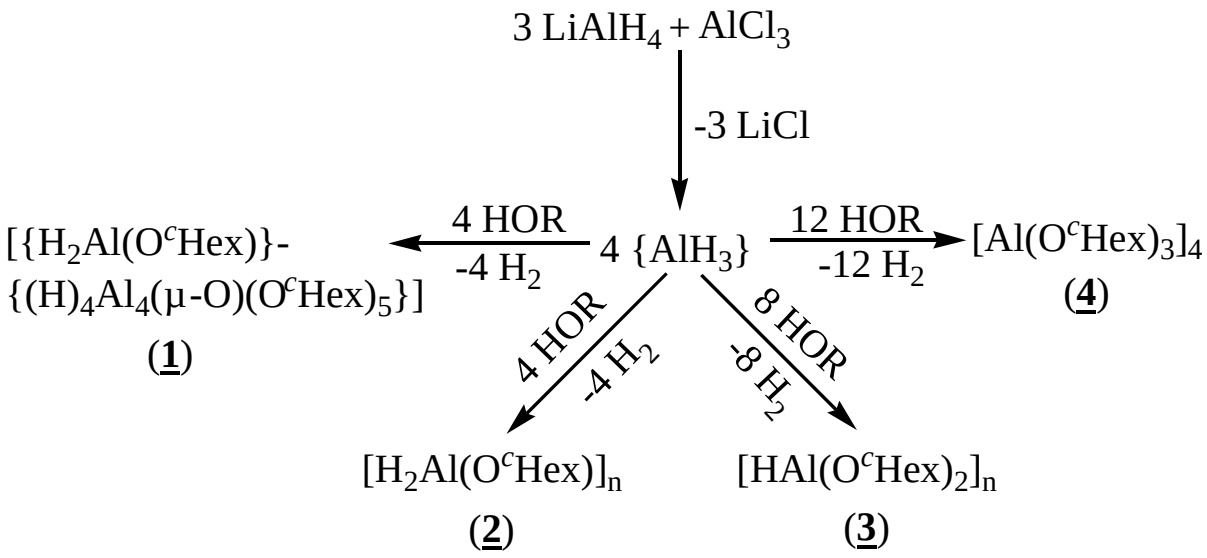

Scheme 1.2. Synthetic reactions for the preparation of compounds **1**-**4**

1.2. Spectroscopic Characterization

All the four compounds (**1**-**4**) have been characterized by ^{1}H, ^{13}C NMR and IR spectroscopy as well. In the ^{1}H-NMR spectrum of compound **1**, a broad peak at 4.53 ppm has been obtained which is the characteristic peak of hydrido ligands at Al centre [28, 79]. The peak broadened due to the influence of the high quadruple moment of Al centre. This peak could be due to the aluminium dihydride since it is difficult to see the peak for aluminium monohydride due to extraordinary broadness of the peak for monohydrides. A multiplet with a centre at 3.97 ppm has been observed which is due to the proton attached to α-carbon of the cyclohexyl ring. Multiple peaks in the range of 1.04 ppm to 2.34 ppm have been observed for the $-CH_2-$ protons of the cyclohexyl ring. As the chemical environments of these protons are nearly identical, therefore, it is quite difficult to resolve these peaks into individual peaks. ^{13}C-NMR spectroscopy gives peaks for all the carbons of the ring. ^{27}Al-NMR spectrum gives a broad peak spread over a large scale that is 0 ppm to 200 ppm with a maximum at around 40 ppm. It seems that the Al peaks of the compound strongly overlap with the Al peak of the sample holder. The IR spectrum of compound **1** gives characteristic peak of the Al–H stretching vibration. The peak is relatively broad and has a shoulder which indicates that there are two different types of hydrides. The minimum transition of the peak is found at 1816 cm^{-1} and lies well in the Al–H stretching vibration range [28, 79-80].

The ^{1}H-NMR spectrum of compound **2** shows peaks at 4.51 ppm and 4.32 ppm for the hydrogen atoms attached to the Al centre and the values lie well in the typical range [28, 79]. The integral ratio of the two different peaks appeared at 4.51 ppm and 4.32 ppm is 2:1, respectively. A multiplet with the centre at 3.98 ppm has been observed for the proton attached to α-carbon which is in accordance with that of compound **1**. Poorly resolved peaks can be seen in the range of 1.03-2.39 ppm. These peaks are due to the $-CH_2-$ protons of the cyclohexyl ring. The chemical environments of these protons are not too much different. Therefore, the peaks are difficult to be resolved into clear and individual peaks for each $-CH_2-$ group. ^{13}C-NMR spectroscopy gives four peaks for the four chemically different carbons at 73.91, 35.44, 25.20 and 24.73 ppm. This indicates that the organic moieties are identical.

The IR spectrum shows two different peaks for Al–H stretching vibration, a sharp peak at 1852 cm^{-1} and a relatively broad peak at 1830 cm^{-1}. It is noteworthy that the IR spectra were measured in the solid state. These peaks disappeared after exposure of the powder to air for 10 minutes and the compound decomposed. The ^{27}Al solution NMR spectrum in benzene did not show any peak, which may be due to the unsymmetrical Al centres. This indicates that the molecules are associated through certain bindings in solution and makes the Al centres unsymmetrical. Normally, the dihydridoaluminium alkoxides exists as dimers in solution and gives characteristic peaks for tetra-coordinated Al centres in ^{27}Al NMR spectra [80]. The absence of peaks in ^{27}Al NMR spectrum for compound **2** indicates that the Al centres are unsymmetrical and of some other coordination numbers instead 4. However, the solid state ^{27}Al-NMR spectrum gives very clear and distinct peaks at 96.05 and 1.18 ppm for coordination numbers 5 [80] and 6 [140-141], respectively (Figure 1.9). These observations indicate that there are two different Al centres having different coordination numbers. Roughly speaking the ratio between the peaks for coordination number 5 and 6 is 2:1. The peaks are not extraordinarily broad indicating that the Al centres are coordinated fairly symmetrical in the solid state. The results obtained from ^{1}H, ^{13}C, ^{27}Al solution as well as solid state NMR and IR spectroscopy is in good agreement with each other. It means that the bulk of cyclohexyl group is not sufficient to stop the intermolecular association in solid as well as in solution. The appearance of two different types of hydride ligands as well as Al centres concluded from ^{1}H and ^{27}Al NMR coupled with IR spectroscopy reveals that the compound exists as dimers which are associated through hydrogen bridging. The dimers and their

association via hydrogen bridging were confirmed by single crystal analysis (given in the coming section).

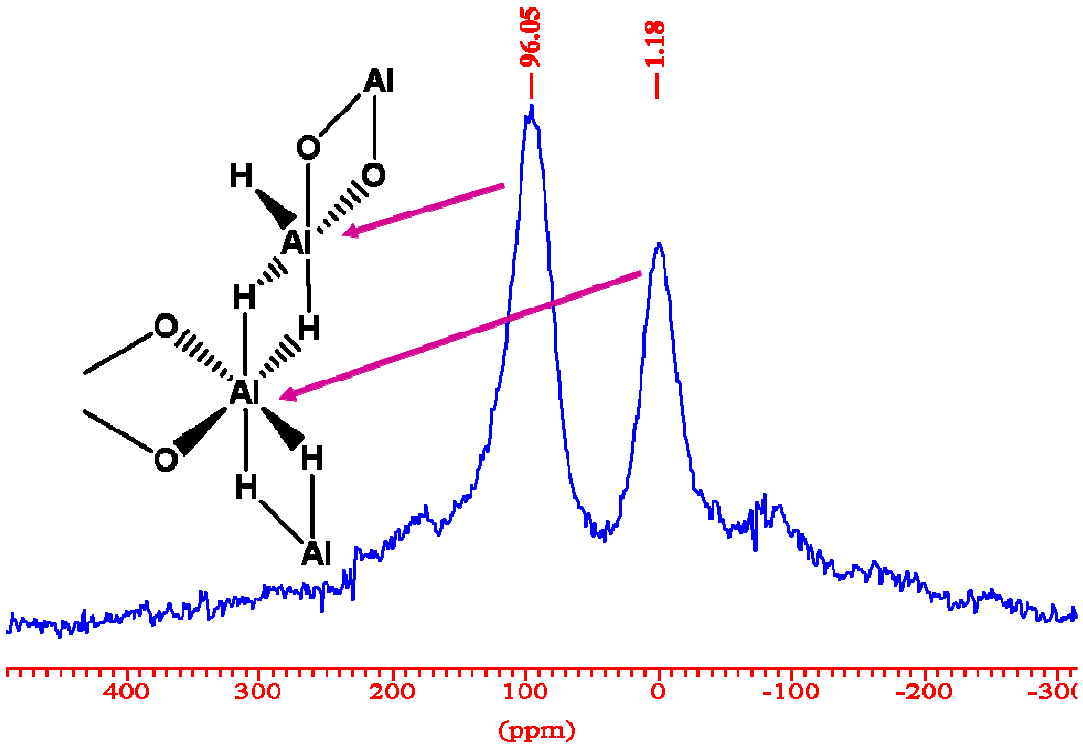

Figure 1.9. Solid state ^{27}Al-NMR spectrum of $[H_2Al(O^cHex)]_n$ **2**

Different spectroscopic techniques have been used for characterization of compound **3** which includes ^{1}H, ^{13}C, ^{27}Al (solution and solid state) and IR spectroscopy. The ^{1}H-NMR spectrum gives two different multiplets at 4.20 and 4.08 ppm for the proton attached to the α-carbon. Two signal sets typical for the cyclohexyl ring have been obtained in the range of 1.01-2.52 ppm, which indicates that there are two chemically different cyclohexyl rings. This was further confirmed by ^{13}C-NMR spectroscopy where paired peaks have been noticed for all four chemically different carbon atoms of the cyclohexyl ring. The α-carbon gives a pair of peaks at 73.95 ppm and 69.66 ppm which could be assigned to the bridging and terminal organic moieties, respectively. The former peak is closely related to the bridging organic moiety for compound **2**. The solution ^{27}Al-NMR spectrum measured in different solvents (for example diethylether, benzene) gives a sharp peak at 4.88 ppm (Figure 1.10). A very broad peak in the range of 180-15 ppm has been observed which is due to the Al present in the

sample holder. It is difficult to see any sort of other peaks in this region since the peak due to the Al present in the sample holder strongly overlaps. However, the solid state ^{27}Al-NMR spectrum gives two peaks: a broad peak at about 100.73 ppm and a narrow peak at 0.012 ppm (Figure 10 inset). These peaks match well to those obtained for compound **2** measured in the solid state, which are distinctive peaks for the penta- and hexa-coordinated Al centres reported earlier [140-141]. Therefore, it is clear that compound **3** has also two different Al centres with coordination numbers 5 and 6. IR spectroscopy gives a relatively broad peak at 1839cm^{-1} which lies in the characteristic range of Al–H stretching vibrations. Normally the Al–H stretching vibration peak in monoalkoxyalanes appears at higher values in comparison to the dialkoxyalanes. It is due to the incorporation of -I electron withdrawing oxygen for hydrogen and it increase the ionic character of Al-H bond and thus its strength. However, in case of compound **3** the situation is reversed which indicates that the hydrogen is bridged between two Al centres making the Al-H bond less strong. The bridging of hydrogen between the two Al centres could be deduced from the broadness of the peak which for terminal hydrido ligands is sharp and intense.

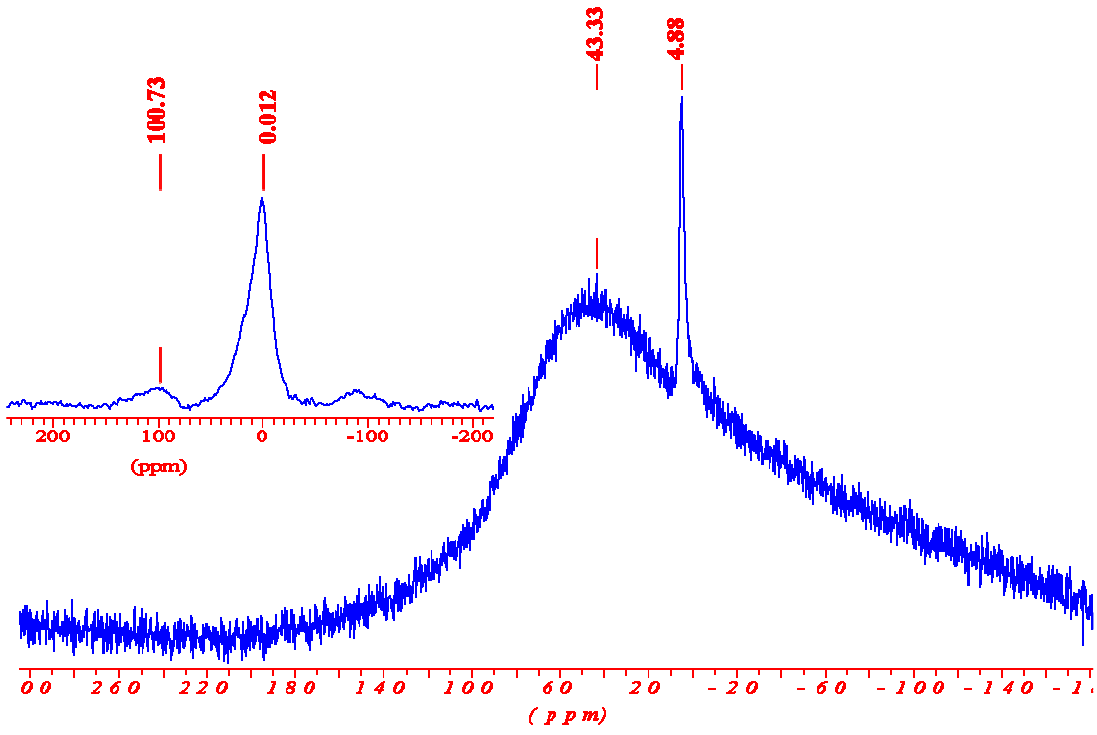

Figure 1.10. Solution ^{27}Al-NMR spectrum of $[HAl(O^cHex)_2]_n$ **3** (The broad peak is due to sample probe); inset is the Solid state ^{27}Al-NMR spectrum

The ^{1}H-NMR spectrum of compound **4** gives a broad multiplet at 4.10 ppm due to the resonance of the protons attached to the α-carbon of the alkyl group. Very clear peaks for the protons of the β-carbon atoms at 2.52 and 2.10 ppm have been observed, which indicates that there are two different alkyl groups in the molecule. Multiple peaks appeared in the range of 1.10 ppm to 1.82 ppm for the rest of the $–CH_2$- protons of the cyclohexyl ring. The organic moieties have also been confirmed by the ^{13}C-NMR spectrum, in which a pair of peaks could be seen for each carbon of the cyclohexyl ring. The ratios of peaks are nearly 1:1 which is in accordance with the terminal and bridging carbons being equal in numbers. The ^{27}Al-NMR spectrum recorded in deuterated benzene is highly related to the one reported by Kriz *et. al.* in 1984 for the same compound [142]. However, they did not report the single crystal structure of this compound. The clear and distinct peak appeared at $\partial(^{27}Al)$ = 4.10 ppm is characteristic of the Al centre having coordination number six [142]. While the peak at 59.30 ppm (Figure 1.11) appeared as a shoulder at the Al peak of the sample holder corresponds to the tetra-coordinated Al centres having tetrahedral chemical environment which is composed of oxygen atoms in this case [143]. The organic moieties were also confirmed by IR spectroscopy where all the corresponding vibrations have been observed in the IR spectrum of compound **4**.

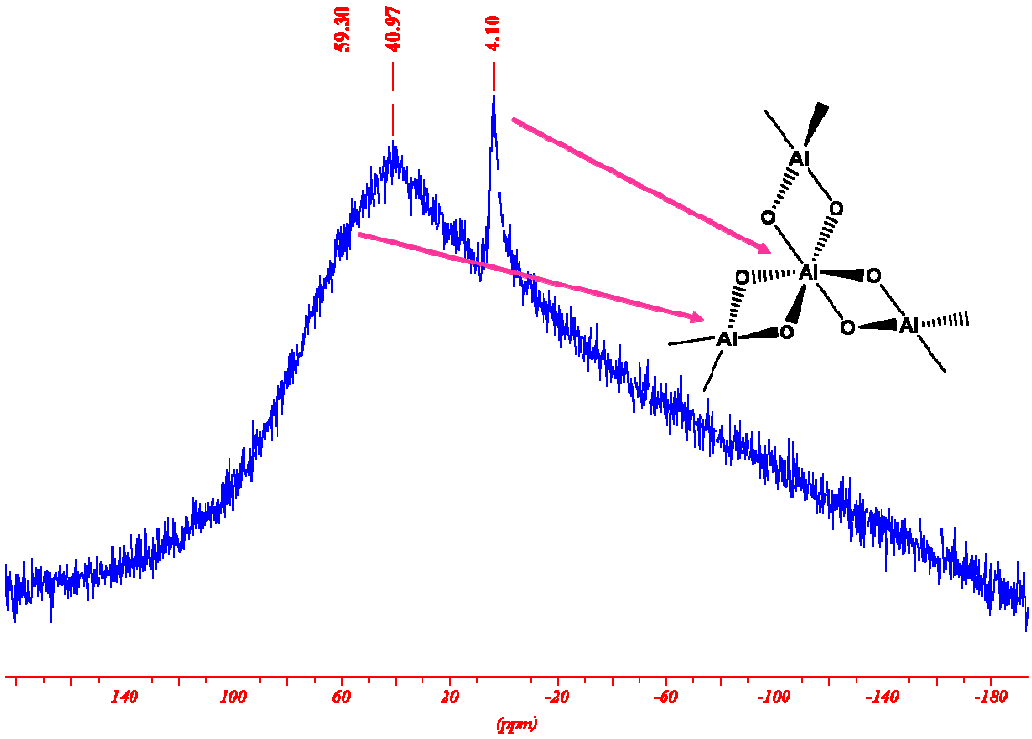

Figure 1.11. Solution ^{27}Al-NMR of compound $[Al(O^{c}Hex)_3]_4$ **4**. The broad peak is due to sample probe

1.3. Solid State Structures

Colourless crystals of compound $[(HAl)_4(H_2Al)O(O^cHex)_7]$ **1** were grown at +4°C in refrigerator. A suitable single crystal was selected and measured by single crystal X-ray diffraction analysis at 153 K temperature. The crystal structure resolved from the collected data belongs to the monoclinic crystal system and possesses $P2_1/m$ space group. The crystal lattice of compound **1** also contains a solvent molecule (diethyl ether). The molecule possesses a plane of symmetry defined by the atoms Al1-Al3-Al4 and thus having point symmetry C_s. The crystal data are organized in Table 1 and the pertinent bond lengths and angles are presented in Table 2. The molecular structure (Figure 1.12) of **1** shows a cluster arrangement of five Al atoms bridged by the oxygen atoms of the alkoxygroups. Four of the five Al atoms share a common oxo-group lacking any organic substituent. Therefore, we can observe five Al_2O_2 four membered rings with one common corner occupied by the naked oxygen atom. The structure of **1** also gives six and eight membered rings composed of alternative Al and oxygen atoms. There are two different types of Al atoms based upon the coordination numbers. Four of the five Al atoms (that is Al1, Al2, Al2(a) and Al3) have coordination number 5 and one of the five Al atoms (that is Al4) has coordination number 4. Each of the former is attached to four oxygen atoms making the bridges between the Al centres, and one terminal hydrogen atom. These Al atoms show pseudo trigonal bipyramidal geometry where the bond angles have a high degree of distortion. The fifth Al atom having coordination number 4 is attached to two bridging oxygen and two terminal hydrogen atoms forming a distorted tetrahedral surrounding. The Al–O bond lengths for penta-coordinated Al centres are larger than the tetra-coordinated Al centre as expected. However, they fit well into the range for Al–O bond lengths according to the reported literature for such type of compounds [28, 80]. The average Al-O bond length of the penta-coordinated Al centres and the central oxo-group is 1.914(1)Å. While the average Al to the bridging oxygen atoms bond length is 1.851(1)Å. The Al-H bond length lies well in its peculiar range and the average bond length is 1.538(1)Å [28, 80]. The central oxygen surrounded by four Al atoms has highly distorted tetrahedral geometry with one of the angle composed by Al2–O1–Al2 is as larg as 153.728(2)°. However, all other angles formed by Al–O–Al are below 100°. The rest of the bridging oxygen atoms have trigonal planar geometry deduced from the sum of angles around them which is in between 355°-359° [28, 80]. The Al–O–Al bond angles in the Al_2O_2 four membered rings are the most characteristic ones and the angles lie between 102-103° [28, 80]. However, the Al–O–Al angle in the six membered ring is quite large reaching a value of

117.517(2)°. The acute angels lie around the Al atom in the Al_2O_2 four membered rings as expected with angles in between 78-80°. The O–Al–O angles in the six membered ring are 90.645(2)° and 104.966(1)° for the penta-coordinated and tetra-coordinated Al centres, respectively.

The structure of **1** indicates that it is an unusual compound and there is no such example in the published literature. However, a somewhat resembling compound containing four metals centres of which one is lithium has been reported [80]. The four metals centres share a common central hydrogen atom instead of oxygen which is observed in case of compound **1**.

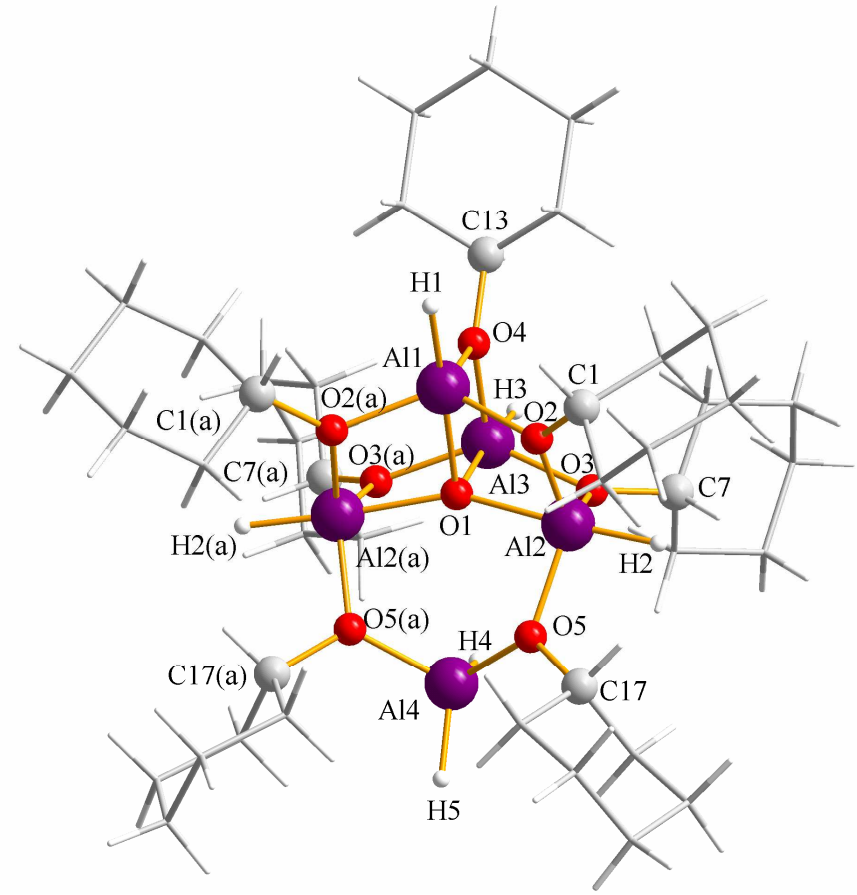

Figure 1.12. Molecular structure of **1** (The C and H atoms of the rings are shown as sticks for simplicity)

Table 1. Crystal Data of Compound **1**

Identification code	**[{$H_2Al(O^cHex)_2$}{$(H)_4Al_4(\mu$-O)$(O^cHex)_5$}]**
Empirical formula	C49 H91 Al5 O8
Formula weight	943.12
Temperature	153(2) K
Wavelength	0.71073 Å
Crystal system	Monoclinic
Space group	$P2_1/m$
Unit cell dimensions	a = 9.577(1) Å b = 20.956(2) Å c = 13.688(1) Å α= 90° β= 102.7120(10)° γ = 90°
Volume	2679.85(13) $Å^3$
Z	2
Density (calculated)	1.169 Mg/m^3
Absorption coefficient	0.151 mm^{-1}
F(000)	1028
Crystal size	0.38 x 0.22 x 0.08 mm^3
Theta range for data collection	1.53 to 26.37°.
Index ranges	-11<=h<=11, -17<=k<=26, -17<=l<=17
Reflections collected	21982
Independent reflections	5624 [R(int) = 0.0477]
Completeness to theta = 26.37°	99.9 %
Absorption correction	Multiscan
Max. and min. transmission	0.9874 and 0.9448
Refinement method	Full-matrix least-squares on F^2
Data / restraints / parameters	5624 / 0 / 297
Goodness-of-fit on F^2	1.015
Final R indices [I>2sigma(I)]	R1 = 0.0571, wR2 = 0.1466
R indices (all data)	R1 = 0.0829, wR2 = 0.1636
Largest diff. peak and hole	1.182 and -0.760 $e.Å^{-3}$

Table 2. Bond Angles and Lengths of Compound **1**

Bond	Length (Å)	Bond	Angle (°)	Bond	Angle (°)
Al(1)-O(2)	1.845(2)	O(2)a-Al(1)-O(2)	125.8(1)	Al(2)a-O(1)-Al(2)	153.7(1)
Al(1)-O(4)	1.856(0)	O(2)a-Al(1)-O(4)	110.7(1)	Al(2)a-O(1)-Al(3)	99.7(8)
Al(1)-O(1)	1.959(3)	O(2)-Al(1)-O(4)	110.7(1)	Al(2)-O(1)-Al(3)	99.7(8)
Al(2)-O(3)	1.850(1)	O(2)a-Al(1)-O(1)	77.6(2)	Al(2)a-O(1)-Al(1)	97.5(8)
Al(2)-O(5)	1.859(2)	O(2)-Al(1)-O(1)	77.6(2)	Al(2)-O(1)-Al(1)	97.5(8)
Al(2)-O(2)	1.863(2)	O(4)-Al(1)-O(1)	78.9(2)	Al(3)-O(1)-Al(1)	97.8(1)
Al(2)-O(1)	1.895(5)	O(3)-Al(2)-O(5)	120.3(0)	C(1)-O(2)-Al(1)	126.0(1)
Al(3)-O(4)	1.861(3)	O(3)-Al(2)-O(2)	117.7(0)	C(1)-O(2)-Al(2)	130.4(1)
Al(3)-O(3)	1.861(2)	O(5)-Al(2)-O(2)	117.0(4)	Al(1)-O(2)-Al(2)	102.8(1)
Al(3)-O(1)	1.905(3)	O(3)-Al(2)-O(1)	78.1(0)	C(7)-O(3)-Al(2)	125.9(2)
Al(4)-O(5)	1.823(2)	O(5)-Al(2)-O(1)	90.7(0)	C(7)-O(3)-Al(3)	130.5(4)
Al(1)-H(1)	1.557(0)	O(2)-Al(2)-O(1)	78.8(2)	Al(2)-O(3)-Al(3)	103.0(9)
Al(2)-H(2)	1.503(0)	O(4)-Al(3)-O(3)a	105.3(0)	C(13)-O(4)-Al(1)	131.9(2)
Al(3)-H(3)	1.622(0)	O(4)-Al(3)-O(3)	105.3(0)	C(13)-O(4)-Al(3)	124.9(2)
Al(4)-H(4)	1.523(0)	O(3)a-Al(3)-O(3)	136.3(3)	Al(1)-O(4)-Al(3)	103.1(1)
Al(4)-H(5)	1.521(0)	O(4)-Al(3)-O(1)	80.2(0)	C(17)-O(5)-Al(4)	123.6(1)
		O(3)a-Al(3)-O(1)	77.7(0)	C(17)-O(5)-Al(2)	117.5(1)
		O(3)-Al(3)-O(1)	77.7()	Al(4)-O(5)-Al(2)	117.5(0)
		O(5)-Al(4)-O(5)a	104.9(0)	O(2)-C(1)-C(6)	110.1(2)

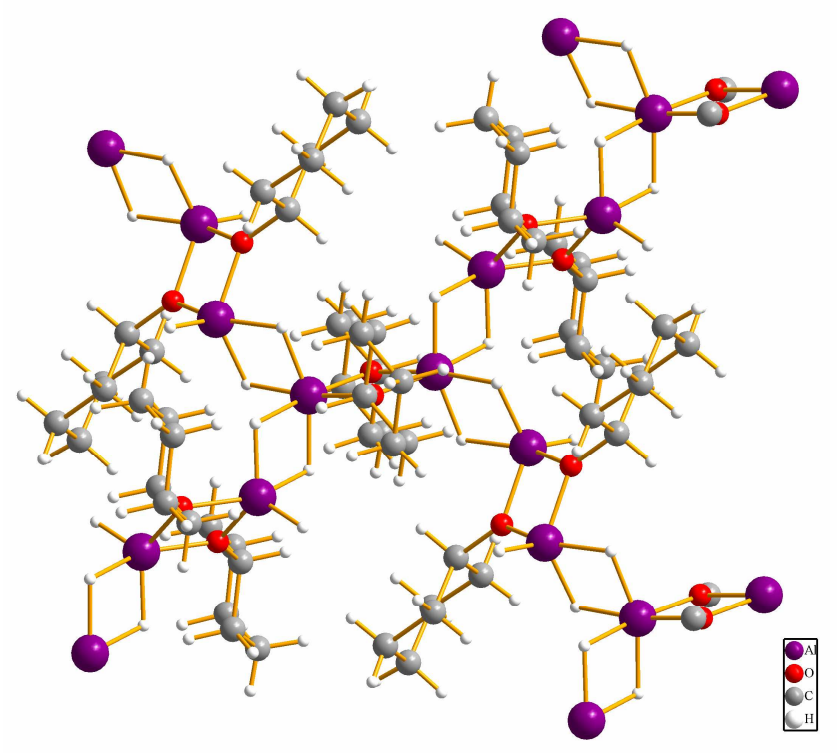

Figure 1.13. Molecular structure of compound **2**

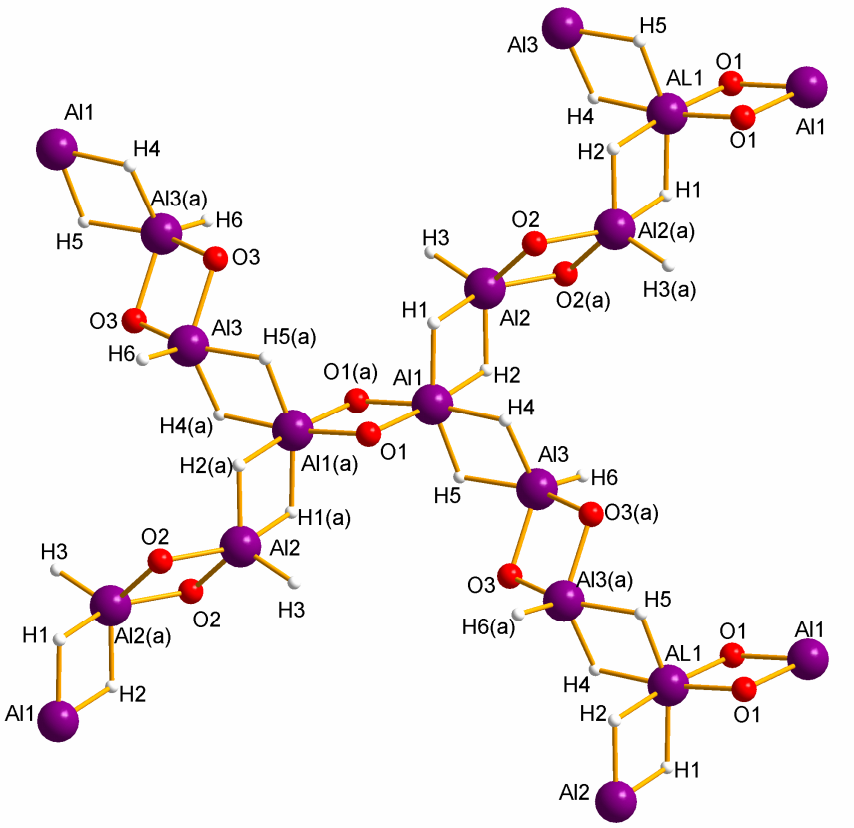

Figure 1.14. Molecular structure of compound **2**. Organic moieties are removed for clarity

The molecular structure of the compound $[H_2Al(OcHex)]_n$ **2** is depicted in Figure 1.13. In Figure 1.14, the molecular structure of **2** is presented without the organic moieties to see more clearly into its structural features. The crystal data are arranged in Table 3 and the pertinent bond lengths and angles are compiled in Table 4. The single crystal X-ray diffraction gives a two dimensional polymeric network like structure of **2**. The network is formed of Al_2O_2 four membered cyclic rings associated through hydrogen bridges. Each dimeric ring is centrosymmetric having point symmetry C_i. The rings can be arbitrarily classified into two different types based upon the coordination numbers of the Al atoms. Those having Al atoms of coordination number 6 and those having Al atoms of coordination number 5. The ratio between the Al atoms of coordination number 6 and 5 is 1:4 which is deduced from the molecular structure of the compound. Therefore, the ratio between the rings composed of Al atoms having coordination number 6 and 5 is also 1:4. Each dimer is formed of two $H_2Al(O^cHex)$ monomeric units bridged together through oxygen of the alkoxy group. The structure resembles *iso*-propoxyalane [80] where association of dimers through hydrogen bridges have been reported. The similarities in structures of *iso*-propoxyalane and cyclohexoxyalane, compound **2**, could be attributed to the nearly same steric bulk of the two organic moieties that is *iso*-propyl and cyclohexyl. Each of the Al atoms having coordination number 6 has a highly distorted octahedral geometry while the penta-coordinated Al centre has pseudo-trigonal bipyramidal environment (Figure 1.15). The octahedron of the hexa-coordinated Al atoms is composed of four hydrogen atoms and two oxygen atoms; all are shared by two Al centres. On the other hand the trigonal bipyramidal geometry of the penta-coordinated Al atoms is formed of three hydrogen atoms and two oxygen atoms. All the atoms are shared by two Al centres except one of the hydrogen which exists as terminal group.

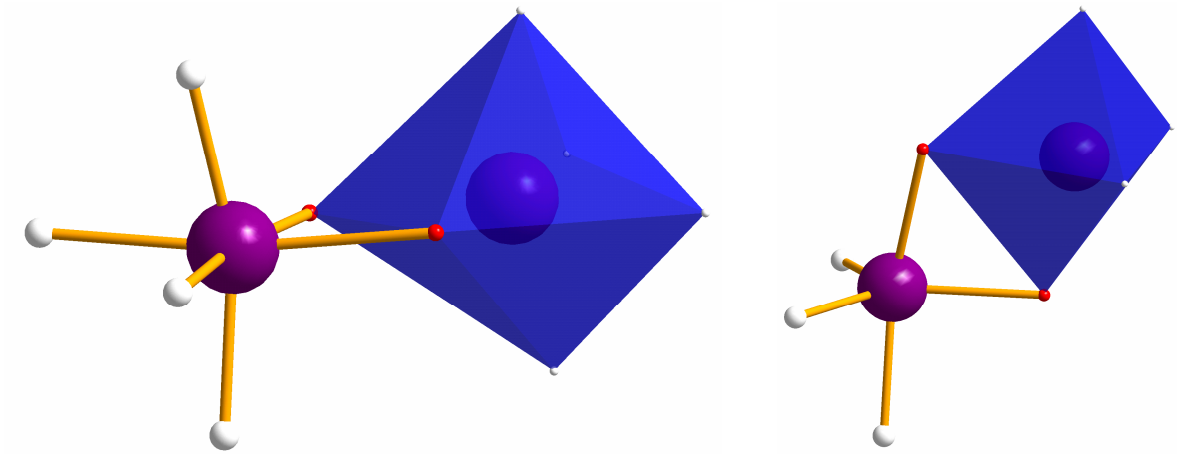

Figure 1.15. Al centres having octahedral (left) and trigonal bipyramidal geometry (right)

The Al–(μ-O) bond lengths are different for the crystallographically different dimeric units of the molecule. However, the difference is not too much significant. The average Al–(μ-O) bond length is 1.854(1)Å, which is in the characteristic range of Al_2O_2 cyclic compounds [28, 80]. The bond lengths of the Al–(μ-H) are larger by approximately 0.2-0.3 Å compared to the terminal Al–H bond lengths. The bridging hydride-aluminium bond lengths have an average value of 1.72(1)° while the average value for the terminal hydride-aluminium bond lengths is 1.51(1)°. The Al(μ-H)$_2$ bridging are sufficiently symmetrical, for example Al–(μ-H)$_1$ and Al–(μ-H)$_2$ has a difference of only 0.07Å which contrasts with the other hydride bridged species [128, 144-145] having highly unsymmetrical Al(μ-H)$_2$ bridging with varying distances in the range of 0.3-0.5Å.

The smallest angles formed by O-Al-O atoms within the Al_2O_2 rings are found at Al centre as expected having values ranging between 77.8-80.0° [28, 80]. In terms of the geometries, there are two different types of Al centres that is octahedral and trigonal bipyramidal. However, in terms of bond lengths and bond angles there are three different Al centres. Therefore, there are three different acute angles formed by O-Al-O atoms. The angle at Al_1 atom formed by O_1-Al_1-O_{1a} is 80.1(1)° which is larger than the angle at Al_2 (O_2-Al_2-O_{2a}) and Al_3 (O_3-Al_3-O_{3a}) having values 78.7(1)° and 77.8(1)°, respectively. However, in general very close to the O-Al-O angles reported earlier for the compounds having Al_2O_2 four membered rings [28, 80]. This difference in bond angles is due to the different geometries of the different Al centres. For example Al_1 has octahedral geometry while Al_2 and Al_3 have trigonal bipyramidal geometries

whose angle difference is also not very significant. The hexacoordinated aluminium centres features highly distorted octahedral geometry. The apexial bond angles formed by O-Al-H are larger than the bond angles formed by H-Al-H, although both have remarkable deviation from the ideal 180°. The square planar angles formed by O-Al-H are larger (>90°) than the angles formed by H-Al-H and again both have deviation from the ideal 90°. The deviation is due to the unequal groups forming the octahedron and the presence of bulky organic moiety upon the oxygen atoms. In the trigonal bipyramidal geometries around Al centres, two of the three hydrogen atoms occupy equatorial positions and the other one goes to the axial position. The O-Al-H apexial angle is distorted by ~25° from the normal 180°. The trigon of the bipyramidal structure is distorted and the O-Al-O angle is large than the H-Al-H angle. This is because of the unequal atoms surrounding Al centre and also the presence of bulky organic moiety over the oxygen atom. The sum of angle around the oxygen atoms is ~360° which gives that the oxygen atoms have trigonal planar environment as well as sp^2 hybridization [80, 146-147].

Table 3. Crystal Data of Compound $[H_2Al(O^cHex)]_n$ **2**

Identification code	**$[H_2Al(O^cHex)]_n$**
Empirical formula	C36 H78 Al6 O6
Formula weight	768.86
Temperature	132(2) K
Wavelength	0.71073 Å
Crystal system	Triclinic
Space group	P-1
Unit cell dimensions	a = 9.319(1) Å b = 9.917(2) Å c = 12.973(2) Å α= 107.451(1)°. β= 100.156(1)°. γ = 102.912(1)°.
Volume	1075.96(6) $Å^3$
Z	1
Density (calculated)	1.187 Mg/m^3
Absorption coefficient	0.189 mm^{-1}
F(000)	420

Crystal size	0.61 x 0.36 x 0.15 mm^3
Theta range for data collection	1.70 to 31.70°.
Index ranges	-13<=h<=13, -14<=k<=14, -19<=l<=19
Reflections collected	26488
Independent reflections	7242 [R(int) = 0.0216]
Completeness to theta = 31.70°	99.3 %
Absorption correction	Multiscan
Max. and min. transmission	0.9722 and 0.8937
Refinement method	Full-matrix least-squares on F^2
Data / restraints / parameters	7242 / 0 / 373
Goodness-of-fit on F^2	1.034
Final R indices [I>2sigma(I)]	R1 = 0.0318, wR2 = 0.0859
R indices (all data)	R1 = 0.0407, wR2 = 0.0912
Largest diff. peak and hole	0.432 and -0.376 e.$Å^{-3}$

Table 4. Bond Angles and Lengths for Compound $[H_2Al(O^cHex)]_n$ **2**

Bond	Length (Å)	Bond	Length (Å)	Bond	Angle (°)
Al(1)- O(1)	1.839(1)	Al(1)- H(2)	1.748(1)	O(1)-Al(1)-O(1)a	80.08(3)
Al(1)- O(1)a	1.868(2)	Al(1)- H(4)	1.776(2)	O(2)-Al(2)-O(2)a	78.71(4)
Al(2)- O(2)	1.819(1)	Al(1)- H(5)	1.661(2)	O(3)a-Al(3)-O(3)	77.79(3)
Al(2)- O(2)a	1.887(1)	Al(1)- H(3)	1.513(1)	Al(1)-O(1)-Al(1)a	99.92(3)
Al(3)- O(3)a	1.837(1)	Al(2)- H(1)	1.775(2)	Al(2)-O(2)-Al(2)a	101.29(4)
Al(3)- O(3)	1.871(1)	Al(2)- H(2)	1.650(0)	Al(3)a-O(3)-Al(3)	102.21(3)
O(1)- Al(1)a	1.868(2)	Al(3)- H(4)	1.680(0)	C(1)-O(1)-Al(1)	133.45(6)
O(2)- Al(2)a	1.887(1)	Al(3)- H(5)	1.769(0)	C(1)-O(1)-Al(1)a	123.94(5)
O(3)- Al(3)a	1.837(1)	Al(3)- H(6)	1.503(0)	C(7)-O(2)-Al(2)	127.18(6)
Al(1)- H(1)	1.681(2)			C(7)-O(2)-Al(2)a	131.53(6)
				C(13)-O(3)-Al(3)a	124.93(6)
				C(13)-O(3)-Al(3)	132.74(6)

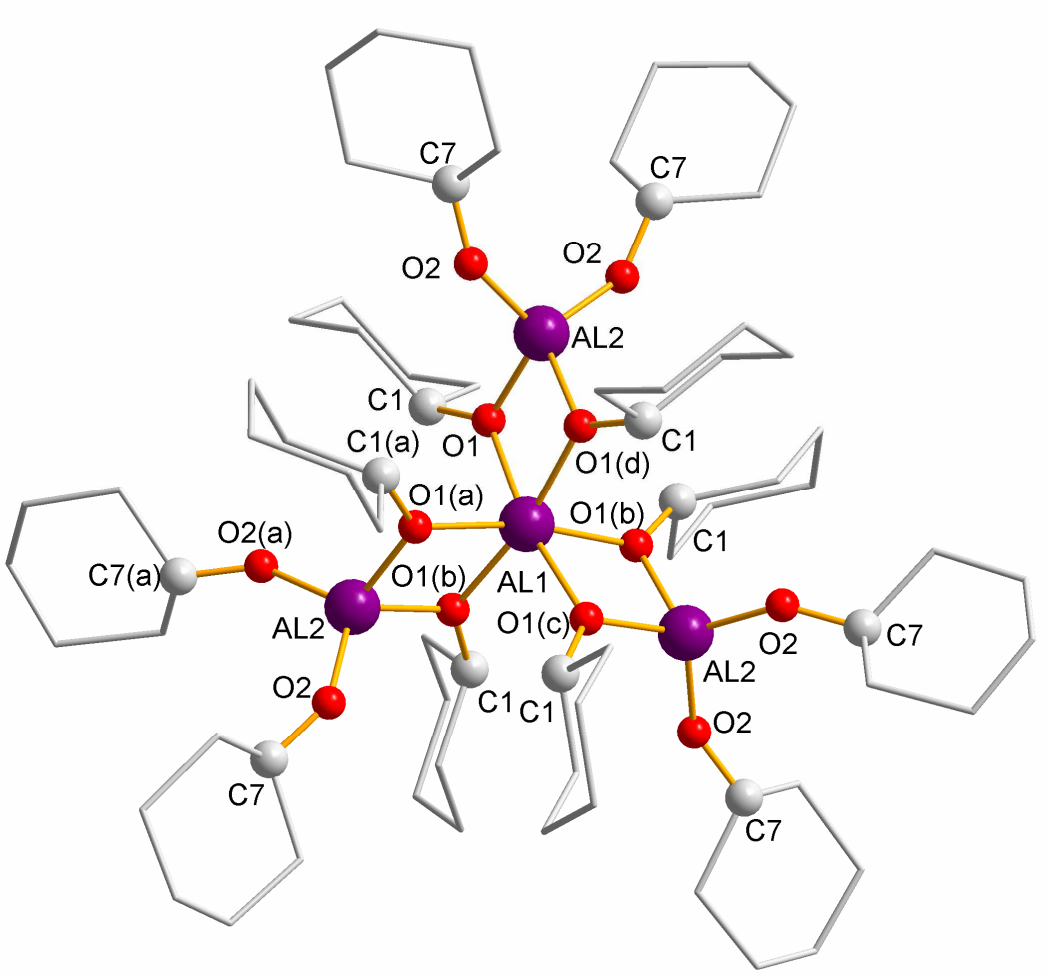

Figure 1.16. Molecular structure of $[Al(O^cHex)_3]_4$ **4**. The cyclohexyl rings are shown as sticks for clarity

Compound **4** has been predicted by Kriz *et. al*. in 1984 using ^{27}Al-NMR spectroscopy [142]. However, its single crystal structure was a mystery up till now. B. Neumüller has reported a trimer contrary to the predicted tetramer with the central Al atoms possessing trigonal bipyramidal geometry [143]. The two different structures obtained for one $[Al(O^cHex)_3]_n$ (n = 3 and/or 4) could be explained upon the interconversion phenomenon of trimer and tetramer reported for $[Al(O^iPr)_3]_4$ too (Scheme 1.3).

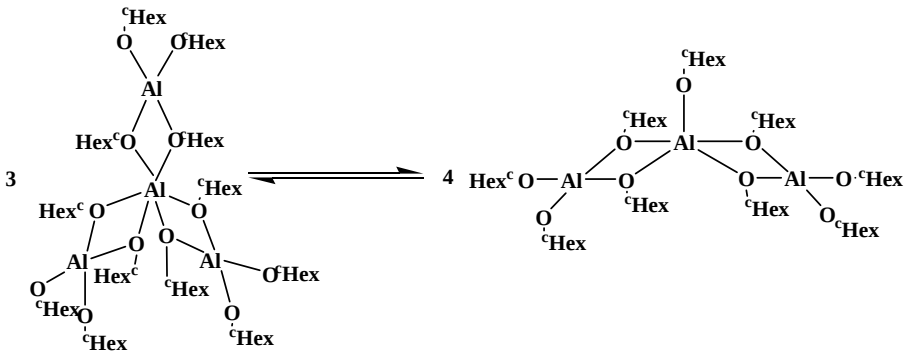

Scheme 1.3. Tetramer-Trimer interconversion equilibrium of $[Al(O^cHex)_3]_n$

The crystal data of **4** are presented in Table 5 while the most relevant bond lengths and angles are organized in Table 6. The crystal lattice of compound **4** possesses one solvent molecule (toluene) which is highly disordered. The structural features of compound **4** are quite similar as those of $[Al(OiPr)_3]_4$ [118-119], $[Al\{(\mu\text{-}OEt)_2AlMe_2\}_3]$, $[Al\{(\mu\text{-}OEt)_2GaMe_2\}_3]$ [125]. Compound **4** (Figure 1.16) is built up of three planar Al_2O_2 four membered rings. The molecular structure of **4** possesses three two fold axis of rotation C_2 passing through Al_1 having coordination number six and each Al_2 having coordination number four. There is another three fold axis of rotation C_3 perpendicular to the plane of the four Al atoms (Figure 1.17). It is the principal axis of rotation; therefore, the final point symmetry of the molecule is D_3.

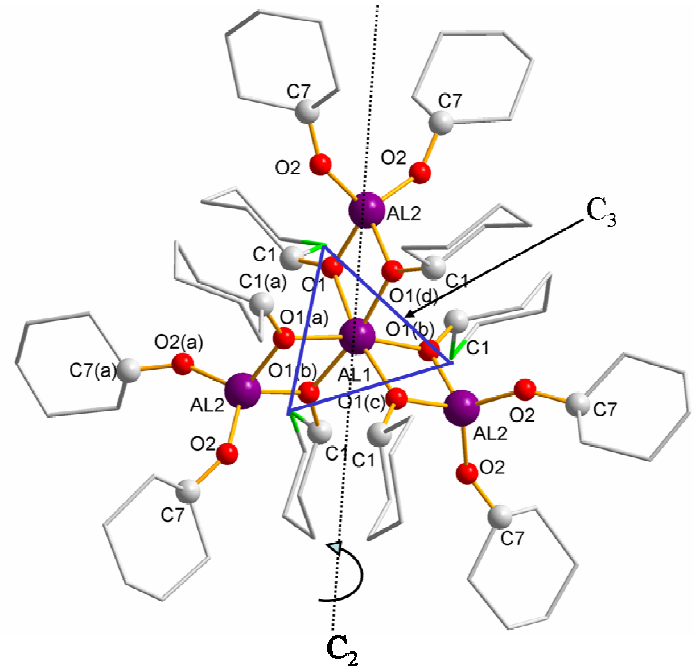

Figure 1.17. Projection of $[Al(O^cHex)_3]_4$ on metal atoms plane

The central aluminium atom is surrounded by three bidentate $[Al(^{c}Hex)_4]^{-1}$ units and gives octahedral geometry. The octahedron at the central aluminium atom is distorted from the ideal. However, it is highly symmetrical in terms of bond lengths and angles. All the Al-O bonds lengths in the octahedron are equal having value of 1.945(1)Å. It is in good agreement with the typical hexa-coordinated Al centres reported elsewhere for structurally similar compounds [119]. However, it is larger than the axial Al-O (1.905-1.898Å) bond lengths for penta-coordinated Al centre in trimeric *tri*-cyclohexoxyaluminum reported by B. Neumüller [143]. This slight increase in bond length of hexa-coordinated aluminium centre may be due to the increased coordination numbers. The axial bond angles in the distorted octahedron are all equal (169.407(1)°) although lower than the normal 180°. The square planar angles show also deviation from the normal 90°.

The three aluminium centres with coordination number four build almost ideal tetrahedra with two bridging and two terminal cyclohexoxy groups. In all the three tetrahedra, the Al-(μ-O) bond lengths are equal having value of 1.805(0) Å and is in good agreement with the Al–(μ-O) reported for Al_2O_2 four membered rings compound [28, 80, 126, 142, 148]. The equal bond lengths may correspond to the high symmetry possesses by the molecule. In the same fashion the aluminium to terminal oxygen bond lengths are equal (1.770(1) Å) but quite longer than those reported by B. Neumüller [143] for Al-O (1.702 Å) bonds. The tetrahedra are highly distorted due to the unequal cyclohexoxy groups since two of them are free as terminal groups and two are making bridges with the central hexa-coordinated aluminium centre. Overall the Al-O bond lengths follow the trend ^{4}Al-O < ^{4}Al–(μ-O) < ^{6}Al–(μ-O) which is same as for structurally similar compounds [119]. The superscript numbers indicates the coordination numbers at Al centres. The structure is similar to the one obtained for tris-(*iso*-propoxy)aluminium [119] and the $Al[(\mu\text{-}O)_2Al]_3$ core adopts a Mitsubishi motif, a term introduced by Caulton *et. al.* [119] and presented in Figure 1.18.

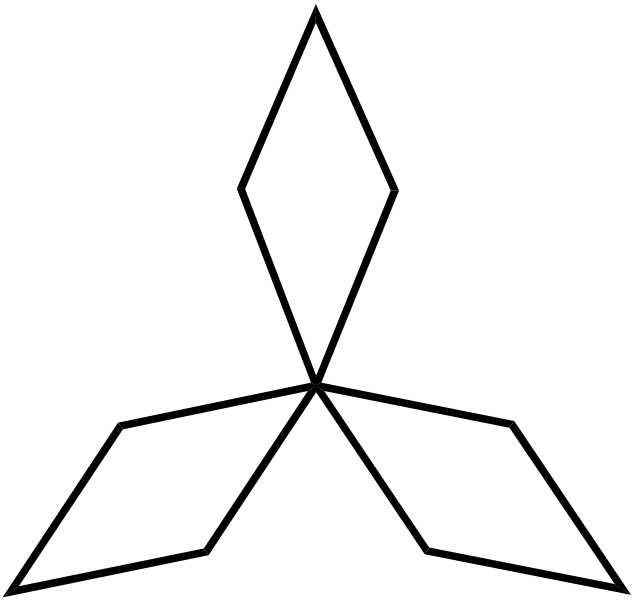

Figure 1.18. The $Al\{(\mu\text{-}O)_2Al\}_3$ core of compound **4** having Mitsubishi motif like structure

Table 5. Crystal Data of Compound **4**

Identification code	**$[Al(O^cHex)_3]_4$**
Empirical formula	C72 H132 Al4 O12
Formula weight	1297.70
Temperature	202(2) K
Wavelength	0.71073 Å
Crystal system	Rhombohedral
Space group	R-3c
Unit cell dimensions	a = b = 20.301(6) Å c = 40.431(1) Å α= β = 90° γ = 120°.
Volume	14430.4(7) $Å^3$
Z	6
Density (calculated)	0.896 Mg/m^3
Absorption coefficient	0.092 mm^{-1}
F(000)	4272

Crystal size	0.43 x 0.20 x 0.11 mm^3
Theta range for data collection	1.53 to 26.44°.
Index ranges	-25<=h<=24, -25<=k<=25, -50<=l<=50
Reflections collected	69371
Independent reflections	3313 [R(int) = 0.1247]
Completeness to theta = 15.04°	99.8 %
Absorption correction	Multiscan
Max. and min. transmission	0.9903 and 0.9613
Refinement method	Full-matrix least-squares on F^2
Data / restraints / parameters	3313 / 0 / 147
Goodness-of-fit on F^2	1.876
Final R indices [I>2sigma(I)]	R1 = 0.0851, wR2 = 0.2407
R indices (all data)	R1 = 0.1665, wR2 = 0.2620
Largest diff. peak and hole	0.934 and -0.326 e.$Å^{-3}$

Table 6. Bond Angles and Lengths for Compound **4**

Bond	Length (Å)	Bond	Length (Å)	Bond	Angle (°)
Al(1)- O(1)	1.917(9)	O(1)-Al(1)-O(1)b	96.0(3)	O(2)-Al(2)-O(1)a	117.8(4)
Al(1)- O(1)a	1.917(9)	O(1)-Al(1)-O(1)	168.7(5)	O(1)-Al(2)-O(1)d	82.4(7)
Al(2)- O(1)	1.794(9)	O(1)-Al(1)-O(1)c	76.1(5)	Al(1)-O(1)-Al(2)	100.8(5)
Al(2)- O(1)a	1.794(9)	O(1)-Al(1)-O(1)a	92.9(4)	C(1)-O(1)-Al(2)	126.1(7)
Al(2)- O(2)	1.759(2)	O(2)-Al(2)-O(2)a	116.2(9)	C(1)-O(1)-Al(1)	132.4(7)
Al(2)- O(2)a	1.759(2)	O(2)-Al(2)-O(1)b	109.2(4)	C(7)-O(2)-Al(2)	139.1(15)
O(1)- C(1)	1.448(3)				
O(2)- C(7)	1.190(2)				

2. $[H_nAl(O^cHex\mathit{Me}\text{-}1)_{3-n}]_2$ (n = 2 **5**, 1 **6**, 0 **7**)

2.1. Synthetic Aspects

The procedure for the synthesis of compounds **5**-**7** was adopted from an established route reported elsewhere [79]. The synthetic reaction procedures have been summarized in the

following scheme (Scheme 1.4). Stoichiometric amounts of $AlCl_3$ and $LiAlH_4$ dissolved in ether (under cooling in case of $AlCl_3$) were mixed together and stirred at room temperature for one hour. LiCl precipitated out as white residue suspended in the solution mixture. The required amounts of 1-*methylcyclo*hexanol (HOC_6H_{10}*Me*-1) were added into the above reaction mixture drop by drop and evolution of hydrogen was observed. The solid residue, LiCl salt was removed by filtration and filtrate was collected into a falsk. The volatiles, mostly the solvent in the resulting filtrate were removed under low pressure and condensed into a cooling trap. Compounds **5** and **7** were obtained as white powders, while compound **6** was a highly viscous colourless liquid. All the efforts for crystallization of **6** failed since it remained liquid in either case. However, **5** and **7** gave colourless crystals in refrigerator at +4°C after re-dissolving small amounts of their powders in 5 mL diethylether. All the three compounds are well soluble in common organic solvents, however react violently with water. Compound **7** is relatively stable in air though decompose upon longer exposure. Compounds **5** and **6** are highly air sensitive. The decomposition has been occurred of these two compounds as soon as exposed to air and a white smoke evolved from their reservoirs.

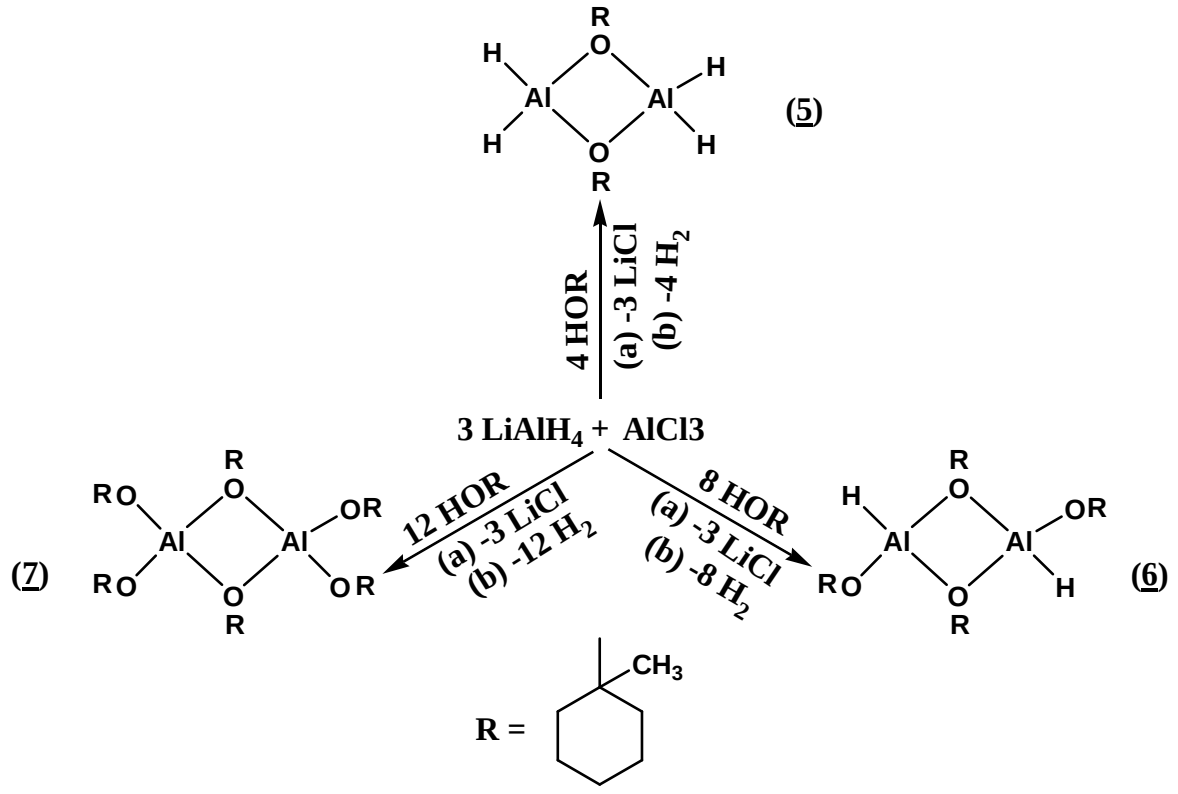

Scheme 1.4. Reaction scheme for the synthesis of **5**, **6** and **7**

2.2. Spectroscopic Characterization

Compounds **5**-**7** have been characterized by NMR and IR spectroscopy. NMR spectra were recorded in deutrated benzene and were referred to tetramethylsilane. ^{1}H-NMR spectrum of **5** gives a broad peak at 4.52 ppm in the peculiar range of protons attached to Al centre in alkoxyalanes [28, 80]. A sharp peak appeared at 1.34 ppm which is due to the methyl group and highly overlapping peaks have been obtained in the range of 1.09-1.74 ppm for the ring of the alkoxy group. ^{13}C-NMR gives peaks for all the five different types of carbons at 77.97 ppm, 39.05 ppm, 26.38 ppm, 24.62 ppm and 22.67 ppm. The Al centre is tetra-coordinated which has been confirmed by the ^{27}Al-NMR where two peaks have been appeared at 98.14 ppm and 48.79 ppm (Figure 1.19). The peak appearing at 48.79 ppm is due to the Al of the sample probe. While the peak appearing at 98.14 ppm is comparable to the tetra-coordinated Al centres in compounds of the type $[H_2Al(OR)]_2$ [80, 129].The IR spectrum of compound **5** gives a sharp peak at 1829cm^{-1} for Al–H stretching vibration [28, 80]. Besides this peak, the IR spectrum also gives peaks for the organic moiety of the compound.

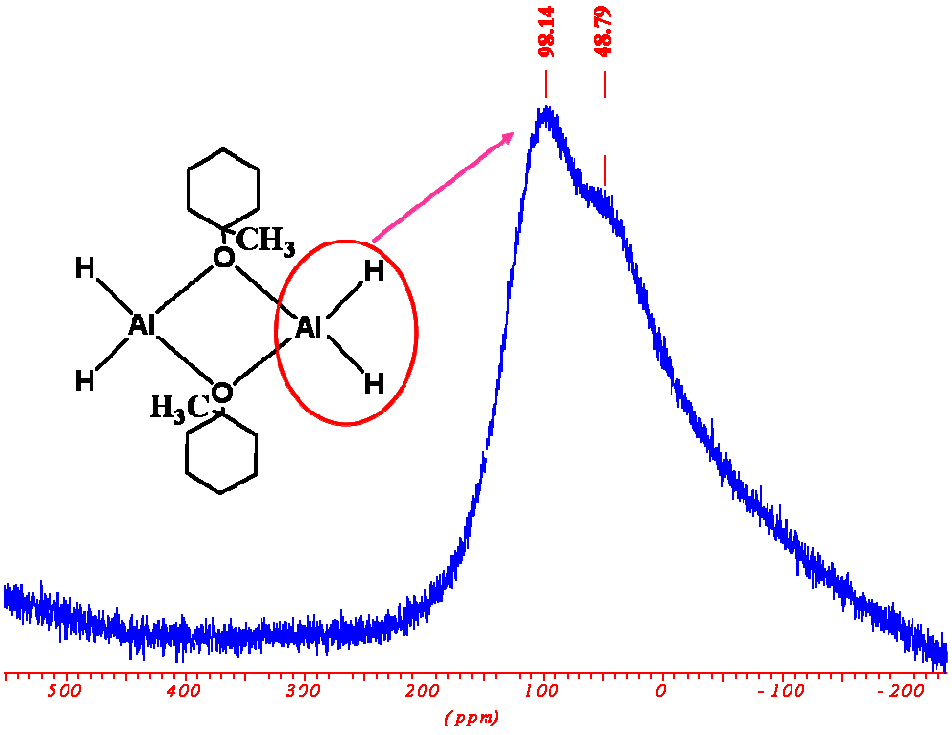

Figure 1.19. ^{27}Al-NMR spectrum of compound $[H_2Al(O^cHexMe\text{-}1)]$ **5**. The broad peak at 48.79 ppm is due to sample probe

Compound **6** has been obtained as viscous oil and therefore, we were unable to analyze its single crystal in solid state by X-ray diffraction. However, it was characterized using NMR and IR spectroscopy. ^{1}H-NMR spectrum gives a very broad peak at 4.10 ppm for the proton attached to the Al centre. Normally, due to the asymmetric Al centre, ^{1}H-NMR peak for this proton is very difficult to observe due to its extraordinary broadening, but for compound **6** it was made possible by adding a small amount of deutrated benzene into the already liquid compound. The peak is sufficiently broad which can be seen in ^{1}H-NMR spectrum given in Figure 1.20. Three different peaks for the methyl protons of 1-methylcyclohexyl moiety are obtained at 1.47 ppm, 1.32 ppm and 1.31 ppm. The first peak at 1.47 ppm is due to the bridging methyl protons while the last two peaks at 1.32 ppm and 1.31 ppm are for the terminal protons of *trans*- and *cis*-isomers, respectively. This indicates that the compound is dimer in solution possessing two different isomers that is *cis*- and *trans*-isomers. ^{13}C-NMR spectrum gives two peaks at 78.2 ppm and 70.0 ppm for bridging and terminal α-carbon of the organic moiety, respectively. In the same way paired peaks for bridging and terminal β-carbon appears at 40.08 ppm and 40.13 ppm, respectively. The peaks for bridging and terminal methyl carbon appear at 31.6 ppm and 30.8 ppm, respectively. It is noteworthy to point out that each peak has a parallel peak which could be due to the presence of two different types of isomers that is *trans*- and *cis*-isomer in solution for compound **6**.

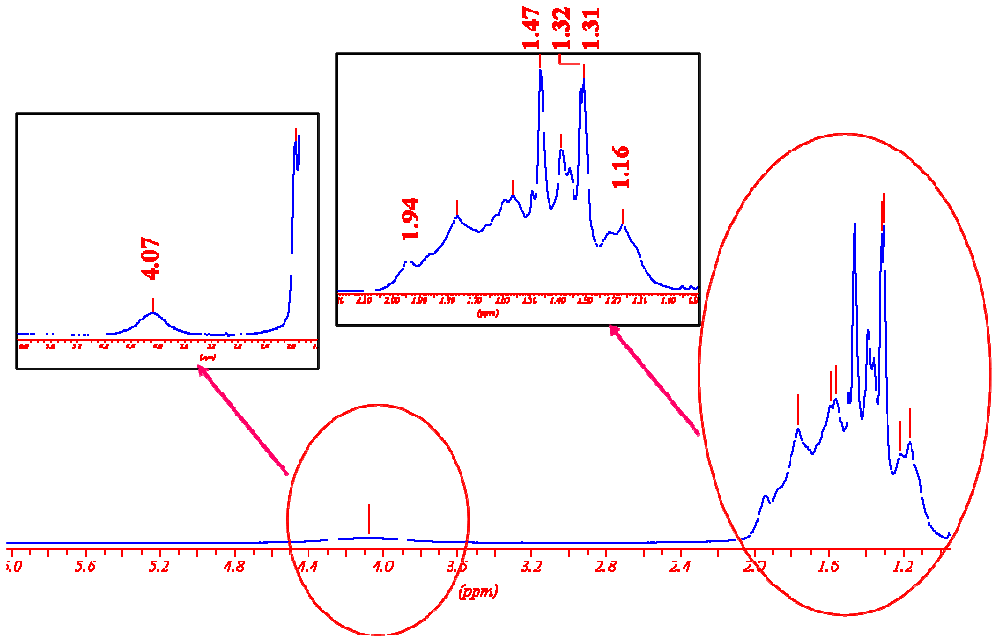

Figure 1.20. ^{1}H-NMR spectrum of **6**, inset is the enlarged parts of spectrum to show the peaks clearly

The ^{27}Al-NMR spectrum gives an irresoluble extra-broad peak with maxima at 41.18 ppm which is due to the Al present in the sample probe. The asymmetric nature of the compound is responsible for disappearance of the tetra-coordinated Al peak of the compound. However, a characteristic Al–H stretching vibration peak has been obtained in the IR spectrum of compound **6** at 1859cm^{-1}. This peak is highly comparable to reported compounds of this type [28, 129]. The IR spectra of compound **5** and **6** are presented in Figure 1.21 for comparison.

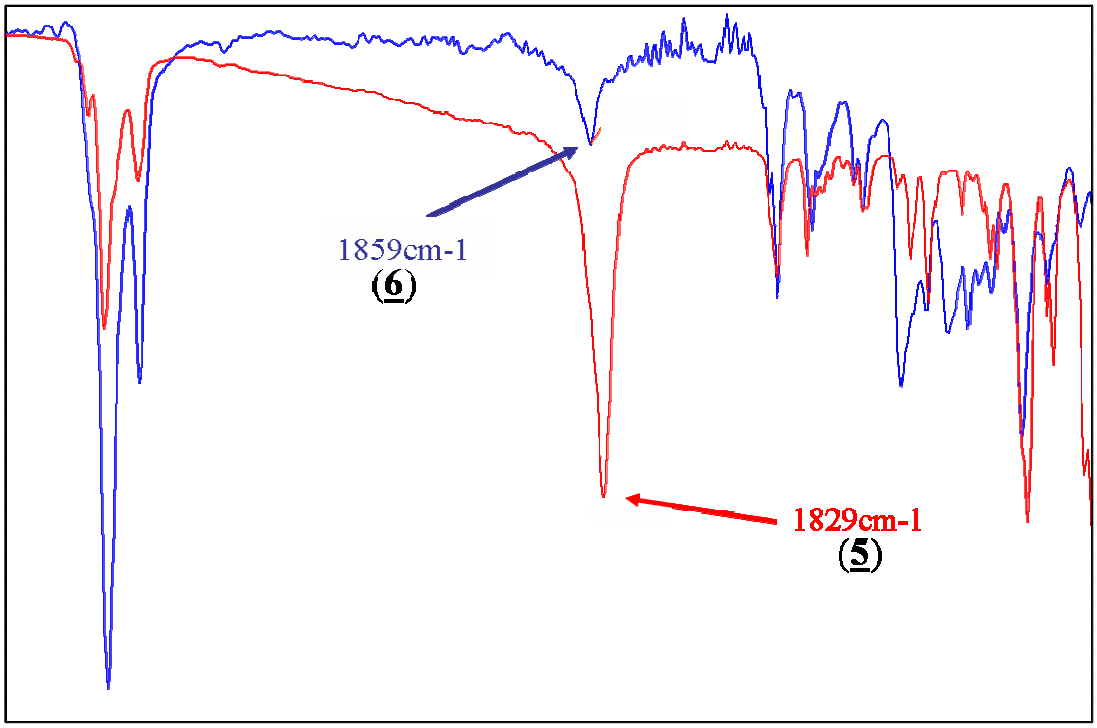

Figure 1.21. IR spectra of compounds **5** (red) and **6** (blue)

The Al-H stretching vibration peaks in the IR spectra of compound **5** (1829 cm^{-1}) and **6** (1859 cm^{-1}) are comparable to that observed for structurally identical compounds $[H_2Al(O^tBu)]_2$ (1845 cm^{-1}) and $[H_2Al(O^tBu)]_2$ (1859 cm^{-1}), respectively [28]. The results show that compound **6** has dimeric structure and exists as *cis*- and *trans*-isomer in solution (Figure 1.22).

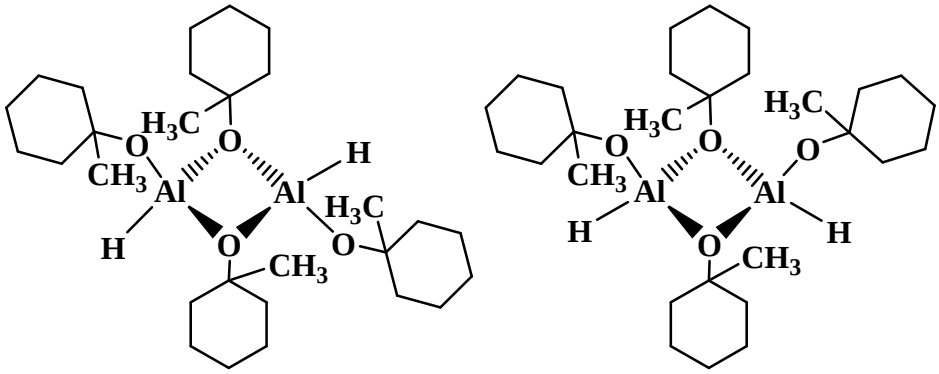

Figure 1.22. Proposed structures for *trans*- (left) and *cis*-isomer (right) of compound **6**

^{1}H-NMR spectrum of compound **7** gives two sharp peaks at 1.63 ppm and 1.51 ppm in 1:2 ratios (Figure 1.23). These peaks are due to the methyl protons of the organic moiety. The two different peaks for a single methyl group indicate that the compound is dimer in solution. The peak appeared at 1.63 ppm is due to bridging methyl protons while the one at 1.51 ppm is due to the terminal methyl protons. The peaks spread over a large δ-scale (1.47-2.19) are due to the $-CH_2-$ protons of the ring. The dimeric nature of **7** in solution was further confirmed by ^{13}C NMR spectroscopy (Figure 1.23-inset). The ^{13}C-NMR spectrum gives two well resolved peaks for the bridging and terminal α-carbon at 78.71 ppm and 70.07 ppm, respectively. The peak for the bridging α-carbon is approximately 8.6 ppm at lower field than that of terminal α-carbon. It is due to the larger deshielding of the bridging α-carbon as the electron withdrawing O-atom is coordinated by two Al centres. The same trend can be seen for the rest of the carbon of the organic moiety. In each pair of peaks for a particular carbon atom the one with higher value is for bridging carbon and the other with lower value is for the terminal carbon. The bridging carbons are experiencing more deshielding effect due to the coordination of electron withdrawing O atoms with two Al centres instead of one in case of terminal groups. Therefore, the peaks for bridging carbons appear at lower field than those for terminal carbons. The organic moieties of the compound have also been confirmed by IR spectroscopy. The spectrum recorded gives peaks for the C-H vibrations in the characteristic regions.

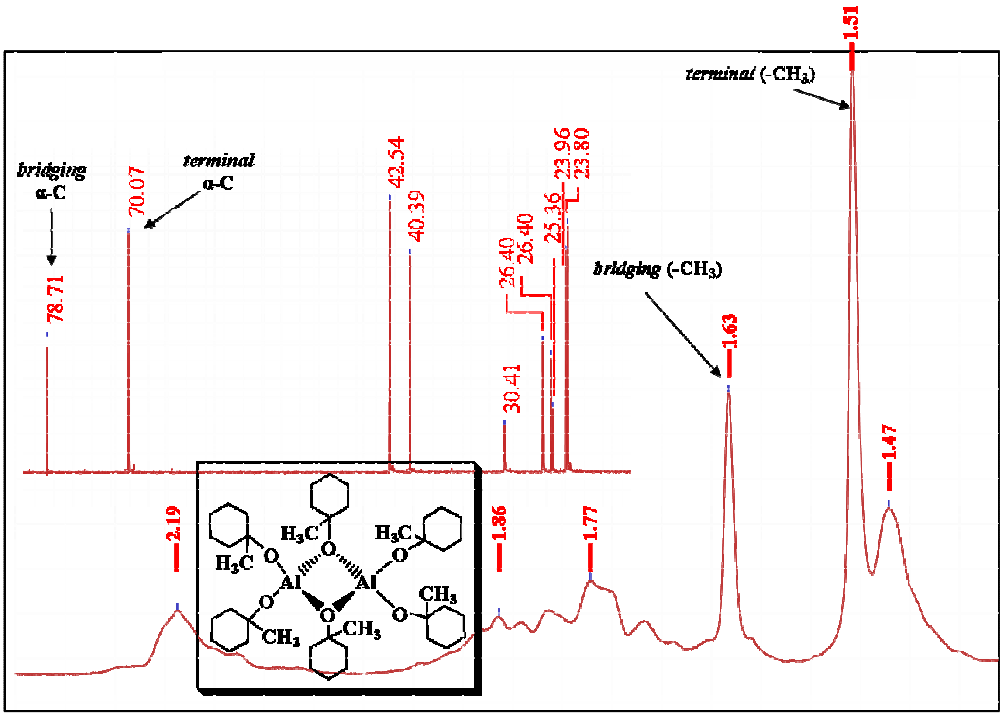

Figure 1.23. ^{1}H and ^{13}C-NMR (inset) spectra of the compound $[Al(O^{c}HexMe\text{-}1)_3]_2$ 7

From the spectroscopic data once can conclude that compound 7 is dimer in solution (Figure 1.24). The dimer is formed by the association of two $Al(O^{c}HexMe\text{-}1)_3$ monomers via oxygen of the 1-methylcyclohexoxy group.

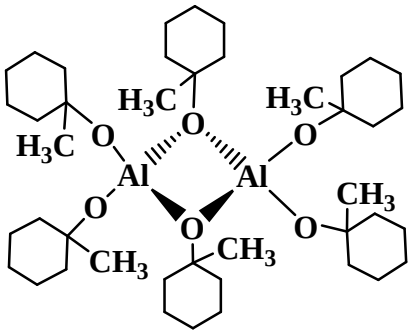

Figure 1.24. Proposed molecular structure of $[Al(O^{c}HexMe\text{-}1)_3]_2$ 7 in solution

2.3. Solid State Structures

Single crystals of compounds **5** and **7** were selected and analysed at 153 K. The structures of compounds **5** and **7** were solved by direct methods and refined with the full-matrix least squares on F^2 using SHELLX software package [149]. All the hydrogen atoms were generated geometrically and anisotropic thermal parameters were assigned to all other non-hydrogen atoms. The most relevant crystal data of compounds **5** and **7** are arranged in Table 7 and 9, respectively. The pertinent bond lengths and angles of compound **5** are summarized in Table 8 while that of compound **7** in Table 10.

The structure of **5** (Figer 1.25) is similar to that of *tert*-butoxyalane [28] and ^{t}Bu$_2$(Me)COAlH$_2$ [80] and the only difference to ^{t}Bu$_2$(H)COAlH$_2$ [129] is that this molecule is tetramer instead of dimer. The compound is a cyclic dimer with central four membered Al_2O_2 planar ring. The molecule of 5 is centrosymmetric possessing point symmetry C_i. Also the molecule possesses a two fold axis of rotation and a vertical mirror plane. The aluminium atoms are tetra-coordinated and having approximately tetrahedral geometry with some sort of distortion. The Al–O bond lengths are in good agreement with the reported compounds of identical structural features [27, 79] and those having an Al_2O_2 ring system [150-153]. The Al_1–(μ-O_1) and Al_1–(μ-$O_{1(a)}$) bond lengths are 1.831(1) Å and 1.835(2) Å, respectively. These bond lengths corresponds well to that of ^{t}BuOAlH$_2$ (1.815(3)Å and 1.810(3)Å) [28] and ^{t}Bu$_2$(Me)COAlH$_2$ (1.854(1) Å and 1.841(1)Å) [80]. The approximate Al-H bond lengths are 1.558(1) Å and 1.467(0) Å which fall well in the reported range [28, 80]. The Al atoms has an acute O-Al-O angle of 81.653(1)° which corresponds to 81.0(2)° for *tert*-butoxyalane [28] and 82.73(6)° for ^{t}Bu$_2$(Me)COAlH$_2$ [80]. The sum of angles around oxygen atoms is 355.51(1)° which suggests planar geometry as well as sp^2 hybridization for these atoms [80]. The organic moieties are uniformly distributed around the Al-O-Al bridges deduced from the nearly equal angles of C1-O1-Al1 and C1-O1-Al1(a).

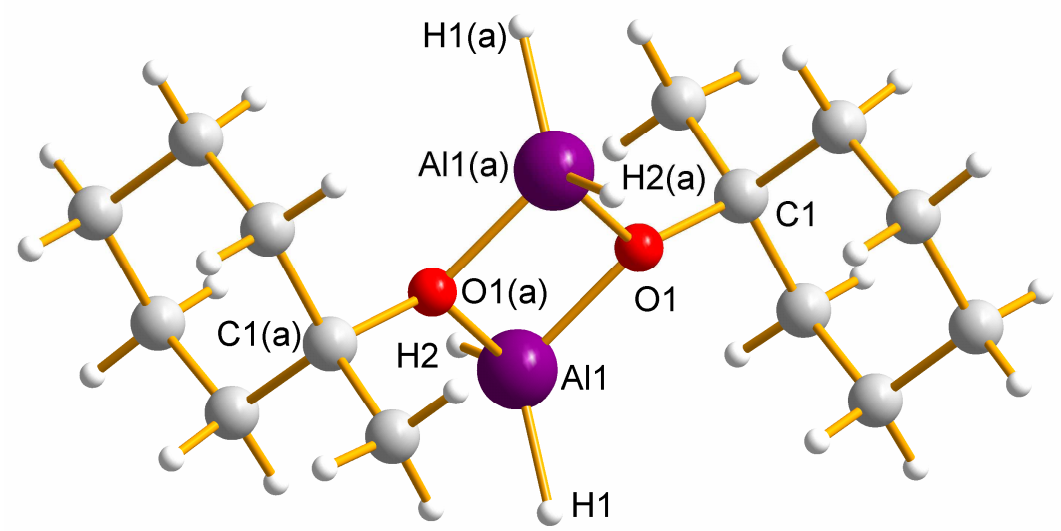

Figure 1.25. Molecular structure of compound $[H_2Al(O^cHexMe\text{-}1)]_2$ **5**

Table 7. Crystal data of compound **5**

Identification code	**$[H_2Al(O^cHexMe\text{-}1)]_2$**
Empirical formula	C14 H30 Al2 O2
Formula weight	284.34
Temperature	153(2) K
Wavelength	0.71073 Å
Crystal system	Orthorhombic
Space group	Pbca
Unit cell dimensions	a = 12.789(1) Å b = 8.451(2) Å c = 15.957(2) Å α = 90°. β = 90°. γ = 90°.
Volume	1724.48(14) $Å^3$
Z	4
Density (calculated)	1.095 Mg/m^3
Absorption coefficient	0.163 mm^{-1}
F(000)	624
Crystal size	0.46 x 0.23 x 0.15 mm^3
Theta range for data collection	2.55 to 31.89°.
Index ranges	-19<=h<=17, -12<=k<=12, -

	23<=l<=23
Reflections collected	37249
Independent reflections	2969 [R(int) = 0.0338]
Completeness to theta = 31.89°	99.9 %
Absorption correction	None
Max. and min. transmission	0.9763 and 0.9282
Refinement method	Full-matrix least-squares on F^2
Data / restraints / parameters	2969 / 0 / 142
Goodness-of-fit on F^2	1.050
Final R indices [I>2sigma(I)]	R1 = 0.0332, wR2 = 0.0930
R indices (all data)	R1 = 0.0454, wR2 = 0.1005
Largest diff. peak and hole	0.350 and -0.282 e.Å^{-3}

Table 8. Selected bond lengths and angles of compound **5**

Bond	Length (Å)	Bond	Angle (°)
Al(1)- O(1)a	1.831(1)	O(1)a-Al(1)-O(1)	81.65(3)
Al(1)- O(1)	1.835(2)	Al(1)a-O(1)-Al(1)	98.35(3)
Al(1)-Al(1)a	2.774(1)	C(1)-O(1)-Al(1)	127.74(5)
O(1)- C(1)	1.469(2)	C(1)-O(1)-Al(1)a	129.42(6)
Al(1)- H(1)	1.558(1)	H(1)-Al(1)-H(2)	116.46(2)
Al(1)- H(2)	1.467(0)	H(1)-Al(1)-O(1)	117.22(2)
		H(2)-Al(1)-O(1)	111.65(1)
		H(1)-Al(1)-O(1)a	111.00(1)
		H(2)-Al(1)-O(1)a	114.03(2)

Figure 1.26 gives the molecular structure of compound **7**. The relevant crystal data is presented in Table 9 and the important bond lengths and angles are summarized in Table 10. Compound **7** is similar in structural aspects as the reported $[Al(^tBu)_3]_2$ [104] and $Al2(NMe3)(^tBu)_5$ [154]. It is comprised of a central Al_2O_2 planar four membered ring. The molecule is centrosymmetric having point symmetry C_i ($\bar{1}$). Each Al centre is surrounded by four alkoxy groups in a pseudo-tetrahedral fashion. The Al–(μ-O) bond length is approximately 1.83(1)Å which is longer than the terminal Al–O bond lengths having average value of 1.68(1)Å. The terminal alkoxy groups lie nearly perpendicular to the central Al_2O_2

plane. The expected acute angle lies at Al centre having value of 81.540(8)°. The oxygen atoms have trigonal planar environment which is deduced from the sum of angles around it (359.91(1)°). It gives also that the oxygen atoms are sp^2 hybridized [80].

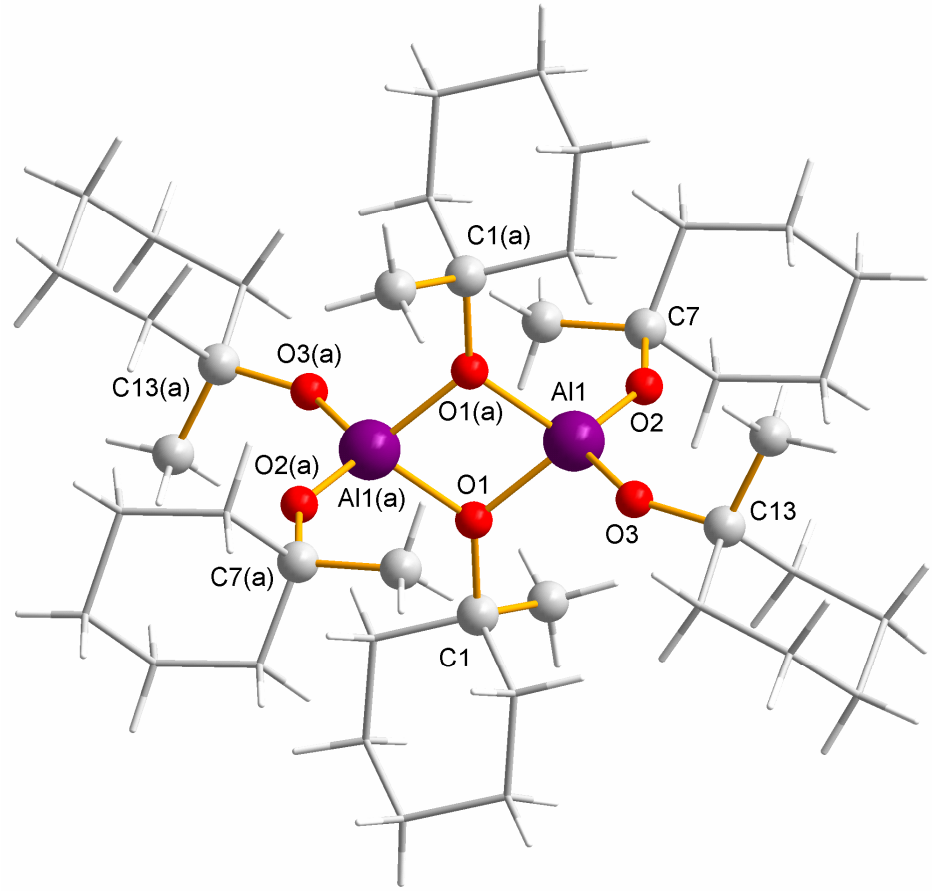

Figure 1.26. Molecular structure of compound $[Al(O^cHexMe\text{-}1)_3]_2$ **7**

Table 9. Crystal data of the compound **7**

Identification code	**$[Al(O^cHexMe\text{-}1)_3]_2$**
Empirical formula	C42 H78 Al2 O6
Formula weight	733.00
Temperature	152(2) K
Wavelength	0.71073 Å
Crystal system	Triclinic
Space group	P-1
Unit cell dimensions	a = 10.535(2) Å

	b = 10.730(1) Å
	c = 10.952(1) Å
	α= 70.98(1)°.
	β= 63.62(2)°.
	γ = 85.30(1)°.
Volume	1045.6(3) $Å^3$
Z	1
Density (calculated)	1.164 Mg/m^3
Absorption coefficient	0.113 mm^{-1}
F(000)	404
Crystal size	0.26 x 0.13 x 0.07 mm^3
Theta range for data collection	2.01 to 29.23°.
Index ranges	-14<=h<=14, -14<=k<=14, -15<=l<=13
Reflections collected	21119
Independent reflections	5655 [R(int) = 0.0539]
Completeness to theta = 29.23°	99.5 %
Absorption correction	Multiscan
Max. and min. transmission	0.9922 and 0.9712
Refinement method	Full-matrix least-squares on F^2
Data / restraints / parameters	5655 / 0 / 382
Goodness-of-fit on F^2	1.049
Final R indices [I>2sigma(I)]	R1 = 0.0447, wR2 = 0.0953
R indices (all data)	R1 = 0.0718, wR2 = 0.1068
Largest diff. peak and hole	0.314 and -0.238 $e.Å^{-3}$

Table 10. Selected bond lengths and angles of the compound **7**

Bond	Length (Å)	Bond	Angle (°)
Al(1)- O(3)	1.676(1)	O(3)-Al(1)-O(2)	116.2(1)
Al(1)- O(2)	1.684(2)	O(3)-Al(1)-O(1)a	111.2(2)
Al(1)- O(1)	1.832(1)	O(3)-Al(1)-O(1)	108.9(2)
Al(1)- O(1)a	1.830(1)	O(2)-Al(1)-O(1)	116.9(1)
Al(1)- Al(1)a	2.774(1)	O(2)-Al(1)-O(1)a	117.2(2)
O(1)- C(1)	1.468(1)	O(1)-Al(1)-O(1)a	81.5(1)

O(2)- C(7)	1.420(2)	Al(1)-O(1)-Al(1)a	98.5(2)
O(3)- C(13)	1.410(1)	C(1)-O(1)-Al(1)a	131.3(2)
		C(1)-O(1)-Al(1)	130.2(2)
		C(7)-O(2)-Al(1)	146.2(2)
		C(13)-O(3)-Al(1)	149.1(2)

3. $[ClAl(H)(O^cHex\mathit{Me}\text{-}1)]_2$ **8** and $[Cl_nAl(O^cHex\mathit{Me}\text{-}1)_{3-n}]_2$ (n = 1 **9** or 2 **10**)

3.1. Synthetic Aspects

Alkoxychloroalane and aluminium chloride alkoxides having general formulae, $[ClAl(H)(O^cHex\mathit{Me}\text{-}1)]_2$ **8** and $[Cl_nAl(O^cHex\mathit{Me}\text{-}1)_{3-n}]_2$ (n = 1 **9** or 2 **10**) have been prepared according to the following reaction strategy (Scheme 1.5). The two step reaction route was adopted from the well know literature procedures reported elsewhere [155]. $LiAlH_4$ was dissolved in diethyl ether in a two neck flask connected to a refluxing condenser. $AlCl_3$ solution in diethylether prepared under cooling was added into the above solution in appropriate molar ratios. LiCl precipitated out after stirring the reaction mixture for 1 hour. 1-methylcyclohexanol was added in stoichiometric ratios into this reaction mixture very slowly and evolution of hydrogen was observed in the reaction flask. The whole reaction mixture was stirred for another four hours for completion of the reaction and the solid residue mostly LiCl was filtered off. The volatiles, mainly the solvent were removed under low pressure and white powder has been obtained for all the three compounds. Small amounts of the powder were re-dissolved in approximately 10 mL diethylether and kept for crystallization in refrigerator at approximately +4.0°C. Colourless crystals have been obtained for all the three compounds after standing for 24 hours. Compound **10** turned yellowish upon standing at room temperature for nearly a week. However, the NMR spectrum recorded shows the same resonances as were observed before. It means that the compound **10** does not decompose upon standing at room temperature.

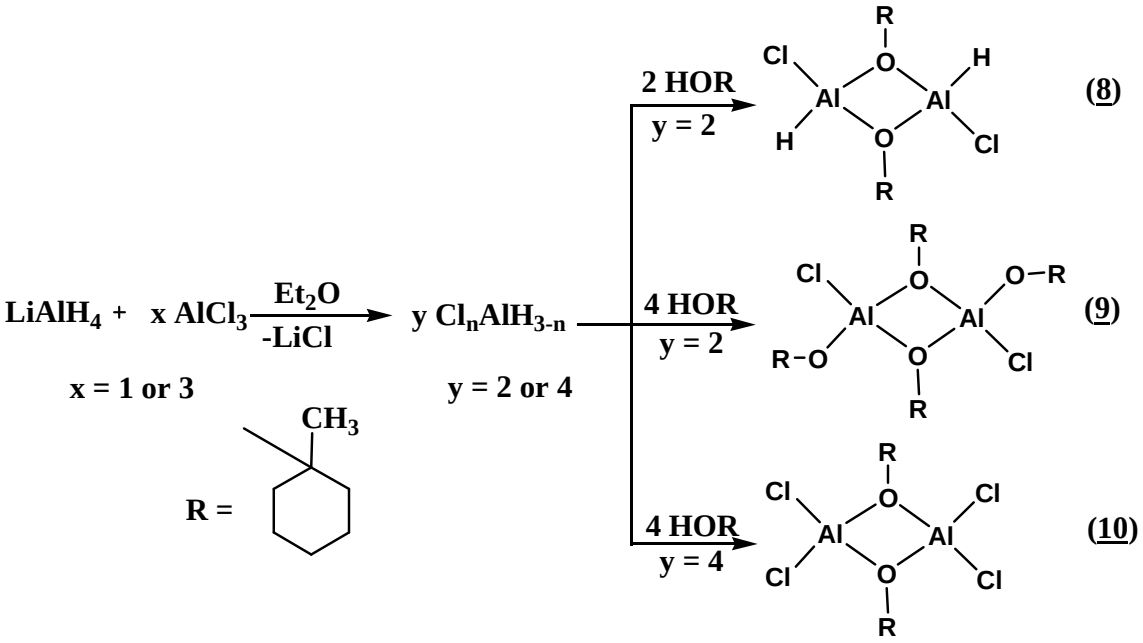

Scheme 1.5. Synthetic strategy for the preparation of compounds **8**, **9** and **10**

3.2. Spectroscopic Characterization

Compounds **8**-**10** have been analysed using different spectroscopic techniques. NMR spectra were recorded in deutrated benzene and diethyl ether for comparison. The IR spectra were recorded in solid state using golden gate method. ^{1}H-NMR spectrum of compound **8** gives two peaks for the methyl protons of the organic moiety at 1.36 ppm and 1.34 ppm (Figure 1.27). The two different peaks for methyl protons of the organic moiety could be explained by considering two different isomers of **8** in solution that is the *cis*- and *trans*-isomers. The peak at 1.36 ppm is for the methyl protons of *trans*-isomer in which the chlorine atoms are oriented opposite to each other around Al_2O_2 cyclic ring. While the peak at 1.34 ppm is for the *cis*-isomer in which the two chlorine atoms are oriented at one side of the Al_2O_2 ring. This notion was further strengthened by the ^{13}C-NMR spectrum in which paired peaks have been appeared for all the five different carbon atoms. A pair of peaks is obtained for α-carbon of the organic moiety at 82.5 ppm and 82.3 ppm for *trans*- and *cis*-isomer, respectively. The same reason has been given by Veith *et. al.* in explanation of the NMR spectra of $[ClAl(H)O^tBu]_2$ [127] which is identical to compound **8** in its structural aspects. The ^{1}H NMR spectrum did not give any signal for terminal hydride bonded to Al atom. This resonance is

hindered by the highly asymmetric Al centre and its quadruple moment, due to which the peak broadened extraordinarily.

^{27}Al-NMR spectrum recorded for compound **8** in deutrated benzene is unusual but matches well with the ^{27}Al-NMR spectra reported for structurally similar compounds [156]. It gives two peaks at 89 ppm and 100 ppm which means that there are two different tetrahedral Al centres. The two peaks obtained for one type of Al centre could not be explained on the basis of *cis*- and *trans*-isomerism phenomenon. Since the chemical shifts in ^{27}Al NMR spectroscopy only depends upon the coordination number and electronic effect of the substituting ligands [157]. Therefore, this could be explained on the basis of two different compounds present in the solution. The peak at 100 ppm is due to the tetra-coordinated Al centre of compound **8** which is in its characteristic range [156]. The peak appeared at 89 ppm may be due to $[Cl_2Al(OR)]_2$ present in the solution as a result of rearrangement which is also mentioned by N. Köhler [156] in his Ph. D work of the same sort of compounds. The hydrides bonded to Al centres were confirmed by the IR spectroscopy. A sharp peak for Al–H stretching vibration has been obtained at 1905cm^{-1} for Al-H stretching vibration in compound **8**. It appears at value higher by approximately 65 cm^{-1} to that reported for $H_2Al(OR)$ [28, 80]. It is due to the higher electronegativity of chlorine atoms which increase the ionic character of Al-H bonds by electrons withdrawing effect.

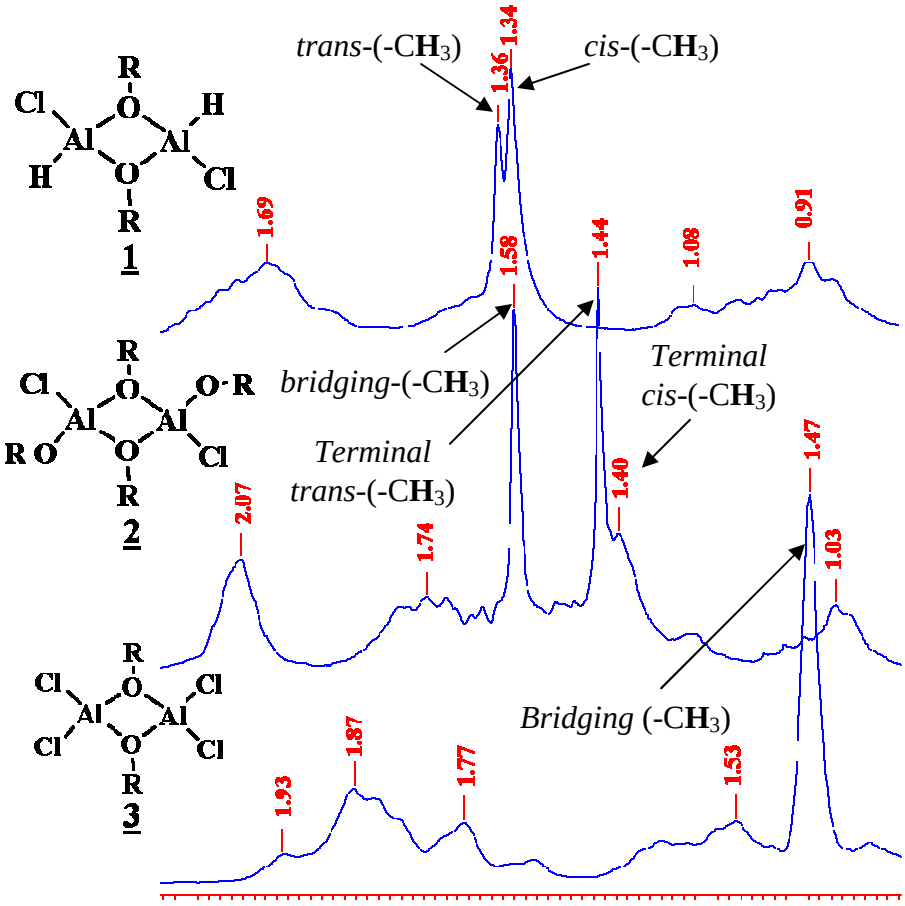

Figure 1.27. ^{1}H-NMR spectra of compounds **8**, **9** and **10**; R = 1-methylcyclohxyl

^{1}H NMR spectroscopy gives a very clear picture of compound **9**, $[ClAl(O^{c}HexMe\text{-}1)_2]_2$ as a dimer (Figure 1.28). There are two different peaks for bridging and terminal methyl protons of the organic moiety appear at 1.58 ppm and 1.44 ppm, respectively. Another important peak appears at 1.40 ppm for the terminal methyl proton. This peak reveals that compound **9** exists as *cis*- and *trans*-isomers in solution. The *cis*- and *trans*-isomers were further proved by ^{13}C NMR spectroscopy which gives three different peaks for α-carbon at 82.27 ppm, 71.25 ppm and 71.18 ppm. The first peak is due to the bridging α-carbon while the last two are for the terminal α-carbon of *trans*- and *cis*-isomers, respectively (Figure 28). An unknown peak at 80.40 ppm has been obtained which could be due to some by-product. The *cis*- and *trans* isomers in solution are also reported by Veith *et. al.* for structurally identical compounds, $[ClAl(O^{t}Bu)_2]_2$ [156]. These observations reveal that compound **9** exists as dimer in solution. Surprisingly, no signal appears in the ^{27}Al NMR spectrum of compound **9**, despite the fact that single peaks are reported for structurally identical compounds [156]. The measurements

were also carried out in different solution but every time the same broad peak appears with a maximum at approximately 45 ppm which is due to the Al present in the sample probe. The signal is so broad that all the peaks disappear under it. One reason for this could be the highly asymmetric Al centre which definitely affects the resulting ^{27}Al NMR signals [158].

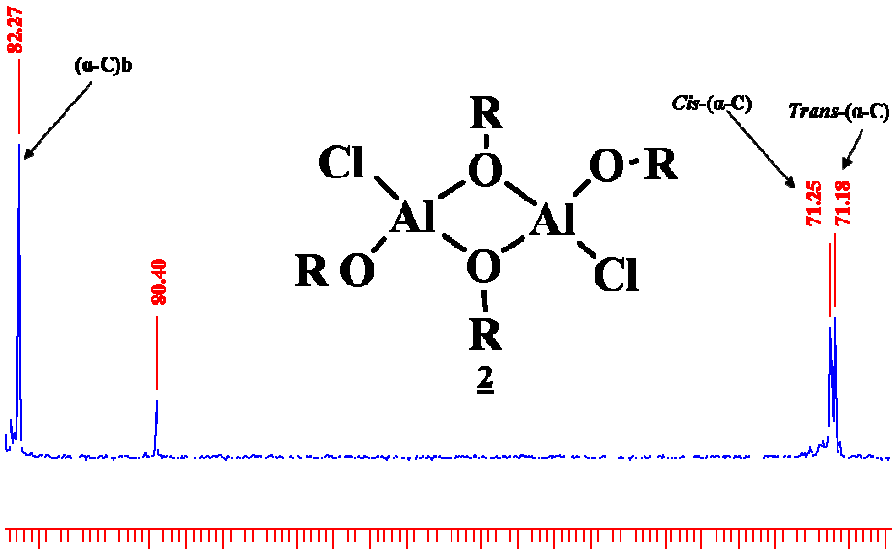

Figure 1.28. ^{13}C NMR spectrum for α-carbon of compound **9**; R = 1-Methylcyclohexyl

^{1}H-NMR spectrum of compound **10** gives a single peak at 1.47 ppm for the methyl protons and irresoluble peaks in the range of 1.53-1.93 ppm for rest of the protons of the cyclohexyl ring (Figure 27). The sharp single peak for methyl protons means that there is only one type of 1-methylcyclohexyl group in the compound. It was further confirmed by the ^{13}C NMR spectroscopy. The spectrum gives peak at 87.4 ppm for the α-carbon of the organic moiety and in the same way single peaks for all other carbons are observed. The ^{27}Al-NMR spectrum gives a single broad peak at 88.95 ppm which corresponds to the tetra-coordinated Al centres reported in similar compounds, $[Cl_2Al(OR)]_2$ having different organic moieties [156, 158-159]. The IR spectrum confirms the organic moiety by giving peaks for C–H stretching vibration. The spectroscopic data reveal that the compound is dimer in solution.

3.3. Solid State Structures

Colourless crystals of all the three compounds (**8**-**10**) have been grown at low temperature in refrigerator. Compound **8** gives crystals at room temperature too as soon as the solution is condensed. The structures were solved by direct method and refined by full-matrix least squares on F^2 using SHELLX software [149]. All the hydrogen atoms were refined with isotropic displacement thermal parameters and non-hydrogen atoms with anisotropic thermal parameters. The structures obtained share some basic characteristics. For example all the three compounds (**8**-**10**) are dimers with a four membered Al_2O_2 planar ring (Figure 1.29). The dimerization of the compounds is the result of electronic deficiency at the Al centre. To complete the electronic shell of the Al atom, the monomers tend to dimerize, oligomerize or even in some cases polymerize depending upon the steric bulk of the organic moiety of the alkoxy group.

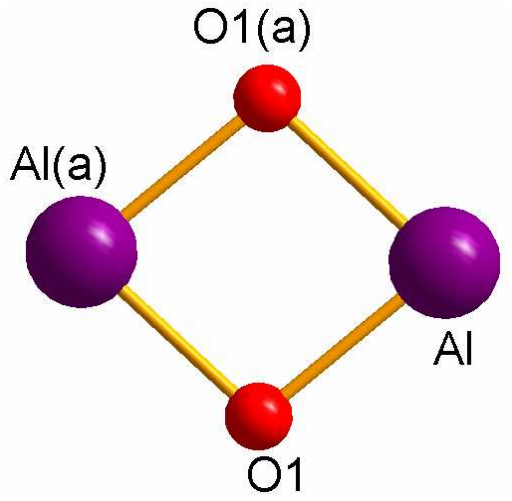

Figure 1.29. Al_2O_2 planar ring forming central unit of compounds **8**, **9** and **10**

The crystal structure of compound **8** was determined at 152K using single crystal X-ray diffractometer. The molecular structure of compound $[ClAl(H)(O^cHexMe\text{-}1)]_2$ **8** is given in Figure 1.30. The relevant crystal data are summarized in Table 11 and the pertinent bond angles and bond lengths are arranged in Table 12. The selected single crystal belongs to monoclinic crystal system having $P2_1/c$ space group. The molecule of **8** is centrosymmetric

possessing point symmetry C_i. The hydrogen and chlorine atoms are *trans*-oriented to each other at Al_2O_2 cyclic ring. Both the Al atoms in the dimer are tetra-coordinated with distorted tetrahedral geometry while the oxygen atoms act as bases to compensate for the electronic deficiency of the Al atoms. The hydrogen atoms are delocalized and difficult to measure exactly due to its lower electronic density especially in the presence of larger atoms, for example chlorine etc [156]. The Al–(μ-O) bond length is 1.82(2)Å which is in good agreement to that reported for ClAl(H)(O^{t}Bu) [127, 156] and other compounds having central Al_2O_2 cyclic ring [28, 104, 129]. The terminal Al-Cl bond distance is 2.12(1) Å which corresponds well to that of compound, ClAl(H)(O^{t}Bu) [126, 159] and falls in the domain of Al–Cl bond distances [169-160]. However, longer than those in adduct of $AlCl_3$ [161] and aluminium chloride alkoxides [160]. The Al-H bond length is 1.64(3) Å which is 0.09Å and 0.13Å longer to those reported for $[H_2Al(O^tBu)]_2$ and $[HAl(O^tBu)_2]_2$ [28], respectively. This is quite surprising since the addition of more electronegative atom into the coordination sphere of Al increases its partial positive character. The larger positive Al atom increases the ionic character of the Al-H bond and thus reduces bond length. It is due to the uncertainty in localization of hydrogen atoms in presence of larger atoms for example chlorine [156].

The smaller angles of 81.3(3)$^\circ$ as expected were found at Al atoms in the Al_2O_2 ring. Since Al atoms are more soft and larger than the oxygen atoms; therefore, more flexible for the stabilization of the four membered ring. The Al atoms have pseudo tetrahedral geometry and the angles of tetrahedron are distorted due to the ring. The oxygen atoms are almost trigonal planar deduced from the sum of angles around them (~358.8°). it indicates that the oxygen atoms are sp^2 hybridized [80]. The C1-O-Al and C1-O-Al(a) angles are nearly the same having values of 130.12° and 129.99°, respectively. This indicates that the organic moieties are uniformly distributed over the Al-O-Al bridges.

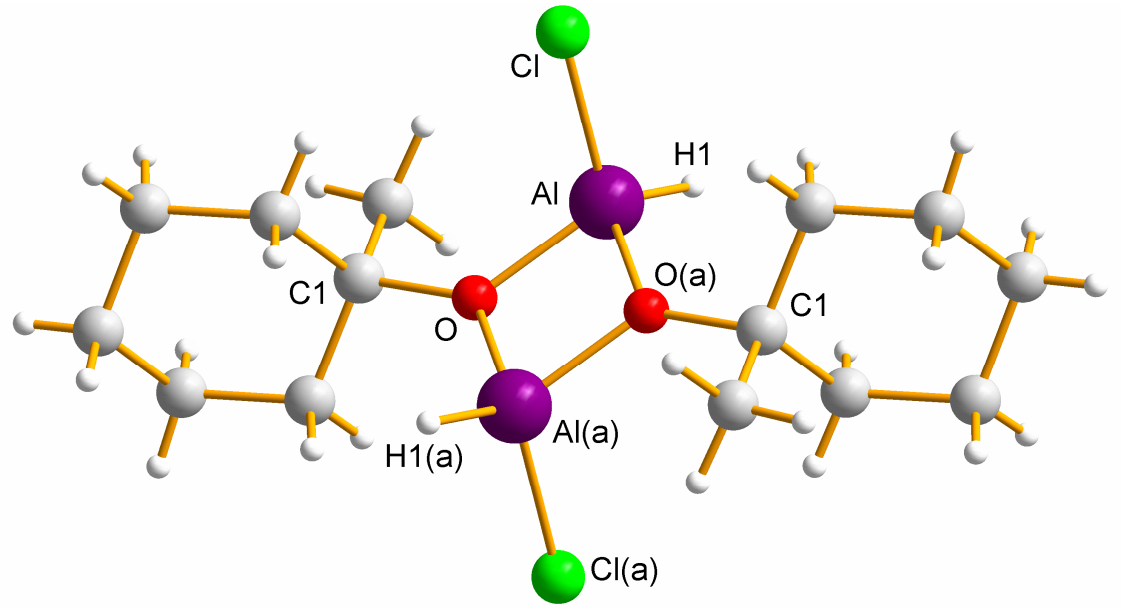

Figure 1.30. Molecular structure of $[ClAl(H)(O^cHexMe\text{-}1)]_2$ **8**

Table 11. Crystal data of compound **8**

Molecular Formula	**ClAl(H)(O^cHex*Me*-1)**
Empirical formula	C14 H28 Al2 Cl2 O2
Formula weight	353.22
Temperature	152(2) K
Wavelength	0.71073 Å
Crystal system	Monoclinic
Space group	$P2_1/c$
Unit cell dimensions	a = 8.934(2) Å b = 8.206(1) Å c = 13.052(2) Å α= 90°. β= 105.05(1)°. γ = 90°.
Volume	923.98(12) $Å^3$
Z	2
Density (calculated)	1.270 Mg/m^3

Absorption coefficient	0.445 mm^{-1}
F(000)	376
Crystal size	0.29 x 0.26 x 0.06 mm^3
Theta range for data collection	2.36 to 27.83°.
Index ranges	-11<=h<=10, -10<=k<=7, -16<=l<=17
Reflections collected	7751
Independent reflections	2190 [R(int) = 0.0464]
Completeness to theta = 27.83°	99.9 %
Absorption correction	Multiscan
Max. and min. transmission	0.9755 and 0.8802
Refinement method	Full-matrix least-squares on F^2
Data / restraints / parameters	2190 / 0 / 147
Goodness-of-fit on F^2	1.066
Final R indices [I>2sigma(I)]	R1 = 0.0459, wR2 = 0.1156
R indices (all data)	R1 = 0.0719, wR2 = 0.1288
Largest diff. peak and hole	0.474 and -0.415 $e.Å^{-3}$

Table 12. Pertinent bond lengths (Å) and angles (°) of **8**

Bond	Length (Å)	Bond	Angle (°)
Al–Cl	2.120(2)	O-Al-O(a)	81.3(1)
Al–H	1.640(2)	O-Al-Cl	111.4(2)
Al–O	1.822(1)	O(a)-Al-Cl	112.8(1)
Al–O(a)	1.823(1)	Al-O-Al(a)	98.7(1)
Al–Al(a)	2.766(1)	C(1)-O-Al	130.1(1)
		C(1)-O-Al(a)	130.0(2)

The Crystal structure of compound **9** is given in Figure 1.31. The crystal data are arranged in Table 13 and the pertinent bond lengths and bond angles are presented in Table 14. The crystal structure resolved is a dimer having two ClAl(O_cHex*Me*-1) units bridged through the oxygen atoms of the alkoxy groups. Compound **9** has a monoclinic crystal system in $P2_1/n$ space group. The molecular structure of **9** is centrosymmetric having point symmetry C_i. The chlorine as well as the terminal alkoxy ligands are *trans* oriented to each other over the central

Al_2O_2 four membered ring. The basic structural features are the same as that of compound **8**. However, due to the incorporation of the alkoxy group for hydride, some changes in the bond lengths and angles are observed. The structure of **9** is similar as that of [ClAl(O^{t}Bu)$_2$] [156] except the organic moiety. The Al1–O1 and Al1–O1(a) bond lengths are 1.816(1)Å and 1.813(1)Å, respectively and comparable to that of [ClAl(O^{t}Bu)$_2$] [156] and compound **8**. The terminal Al–O bond length is smaller by 0.14Å compared to the bridging Al-O bond length. However, all the Al–O bond lengths lie well in the domain of their characteristic range [28, 80, 127, and 156]. The Al-Cl bond length is 2.123(1)Å and corresponds to that of [ClAl(O^{t}Bu)$_2$] [156]. However, it is slightly larger than that observed in the case of compound **8**. This could be due to the incorporation of bulky alkoxy group for hydrogen atom in **9**.

The acute angel has been observed around Al centre as usual having value of 81.67(5)° and is comparable to the earlier reported [28, 80, 127, 156]. Contrarily to compound **8** in which the Cl-Al-H angle was 109°, the Cl-Al-O$_t$ angle (~119°) in compound **9** is more open due to the high bulk of the organic moiety of the alkoxy group. The sum of angles around oxygen atoms is 359.3(2)° which gives that the oxygen atoms have sp^2 hybridization and trigonal planar geometry [80].

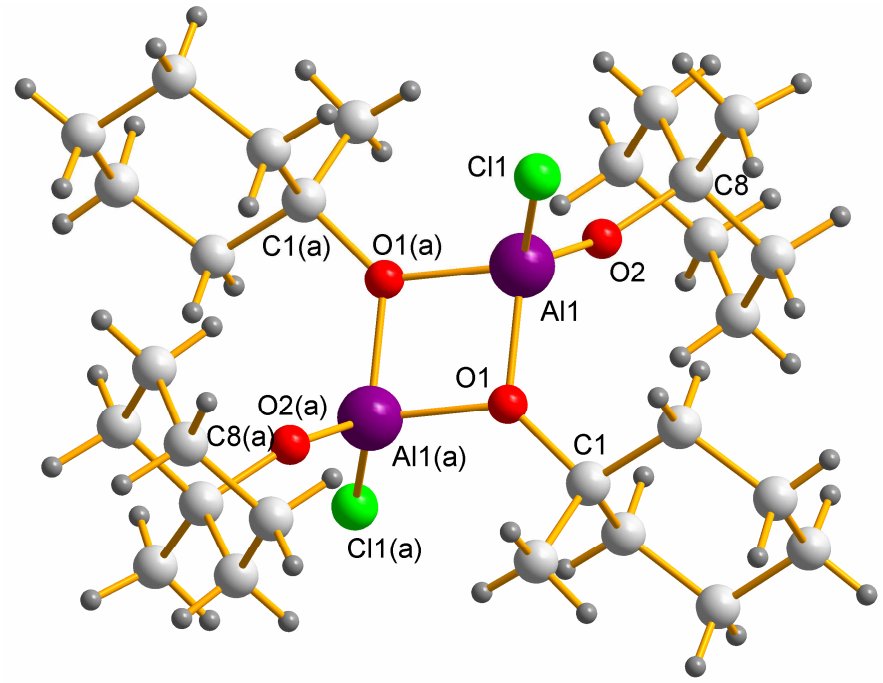

Figure 1.31. Molecular structure of compound [ClAl(O^{c}Hex*Me*-1)$_2$]$_2$ **9**

Table 13. Crystal data of compound **9**

Identification code	**[ClAl(O^{c}Hex*Me*-1)$_2$]$_2$**
Empirical formula	C28 H52 Al2 Cl2 O4
Formula weight	577.56
Temperature	152(2) K
Wavelength	0.71073 Å
Crystal system	Monoclinic
Space group	P2(1)/n
Unit cell dimensions	a = 12.121(1) Å b = 10.613(1) Å c = 12.546(1) Å α = 90°. B = 102.43 (2)°. γ = 90°.
Volume	1576.18(17) Å^3
Z	2
Density (calculated)	1.217 Mg/m^3
Absorption coefficient	0.292 mm^{-1}
F(000)	624
Crystal size	0.56 x 0.43 x 0.27 mm^3
Theta range for data collection	2.12 to 28.73°.
Index ranges	-16<=h<=16, -14<=k<=10, -16<=l<=16
Reflections collected	14833
Independent reflections	4081 [R(int) = 0.0752]
Completeness to theta = 28.73°	99.8 %
Absorption correction	Multiscan
Max. and min. transmission	0.9265 and 0.8537
Refinement method	Full-matrix least-squares on F^2
Data / restraints / parameters	4081 / 0 / 267
Goodness-of-fit on F^2	1.050
Final R indices [I>2sigma(I)]	R1 = 0.0490, wR2 = 0.1304
R indices (all data)	R1 = 0.0619, wR2 = 0.1418
Largest diff. peak and hole	0.914 and -0.282 e.Å^{-3}

Table 14. Pertinent bond lengths (Å) and angles (°) of the compound **9**

Bond	Length (Å)	Bond	Angle (°)
Cl(1)-Al(1)	2.123(1)	O(2)-Al(1)-O(1)(a)	114.8(2)
Al(1)-O(2)	1.670(3)	O(2)-Al(1)-O(1)	114.2(1)
Al(1)-O(1)(a)	1.813(1)	O(1)(a)-Al(1)-O(1)	81.7(2)
Al(1)-O(1)	1.816(2)	O(2)-Al(1)-Cl(1)	118.7(1)
Al(1)-Al(1)(a)	2.746(2)	O(1)(a)-Al(1)-Cl(1)	110.4(2)
O(1)-Al(1)(a)	1.813(1)	O(1)-Al(1)-Cl(1)	111.3(1)
O(2)-C(8)	1.424(2)	C(1)-O(1)-Al(1)(a)	131.1(1)
O(1)-C(1)	1.476(2)	C(1)-O(1)-Al(1)	129.9(2)
		Al(1)(a)-O(1)-Al(1)	98.3(1)
		C(8)-O(2)-Al(1)	146.0(1)

The molecular structure of compound **10** is presented in Figure 1.32. The relevant crystal data are arranged in Table 15 and the pertinent bond lengths and bond angles are summarized in Table 16. The single crystal of compound **10** belongs to the monoclinic crystal system in $P2_1/c$ space group. The centrosymmetric molecule having point symmetry C_i is a dimer in which two ClAl(OcHexMe-1) units are associated via oxygen bridges. The structure is composed of central four membered Al_2O_2 ring forming backbone of the molecule. Each of the Al atoms of the dimer has tetrahedral geometry attached to two chlorine and two oxygen atoms of the alkoxy group. The oxygen atoms act as base to stabilize the electron deficient Al centre carrying +3 charge. The bond lengths and angles in **10** are comparable to those of the same type of compounds, $[Cl_2Al(OR)]_2$ [156, 159-160]. The terminal Al-Cl bond lengths are 2.092(2)Å and 2.097(2)Å which are shorter by approximately 0.026Å and 0.03Å compared to compound **8** and **9**, respectively. However, the Al-Cl bond lengths fall under the characteristic range [159-160]. The bridging Al-O bond lengths are 1.804(1)Å and 1.810(2)Å which are comparable to that observed for structurally similar compound [156]. As expected, the smallest angle, 82.3(1)° is found at Al centre. The sum of angles around oxygen atom is ~359.55° which indicates that oxygen has trigonal planar geometry and is sp^2 hybridized [80].

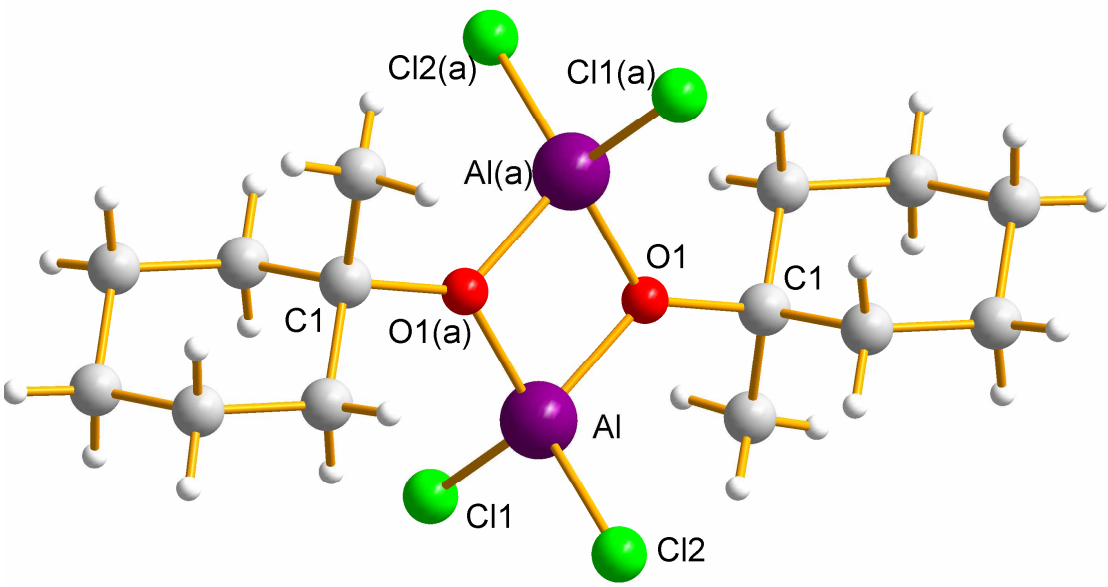

Figure 1.32. Molecular structure of $[Cl_2Al(O^cHexMe\text{-}1)]_2$ **10**

Table 15. Crystal data of compound **10**

Molecular Formula	**$[Cl_2Al(O^cHexMe\text{-}1)]_2$**
Empirical formula	C14 H26 Al2 Cl4 O2
Formula weight	422.11
Temperature	152(2) K
Wavelength	0.71073 Å
Crystal system	Monoclinic
Space group	P2(1)/c
Unit cell dimensions	a = 9.018(2) Å b = 8.682(2) Å c = 13.149(1) Å α= 90°. β= 104.821(2)°. γ = 90°.
Volume	995.19(7) $Å^3$
Z	2
Density (calculated)	1.409 Mg/m^3
Absorption coefficient	0.686 mm^{-1}
F(000)	440
Crystal size	0.47 x 0.37 x 0.31 mm^3

Theta range for data collection	2.34 to 34.95°.
Index ranges	-9<=h<=14, -13<=k<=10, -21<=l<=21
Reflections collected	16344
Independent reflections	4356 [R(int) = 0.0491]
Completeness to theta = 34.95°	99.8 %
Absorption correction	Multiscan
Max. and min. transmission	0.8166 and 0.7406
Refinement method	Full-matrix least-squares on F^2
Data / restraints / parameters	4356 / 0 / 152
Goodness-of-fit on F^2	1.051
Final R indices [I>2sigma(I)]	R1 = 0.0313, wR2 = 0.0835
R indices (all data)	R1 = 0.0394, wR2 = 0.0880
Largest diff. peak and hole	0.413 and -0.296 e.Å^{-3}

Table 16. Pertinent bond lengths (Å) and angles (°) for the compound **10**

Bond	Length (Å)	Bond	Angle (°)
Al1-O1(a)	1.804(1)	O(1)a-Al(1)-O(1)	82.3(1)
Al1-O1	1.808(1)	O(1)a-Al(1)-Cl(1)	113.2(1)
Al1(a)-O1	1.804(1)	O(1)-Al(1)-Cl(1)	114.9(1)
Al1(a)-O1(a)	1.808(1)	O(1)a-Al(1)-Cl(2)	115.7(1)
Al1-Cl1	2.092(2)	O(1)-Al(1)-Cl(2)	113.7(1)
Al1-Cl2	2.097(2)	Cl(1)-Al(1)-Cl(2)	113.5(3)
Al1(a)-Cl1(a)	2.092(2)	C(1)-O(1)-Al(1)a	131.6(1)
Al1(a)-Cl2(a)	2.097(2)	C(1)-O(1)-Al(1)	130.3(2)
Al1-Al1(a)	2.719(1)	Al(1)a-O(1)-Al(1)	97.7(2)

4. Synthsis of $[Ge(OR)_2]_2$ (R = ^{c}Hex **11**, ^{c}Hex*Me*-1 **12** or ^{i}Pr **13**)

4.1. Synthetic Aspects

The title compounds, $[Ge(OR)_2]_2$ (R = ^{c}Hex **11**, ^{c}HexMe-1 **12**, ^{i}Pr **13**) have been obtained by the reaction of $Ge\{N(SiMe_3)_2\}_2$ [162-164] and the corresponding alcohols in a 1:2 ratio, according to the following reaction scheme (Scheme 1.6). $Ge\{N(SiMe_3)_2\}_2$ was freshly prepared and distilled according to the well know reaction process [163]. The synthetic procedure for the preparation of compounds **11**-**13** was adopted from the well established

reported routes which were used in synthesis of same sort of compounds [136, 139, and 165]. As soon as the ethereal solutions of the two reactants were mixed together, the yellow colour of germanium amide disappeared immediately. The reaction is simple and has been carried out at room temperature by stirring the mixture for 3-4 hours. The volatiles were removed from the reaction mixture under low pressure giving white powders for compound **11** and **12**, while compound **13** has been obtained as thick oil like colourless liquid. The yield was satisfactory for all the three compounds (>85%). Small amounts of compounds **11**-**13** were re-dissolved in 5 mL diethylether and kept in refrigerator at about + 4°C. Compound **11** and **12** have been obtained as fine crystals at a period of one day suitable for single crystal X-ray analysis. All the efforts were in vain to get crystals of compound **13**. However, the thick oily stuff was analysed by NMR and IR spectroscopy.

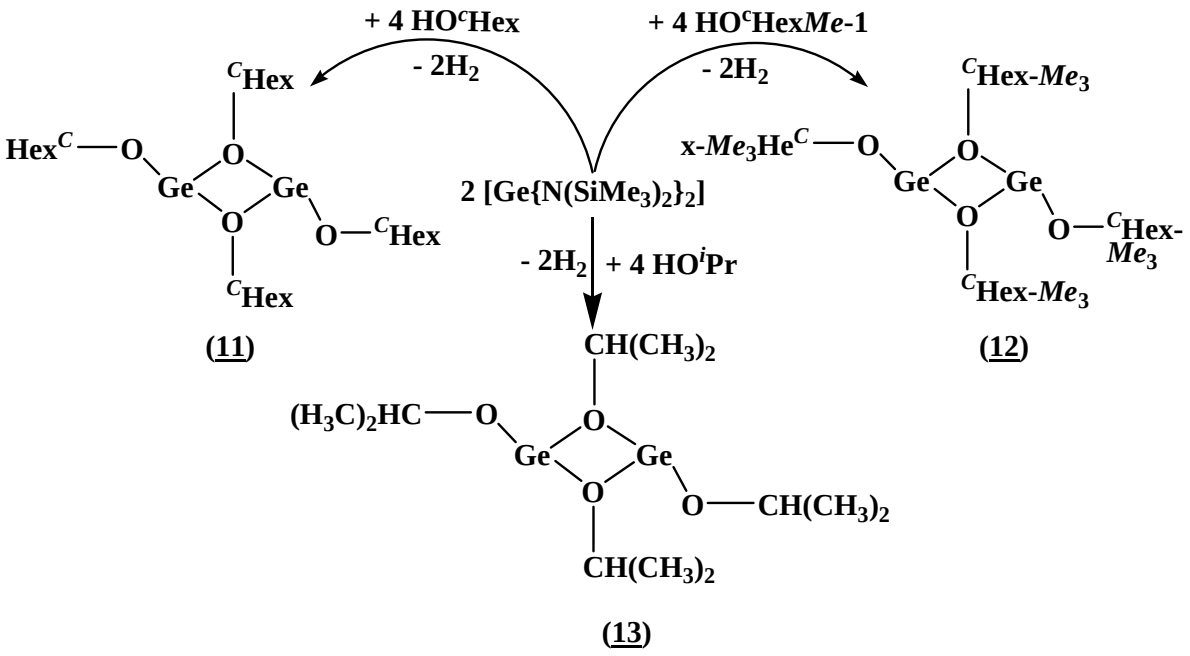

Scheme 1.6. Synthetic reactions for the preparation of **1**, **12** and **13**

4.2. Spectroscopic Characterization

Compound **11**-**13** have been characterized using IR and NMR spectroscopy. No peaks for amide moiety in the IR spectra have been found which shows that the ligand has been replaced completely by the alkoxy groups. The organic moiety of the alkoxy group has been

confirmed by the appearance of C-H stretching vibration peaks in the range of 2950cm^{-1}-2850cm^{-1} for all the three compounds. The ^{1}H and ^{13}C NMR spectra have been recorded in benzene having small amount of deutrated benzene as lock solvent. For comparison purposes the spectra were also measured in diethylether. However, the compounds have showed the same behaviour in the two different solvents.

The ^{1}H NMR spectrum of compound **11** gives a multiple peak at 4.29 ppm which is due to the proton attached to α-carbon of the cyclohexyl ring. Its multiplicity is due to the coupling effect of the protons in its vicinity. The peak is sufficiently broad which gives a hint that the compound is dimeric in solution and the peaks broaden due to the rapid exchange of the terminal and bridging alkoxy group. Therefore, instead of separate peaks for the terminal and bridging organic moieties we observed single but broad peaks. The dimeric nature of the compound in solution could be well deduced from the two distinct peaks observed at 2.17 ppm and 1.85 ppm for the β-protons of the ring. These peaks are also broad but distinctly separated. Multiple peaks in the range of 1.24 ppm-1.70 ppm have been observed for the rest of the cyclohexyl ring protons. ^{13}C NMR gives single peaks for the α-carbon and β-carbon while paired peaks have been observed for the rest of the carbons of the ring (Figure 1.33). The lesser number of peaks seem to be due to the rapid exchange phenomenon of the bridging and terminal groups. Due to this reason the dimeric compound $[Ge(OtBu)_2]_2$ [166-167] give a sinlge peak for the terminal and bridging groups. However, this compound is proved as dimer in solution by molar mass determination study [166-167].

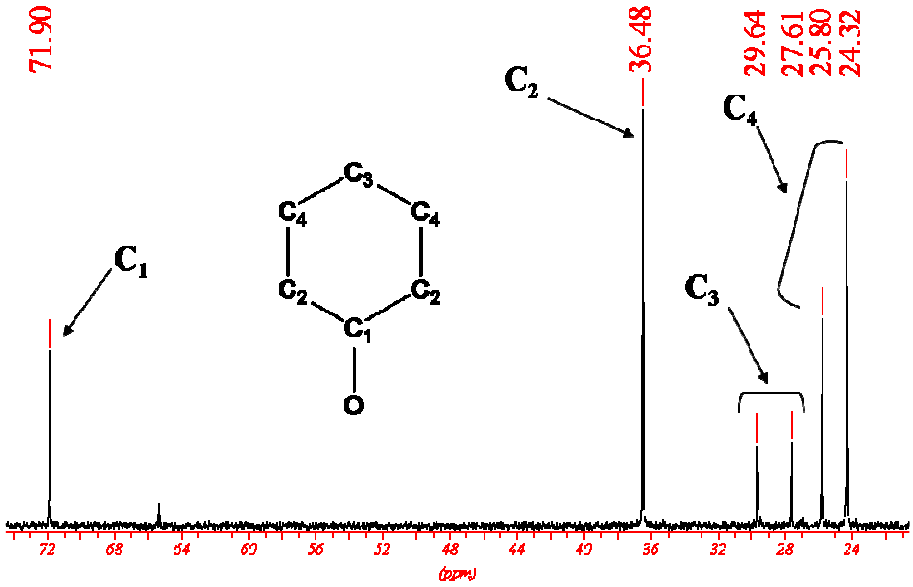

Figure 1.33. ^{13}C-NMR spectrum of Ge(O^{c}Hex)$_2$ **11**

Compound **12** has the same structural aspects in solution as that of [Ge(O^{t}Bu)$_2$]$_2$ [166-167], since the steric bulk of the organic moieties in the two compounds is nearly equal. Therefore, the compound is thought to be dimeric in solution. This has been proven by measuring solution NMR spectra for compound **12**. The methyl group in the organic moiety has a distinct peak in the ^{1}H NMR spectrum compared to that protons of the ring. Therefore, methyl protons will be given preference in structural interpretations of compound **12** by ^{1}H NMR spectroscopy. There are two distinct peaks for the methyl protons of the organic moiety in ^{1}H NMR spectrum of compound **12** (Figure 34). The peak appearing at 1.61 ppm is for bridging while the peak appearing at 1.57 ppm is for terminal methyl protons. The peak appearing at 1.61 ppm has been broadened due to the ligand exchange effect. Peaks in the range of 1.36-1.96 ppm appear for the protons of the ring. The ^{13}C NMR spectrum of compound **11** corresponds to that of **10**. ^{13}C NMR spectrum gives single peaks at 74.7 ppm, 41.5 ppm and 29.8 ppm for α-carbon, β-carbon and methyl carbon of the organic moieties (Figure 1.34). This indicates that the ligands exchange occurs in compound **11** at room temperature.

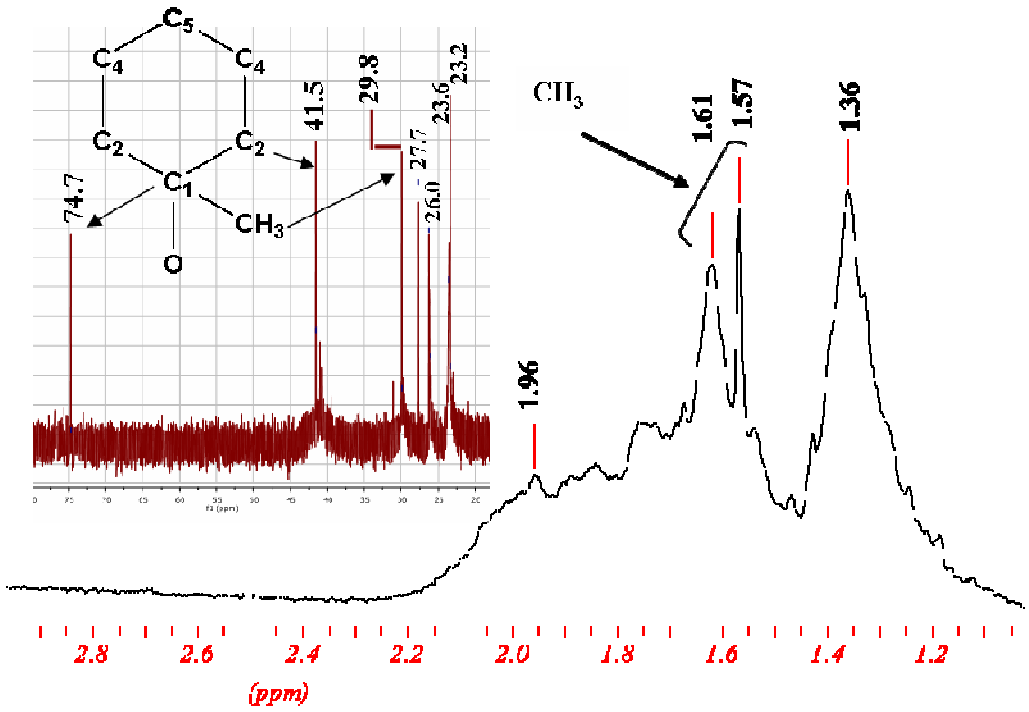

Figure 1.34. ^{1}H and 1^{3}C (inset) NMR spectra of Ge(O^{c}Hex*Me*-1) **12**

Structural predictions of compound **13** are crucial since it is an oily liquid and does not crystallize. It was characterized by spectroscopic techniques specifically NMR spectroscopy. ^{1}H NMR spectrum gives a broad multiplet with a centre at 4.51 ppm for proton attached to the α-carbon. Its multiplicity is due to the coupling effect of the vicinal protons. A doublet has been appeared having peak value of 1.325ppm with j = 5.90 Hz in ^{1}H NMR spectrum of compound **13** for the methyl protons of the *iso*-propoxy group (Figure 1.35). The usually sharp doublet peak is quite broad. The broadening of the peak may be due to the rapid exchange of organic moieties. The ^{13}C NMR gives peaks at 67.4 ppm and 27.0 ppm for the α-carbon and methyl carbon of the organic moiety.

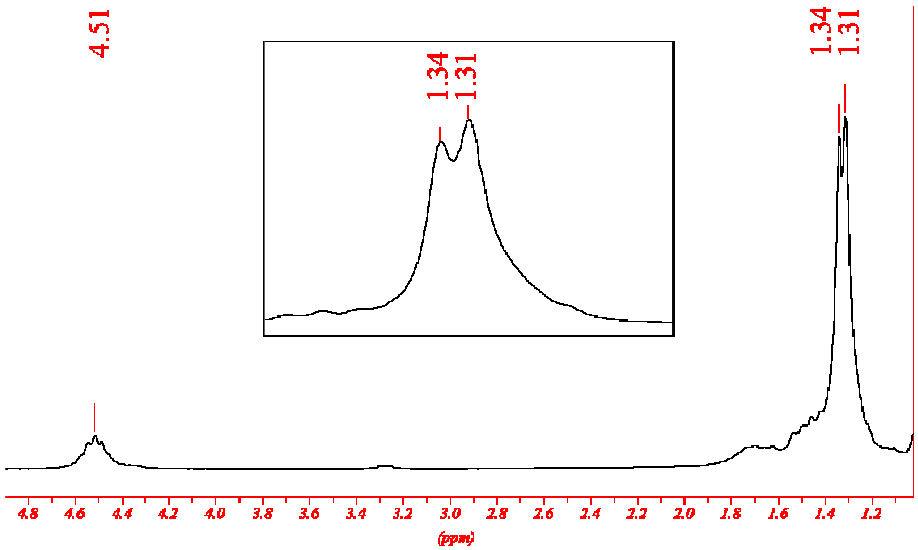

Figure 1.35. ^{1}H-NMR spectrum of compound [Ge(O^{i}Pr)$_2$]$_2$ **13**

The ^{1}H and ^{13}C NMR data correspond to the earlier reported compounds of identical structural features [Ge(O^{t}Bu)$_2$]$_2$ [166-167]. [Ge(O^{t}Bu)$_2$]$_2$ is a dimer in solution confirmed by NMR and molar mass determination. Compound **13** is a dimer having structure depicted in Figure 1.36.

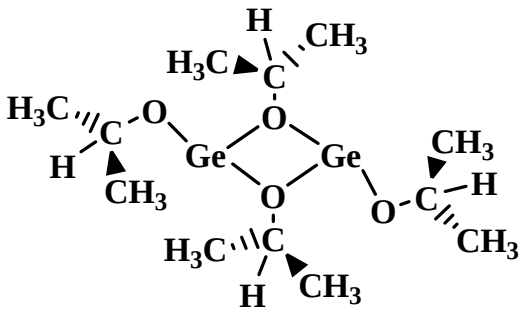

Figure 1.36. Proposed molecular structure of compound [Ge(O^{i}Pr)$_2$]$_2$ **13**

4.3. Solid State Structures

Fine colourless crystals of compounds **11** and **12** have been grown in refrigerator at +4°C. The efforts for the crystallization of compound **13** did not succeed and all the attempts failed

as it is a thick oily liquid. Single crystals have been isolated for structural analysis and measured at 152K. SHELLX software packages [149] have been used for the refinement and solution of the crystal structures. The structures of compounds **11** and **12** were solved by direct methods and refined by full-matrix least squares on F^2. All the non-hydrogen atoms were refined with anisotropic thermal parameters and hydrogen atoms with isotropic thermal parameters. Most of the features of the two structures are similar except the pendant groups which are not identical. Both are dimeric in solid state with the backbone composed of a planar four membered ring comprising of Ge and oxygen atoms, Ge_2O_2 (Figure 1.37). The central four membered Ge_2O_2 ring is similar as Al_2O_2 ring in aluminium alkoxides as well as in alkoxyalanes [157-158, 168-173]. The compounds has similar structural features as those of $[Ge(O^tBu)_2]_2$ [166-170 and 174-175], $[Ge(OAr)_2]_2$ [137] and $[Sn(O^tBu)_2]_2$ [166-167]. The bridging oxygen atoms possess nearly planar geometry in both the compounds which indicate that the lone pairs may be stereochemically inactive. However, the highly strained geometry at each Ge atoms of the Ge_2O_2 cyclic ring shows that the lone pair of Ge atoms is stereochemically active. The terminal alkoxide groups are *trans*-oriented to each other over Ge_2O_2 ring.

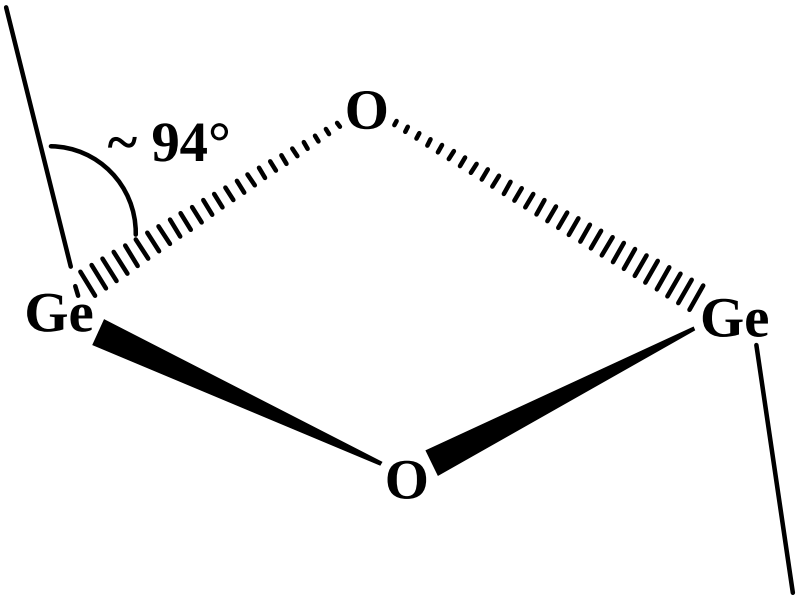

Figure 1.37. Central Ge_2O_2 ring of $[Ge(OR)_2]_2$ (R = ^{c}Hex **11**, or ^{c}Hex*Me*-1 **12**)

The solved and refined structure of compound **11** is presented in Figure 1.38. The most relevant crystal data are summarized in Table 17 and the pertinent bond lengths and bond angles are presented in Table 18. Complete data will be presented at the end of the thesis.

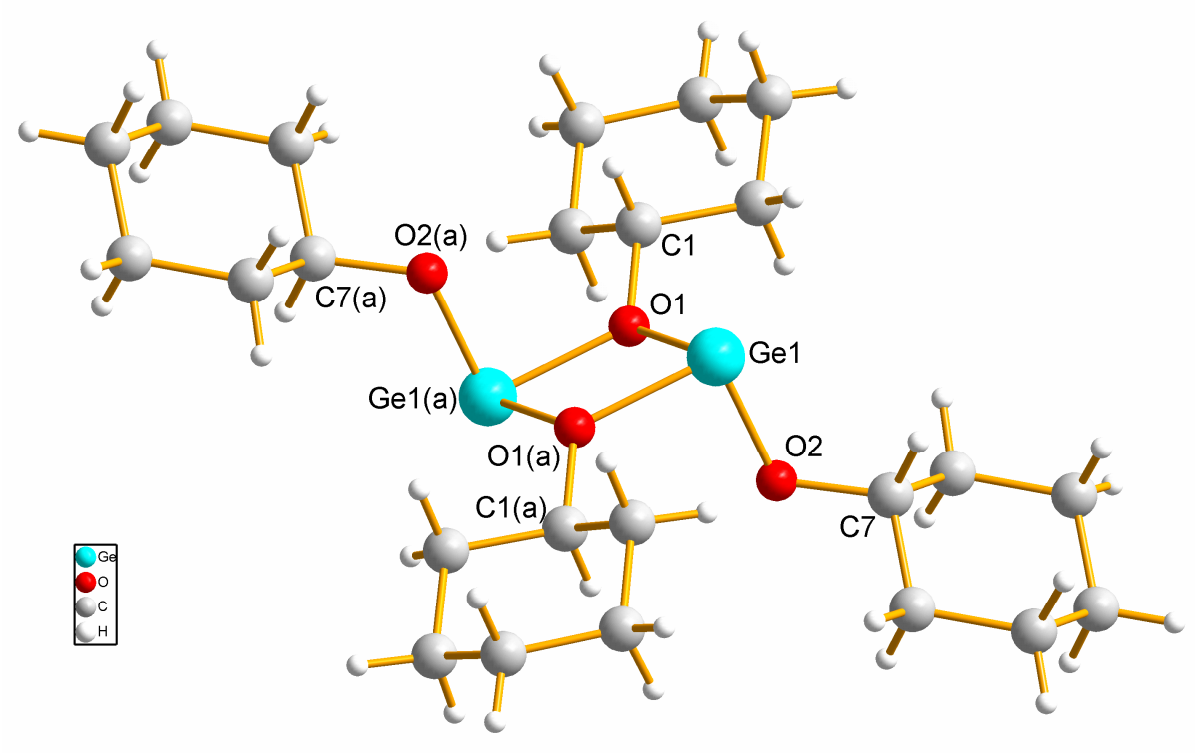

Figure 1.38. Molecular structure of $[Ge(O^cHex)_2]_2$ **11**

Compound **11** has been crystallized in triclinic crystal system with a Pī space group. Both the Ge atoms are in +2 oxidation state. The molecule of compound $[Ge(O^cHex)_2]_2$ **11** is centrosymmetric in point symmetry C_i with trans-orientation of the cyclohexoxy groups with respect to the Ge_2O_2 cyclic ring. The structural motif of **11** is similar as reported for germanium alkoxides (e.g. $[Ge(O^tBu)_2]_2$) [166-167; 174-175]) and aryloxides (e.g. $[Ge(OC_6H_2Me_3\text{-}2,4,6)_2]_2$) [137]. The Ge–(μ-O1) and Ge–(μ-O1a) bond distances are 1.977(1) Å and 1.968(2) Å, respectively which are nearly identical and lie well in its characteristic range [167, 137, 174-178]. The terminal Ge–O bond lengths are equal having value of 1.815(2) Å and corresponds to those of dimeric Ge(II) alkoxides [167, 179]. There is no chance of the Ge-Ge interaction since the distance between the two Ge atoms (3.115(2) Å) in the Ge_2O_2 cyclic ring fall away of the typical Ge-Ge bond lengths [180-187].

The two Ge atoms are bridged by oxygen atoms making Ge_2O_2 four membered planar cyclic ring. The sum of angles around the oxygen atoms is approximately 349.0(1)° which indicates that the oxygen atoms possess trigonal planar geometry as well as sp^2 hybridization [80]. However, the carbon makes a little bit of deviation from plane which could be due to the steric effect of the bridging pendants. The C1-O1-Ge1 angle (122.3(2)°) is nearly the same as the C1-O1-Ge1(a) angle (122.5(2)°) which indicates that the organic moiety is equally distributed around the Ge-O-Ge bridge. The acute angle (75.72°) as expected can be found at Ge centre which is larger and softer than oxygen atoms. Each of the Ge^{II} atoms has trigonal pyramidal geometry. The sum of angles around each Ge^{II} atom is 263.9(1)° which supports the presence of non-bonding lone pair at Ge^{II}. However, the acute endocyclic angle O-Ge-O corresponds to p^3 geometry at each Ge^{II} atom [179].

Table 17. Crystal data of compound **11**

Identification code	**$Ge(O^cHex)_2$**
Empirical formula	C24 H44 Ge2 O4
Formula weight	541.77
Temperature	152(2) K
Wavelength	0.71073 Å
Crystal system	Triclinic
Space group	Pī
Unit cell dimensions	a = 5.627(1) Å b = 10.351(1) Å c = 11.123(1) Å a= 81.23(1)°. b= 82.14(2)°. g = 86.68(1)°.
Volume	633.84(4) $Å^3$
Z	1
Density (calculated)	1.419 Mg/m^3
Absorption coefficient	2.397 mm^{-1}
F(000)	284
Crystal size	0.62 x 0.22 x 0.07 mm^3
Theta range for data collection	1.87 to 38.38°.
Index ranges	-9<=h<=9, -18<=k<=18, -19<=l<=17
Reflections collected	26163
Independent reflections	7057 [R(int) = 0.0254]

Completeness to theta = 38.38°	99.7 %
Absorption correction	Multiscan
Max. and min. transmission	0.8426 and 0.3198
Refinement method	Full-matrix least-squares on F^2
Data / restraints / parameters	7057 / 0 / 224
Goodness-of-fit on F^2	1.029
Final R indices [I>2sigma(I)]	R1 = 0.0231, wR2 = 0.0562
R indices (all data)	R1 = 0.0296, wR2 = 0.0585
Largest diff. peak and hole	0.466 and -0.381 e.$Å^{-3}$

Table 18. Selected bond lengths (Å) and angles (°) of compound **11**

Bond	Length(Å)	Bond	Angle(°)
Ge(1)-O(2)	1.815(2)	O(2)-Ge(1)-O(1)a	93.47(3)
Ge(1)-O(1)	1.977(1)	O(1)a-Ge(1)-O(1)	75.72(3)
O(1)-Ge(1)a	1.968(2)	C(1)-O(1)-Ge(1)	122.25(5)
Ge(1)-O(1)a	1.968(2)	O(2)-Ge(1)-O(1)	94.72(3)
O(1)-C(1)	1.448(2)	C(1)-O(1)-Ge(1)a	122.48(5)
O(2)-C(7)	1.426(1)	Ge(1)a-O(1)-Ge(1)	104.28(3)
		C(7)-O(2)-Ge(1)	117.11(5)

Single crystal suitable for X-ray analysis was selected and measured at 123K by single crystal X-ray diffractometre. The structure resolved belongs to monoclinic crystal system in $P2_1/c$ space group. The solved and refined solid state structure of **12** is presented in Figure 1.39. The crystal data are arranged in Table 19 and the most relevant bond angles and bond lengths are organised in Table 20. Compound **12** has a similar structural motif as that of compound **11** except the pendant group which is 1-methylcyclohexyl instead of cyclohexyl in **11**. The structural features of **12** are not extraordinary and correspond well to the reported structural motifs having Ge_2O_2 cyclic ring [166-167; 137; 174-175] as well as to that of **11**. The structure is dimer in which the two Ge^{II} centres are bridged by 1-methylcyclohexoxy groups. The bridging Ge–O and terminal Ge–O bond distances are longer by approximately 0.1Å compared to those of compound **11**. It may be due to the higher steric demanding organic moiety in compound **12**. The bridging Ge1–O2 and Ge1–O2(a) bond distances are nearly equal having values of 1.982(2) Å and 1.976(1) Å, respectively. The terminal Ge–O bond

lengths are 1.820(1) Å and smaller than the bridging Ge–O bond lengths, as expected. However, the bridging as well as terminal Ge-O bond lengths correspond well to the reported [137; 167; 174-189].

The sum of angles around the bridging oxygen atoms is 354.0(2)° which indicates that the oxygen atoms have trigonal planar environment as usual [80]. The organic moieties attached to the bridging oxygen have moved a little bit out of plane which may be due to the steric effect of the pendant groups. However, the out of plane moment is less than that observed in compound **11**. The C–O–Ge angles at the two sides of Ge-O-Ge bridge are not identical as was the case in compound **11**. C8–O2–Ge1 angle is 126.73(2)° which is larger by 4.46(1)° compared to the C8–O2–Ge1(a) angle having value of 122.28(2)°. The acute angle amounting to 75.11(2)° lie at Ge^{II} atoms in the Ge_2O_2 cyclic ring. It is smaller by 0.61(2)° compared to that in compound **11**. The smaller difference of angles between compound **11** and **12** at Ge^{II} atoms may be due to the difference of bulk of organic moieties. The terminal alkoxy groups are oriented in a *trans*-fashion to each other at the four membered Ge_2O_2 cyclic ring. Each of the Ge^{II} atoms has trigonal pyramidal geometry comparable to that in compound **11**. The sum of angles at Ge^{II} atoms is 263.91(1)° which means that there is a non-bonding lone pair at Ge^{II} atoms responsible for the trigonal pyramidal geometry of Ge^{II} atoms. However, the acute endocyclic angle at Ge^{II} is more consistent with p^3 geometry [179].

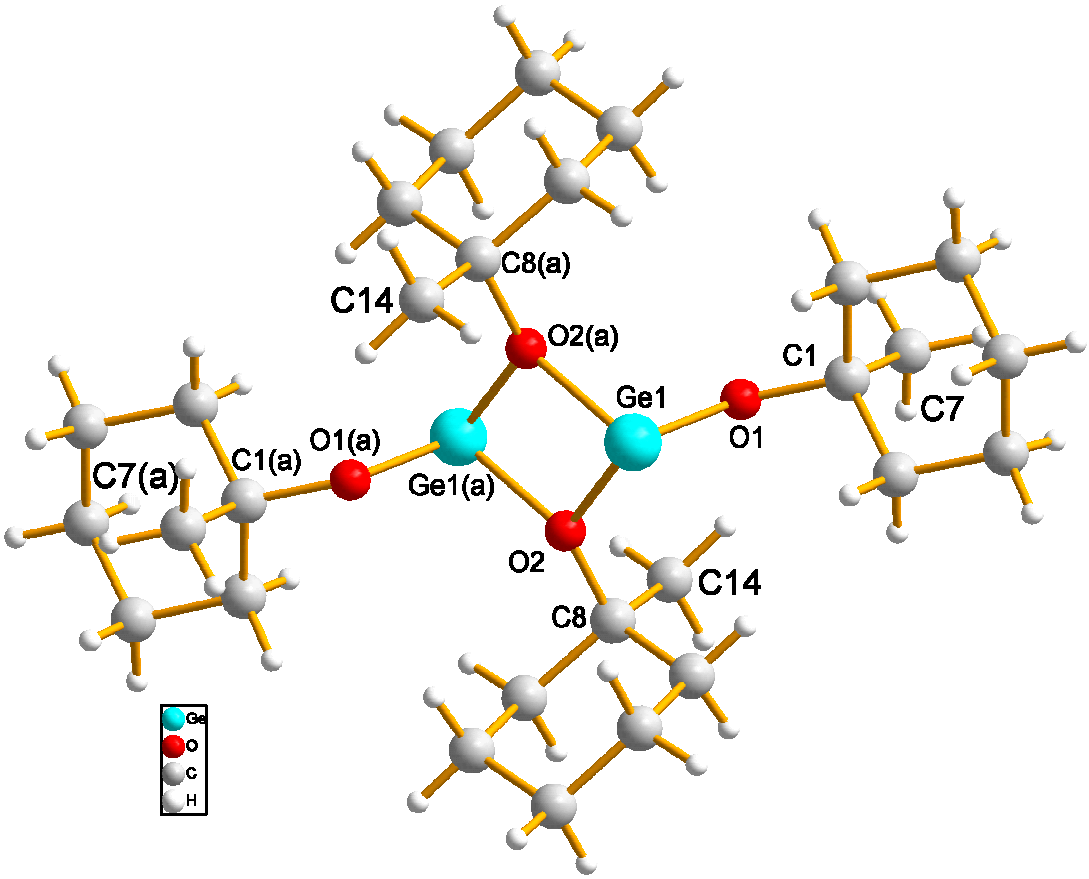

Figure 1.39. Molecular structure of $[Ge(O^{c}HexMe\text{-}1)_2]_2$ **12**

Table 19. Crystal data of compound **12**

Identification code	**Ge(OcHex-Me)2**
Empirical formula	C28 H52 Ge2 O4
Formula weight	597.88
Temperature	123(2) K
Wavelength	0.71073 Å
Crystal system	Monoclinic
Space group	P2(1)/c
Unit cell dimensions	a = 10.932(2) Å b = 9.694(2) Å c = 13.728(1) Å a= 90°. b= 101.31(1)°. g = 90°.

Volume	1426.50(19) $Å^3$
Z	2
Density (calculated)	1.392 Mg/m^3
Absorption coefficient	2.137 mm^{-1}
F(000)	632
Crystal size	0.69 x 0.37 x 0.09 mm^3
Theta range for data collection	1.90 to 41.29°.
Index ranges	-20<=h<=20, -17<=k<=17, -25<=l<=25
Reflections collected	55458
Independent reflections	9520 [R(int) = 0.0397]
Completeness to theta = 41.29°	99.5 %
Absorption correction	None
Max. and min. transmission	0.8375 and 0.3182
Refinement method	Full-matrix least-squares on F^2
Data / restraints / parameters	9520 / 0 / 258
Goodness-of-fit on F^2	1.029
Final R indices [I>2sigma(I)]	R1 = 0.0246, wR2 = 0.0573
R indices (all data)	R1 = 0.0386, wR2 = 0.0621
Largest diff. peak and hole	0.476 and -0.598 $e.Å^{-3}$

Table 20. Selected bond lengths (Å) and angles (°) of **12**

Bond	Length	Bond	Length
Ge(1)-O(1)	1.820(1)	O(1)-Ge(1)-O(2)	94.24(2)
Ge(1)-O(2)a	1.976(1)	O(1)-Ge(1)-O(2)a	94.70(2)
Ge(1)-O(2)	1.982(2)	O(2)-Ge(1)-O(2)a	75.11(2)
O(1)-C(1)	1.439(1)	C(1)-O(1)-Ge(1)	124.70(4)
O(2)-C(8)	1.462(2)	C(8)-O(2)-Ge(1)	126.80(4)
O(2)-Ge(1)	1.982(2)	C(8)-O(2)-Ge(1)a	122.27(4)
		Ge(1)-O(2)-Ge(1)a	104.89(2)

5. Reduction of $Ge\{N(SiMe_3)_2\}_2$ by $[H_2Al(OR)]_2$ (R = ^{t}Bu, ^{c}Hex*Me*-1)

5.1. Synthetic Aspects of the Reactions

In the previous section alkoxide ligands were substituted for *bis*-(*tri*-methylsilyl)amide ligands in a simple one step reactions between $Ge\{N(SiMe_3)_2\}_2$ [162, 164] and the corresponding alcohols. The bis-(*tri*-methylsilyl)amide ligand is chemically labile and suitable to be replaced with other ligands. In this section the reduction reaction between $Ge\{N(SiMe_3)_2\}_2$ and $[H_2Al(OR)]_2$ (R = ^{t}Bu or ^{c}Hex*Me*-1) in a 1:1 molar ratio will be presented.

The reactions between $Ge\{N(SiMe_3)_2\}_2$ and $[H_2Al(OR)]_2$ (R = ^{t}Bu or ^{c}Hex*Me*-1) were carried out at room temperature. The reactions occurred within an hour after addition of ethereal solution of alkoxyalane into an ethereal solution of $Ge\{N(SiMe_3)_2\}_2$ under constant stirring. However, the reaction mixture was stirred for approximately three hours to achieve completion of the reactions. The yellow colour of the germanium amide solution disappeared immediately as soon as all the alkoxyalane were dropped into it. The solutions were condensed into $1/4^{th}$ of its original volumes by removing the volatiles under vacuum. The condensed solutions were placed in refrigerator at +4°C and colourless crystals were obtained after one week. The detailed analysis of the final products by NMR, IR and single crystal X-ray diffraction analysis reveals that the compounds possess the general formula $[HAl(\mu\text{-}OR)(N\acute{R}_2)]_2$ (R = ^{t}Bu **14** or ^{c}Hex*Me*-1 **15**). The reactions routes are summarized according to the following reaction scheme (Scheme 1.7).

When the reaction mixtures were condensed into smaller volumes by removing the volatiles under low pressure, the colour of the solutions turned pale yellow. The yellow colours of the solutions may be due to the suspension of Ge nano-particles. Alkoxyalanes are stronger reducing agents [188]. Therefore, it is assumed that Ge^{+2} have been reduced to Ge^0 which is suspended in the solution mixture (Eq. 1.4). However, neither the Ge^0 nano-particles have been isolated nor their isolation has been taken seriously, as the aim was not to prepare Ge nano-particles. The crystals isolated from the reactions mixtures were analysed by single crystal X-ray diffraction as well as by various spectroscopic techniques.

$$Ge\{N(SiMe_3)_2\}_2 + [H_2Al(O^tBu)]_2 \longrightarrow [HAl(O^tR)\{N(SiMe_3)_2\}_2]_2 + H_2 + Ge^0 \quad (1.4)$$

Where R = *tert*-butyl **14** and/or 1-methylcyclohexyl **15**

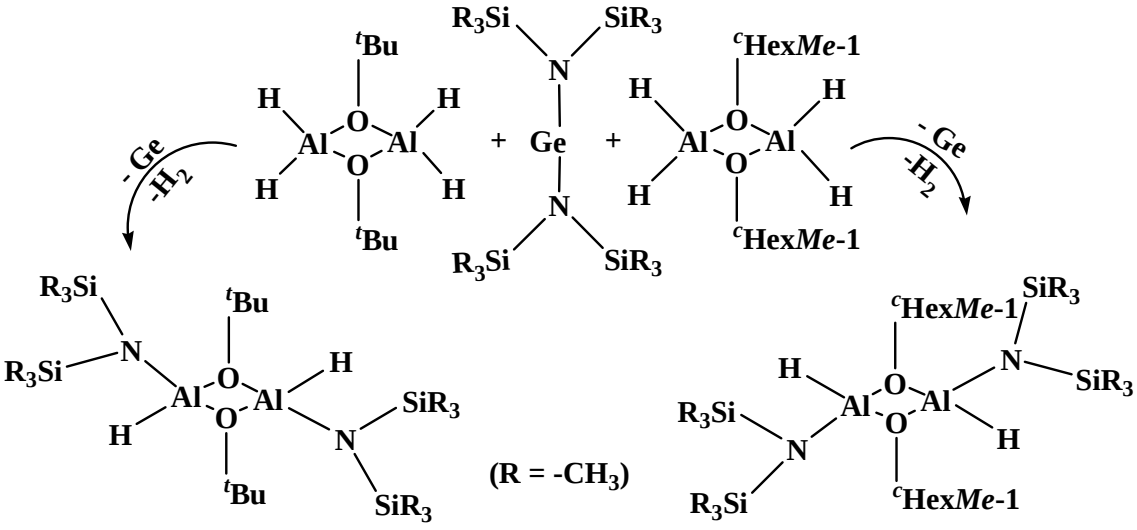

Scheme 1.7. Schematic representation of reactions between $Ge\{N(SiMe_3)_2\}_2$ and $[H_2Al(OR)]_2$

5.2. Spectroscopic Characterization

The compounds obtained of the general formula, $[HAl(\mu\text{-}OR)(N\acute{R}_2)]_2$ (R = *tert*-butyl **14** or 1-methylcyclohexyl **15** and Ŕ = $SiMe_3$) were characterized by NMR and IR spectroscopy. Figure 1.40 gives the ^{1}H-NMR spectra of compound **14** (blue) and **15** (red). ^{1}H-NMR spectrum of compound **14** gives peaks for three chemically different protons at 1.42 ppm, 0.42 ppm and 0.40 ppm. The last two peaks seem to be overlapped with a broad base and sharp two well resolved tips. The first peak at 1.42 ppm is due to the methyl protons of the *tert*-butyl group while the other two peaks are due to the methyl protons of the *tri*-methylsilyl group. Basically, there should be a single peak for the protons of *tri*-methylsilyl groups because all the six methyl groups are chemically identical. However, the appearance of two peaks is due to the lack of rotation along Al–N bond which is restricted by the higher steric

demand of the *bis*-(*tri*-methylsilyl)amide group. Therefore, the two *tri*-methylsilyl groups differ and give two different peaks. This behaviour of the *tri*-methylsilyl groups was also observed in ^{13}C NMR spectrum in which parallel peaks for the chemically equivalent carbons have been obtained. The ^{13}C NMR spectrum gives peaks for *tert*-butyl entity of compound **14** at 77.3 ppm and 31.4 ppm for α-carbon and methyl carbons, respectively. A pair of peaks appears at 5.7 ppm and 5.2 ppm for the methyl carbons of the *bis*-(*tri*-methylsilyl)amide moiety. The same compound was also reported by veith *et. al*. [138] during the reduction reaction of $Pb\{N(SiMe_3)_2\}_2$ [189] with $[H_2Al(OR)]_2$ [28] to produce Pb nano particles. The NMR data of compound **14** match well with that reported in literature [138].

Compound **15** shows the same structural characteristics in solution as showed by compound **14**. The NMR spectra were recorded in deutrated benzene at room temperature. The ^{1}H NMR spectrum gives peaks at 0.45 ppm and 0.46 ppm for the *tri*-methylsilyl protons. The two peaks appear due to lack of rotation along the Al-N bond. The rotation along Al-N bond is hindered by the higher steric demand of the *bis*-(*tri*-methylsilyl)amide group [138]. The peak appears at 1.50 ppm is for the methyl protons of the 1-methylcyclohexyl entity while the peaks appear in the range of 1.03-2.05 ppm are for the protons of the cyclohexyl ring. The restriction of rotation along the Al-N bond has been also confirmed by ^{13}C NMR spectroscopy. The ^{13}C NMR spectrum gives parallel peaks at 5.7 ppm and 5.3 ppm for the methyl carbon of the *bis*-(*tri*-methylsilyl)amide group. Single peaks appear for α-carbon and methyl carbon of the 1-methylcyclohexyl entity at 80.5 ppm and 29.6 ppm, respectively. Single peaks are also observed for the rest of the carbon of 1-methylcyclohexyl. The NMR spectra of compound **15** are in good agreement to that of compound **14** and the reported compounds [138]. The ^{1}H NMR spectra of compound **14** as well as **15** do not give peaks for hydrogen atoms bonded to Al. The peaks are too broad to be observed due to the asymmetrical geometry and quadruple moment of Al atoms [157].

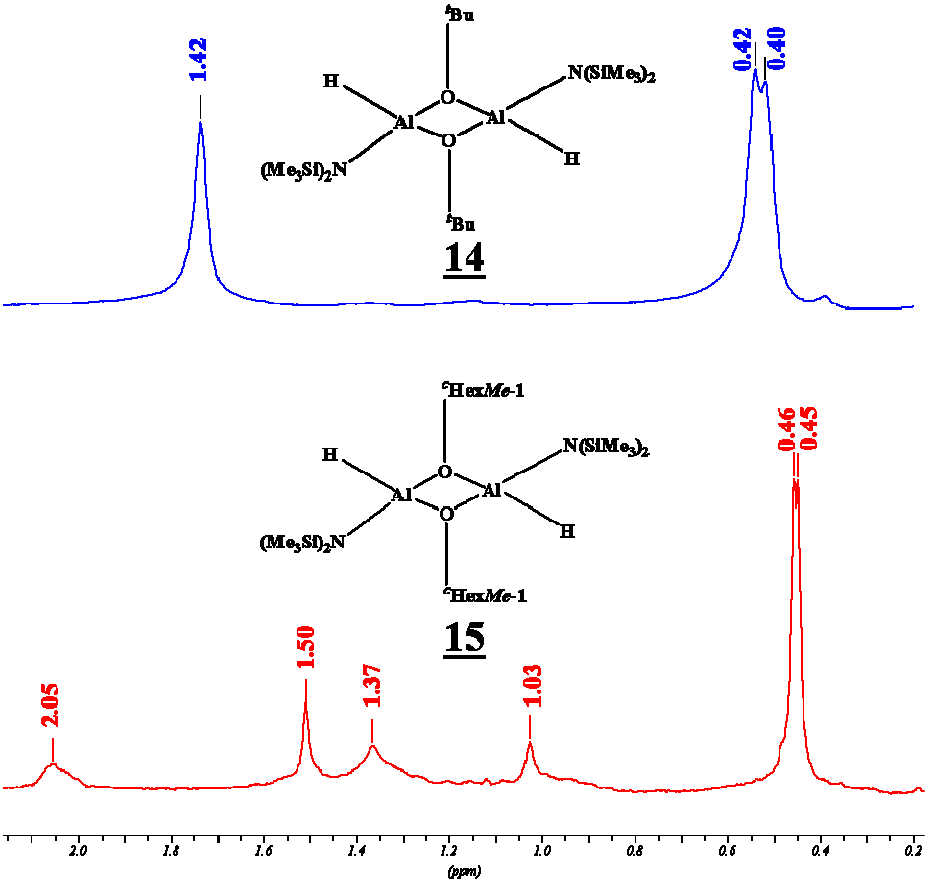

Figure 1.40. ^{1}H-NMR spectra of compounds **14** (blue) and **15** (red)

The Al-H bonds in compounds **14** and **15** were confirmed by IR spectroscopy. Figure 1.41 gives the IR spectra of compounds **14** (red) and **15** (blue). The IR spectra give sharp and characteristic peaks for the Al–H stretching vibrations at 1873 cm^{-1} and 1866 cm^{-1} for compounds **14** and **15**, respectively. The peaks correspond well to that of monoalkoxyalanes, for example $[HAl(O^tBu)_2]_2$ [28].

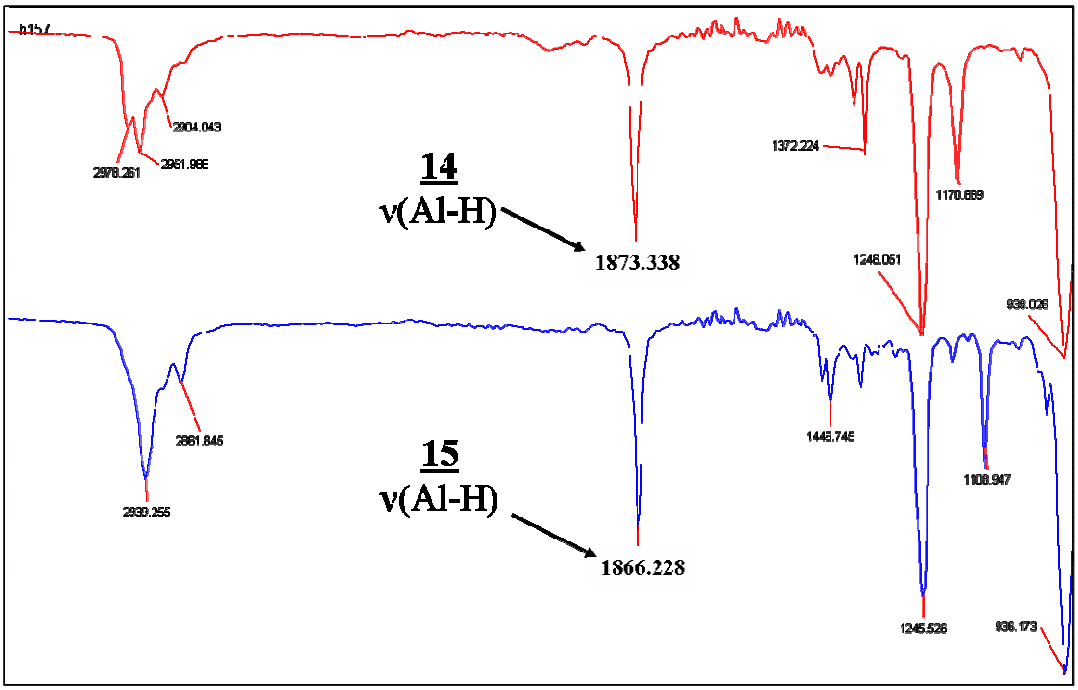

Figure 1.41. IR spectra of compounds **14** (red) and **15** (blue)

5.3. Solid State Structures

Small amounts of compounds **14** and **15** were dissolved in approximately 5 mL diethyl ether and kept in refrigerator at +4°C for crystallization. Colourless crystals were appeared in the solution after 24 hours. Suitable single crystals were selected and mounted into the X-ray diffractometer. The crystals structures were determined at approximately 152K. The structures were solved and refined by appropriate methods using SHELLX software packages [149]. The hydrogen atoms were determined by isotropic and all the non-hydrogen atoms were determined by anisotropic thermal parameters.

Figure 1.42 gives the crystal structure of compound **14**. Veith *et. al.* [138] reported the same structure obtained during the reduction of $Pb\{N(SiMe_3)_2\}_2$ [189] with $[H_2Al(O^tBu)]_2$ [28] to produce Pb nano particles. Therefore, the structural parameters are exactly the same as were reported. Here we are only reproducing the same structure to explained the process since the amide used is Ge(II) amide instead of Pb(II) amide. Besides, the bond lengths and angles in **14** are different to that of reported [138] which are shown in Table 22.

The relevant data of compound **14** are organized in Table 21 and the pertinent bond angles and bond lengths are summarized in Table 22. The compound crystallizes belongs to triclinic crystal system in $P2_1/c$ space group. The structure is quite unique in the sense that there are only very few known compounds [126, 190] in which a single Al centre is tetra-coordinated with H, O and N.

The centrosymmetric (point symmetry, C_i) molecular structure of **14** is composed of a central four membered Al_2O_2 cyclic ring which is similar as that in its parent compound $[H_2Al(OtBu)]_2$ [28]. The hydrides and amides lignads are trans-oriented to each other at the Al_2O_2 cyclic ring. No *cis*-isomer has been obtained in solid state. The bridging Al–O bond lengths are nearly equal having values of 1.842(2) Å and 1.843(1) Å and corresponds to those reported for structurally equivalent compounds [126, 170, 191-196]. The bridging Al-O bond distances are larger by approximately 0.03Å compared to that in $[H_2Al(OtBu)]_2$ [28]. It may be due to the substitution of bulky *bis*-(*tri*-methylsilyl)amide groups for lesser bulky hydrides. The terminal Al–N bond lengths are equal having value of 1.824(1) Å and are in good agreement to that reported for structurally identical compounds [80, 170, 190-196]. The terminal Al-H bond lengths are also equal having values of 1.520(1)Å and corresponds well to that of *mono*- and *bis*-(*tert*-butoxy)alanes [28].

The acute angle, as expected, is observed at Al centre in the Al_2O_2 four membered cyclic ring having value of 80.80(4)°. The O-Al-O and Al-O-Al bond angles are approximately the same as those in $[H_2Al(OtBu)]_2$ [28]. It indicates that the substitution of *bis*-(*tri*-methylsilyl)amide entity for hydride ligands does not affect the central Al_2O_2 ring except for slight increase in the Al-O bond lengths. The two methylsilyl (-$SiMe_3$) groups attached to the N centre are inequivalent which is deduced from the difference in Si-N-Al angles and N-Si bond lengths. The Si1-N1 and Si2-N1 bond lengths are 1.749(1) Å and 1.736(2) Å, respectively. While the Si1-N1-Al1 and Si2-N1-Al1 bond angles are 113.95(1)° and 125.56(2)°, respectively. The difference between the two methylsilyl entities attached to a common N atom is due to the lack of free rotation along the Al-N bond. The free rotation along the Al-N bond is hindered by the larger bulk of the *bis*-(*tri*-methylsilyl)amide group. The oxygen atom has trigonal planar geometry as usual which is deduced from the sum of angles around it amounting to 359.42(0)°.

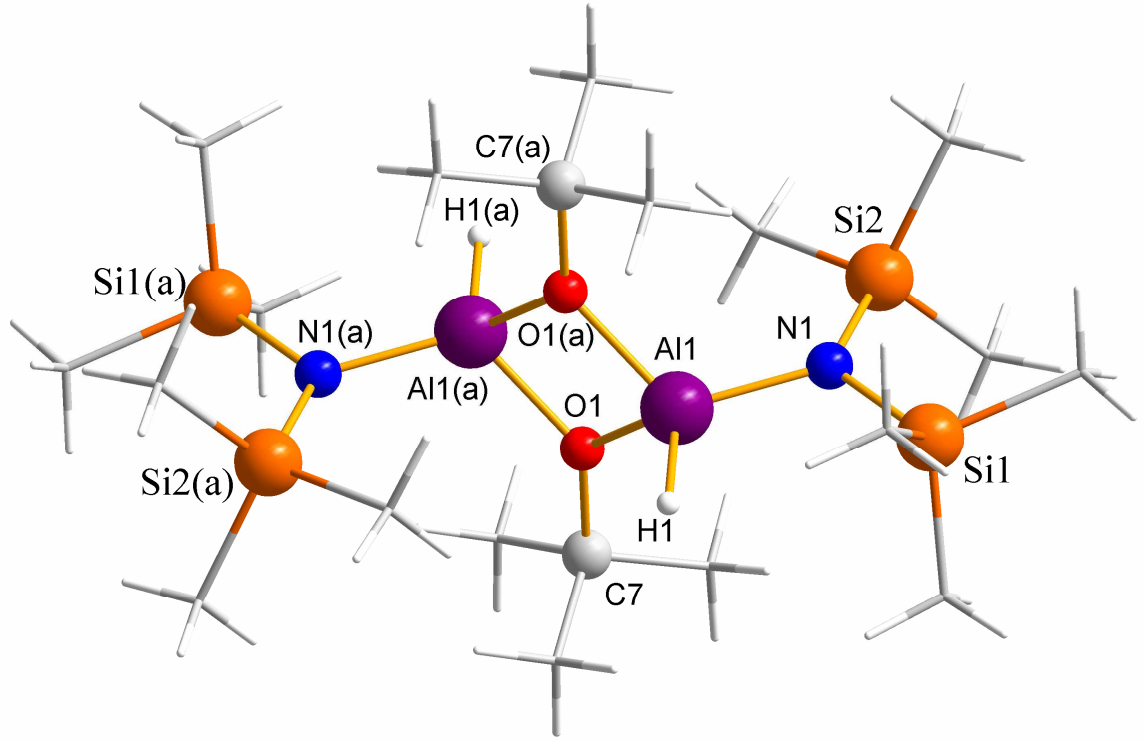

Figure 1.42. Molecular structure of compound [HAl(O^{t}Bu){N(SiMe$_3$)$_2$}]$_2$ **14**; the sticks show carbon and/or hydrogen atoms

Table 21. Relevant crystal data of [HAl(O^{t}Bu){N(SiMe$_3$)$_2$}]$_2$ **14**

Identification code	**[HAl(O^{t}Bu){N(SiMe$_3$)$_2$}]$_2$**
Empirical formula	C20 H56 Al2 N2 O2 Si4
Formula weight	522.99
Temperature	152(2) K
Wavelength	0.71073 Å
Crystal system	Monoclinic
Space group	P2$_1$/c
Unit cell dimensions	a = 11.168(2) Å b = 14.352(2) Å c = 10.239(1) Å α= 90°. β= 99.95(2)°. γ = 90°.
Volume	1616.45(12) Å^3

Z	2
Density (calculated)	1.075 Mg/m^3
Absorption coefficient	0.256 mm^{-1}
F(000)	576
Crystal size	0.57 x 0.24 x 0.11 mm^3
Theta range for data collection	1.85 to 29.38°.
Index ranges	-15<=h<=15, -18<=k<=19, -12<=l<=14
Reflections collected	17495
Independent reflections	4450 [R(int) = 0.0492]
Completeness to theta = 29.38°	100.0 %
Absorption correction	Multiscan
Max. and min. transmission	0.9724 and 0.8675
Refinement method	Full-matrix least-squares on F^2
Data / restraints / parameters	4450 / 0 / 149
Goodness-of-fit on F^2	1.031
Final R indices [I>2sigma(I)]	R1 = 0.0351, wR2 = 0.0875
R indices (all data)	R1 = 0.0511, wR2 = 0.0954
Largest diff. peak and hole	0.371 and -0.238 $e.Å^{-3}$

Table 22. Selected bond lengths (Å) and bond angles (°) of compound **14**

Bond	**Length**		**Bond**	**Angle**	
	14	**[138]**		**14**	**[138]**
Al(1)-N(1)	1.824(1)	1.830(2)	N(1)-Al(1)-O(1)a	118.63(5)	118.92(7)
Al(1)-O(1)a	1.842(2)	1.848(1)	N(1)-Al(1)-O(1)	119.94(5)	120.21(7)
Al(1)-O(1)	1.843(1)	1.847(1)	O(1)-Al(1)-O(1)a	80.80(4)	80.59(7)
Al(1)-Al(1)a	2.806(1)	-	Al(1)-O(1)-Al(1)a	99.20(4)	99.41(7)
O(1)-C(7)	1.477(1)	1.481(2)	C(7)-O(1)-Al(1)a	131.01(8)	-
Al(a)-H(1)	1.521(2)	1.516(6)	C(7)-O(1)-Al(1)	129.20(1)	-
N(1)-Si(1)	1.749(1)	1.743(2)	Si(1)-N(1)-Al(1)	113.95(1)	114.0(1)
N(1)-Si(2)	1736(2)	1.757(2)	Si(2)-N(1)-Al(1)	125.56(2)	125.7(1)

Compound **15** has been crystallized into triclinic crystal system in P-1 space group and has similar structural features as those of compound **14** except the alkoxy group which is 1-mthylcyclohexoxy in **15** instead of *tert*-butoxy in **14**. The molecular structure of **15** is shown in Figure 1.43. The relevant crystal data are summarized in Table 23 and the pertinent bond lengths and angles are presented in Table 24. The molecule of **15** is centrosymmetric (point symmetry C_i). The *bis*-(*tri*-methylsilyl)amide and hydrogen atoms are *trans*-oriented at the four membered Al_2O_2 cyclic ring. The Al atoms are tetra-coordinated showing distorted tetrahedral geometry due to the ring. The bridging Al–O bond lengths are nearly equal having values of 1.836(2) Å and 1.845(1) Å and lie in the characteristic range [126, 170, 191-196]. The terminal Al–H bond lengths are equal having values of 1.655(1) Å. However, the Al-H bond lengths are longer than those observed in **14** and in alkoxyalanes [28]. It is due to the high uncertainty in prediction of the hydrogen position in XRD spectrum, especially in presence of larger groups. The terminal Al–N bond length is 1.823(1) Å and is comparable to that of compound **14** (1.824(1) Å) as well as those reported in literature [170, 190-196].

The acute angle, O–Al–Oa is 80.00(6)° which lie at Al atoms of the four membered Al_2O_2 cyclic ring as expected. The sum of angles around bridging oxygen atoms amounting to 359.06(1)° which shows that the oxygen atoms are sp^2 hybridized having trigonal planar geometries [80]. The methylsilyl moieties of the *bis*-(*tri*-methylsilyl)amide ligands are inequivalent deduced from the difference between Si-N bond lengths and Si-N-Al bond angles. The Si1-N1 and Si2-N1 bond lengths are 1.740(1) Å and 1.749(1) Å, respectively. While the Si1-N1-Al1 and Si2-N1-Al1 bond angles are 125.53(2)° and 114.18(1)°, respectively. The difference arises due to high bulk of the *bis*-(*tri*-methylsilyl)amide group which restricts the rotation along the Al–N bond.

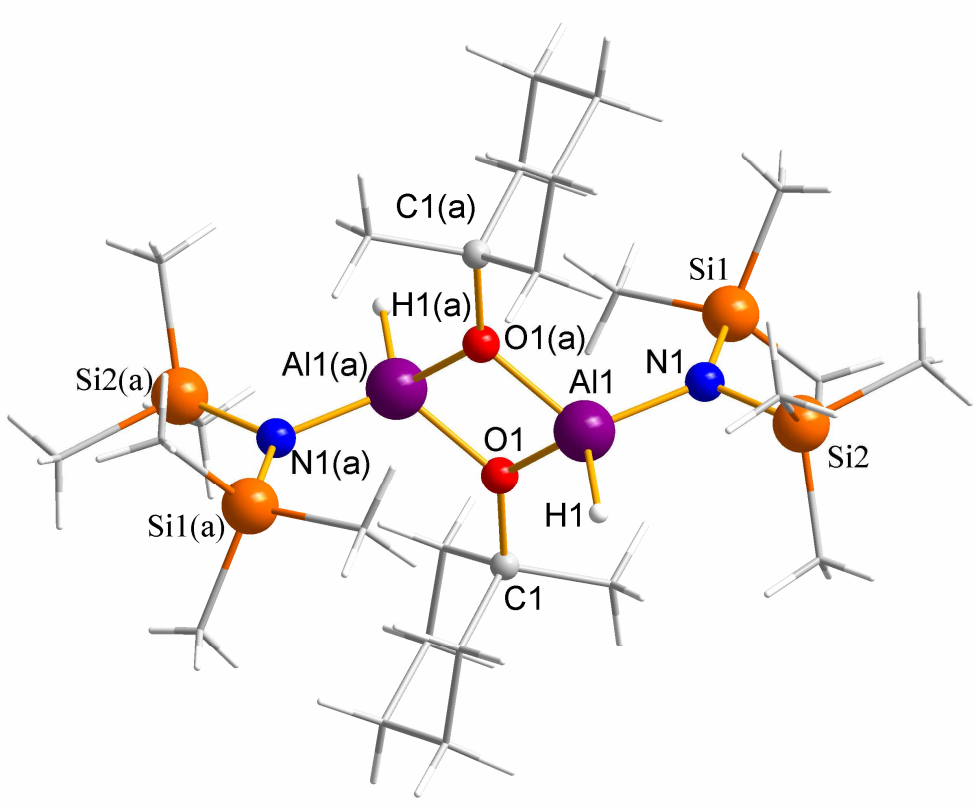

Figure 1.43. Molecular structure of compound [HAl(O^{c}Hex*Me*-1){N(SiMe$_3$)$_2$}]$_2$ **15**; the sticks represents carbon and/or hydrogen atoms

Table 23. Relevant crystal data of the compound **15**

Identification code	**[HAl(O^{c}Hex*Me*-1){N(SiMe$_3$)$_2$}]$_2$**
Empirical formula	C13 H32 Al N O Si2
Formula weight	301.56
Temperature	123(2) K
Wavelength	0.71073 Å
Crystal system	Triclinic
Space group	P-1
Unit cell dimensions	a = 9.135(2) Å
	b = 12.186(1) Å
	c = 17.577(2) Å
	α= 82.076(1)°.
	β= 77.642(1)°.

	γ = 70.006(1)°.
Volume	1791.64(6) $Å^3$
Z	4
Density (calculated)	1.118 Mg/m^3
Absorption coefficient	0.239 mm^{-1}
F(000)	664
Crystal size	0.37 x 0.21 x 0.13 mm^3
Theta range for data collection	1.19 to 27.94°.
Index ranges	-12<=h<=11, -16<=k<=16, -22<=l<=23
Reflections collected	31958
Independent reflections	8517 [R(int) = 0.0538]
Completeness to theta = 27.94°	99.4 %
Absorption correction	Multiscan
Max. and min. transmission	0.9687 and 0.9176
Refinement method	Full-matrix least-squares on F^2
Data / restraints / parameters	8517 / 0 / 581
Goodness-of-fit on F^2	1.029
Final R indices [I>2sigma(I)]	R1 = 0.0467, wR2 = 0.1209
R indices (all data)	R1 = 0.0619, wR2 = 0.1309
Largest diff. peak and hole	1.418 and -0.318 $e.Å^{-3}$

Table 24. Selected bond lengths (Å) and bond angles (°) of compound **15**

Bond	Length	Bond	Angle
Al(1)-N(1)	1.8236(18)	N(1)-Al(1)-O(1)	120.34(7)
Al(1)-O(1)	1.8359(14)	N(1)-Al(1)-O(1)(a)	118.87(7)
Al(1)-O(1)(a)	1.8451(14)	O(1)-Al(1)-O(1)(a)	80.00(6)
Al(1)-Al(1)(a)	2.8197(12)	C(1)-O(1)-Al(1)	129.57(12)
O(1)-Al(1)(a)	1.8451(14)	C(1)-O(1)-Al(1)(a)	129.49(12)
O(1)-C(1)	1.471(2)	Al(1)-O(1)-Al(1)(a)	100.00(7)
Al(1)-H(1)	1.6551(0)	N(1)-Al(1)-H(1)	108.131(0)

N(1)-Si(1)	1.740(1)	O(1)-Al(1)-H(1)	111.297(1)
N(1)-Si(2)	1.749(1)	O(1)(a)-Al(1)-H(1)	115.200(1)
		Si(1)-N(1)-Al(1)	125.53(2)
		Si(2)-N(1)-Al(1)	114.18(1)

It is quite interesting that only one of the hydrides has been replaced with the *bis*-(*tri*-methylsilyl)amide group. M. Veith *et. al.* tried all the possible reaction routes to replace the second hydride but all in vain [138]. However, the reduction reaction between $Me_2Si(N^tBu)_2Sn$ and $[H_2Al(OR)]_2$ resulted into complete removal of the hydrides [197]. The different reaction behaviour of $[H_2Al(OR)]_2$ with $Ge\{N(SiMe_3)_2\}_2$ and $Me_2Si(N^tBu)_2Sn$ may be due to the different steric demand of $(Me_3Si)_2N$ and $Me_2Si(N^tBu)_2$.

6. $[M\{(OR)_{3-n}AlH_n\}_2]$ (M = Ge(II), Ni(II), Eu(II); n = 0, 1, 2)

Hydride-modified heterometallic alkoxides of the general formula $[M\{(OR)_{3-n}AlH_n\}_2]$ are interesting single source precursor for the preparation of new material. The manifold advantages of these compounds especially their use in chemical vapour deposition (CVD) and Sol-Gel techniques for the preparation of nano-materials is highly desirable. But the library of such compounds is nearly empty. The only compound of the type is $[Mg\{(O^tBu)_2AlH_2\}_2]$ which was reported in 1999 by M. Veit *et. al.* [29]. The compound, $[Mg\{(O^tBu)_2AlH_2\}_2]$ was used for the synthesis of $MgAl_2O_4$ spinel by CVD technique and has showed manifold advantages as a single source precursor over the conventional molecules used for the synthesis of MAl_2O_4 type spinels. Low decomposition temperatures, high purity, homogeneity and desired elemental composition of the final product are some highly attractive features of these molecules as single source precursors for material synthesis.

Tries were made in this work to extend and utilize the concept for the synthesis of $[M\{(O^tBu)_2AlH_2\}_2]$ compounds. The metals used in this study were Ge, Ni, and Eu in oxidation state +2. Although none of the efforts brought fruit but the study gave some very useful insights into future work. The following sections will give the details of the synthetic strategies used during the study and will elaborate some crucial points to be consider in future works.

6.1. Efforts for the Synthesize [Ge{$H_nAl(OR)_{3-n}$}$_2$] (n = 0, 1 or 2; R = ^{t}Bu or ^{c}Hex*Me*-1)

Different reaction strategies were used to get hydride modified heterometal alkoxides of Al with Ge(II) having general formula, [Ge{$H_nAl(OR)_{3-n}$}$_2$] (where n = 0, 1, 2 and R = ^{t}Bu, ^{c}Hex*Me*-1). The salt elimination reaction has been utilized previously but did not work [121]. Therefore, we tried some alternative routs, specifically the condensation type reactions.

At first place the reactions between germanium(II) *bis*-(*tri*-methylsilyl)amide, Ge{$N(SiMe_3)_2$}$_2$ and [$H_nAl(OR)_{3-n}$]$_2$ (where n = 0, 1, or 2 and R = ^{t}Bu or ^{c}Hex*Me*-1) have been brought at ambient conditions. The Ge{$N(SiMe_3)_2$}$_2$ reactant was prepared according to the well known and reported routes [163, 198]. The selection of Ge{$N(SiMe_3)_2$}$_2$ as a reactant has the advantage of chemically labile Ge-N bonding. The low enthalpy of Ge-N bond [71] could work as driving force for the reaction to occur at ambient conditions.

As shown in the previous section the reaction between Ge{$N(SiMe_3)_2$}$_2$ and [$H_2Al(OR)$]$_2$ resulted into ligand exchange reaction between the two metal centres. The *bis*-(*tri*-methylsilyl)amide groups transfer from the Ge centre to the Al centre. The reaction is feasible in context of the bond enthalpies. The lower Ge-N bond enthalpy force the reaction to occur compared to the higher Al-N bond enthalpy. One of the hydrogen was replaced by the *bis*-(*tri*-methylsilyl)amide group while the second one remained intact. The molar ratio between Ge{$N(SiMe_3)_2$}$_2$ and [$H_2Al(OR)$]$_2$ was changed from 1:1 to 2:1 to remove the second hydride. But the second hydrogen remained intact even using excess of Ge{$N(SiMe_3)_2$}$_2$ as well as refluxing the reaction mixture overnight (~ 24 hours). The reaction mixture was also refluxed for 48 hours but nothing happened to the second hydrogen. The bulky *bis*-(*tri*-methylsilyl)amide group retard the excess of second *bis*-(*tri*-methylsilyl)amide ligand to the Al centre. However, the addition of alcohol into the reaction mixture of Ge{$N(SiMe_3)_2$}$_2$ and [$H_2Al(OR)$]$_2$ in a way in which the molar ratio between alcohol and [$H_2Al(OR)$]$_2$ is 2:1 resulted into removal of the second hydrogen as well as *bis*-(*tri*-methylsilyl)amide ligands. As soon the alcohol was added into the reaction mixture of Ge{$N(SiMe_3)_2$}$_2$ and [$H_2Al(OR)$]$_2$ in appropriate molar ratio, a yellow residue settled down in the bottom of the reaction flask. The yellow residue was filtered off and the filtrate was collected into a clean flask and condensed under reduced pressure. The resulting condensed reaction mixture gives a complex NMR spectrum which upon analysis has shown [$Al(OR)_3$]$_2$ and $HN(SiMe_3)_2$ besides some unidentified species. The whole reaction process can be summarized according to the

following reaction scheme (scheme 1.8). The yellow residue left behind was thought to be Ge and/or its product which was insoluble in organic solvent as well as in water. The XRD measured for the yellow residue does not give a single peak which means that the residue was amorphous.

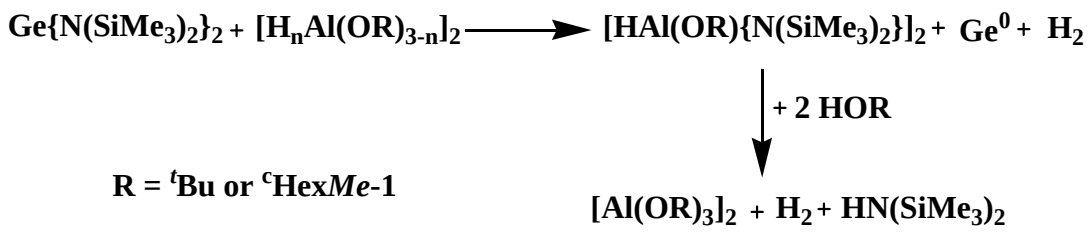

Scheme 1.8. Reduction of $Ge\{N(SiMe_3)_2\}_2$ by $[H_2Al(OR)]_2$

The unusual stability of Al-H bond in the above case increased the curiosity. Therefore, bis(alkoxy)aluminium hydride, $[HAl(OR)_2]_2$ was reacted with germanium(II) *bis*-(*tri*-methylsilyl)amide in a 1:1 ratio. Contrarily to the observations in the above reaction in which the colour of germanium(II) *bis*-(*tri*-methylsilyl)amide lost immediately upon addition of monoalkoxyalane, the colour of the reaction mixture remained unchanged. Even at refluxing the mixture for 48 hours nothing happened to the colour of the solution. The different volatile components of the reaction mixture were separated by fractional distillation and the solid residue left behind in the flask was purified by sublimation. The NMR spectra confirmed the distilled fractions as diethylether and $Ge\{N(SiMe_3)_2\}_2$. The NMR of the solid residue was the same as that of the starting materials, $[HAl(OR)_2]_2$. The observations show that the reactants remained unreacted (eq. 1.5).

(1.5)

To the reaction mixture shown in equation 7, alcohol were added in a proportion to give molar ratio 2:1 between alcohol and $[HAl(OR)_2]_2$. As soon as a small portion of alcohol was added into the reaction mixture from a dropping funnel, a yellow coloured solid residue precipitated out. The solid residue was filtered off which was completely insoluble in the common organic solvents. The yellow coloured solid residue was analysed by powder XRD which shows that

the residue is amorphous. The filtrate obtained from the reaction mixture was condensed under reduced pressure and analysed by NMR spectroscopy. The NMR spectra give clear peaks which corresponds to that of compounds $[Al(OR)_3]_2$ and $HN(SiMe_3)_2$. The compound $HN(SiMe_3)_2$ was fractionally distilled at 45°C leaving behind white powder of $[Al(OR)_3]_2$. The two compounds were confirmed by NMR spectroscopy. The same reaction was also performed under cooling at approximately -29°C. As soon as the alcohol were added into the mixture of $[Al(OR)_3]_2$ and $HN(SiMe_3)_2$ at -29°C in appropriate proportion, the colour of the solution turned colourless. The reaction mixture was followed by NMR spectroscopy and the NMR spectra measured gives peaks for $Ge(OR)_2$ beside those of $[HAl(OR)_2]_2$. However, as soon as the reaction mixture was allowed to warm up to the room temperature, yellow residue precipitated out which was filtered off and the filtrate was condensed under reduced pressure. The NMR spectra of the condensed mixture were shown the same peaks as were observed for the reaction carried out at room temperature. it means that alcohol first react with $Ge\{N(SiMe_3)_2\}_2$ giving $Ge(OR)_2$. The $Ge(OR)_2$ is then reduced by $[HAl(OR)_2]_2$ giving $[Al(OR)_3]_2$, Ge^0 and H_2 according to the following reaction scheme (Scheme 1.9). However, the XRD diffractogram did not show patterns for metallic Ge.

$$\mathbf{Ge\{N(SiMe_3)_2\}_2 + 2\ HOR \longrightarrow Ge(OR)_2 + 2\ HN(SiMe_3)_2}$$

$$\mathbf{Ge(OR)_2 + [HAl(OR)_2]_2 \longrightarrow [Al(OR)_3]_2 + Ge^0}$$

R = ^{t}Bu or ^{c}Hex*Me*-1

Scheme1.9. Reduction of $Ge\{N(SiMe_3)_2\}_2$ by $[HAl(OR)_2]_2$

The reaction between $Ge\{N(SiMe_3)_2\}_2$ and $[Al(O^tBu)_3]_2$ has been performed but no reaction was observed. The two reactants that is $Ge\{N(SiMe_3)_2\}_2$ and $[Al(O^tBu)_3]_2$ were mixed together in a 1:1 ratio and stirred for approximately 4 hours at room temperature. The colour of the reaction mixture remained unchanged. The solvent were removed under reduced pressure by condensing into a cold trap giving a bright red colour liquid. The obtained red coloured liquid was distilled at 45°C separating intense red colour liquid compound and leaving behind white powder. The red liquid separated by distillation from the reaction

mixture was characterized by NMR spectroscopy and identified as $Ge\{N(SiMe_3)_2\}_2$. The white solid residue was sublimed at approximately 90°C and characterized by NMR as $[Al(O^tBu)_3]_2$. It indicates that the two reactants remained unreacted. In a second attempt, the reaction mixture prepared by the addition of $Ge\{N(SiMe_3)_2\}_2$ and $[Al(O^tBu)_3]_2$ in a 1:1 molar ratio was refluxed for approximately 48 hours. However, the results were no different than those observed at room temperature. No reaction was occurred at elevated temperatures too (eq. 1.6).

$$\mathbf{Ge\{N(SiMe_3)_2\}_2 + [Al(OR)_3]_2} \not\longrightarrow \qquad (1.6)$$

tert-Butanol was added into the stoichiometric reaction mixture of $Ge\{N(SiMe_3)_2\}_2$ and $[Al(O^tBu)_3]_2$ in equation 8. The molar ratio of *tert*-butanol and $[Al(O^tBu)_3]_2$ was kept 2:1, respectively. The colour of the solution disappeared as soon as a small amount of *tert*-Butanol was added into the reaction mixture of $Ge\{N(SiMe_3)_2\}_2$ and $[Al(O^tBu)_3]_2$. The whole reaction mixture was stirred for 4-5 hours at ambient conditions. When the volatiles were removed under reduced pressure, white powder was obtained in the reaction flask. Very clear ^{1}H-NMR spectrum was recorded for the obtained white powder giving three well resolved peaks at 1.52 ppm, 1.48 ppm and 1.42 ppm. The peaks at 1.52 ppm and 1.42 ppm are the characteristic peaks of the compound $[Al(O^tBu)_3]_2$ and the one at 1.48 ppm is that of $[Ge(O^tBu)_2]_2$. The powder was sublimed at 60°C under reduced pressure (10^{-2} mbar) for an hour and the ^{1}H-NMR spectrum recorded for the sublimed product gives only one peak at 1.48 ppm which is the characteristic of $[Ge(O^tBu)_2]_2$ (Figure 1.44). The peaks for the $[Al(O^tBu)_3]_2$ disappeared in the ^{1}H NMR spectrum of the sublimed product. The small characteristic peaks of $[Al(^tBu)_3]_2$ appeared in the spectrum of the sublime product indicates that very limited amount of $[Al(^tBu)_3]_2$ sublimed below 90°C which is its characteristics sublimation temperature [199-200]. The volatiles condensed into the cold trap was fractionally distilled and the NMR spectra of the two main fraction shows peaks for diethylether and *bis*-(*tri*-methylsilyl)amine. This observation could lead to summarize the reaction into the following reaction equation (Eq. 1.7).

$$\mathbf{Ge\{N(SiMe_3)_2\}_2 + [Al(OR)_3]_2 \xrightarrow[-\,2\,HN(SiMe_3)_2]{+\,2\,HOR} 1/2\,[Ge(OR)_2]_2 + [Al(OR)_3]_2} \qquad (1.7)$$

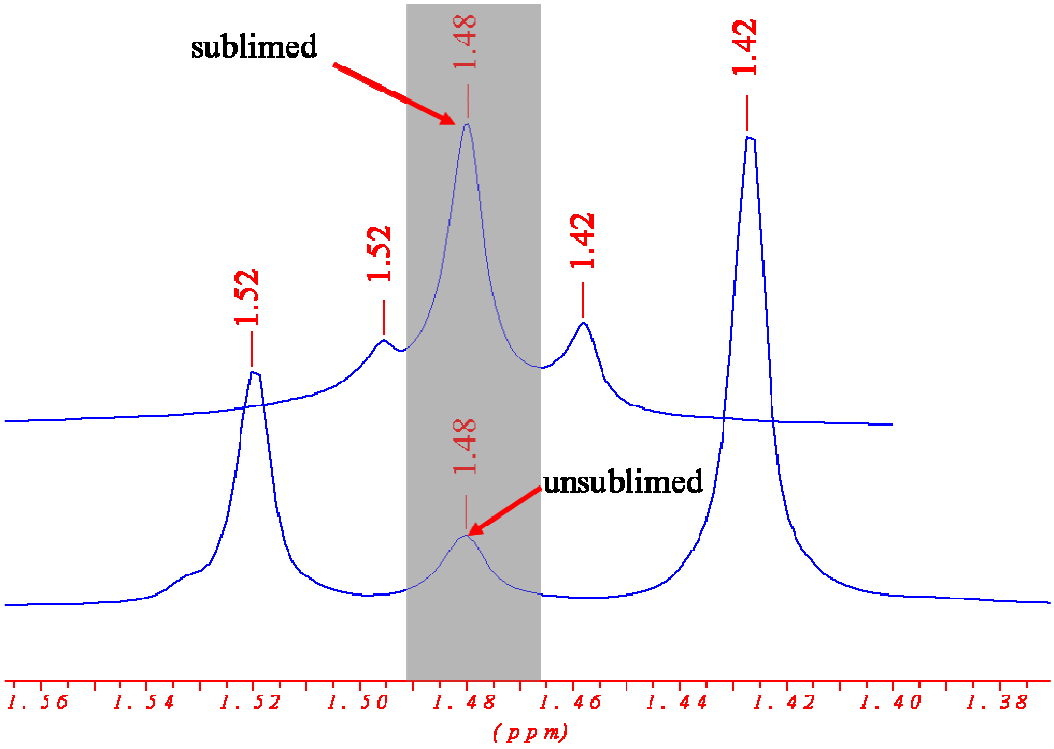

Figure 1.44. ^{1}H-NMR spectrum of the reaction mixture before and after sublimation

The reaction mixture of $[Al(O^tBu)_3]_2$ and $Ge\{N(SiMe_3)_2\}_2$ in a 1:1 molar ratio was refluxed for approximately 8 hours for any possible reaction. However, the white powder obtained upon removal of the volatiles was the mixture of $[Al(O^tBu)_3]_2$ and $[Ge(O^tBu)_2]_2$ and no reaction was observed. It means that the alcohols react with $Ge\{N(SiMe_3)_2\}_2$ giving $[Ge(O^tBu)_2]_2$. however, $[Ge(O^tBu)_2]_2$ and $[Al(O^tBu)_3]_2$ present in the reaction mixture does not react further. To check this phenomenon the reaction between pure $[Ge(O^tBu)_2]_2$ and $[Al(O^tBu)_3]_2$ was performed in diethyl ether, initially at room temperature and latter on at refluxing conditions. In both the reaction conditions, the reactants remained unreacted which was confirmed by NMR spectroscopy (Eq. 1.8).

$$\mathbf{[Ge(OR)_2]_2 + [Al(OR)_3]_2} \not\longrightarrow \qquad (1.8)$$

The observations indicates that is Ge(II) is susceptible to reduction in presence of *mono*- and *bi*-alkoxyalanes which work as reducing agent in the reaction.

6.2. Efforts for the Synthesize $[Ni\{H_2Al(O^tBu)\}_2]$

The synthetic efforts include a salt elimination reaction adopted from the earlier reported synthetic strategies [29]. Stoichiometric amounts of $NiCl_2$ suspended in diethyl ether and $LiAlH_2(O^tBu)_2$ (prepared by the addition of 2 molar solution of *tert*-butanol into 1 molar solution of $LiAlH_4$) were mixed together and stirred at room temperature for 6 hours. The addition of $NiCl_2$ gives rise to two remarkable observations. One the evolution of hydrogen as soon as the two reactants were mixed and second the colour of the solution turned black. After stirring for nearly six hours the solid residue was filtered off and was confirmed by XRD as LiCl. The residue is free of any sort of organic compounds which were confirmed by the IR spectroscopy. The IR spectrum does not give any peak for organic entities.

The filtrate was condensed under reduced pressure by removing the volatiles (mostly the solvent) into cold trap. The black solid obtained was sublimed at approximately 90°C and the sublimation gave colourless crystals leaving behind a fine black powder. ^1H and ^{13}C-NMR spectra measured for the colourless crystals shows peaks which corresponds to that of $[Al(OtBu)_3]_2$ (Figure 1.45). It means that the sublimed product is $[Al(OtBu)_3]_2$. The fine black powder was analysed by powder XRD and was confirmed as Ni. However, when the Ni powder was analysed by IR spectroscopy, peaks were observed for C-H stretching vibrations. It means that the Ni powder left behind after sublimation of $[Al(OtBu)_3]_2$ contains some unidentified compounds. All the efforts to isolate these by-products were failed. The fine Ni powder is air sensitive and reacts violently with the air as soon as is exposed to it. it may be due to presence of some compounds having Al-H bondigs.

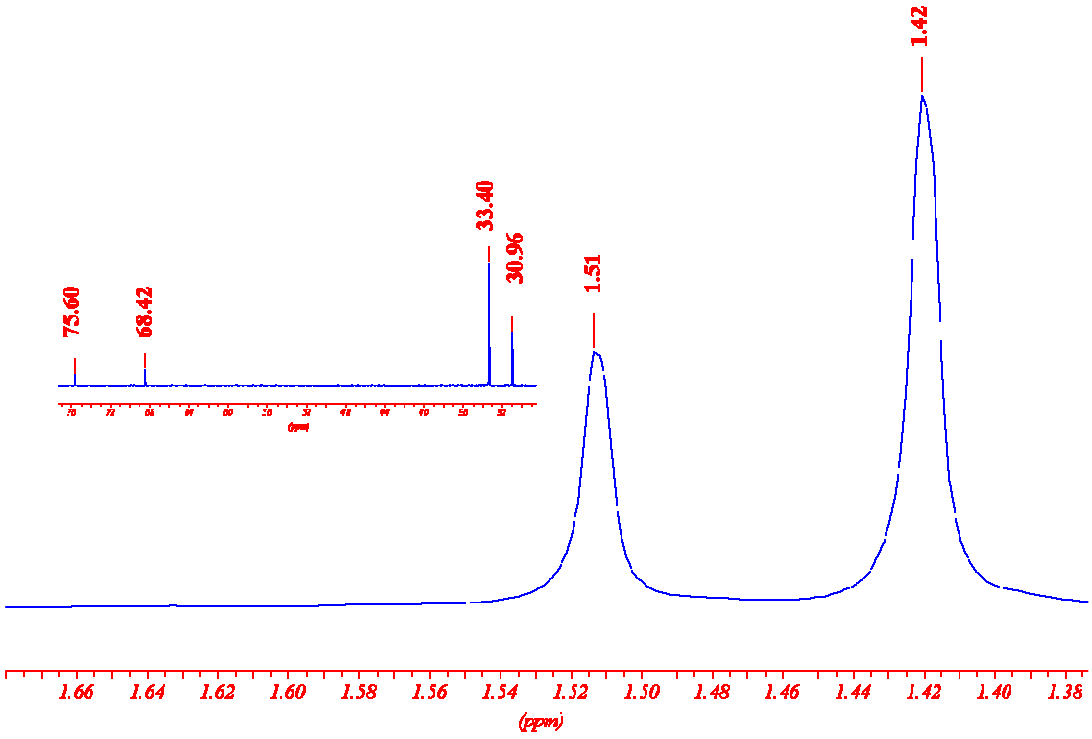

Figure 1.45. ^{1}H and ^{13}C NMR spectra of the sublimed product

The stoichiometric reaction mixture of $NiCl_2$ and $LiAlH_2(O^tBu)_2$ was prepared and refluxed for 8 hours. The addition of the reactants shown an immediate release of the hydrogen gas and the colour of the reaction mixture turned black. The solid residue was filtered off and was confirmed again as LiCl by XRD. The black powder obtained after removal of the volatiles was sublimed into fine colourless crystals of $[Al(O^tBu)_3]_2$ and the fine powder left behind was confirmed as Ni by powder XRD. Based upon these observations and results discussed so far, the following reaction scheme (scheme 1.10) was proposed. The Ni^{+2} reduce to Ni^0 which is dispersed in the solvent and difficult to isolate by simple filtration.

$$2LiAlH_4 + 4\,HO^tBu \longrightarrow 2LiAlH_2(O^tBu)_2$$

$$2LiAlH_2(O^tBu)_2 + NiCl_2 \longrightarrow Ni + 2LiCl + [Al(OtBu)_3]_2 + 2H_2 + \text{unidentified products}$$

Scheme 1.10. Schematic representation of the reaction between $LiAlH_2(O^tBu)_2$ and $NiCl_2$

6.3. Efforts for the Synthesis of [Eu{$H_2Al(O^tBu)$}$_2$]

Following salt elimination reaction procedures [29], 2 molar solution of $LiAlH_2(OtBu)_2$ (prepared by the mixing of $LiAlH_4$ and HO^tBu in a 1:2 ratio, respectively) was taken in the reaction flask with THF as solvent and was fed with a THF solution of EuI_2. The whole reaction mixture was stirred for approximately 8 hours. A solid residue precipitated out which was filtered off. The powder X-ray diffraction analysis of the solid residue confirmed only EuI_2. it means that no reaction has occurred and the reactants remained as such (eq. 1.9).

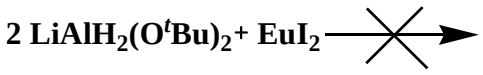

(1.9)

It was further proved by analyzing the filtrate obtained which was condensed into white powder by removing the volatiles under reduced pressure. The ^{1}H-NMR spectrum gives a single peak at 1.44 ppm corresponds to the methyl protons of the *tert*-butoxy group. This was further confirmed by ^{13}C-NMR where we have observed only two peaks at 69.34 ppm and 32.88 ppm which are characteristic of the two chemically different carbon of *tert*-butoxy group. Hydrides bonded to the Al centre have been confirmed by the IR spectroscopy in which characteristic peak was obtained for the Al–H stretching vibration at 1843 cm^{-1}.

In second try we have refluxed the reaction for approximately 8 hours. However, the reaction does not occurs which was confirmed by powder XRD, NMR and IR spectroscopy. It means that the reaction does not occur at the aforementioned conditions.

Summary

At the end, it is now easier to classify the different compounds obtained into different series based upon the similarities in molecular structures and their chemical compositions.

- In the first series are classified hydride-modified aluminium alkoxides, $[H_nAl(OR)_{3-n}]_x$ (R = ^{c}Hex and n = 2 **1** & **2**, 1 **3**; R = ^{c}Hex*Me*-1 and n = 2 **5**, 1 **6**), hydride-modified aluminium alkoxides amide, $[HAl(OR)(N\acute{R}_2)]_2$ (R = tBu **14**, ^{c}Hex*Me*-1 **15**; $\acute{R}$ = $Si(Me_3)_2$) and hydride-modified aluminium chloride alkoxides, $[ClAl(H)(O^cHe\mathit{Me}\text{-}1)]_2$ **8**. These compounds have two very common bases. One, all the compounds have central Al_2O_2 cyclic unit and second, in all these compounds there is at least one Al-H bond. Due to the electronic deficient aluminium centre, these compounds tend to associate via alkyloxo bridging to form dimers. Therefore, all the compounds possess one or more than one central four membered Al_2O_2 cyclic ring (Figure 50).

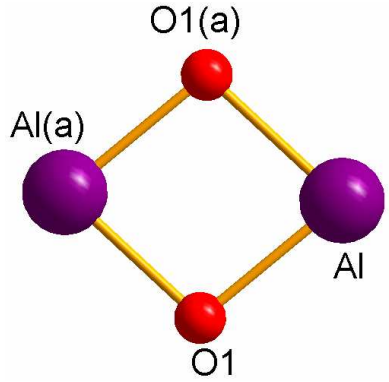

Figure 50. Central four membered Al2O2 cyclic rings

However, the degree of association depended upon the steric bulk of the alkyl moiety of the alkoxy groups. Therefore, the compounds range between dimers and polymers. For example *cyclo*-hexoxyaluminium hydrides are all polymers (Figure 51a) contrary to the 1-methylcyclohexoxyaluminium hydrides (Figure 51b) which are all dimers. It was also observed that the steric bulk in the immediate vicinity is more effective than that at some far away positions. For example $^tBu_2C(H)OAlH_2$ [128] is tetramer despite the bulkier $^tBu_2C(H)$ organic moiety contrary to compound **5** which is dimer. Instead of hydrogen, the presence of methyl group in the immediate vicinity in compound **5** impart more steric demand and block further association of the molecules.

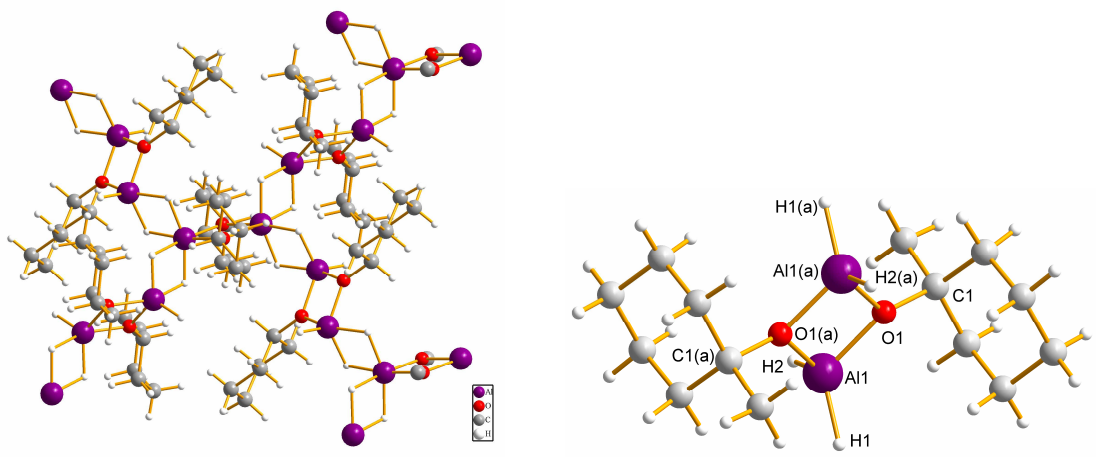

(a) **(b)**

Figure 51. (a) *cyclo*-hexoxy-, and (b) 1-methylcyclohexoxy-aluminium hydrides

The different terminal groups in these compounds oriented in *trans*-fashion to each other at the Al_2O_2 cyclic ring in solid state. For example hydrido-aluminium chloride alkoxides (Figure 52a) and hydrido-aluminium bis-(*tri*-methylsilyl)amide alkoxides. However, in solution hydrido-aluminium chloride alkoxides compounds showed some rearrangements to give another compound of the chemical formula, $[Cl_2Al(OR)]_2$ which was confirmed by ^{27}Al NMR spectroscopy. The two silyl groups of the bis-(*tri*-methylsilyl)amide moiety in the $[HAl(OR)\{N(SiMe_3)_2\}]_2$ compounds are different. The higher bulk is responsible for their different behaviour which retards the rotation along N-Al bond.

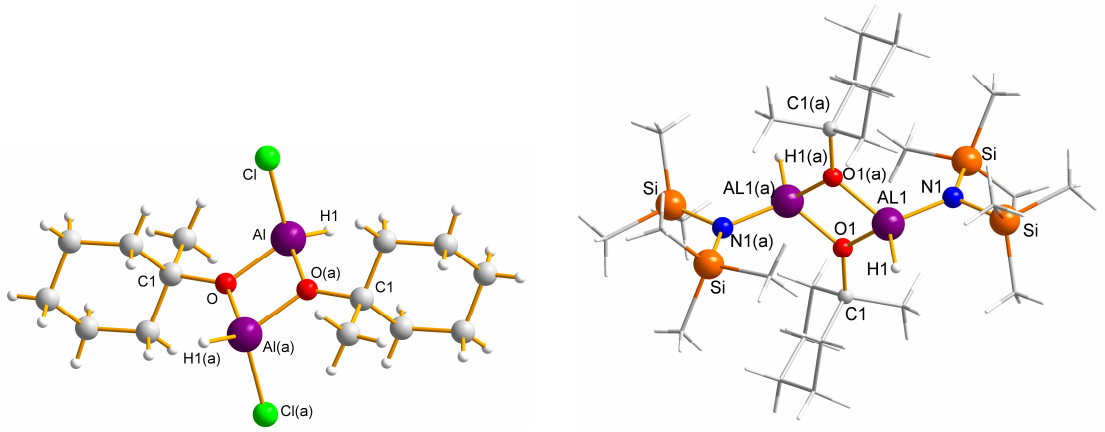

(a) **(b)**

Figure 52. Molecular structures of compound **8** and **15**

- The second series is comprised of aluminium alkoxides, $[Al(OR)_3]_n$ (R = ^{c}Hex **4**, ^{c}Hex*Me*-1 **7**; n = 4 **4**, 2 **7**). In this series the compounds are either dimers or oligomers. The dimers possess comparable structural features as were observed in hydride-modified alumnium alkoxides. There is a central four membered Al_2O_2 planar cyclic ring in all the compounds (Figure 53).

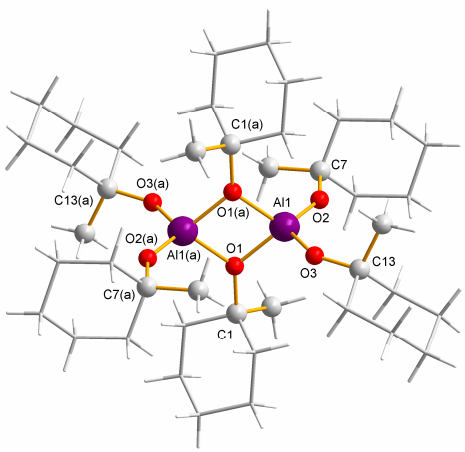

Figure 53. $[Al(OR)_3]_n$ (R = ^{c}Hex*Me*-1 and n = 2)

However, the less bulky hexoxy group gives a tetramer having a structure like Mitsubishi motif (Figure 54). This structure is similar to that reported for aluminium *iso*-propoxide [118]. The structure is composed of three $[Al(O^cHex)_4]^{-1}$ anions surrounding an Al^{+3} cation.

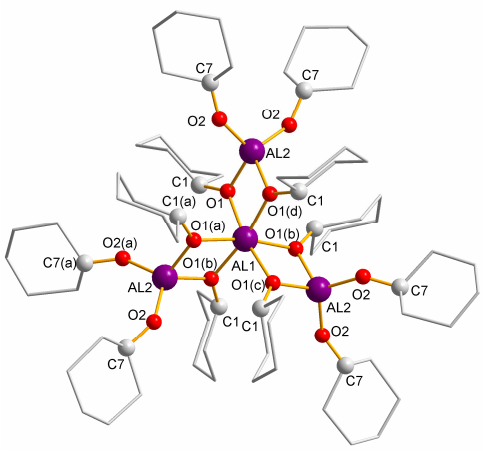

Figure 54. Tetramer structure of $[Al(OR)_3]_n$ (R = ^{c}Hex and n = 4)

- The third series comprises compounds having at least one Al-Cl bond. The compounds of general formula $[Cl_nAl(OR)_{3-n}]_2$ (R = ^{c}Hex*Me*-1; n = 1 **9**, 2 **10**) are all dimers having central four membered Al_2O_2 planar cyclic ring. For example $[Cl_2Al(O^cHexMe\text{-}1)]$ depicted in Figure 55. The intermolecular association as expected is due to the electronic deficient aluminium centre. The bulk of the alkyl moiety is sufficient to stop polymerization of the compound and comparable to that of *tert*-butyl. The different terminal groups are oriented in *trans*-fashion to each other around the Al_2O_2 ring in solid state. However, in solution both *cis*- and *trans*-isomers have been confirmed by NMR spectroscopy for compound **9**.

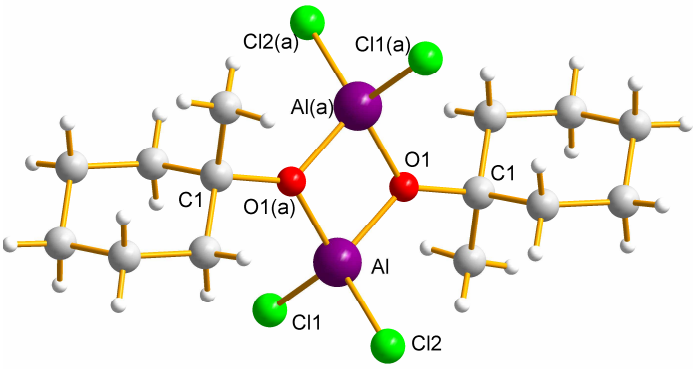

Figure 55. Dimeric structure of $[Cl_2Al(O^cHexMe\text{-}1)]$

- The fourth series of the compounds is comprised of the germanium(II) alkoxides having general formula, $[Ge(OR)_2]_2$ (R = ^{c}Hex **11**, ^{c}Hex*Me*-1 **12,** ^{i}Pr **13**). All the compounds are dimers in solid state having central Ge_2O_2 four membered cyclic ring (an example is given in Figure 56). Germanium is in +2 oxidation state in all the compounds having pyramidal geometry. The compounds are dimers in solution too which were confirmed by the solution NMR spectroscopy.

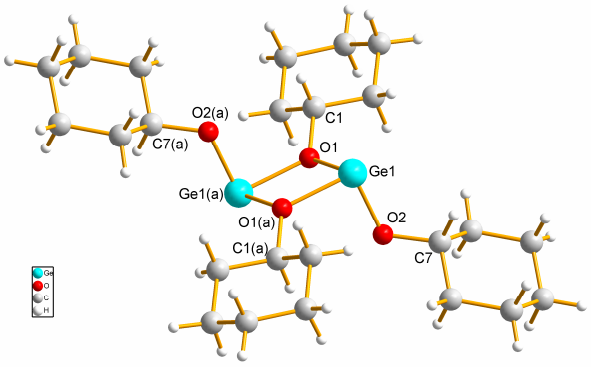

Figure 56. Dimeric molecular structure of $[Ge(O^cHex)_2]_2$

- Efforts were made for the preparation of compounds having general formula, $M\{H_2Al(OR)_2\}$ (R = ^{t}Bu, ^{c}Hex*Me*-1 and M = Ge^{II}, Ni^{II}, Eu^{II}). However, all the efforts gone in vain and none of the desired product was obtained.

1. General

Most of the compounds are air and moisture sensitive. Therefore, all the experimental procedures were carried out under inert atmosphere using Stock apparatus connected to a nitrogen carrier line and mechanical vacuum pump. A mechanical vacuum pump has been used for evacuation of the line with a base pressure of ca. 1.0×10^{-2} mbar. The organic solvents (diethylether, THF, toluene, benzene) are purified and dried over sodium wires using sodium-benzophenone as indicator. The freshly distilled solvents were kept over sodium wire and under nitrogen atmosphere. The corresponding alcohols (*tert*-butanol, *iso*-propanol, cyclohexanol and 1-methylcyclohexanol) were dried over magnesium turnings and kept over molecular sieves. The salts ($LiAlH_4$, SmI_2, EuI_2 and $NiCl_2$, $GeCl_4$) were purchased from Sigma-Aldrich and used as received. $HN(SiMe_3)_2$ was distilled and $AlCl_3$ was freshly sublimed before use. $GeCl_2$.1,4-dioxane [208], $LiN(SiMe_3)_2$ [209] and $Ge\{N(SiMe_3)_2\}_2$ [165-167] were prepared according to the cited literature.

2. Elemental analysis

Elemental (C, H and N) measurements were carried out using a LECO CHN 900 elemental analyzer. The metal contents (Al and Ni) of the compounds were determined by complexometric titration methods using EDTA as complexing agent. Chlorine was determined by titrimetry with $AgNO_3$. The theoretical molar masses were calculated using relative masses of the elements from the IUPAC tables [2001].

3. Spectroscopic Methods

3.1. Nuclear Magnetic Resonance (NMR) Spectroscopy

^1H and ^{13}C-NMR measurements were performed using an ACF 200 NMR spectrometer operated at 200.1 MHz and 50.3 MHz frequency, respectively. The samples were prepared by dissolving small amounts of compounds in appropriate deuterated solvents (C_6D_6). Deuterated benzene has been used as lock solvent. δ-scale has been used for the values of chemical shifts and presented in ppm units. The peaks were reference to the δ values of benzene which are

7.16 and 128.00 ppm for ^{1}H and ^{13}C nuclei. The ^{27}Al NMR spectra were recorded upon multinuclear ACF 200 NMR spectrometer operated at 200.1 MHz. The abbreviations used for multiplicity of peaks are summarized in the following Table.

Multiplicity	Abbreviation
Singlet	s
Doublet	d
Triplet	t
Multiplet	M
Broad	b

3.2. Infra-red spectroscopy

IR spectra were recorded on a Varian 2000 FT-IR spectrophotometer. The measurements were carried out in solid state using golden gate technique. The chamber was flushed with dryed gaseous N_2 before starting and during the measurements. The bands were labelled using Varian pro software. The abbreviations used for the relative intensity of the bands are summarized in the following table.

Band	Abbreviation
Strong	*s*
Weak	*w*
Broad	*br*

4. Single crystal determination

The single crystal X-ray diffraction analysis was performed on a Stoe imaging plate diffractometer (IPDS) at -70 °C and a BrukerAxs X8 Apex II diffractometer at -170°C using graphite monochromated Mo Kα X-ray radiation (λ = 0.71073 Å). The crystal structures were solved by direct methods and refined by full-matrix least squares on F2 using the SHELX

software package for crystal structure solution and refinement [152]. All non-hydrogen atoms were refined with anisotropic thermal parameters in the later cycles of refinement.

5. Synthetic Procedures

5.1. Synthesis of $[H_nAl(O^cHex)_{3-n}]_n$

5.1.1. $[\{H_2Al(O^cHex)_2\}\{(H)_4Al_4(\mu\text{-}O)(O^cHex)_5\}]$ **1**

Following established routes [78-79], 0.854 g (22.50 mmol) of $LiAlH_4$ were dissolved in 50 ml of diethyl ether in a flask with a reflux condenser. Aluminiumtrichloride (1.007 g; 7.55 mmol) were dissolved under cooling in 50 ml of diethyl ether and added to the lithium aluminium hydride in a steady flow at room temperature. LiCl precipitates from the mixture. To this suspension, 3.01 g (30.00 mmol) of cyclohexanol were added dropwise and formation of hydrogen was observed. The reaction was completed by stirring the reaction mixture at ambient temperature for 4 h. After filtration of the lithium chloride, the solvent was condensed in a cooling trap under reduced pressure and the residue was redissolved in a small amount (ca. 10 ml) of diethyl ether. Colourless crystals of $[\{H_2Al(O^cHex)_2\}\{(H)_4Al_4(\mu\text{-}O)(O^cHex)_5\}]$ **1** were obtained overnight at +4°C. Isolated yield: 90.4% (2.59g).

^{1}H-NMR(C_6D_6): δ=4.53 ppm (b, Al-H), δ=3.97 ppm (m, -O-C**H**-), δ=1.04-2.34 ppm (-CH_2-ring); ^{13}C-NMR: δ= 74.46 ppm (-$\mathbf{C_1}$), 35.97 ppm (-$\mathbf{C_2}$), 25.96 ppm ($\mathbf{C_3}$) and 25.27 ppm ($\mathbf{C_4}$); IR: ν=1816 cm^{-1}(br, Al-H). Elemental Analysis: Calcd. (Found): H 9.83 (10.37), C 59.28 (62.32), Al 15.85 (16.20).

5.1.2. $[H_2Al(O^cHex)]_n$ **2**

0.854g (22.50mmol) of $LiAlH_4$ was dissolved in 50 ml of diethyl ether in a flask with a reflux condenser. Aluminiumtrichloride (1.007g; 7.55 mmol) were dissolved under cooling in 50ml diethyl ether and added to the lithium aluminium hydride in a steady flow at room temperature. LiCl precipitates from the mixture. To this suspension 3.01g (30.00 mmol) cyclohexanol were added dropwise and formation of hydrogen was observed. The reaction was completed by stirring the reaction mixture at ambient temperature for 4 h. After

separation of the lithium chloride by filtration, the solvent was condensed into a cooling trap under reduced pressure and the residue was redissolved in a small amount (ca. 10 ml) of diethyl ether. Colourless crystals of $[H_2Al(O^cHex)]_n$ **2** were obtained after overnight stay (ca. 12 h) in refrigerator at +4°C. Isolated yield: 92.6% (2.65g).

^{1}H-NMR(C_6D_6): δ=4.50 ppm (b, 2H, Al-μ-H), δ=4.32 ppm (b, 1H, Al-H), δ=3.98 ppm (m, 3/2H, -O-C**H**-), δ=1.03-2.29 ppm (15H, -CH_2-ring); ^{13}C-NMR: δ=71.87 ppm(**C_1**), 36.48 ppm (**C_2**), 25.79 ppm (**C_3**) and 24.31 ppm (**C_4**); IR: ν=1860 cm^{-1} (s, Al-H), ν=1830 cm^{-1} (br, Al-μ-H). Elemental Analysis: Calcd. (Found): H 10.22 (10.37), C 57.98 (57.31), Al 21.05 (20.57).

5.1.3. $[HAl(O^cHex)_2]_n$ 3

Compound **3** was prepared by the reaction of $LiAlH_4$, $AlCl_3$ and Cyclohexanol. 0.43g (11.33 mmol) of $LiAlH_4$ was dissolved in 50 ml of diethyl ether in a flask with a reflux condenser. 0.5g (3.75 mmol) of aluminiumtrichloride were dissolved under cooling in 50ml diethyl ether and added to the lithium aluminium hydride in a steady flow at room temperature. LiCl precipitates from the mixture. To this suspension 3.00g (29.45 mmol) cyclohexanol was added dropwise and formation of hydrogen was observed. The reaction was completed by stirring the reaction mixture at ambient temperature for 4 h. After separation of the lithium chloride by filtration, the solvent was condensed into a cooling trap under reduced pressure and the residue was redissolved in small amount (ca. 10 ml) of diethyl ether for crystallization. After several attempts we were unable to get crystals of **3**. Isolated yield: 90.3% (2.29g).

^{1}H-NMR(C_6D_6): δ=4.27 ppm (b, 1H, Al-H), 4.08 ppm (m, 2H, -O-C-μ-**H**-), 1.11-2.40 (20H, -CH_2-ring); ^{13}C-NMR: δ=73.95 ppm (μ-**C_1**), 38.32 ppm (μ -**C_2**), 26.00 ppm (μ –**C_3**), and 24.32 ppm (μ-**C_4**); IR: ν=1841 cm^{-1} (s, Al-H), 676 cm^{-1} (δ-Al-H). Elemental Analysis: Calcd. (Found); H 10.24 (10.01), C 63.69 (63.31), Al 11.92 (11.89).

5.1.4. $[Al(O^cHex)_3]_4$ 4

Compound **4** was prepared by dissolving 0.500g (13.18mmol) of $LiAlH_4$ in 50 ml of diethyl ether in a flask with a reflux condenser. 0.586g (4.39mmol) of aluminiumtrichloride were

dissolved under cooling in 50ml diethyl ether and added to the lithium aluminium hydride in a steady flow at room temperature. LiCl precipitates from the mixture. To this suspension, 15.84g (158.18mmol) of cyclohexanol was added dropwise and formation of hydrogen was observed. The reaction was completed by stirring the reaction mixture at ambient temperature for 4 h. After separation of the lithium chloride by filtration, the solvent was condensed into a cooling trap under reduced pressure and the residue was redissolved in small amount (ca. 10 ml) of diethyl ether. Colourless crystals of $[Al(O^cHex)_3]_4$ **4** were obtained after overnight stay (ca. 12 h) in refrigerator at +4°C. Isolated yield: 92.8% (3.93g).

^{1}H-NMR(C_6D_6): δ=4.20 ppm (m, 6H, μ-O-C**H**-), 3.59 ppm (m, 6H, -O-C**H**-), 1.09-2.57 ppm (120H, -CH_2-ring); ^{13}C-NMR: δ=73.73 ppm (μ-**C$_1$**), 70.09 ppm (-**C$_1$**), 35.51 ppm (μ -**C$_2$**), 35.23 ppm (**C$_2$**), 25.76 ppm (μ –**C$_3$**), 25.32 ppm (-**C$_3$**), 24.38 ppm (μ –**C$_4$**) and 23.97 ppm (-**C$_4$**); IR: ν=2922 cm^{-1} (asym., C-H), 2853 cm^{-1} (sym., C-H). Elemental Analysis: Calcd. (Found); H 10.25 (10.54), C 66.64 (66.04), Al 8.32 (8.12).

5.2. Synthesis of $[H_nAl(O^cHex$*Me*$-1)_{3-n}]_n$

5.2.1. $[H_2Al(O^cHex$*Me*$-1)]_2$ 5

0.414g (10.90 mmol) of $LiAlH_4$ was dissolved in 50 ml of diethyl ether in a flask with a reflux condenser. 0.485g (3.65 mmol) of aluminiumtrichloride were dissolved under cooling in 50ml diethyl ether and added to the lithium aluminium hydride in a steady flow at room temperature. LiCl precipitates from the mixture. To this suspension, 1.661g (14.55 mmol) 1-methylcyclohexanol was added dropwise and formation of hydrogen was observed. The reaction was completed by stirring the reaction mixture at ambient temperature for 4 h. After separation of the lithium chloride by filtration, the solvent was condensed into a cooling trap under reduced pressure and the residue was redissolved in small amount (ca. 10 ml) of diethyl ether. Colourless crystals of $[H_2Al\{O^cHex\text{-}CH_3)\}]_2$ **5** were obtained after overnight stay (ca. 12 h) in refrigerator at +4°C. Isolated yield: 90.4% (1.40g).

^{1}H-NMR(C_6D_6): δ=4.47 ppm (b, 4H, Al-H), 1.34 ppm (6H, -C(C**H$_3$**)), 1.08-1.89 ppm (20H, C**H$_2$**-ring); ^{13}C-NMR (C_6D_6): δ=77.96 ppm (-**C$_1$**), 39.06 ppm (-**C$_2$**), 26.38 ppm (-**C$_3$**), 24.77 ppm (-**C$_4$**) and 22.66 ppm (-**C$_5$**); IR: ν=1829 cm^{-1} (s, Al-H), 744 cm^{-1} (s, b, δAl-H); Elemental Analysis: Calcd. (Found); H 10.63 (10.47), C 59.14 (58.49), Al 18.98 (19.04).

5.2.2. $[HAl(O^cHex\mathit{Me}\text{-}1)_2]_2$ 6

0.433g (11.40 mmol) of $LiAlH_4$ was dissolved in 50 ml of diethyl ether in a flask with a reflux condenser. 0.507g (3.80 mmol) of aluminiumtrichloride were dissolved under cooling in 50ml diethyl ether and added to the lithium aluminium hydride in a steady flow at room temperature. LiCl precipitates from the mixture. To this suspension 3.47g (30.40 mmol) 1-methycyclohexanol was added dropwise and formation of hydrogen was observed. The reaction was completed by stirring the reaction mixture at ambient temperature for 4 h. After separation of the lithium chloride by filtration, the solvent was condensed into a cooling trap under reduced pressure. A colourless thick liquid of **6** was obtained and all the efforts to get a crystal gone in vain. Isolated yield: 91.1% (2.64g).

^{1}H-NMR (C_6D_6): δ=4.07 ppm (b, 2H, Al-H), 1.39 ppm (6H, -C-μ-(C**H**$_3$)), 1.30 ppm (6H, -C-(C**H**$_3$)) and 1.16-1.93 ppm (40H, C**H**$_2$-ring); ^{13}C-NMR (C_6D_6): δ=78.97 ppm (μ-**C**$_1$), 70.87 ppm (-**C**$_1$), 42.70 ppm (μ-**C**$_2$), 40.69 ppm (-**C**$_2$), 32.12 ppm (μ-**C**$_3$), 27.42 ppm (**C**$_3$), 26.26 ppm (μ-**C**$_4$), 25.65 ppm (-**C**$_4$), 23.93 ppm (μ-**C**$_5$) and 23.64 ppm (-**C**$_5$); IR: ν=1859 cm^{-1} (s, Al-H), 673 cm^{-1} (s, br, δ-Al-H); Elemental Analysis: Calcd. (Found); H 10.70 (10.90), C 66.11 (65.95), Al 10.61 (10.64).

5.2.3. $[Al(O^cHex\mathit{Me}\text{-}1)_3]_2$ 7

1.742g (45.90 mmol) $LiAlH_4$ were dissolved in 80 ml of diethyl ether in a flask with a reflux condenser. 2.041g (15.31 mmol) of aluminiumtrichloride were dissolved under cooling in 80ml diethyl ether and added to the lithium aluminium hydride in a steady flow at room temperature. LiCl precipitates from the mixture. To this suspension, 22.82g (200.00 mmol) 1-methycyclohexanol was added dropwise, and formation of hydrogen was observed. The reaction was completed by stirring the reaction mixture at ambient temperature for 4 h. After separation of the lithium chloride by filtration, the solvent was condensed into a cooling trap under reduced pressure and the residue was redissolved in small amount (ca. 10 ml) of diethyl ether. Colourless crystals of $[Al\{O^cHex\text{-}CH_3)\}_3]_2$ 7 after overnight stay (ca. 12 hours) in refrigerator at +4°C were obtained. Isolated yield: 92.8% (15.61g).

^{1}H-NMR (C_6D_6): δ=1.47 ppm (6H, μ-O-C(C**H**$_3$)), 1.51 ppm (12H, O-C(C**H**$_3$)), 1.18-2.19 ppm (60H, -CH_2-ring); ^{13}C-NMR (C_6D_6): δ=78.38 ppm (μ-**C**$_1$), 69.84 ppm (-**C**$_1$), 42.31 ppm (μ-

C₂), 40.10 ppm (-**C₂**), 30.18 ppm (μ-**C₃**), 26.29 ppm (**C₃**), 25.29 ppm (μ-**C₄**), 25.12 ppm (-**C₄**), 23.79 ppm (μ-**C₅**) and 23.57 ppm (-**C₅**); IR: ν=2922 cm^{-1} (asym. C-H), 2854 cm^{-1} (sym. C-H). Elemental Analysis: Calcd. (Found); H 10.73 (11.01), C 68.82 (68.23), Al 7.36 (7.32).

5.3. Synthesis of $[ClAl(H)(OR)]_2$ and $[Cl_nAl(OR)_{3-n}]_2$

5.3.1. $[ClAl(H)(O^cHex\mathit{Me}\text{-}1)]_2$ **8**

To a suspension of 0.268 g (7.06 mmol) lithium aluminium hydride in 75 mL diethyl ether was added a solution of 0.940 g (7.06 mmol) of aluminiumtrichloride prepared in 75 mL diethyl ether under cooling. After 1 h stirring, 1.76 mL (14.12 mmol) of 1-methylcyclohexanol was added drop by drop to the above reaction mixture and stirred for additional 3 hrs. The solution mixture was reduced to half by removing solvent under reduced pressure and then 50 mL hexane was added to the resulting mixture to complete the precipitation of lithium chloride. The lithium chloride salt was separated by filtration and the volume of the filtrate was reduced under reduced pressure to allow the formation of 2.15 g (86.34%) of colorless crystals of $[ClAl(H)(OR)]_2$ **8** in refrigerator at +4°C.

^{1}H-NMR (C_6D_6): δ=1.34 ppm (s, CH_3, 3H), 1.36 ppm (s, CH_3-, 3H), 0.9-1.7 ppm (m, -CH_2-ring, 10H); ^{13}C-NMR (C_6D_6): δ=82.25 ppm (s, 1-CH), 82.27 ppm (s, α-CH_2), 39.74 ppm (s, 2-CH_2), 39.56 ppm (s, 2- CH_2), 24.31 ppm (s, CH_3), 22.78 ppm (s, CH_3); ^{27}Al-NMR: δ=100.00 ppm, 89.34 ppm; IR (Al-H): ν=s, 1905cm^{-1}; Elemental Analysis: Calcd. (Found); C 47.60 (42.45), H 7.99 (7.29), Al 15.28 (15.36); Cl 20.07 (19.72).

5.3.2. $[ClAl(O^cHex\mathit{Me}\text{-}1)_2]_2$ **9**

To a suspension of 0.334 g (8.80 mmol) of lithium aluminium hydride in 75 mL diethyl ether was added a solution of 1.173g (8.80 mmol) of aluminiumtrichloride prepared in 75 mL diethyl ether under cooling. After 1 h stirring, 4.4 mL (35.20 mmol) of 1-methylcyclohexanol was added drop by drop to the above reaction mixture and stirred for additional 3 hrs. The solution mixture was reduced to half by removing diethylether under reduced pressure and then 50 mL hexane was added to the resulting mixture to complete the precipitation of lithium chloride. The lithium chloride salt was separated by filtration and the volume of filtrate was

reduced under low pressure to allow the formation 2.31 g (91.70%) colorless crystals of $[ClAl(OR)_2]_2$ **9**.

^{1}H-NMR (C_6D_6): δ=1.58 ppm (s, μ-CH_3, 3H), 1.44 ppm (s, CH_3, 3H), 1.02-2.06 ppm (m, ring-CH_2, 20H); ^{13}C-NMR: δ=82.27 ppm (s, μ-**C**H{1}-), 71.25 ppm (s, **C**H{1}-), 41.96 ppm (s, μ-**C**H_2{2}-), 39.99 ppm (s, -**C**H_2{2}-), 30.25 ppm (s, μ-**C**H_3{3}), 29.71 ppm (s, -**C**H_3{3}), 25.84 ppm (s, μ-**C**H_2{4}), 24.68 ppm (s, -**C**H_2{4}), 23.42 ppm (s, μ-**C**H_2{5}), 23.25 ppm (s, -**C**H_2{5}); IR: (C-H) ν=2931cm^{-1}. Elemental Analysis: Calcd. (Found); C 58.64 (55.67), H 8.44 (8.82), Al 9.41 (10.04); Cl 12.36 (12.20).

5.3.3. $[Cl_2Al(O^cHex\textit{Me}\text{-}1)_2]$ 10

To a suspension of 0.104 g (2.77 mmol) lithium aluminium hydride in 75 mL diethyl ether was added a solution of 1.099 g (8.24 mmol) of aluminiumtrichloride prepared in 75 mL diethyl ether under cooling. After 1 h stirring, 1.36 mL (10.95 mmol) of 1-methylcyclohexanol was added drop by drop to the above mixture and stirred for additional 3 hrs. The solution mixture was reduced to half by removing diethylether under reduced pressure and then 50 mL hexane was added to the resulting mixture to complete the precipitation of lithium chloride. The lithium chloride salt was separated by filtration and the volume of the filtrate was reduced under reduced pressure to allow the formation 1.75 g (75.75%) of colorless crystals of $[Cl_2Al(OR)]_2$ **10**.

^{1}H-NMR (C_6D_6): δ=1.47 ppm (s, CH_3, 3H), 1.41-1.87 ppm (m, ring-CH_2, 10H); ^{13}C-NMR: δ=87.44 ppm (s, 1-CH), 40.62 ppm (s, 2-CH_2), 25.21 ppm (s, 5-CH_2), 24.17 ppm (s, 4- CH_2); ^{27}Al-NMR: δ = 88.95 ppm; IR: (C-H) ν=2936cm^{-1}. Elemental Analysis: Calcd. (Found); C 39.83 (38.46), H 6.21 (5.40), Al 12.78 (11.99); Cl 33.59 (34.05).

5.4. Synthesis of $[Ge(OR)_2]_2$

5.4.1. $[Ge(O^cHex)_2]_2$ 11

Compound **11** was prepared following a reported route [118]. To a 2.94 mmol (1.16g) ethereal solution of $Ge\{N(SiMe_3)_2\}_2$ was added 5.88 mmol (0.589g) cyclohexanol dissolved in diethyl ether. The pale yellow colour of $Ge\{N(SiMe_3)_2\}_2$ solution disappeared as soon as

all the cyclohexanol was dropped into it and the whole reaction mixture was stirred for 4 h to complete the reaction process. The volatiles (diethyl ether and hexamethyldisilazane) were removed under reduced pressure and condensed into liquid nitrogen cold trap. Small amount of the white powder left behind in the flask was dissolved in 5mL diethyl ether and kept in refrigerator for crystallization at +4°C. Fine colourless crystals of $[Ge(O^cHex)_2]_2$ **11** were obtained after overnight stay (~12 hours) of the solution in refrigerator. Isolated yield: 2.38 g (72.6%).

^{1}H-NMR (C_6D_6): δ=4.29 ppm (m, -OC{**H**}-ring), 1.45-2.17 ppm (m, -CH_2-ring); ^{13}C-NMR: δ=71.87 ppm (s, 1-CH-ring), 36.48 ppm (s, 2-CH_2-ring), 25.79 ppm (s, 3-CH_2-ring), 24.31 ppm (s, 4-CH_2-ring); IR: ν(C-H)=2924 cm^{-1}(asymetric), 2852 cm^{-1} (symetric); Elemental Analysis: Calcd. (Found); C 53.20 (51.46), H 8.19 (8.13).

5.4.2. $[Ge(O^cHex\mathit{Me}\text{-}1)_2]_2$ 12

To a 9.30 mmol (3.657g) ethereal solution of $Ge\{N(SiMe_3)_2\}_2$ was added 18.60 mmol (2.123g) 1-methylcyclohexanol dissolved in diethyl ether. The pale yellow colour of $Ge\{N(SiMe_3)_2\}_2$ solution disappeared as soon as all the 1-methylcyclohexanol was added into it and the whole reaction mixture was stirred for 4 h to complete the reaction process. The volatiles (diethyl ether and hexamethyldisilazane) were removed under reduced pressure and condensed into liquid nitrogen cold trap. Small amount of the white powder left behind in the flask was dissolved in 5mL diethylether and kept in refrigerator for crystallization. Fine colourless crystals of $[Ge(^cHex\mathit{Me}\text{-}1)_2]_2$ **12** were obtained after overnight stay (~12 hours) of the solution in refrigerator at +4°C. Isolated yield: 1.50 g (59.2%).

^{1}H-NMR (C_6D_6): δ=1.56 ppm (s, -OC{C**H$_3$**}-ring), 1.36-1.96 ppm (m, -CH_2-ring); ^{13}C-NMR: δ=74.54 ppm (s, 1-C-ring), 41.12 ppm (s, 2-CH_2-ring), 29.45 ppm (s, 3-CH_3), 25.67 ppm (s, 4-CH_2-ring), 22.87 ppm (s, 5-CH_2-ring); IR: ν(C-H) = 2953 cm^{-1}(asymetric), 2875 cm^{-1} (symetric); Elemental Analysis: Calcd. (Found); C 56.24 (55.23), H 8.77 (8.08).

5.4.3. $[Ge(O^iPr)_2]_2$ 13

To a 2.15 mmol (0.846g) ethereal solution of $Ge\{N(SiMe_3)_2\}_2$ was added 4.30 mmol (0. 258g) *iso*-propanol dissolved in diethyl ether. The pale yellow colour of $Ge\{N(SiMe_3)_2\}_2$

solution disappeared as soon as all the *iso*-propanol was added into it and the whole reaction mixture was stirred for 4 h to complete the reaction process. The volatiles (diethyl ether and hexamethyldisilazane) were removed under reduced pressure and condensed into liquid nitrogen cold trap. Small amount of the white powder left behind in the flask was dissolved in 5mL diethylether and kept in refrigerator for crystallization at +4°C. However, all the efforts failed to get crystals of $[Ge(^{i}Pr)_2]_2$ **13**. Isolated yield: 87.2%.

^{1}H-NMR (C_6D_6): δ=4.51 ppm (m, -OC{**H**}), 1.34 ppm (s, μ-CH_3), 1.31 ppm (s, -CH_3); ^{13}C-NMR: δ=77.45 ppm (s, μ-O{**C**}), 64.77 ppm (s, -O{**C**}), 27.00 ppm (s, μ-**C**H_3), 26.60 ppm (s, -CH_3); IR: ν(C-H) = 2961 cm^{-1}(asymetric), 2883 cm^{-1} (symetric); Elemental Analysis: Calcd. (Found); C 37.77 (37.51), H 7.40 (7.19).

5.5. Synthesis of [HAl(OR)(NŔ)]$_2$

5.5.1. [HAl(O^{t}Bu)(N{SiMe$_3$}$_2$)]$_2$ 14

0.51g (2.5 mmol) of $[H_2Al(O^{t}Bu)]_2$ was dissolved in 20 mL diethyl ether and was added dropwise into 0.98g (2.5 mmol) of $Ge(N\{SiMe_3\}_2)_2$ solution prepared in 20mL diethyl ether under stirring and the whole reaction mixture was stirred at room temperature for another 6 h. The colour of the solution changed from yellow to pale yellow. The transparent pale yellow solution was condensed to one third of its original volume under reduced pressure and was kept for crystallization in refrigerator. After one night (ca. 12 h) colourless crystals of $[HAl(O^{t}Bu)\{N(SiMe_3)_2\}]_2$ **14** dispersed in pale yellow solution have been obtained at +4°C. Isolated yield: 83.7% (1.09g).

^{1}H-NMR (C_6D_6): δ=1.42 ppm (s, μ-CH_3, 18H), 0.42 ppm (s, Si-$\{CH_3\}_3$, 18H), 0.40 ppm (s, Si-$\{CH_3\}_3$, 18H); ^{13}C-NMR: δ=77.30 ppm (s, μ-**C**$\{CH_3\}_3$), 31.43 ppm (s, μ-C{**C**$H_3\}_3$), 5.65 ppm (s, -Si{**C**$H_3\}_3$), 5.23 ppm (s, -Si{**C**$H_3\}_3$); IR: (C-H) ν = s, 1873cm^{-1}. Elemental Analysis: Calcd. (Found); C 45.93 (44.79), H 10.79 (10.15), N 5.36 (5.06), Al 10.32 (10.70).

5.5.2. [HAl(O^{c}Hex*Me*-1)(N{SiMe$_3$}$_2$)]$_2$ 15

0.69g (2.4 mmol) of $[H_2Al(O^{c}Hex\textit{Me}\text{-}1)]_2$ was dissolved in 20 mL diethyl ether and was added dropwise to 0.96g (2.4 mmol) of $Ge(N\{SiMe_3\}_2)_2$ solution prepared in 20mL diethyl

ether under stirring and the whole reaction mixture was stirred at room temperature for another 6 h. The colour of the solution changed from yellow to pale yellow. The transparent pale yellow solution was condensed to one third of its original volume under reduced pressure and was kept for crystallization in refrigerator. After one night (ca. 12 h) colourless crystals of $[HAl(\mu\text{-}O^{c}Hex\textit{Me}\text{-}1)\{N(SiMe_3)_2\}]_2$ **15** dispersed in pale yellow solution were obtained at +4°C. Isolated yield: 89.2% (1.25g).

^{1}H-NMR (C_6D_6): δ=1.50 ppm (s, μ-**C**H_3, 6H), 0.46 ppm (s, Si-{CH_3}$_3$, 18H), 0.45 ppm (s, Si-{CH_3}$_3$, 18H), 1.03-2.05 ppm (s, μ-**C**H_2{ring}, 20H),; ^{13}C-NMR: δ=80.45 ppm (s, μ-**C**{ring-1}), 40.81 ppm (s, μ-**C**H_2{ring-2}), 29.65 ppm (s, μ-**C**H_3{ring-3}), 25.47 ppm (s, μ-**C**H_2{ring-4}), 23.59 ppm (s, μ-**C**H_2{ring-5}), 5.74 ppm (s, -Si{**C**H_3}$_3$), 5.25 ppm (s, -Si{**C**H_3}$_3$); IR: (C-H) ν=s, 1866cm^{-1}. Elemental Analysis: Calcd. (Found); C 49.78 (50.32), H 11.14 (10.26), N 4.84 (4.53), Al 9.32 (10.70).

References

[1] R. Kuhlman, *Ann.*, 33, 97, **1840**.

[2] J. J. Ebelman and M. Bouquet, *Ann. Chim. Phys*., 17, 54, **1846**.

[3] J. J. Ebelman, *Ann*., 57, 331, **1846**.

[4] W. Tischtschenko, *Chem, Zentr*., 77, 1309, 1556, 1558, **1906**.

[5] M. S. Kulpinski and F. F. Nord, *Nature*, 151, 363, **1943**.

[6] Idem, *J. Org. Chem.*, 8, 256, **1943**.

[7] F. J. Villani and F. F. Nord, *J. Am. Chem. Soc*., 69, 2605, **1947**.

[8] D. C. Bradley, in *Progress in Inorg. Chem.*, 2, ed. F. A. Cotton, Interscience Publ., New York, 304, **1960**.

[9] D. C. Bradley, A. H. Westlake, Proc. *Symp. Coord. Chem*., Tihany, Hungary, **1964**, Acad. Kiado, Budapest, 309, **1965**.

[10] D. C. Bradley, in *Adv. in Inorg. Chem. and Radiochem.*, 15, 259, **1972**.

[11] D. C. Bradley, R. C. Mehrotra, D. P. Gaur, *Metal Alkoxides*, Academic Press, London, **1978**.

[12] H. Adkins, *J. Am. Chem. Soc*., 44, 2175, **1922**.

[13] H. Meerwein, *US Patent*, 1,689,356, **1929**.

[14] H. Meerwein, *Chem. Abstr*., 23, 156, **1929**.

[15] H. Meerwein and T. Bersin, *Ann*., 476, 113, **1929**.

[16] H. Meerwein and T. Bersin, *Chem. Abstr*, 24, 586, **1930**.

[17] N. Y. Sidgwick, *The Chemical Elements and Their Compounds*, Vol. 1, Oxford Univ. Press, London, **1950**.

[18] G. E. M. Jones and O. L. Hughes, *J. Chem. Soc*., 1197, **1934**.

[19] M. W. Rupich, B. Lagos and J. P. Hachey, *Appl. Phys. Lett*., 55, 2447, **1989**.

[20] S. N. Putlin, E. V. Antipov, O. Chmaisson and M. Marezio, *Nature*, 363, 56, **1993**.

[21] H. Maeda, Y. Tanaka, M. Fukutomi and T. Asane, *Jpn. J. Appl. Phys*., 27, L209, **1988**.

[22] M. H. Chisholm, *Inorganic Chemistry Toward the 21st Century*; p. 243. American Chemical Society: Washington DC. **1983**.

[23] D. C. Bradley, *Chem. Rev*., 89, 1317, **1989**.

[24] U. Schuber, *J. Chem. Soc., Dalton Trans*. 3343, **1996**.

[25] M. Veith, S. Mathur and C. Mathur, *Polyhedron*, 17, 1005, **1998**.

[26] M. Veith, *J. Chem. Soc., Dalton Trans*., 12, 2405, **2002**.

[27] Prof. Dr. Dr. h. c. Michael Veith, Institute of Inorganic Chemistry, Saarland University, Saarbrücekn (Germany).

[28] M. Veith, S. Faber, H. Wolfanger and V. Huch, *Chem. Ber*., 129, 381, **1996**.

[29] M. Veith, A. Alther and H. Wolfanger, *Chem. Vap. Deposition*, 5, 87, **1999**.

[30] Ethyl Corpn., *Brit. Patent*, 727,923, **1995**; *Chem. Abstr*., 50, 5018, **1956**.

[31] L. Lochmann, D. Lim and J. Coupek, *Ger. Offen. Patent*, 2,035,260, **1971**.

[32] L. Lochmann, D. Lim and J. Coupek, *Chem. Abstr*., 74, 87355, **1971**.

[33] Mathieson Alkali Works, *Fr. Patent*, 850,126, 1939.

[34] Mathieson Alkali Works, *Chem. Abstr*., 36, 1619, **1942**.

[35] K. S. Mazdiyasni, R. T. Dolloff and J. F. Smith II, *J. Am. Ceram. Soc*., 52, 523, **1969**.

[36] J. F. Smith II, R. T. Dolloff and K. S. Mazdiyasni, *J. Am. Ceram. Soc*., 53, 91, **1970**.

[37] N. Y. Turova, A. V. Novoselova and K. N. Semenenko, *Zh. Neorg. Khim*., 4, 997, **1959**.

[38] N. Y. Turova, A. V. Novoselova and K. N. Semenenko, *Chem. Abnstr*., 54, 8397, **1960**.

[39] C. A. Cohen, *US Patent*, 2,287,088, **1943**.

[40] C. A. Cohen, *Chem. Abnstr*., 37, 141, **1943**.

[41] S. J. Teichner, *Compt. Tend*., 237, 810, **1953**.

[42] G. C. Whitaker, *Metal Organic Compounds*, Advances in Chem. Series, No. 23, 184, **1959**.

[43] K. S. Mazdiyasni, C. R. Lynch and J. S. Smith, *Inorg. Chem*., 5, 342, **1966**.

[44] L. M. Brown and K. S. Mazdiyasni, *Inorg. Chem*., 9, 2783, **1970**.

[45] B. Szilard, *Z. Electrochem*., 12, 393, **1906**.

[46] T. G. Tripp, *Ger. Offen. Pat.* 2005835, **1970**; 2121732, **1972**; *Brit. Pat*. 1246032, **1971**; *Fr. Pat*. 2091229, **1972**.

[47] V. A. Shreider, E. P. Turevskaya, N. I. Kozlova and N. Ya. Turona, *Inorg. Chim. Acta*, 13, L73, **1981**.

[48] H. Lehmkul and W. Eisenbach, *Ann*., 672, **1975**.

[49] R. Marmodee, W. Schäfer and K. Andrä, *Z. Anorg. Allg. Chem*., 551, 61, **1987**.

[50] E. P. Kovsman, S. I. Andrusewa, L. I. Solovjeva, V. I. Fedyaev, M. N. Adamova and T. V. Rogova, *J. Sol-Gel Sci. Technol*., 2, 61, **1994**.

[51] E. P. Turevskaya, N. I. Kozlova, N. Ya. Turona, A. I. Belokon', D. V. Berdyev, V. G. Kessler and Yu. K. Grishin, *Russ. Chem. Bull*., 734, **1995**.

[52] T. Colclough, W. Gerrard and M. F. Lappert, *J. Chem. Soc.*, 3006, **1966**.

[53] M. F. Lappert, *Chem. Rev*., 56, 959, **1956**.

[54] D. C. Bradley, R. C. Mehrotra and W. Wardlaw, *J. Chem. Soc.*, 5020, **1952**.

[55] G. O. Doak and L. D. Freedmann, *Chem. Rev*., 61, 31, **1961**.

[56] R. C. Mehrotra, T. N. Misra and S. N. Misra, *J. Indian Chem. Soc*., 42, 351, **1965**.

[57] A. Rosenheim, V. Samter and J. Davidsohn, *Z. Anorg. Allg. Chem*., 35, 447, **1903**.

[58] N. V. Sidgwick, *J. Chem. Soc*., 125, 2672, **1924**.

[59] J. U. Nef, *Ann*., 308, 329, **1899**.

[60] D. L. Tabern, W. R. Orndorff and L. M. Dennis, *J. Amer. Chem. Soc.*, 47, 2039, **1925**.

[61] D. C. Bradley, L. Kay and W. Wardlaw, *Chemistry & Industry*, 746, **1953**.

[62] V. E. Tishschenko, *Zhurn. Russ. Fiz.-Khim. Obsch*, 31, 694, **1899**.

[63] R. C. Mehrotra, *J. Indian Chem. Soc*., 30, 585, **1953**.

[64] G. F. Wheite, A. B. Morrison and E. G. Anderson, *J. Amer. Chem. Soc.*, 46, 961, **1924**.

[65] R. G. Jones, G. Karmas, G. A. Martin and H. Gilman, *J. Amer. Chem. Soc.*, 78, 4285, **1956**.

[66] D. C. Bradley, in *Preparative Inorg. Reactions*, 2, ed. W. L. Jolly, Interscience. Publ., New York, 226, **1965**.

[67] M. Akiyama, M. H. Chisholm, F. A. Cotton, M. W. Extine, D. A. Haitko, D. Little and P. E. Eanwick, *Inorg. Chem*., 18, 2266, **1979**.

[68] D. C. Bradley, M. H. Chisholm, M. W. Extine, *Inorg. Chem*., 16, 1791, **1977**.

[69] B. Horvath, E. G. Horvath, *Z. Anorg. Allg. Chem*., 449, 41, **1979**.

[70] B. Horvath, E. G. Horvath, *Z. Anorg. Allg. Chem*., 457, 51, **1979**.

[71] M. F. Lappert, P. P. Power, A. R. Sanger, R. C. Srivastava, *Metal and Metalloid Amides*, 1st ed., Halsted Press: Chichester, U. K., **1980**.

[72] W. C. Child and H. Adkins, *J. Amer. Chem. Soc*., 45, 3013, **1923**.

[73] A. Edelstein and R. C. Cammerata, *eds.*, *Nanomaterials: Synthesis, Properties and Applications*, Institute of Physics Publishing, Bristol, UK, and Philadelphia, USA, **1996**.

[74] K. E. Sickfaus and J. M. Wills, *J. Amer. Chem. Soc*., 82, 3279, **1998**.

[75] P. P. Phule and S. H. Risbud, *J. Mater. Sci*., 25, 1169, **1990**.

[76] J. Satge, *Bull. Soc. Chim. France*, 630, **1964**.

[77] R. E. A. Dear, *J. Org. Chem*., 33, 3959, **1968**.

[78] A. J. Bloodworth and A. G. Davies, *Organotin Compounds*, Ed. by A. K. Sawyer, Vol. 1, Marcel Dekker, New York, **1971**.

[79] H. Nöth and H. Suchy, *Z. Anorg. Allg. Che*., 368, 44, **1968**.

[80] H. Nöth, A. Schlegel, J. Knizek and H. Schwenk, *Angew. Chem. Int. Ed. Engl.*, 36, 2640, **1997**.

[81] N. V. Sidgwick and L. E. Sutton, *J. Chem. Soc*., 1461, **1930**.

[82] L. F. Dahl, G. L. Davies, D. L. Wampler and K. West, *J. Inorg. Nucl. Chem.*, 24, 357, **1962**.

[83] E. Weis, H. Alsdorf and H. Kuhr, *Angew. Chem. Intl. Ed. Eng*., 6, 801, **1967**.

[84] E. Weis, H. Alsdorf and H. Kuhr, *Chem. Abstr.*, 67, 120706, **1967**.

[85] E. Weis and H. Alsdorf, *Angew. Chem.*, 79, 816, **1967**.

[86] E. Weis, H. Alsdorf and H. Kühr, *Chem. Ber*., 101, 3777, **1968**.

[87] R. E. A. Dear, F. W. Fox, R. J. Fredericks, G. E. Gilbert and D. K. Huggins, *Inorg. Chem.*, 9, 2590, **1970**.

[88] H. M. M. Shearer and C. B. Spencer, *Chem. Commun*., 194, **1966**.

[89] G. E. Hartwell and T. L. Brown, *Inorg. Chem*., 5, 1257, **1966**.

[90] M. S. Bains, *Can. J. Chem*., 42, 945, **1964**.

[91] N. I. Kozlova, N. Ya. Turova, *Russ. J. Coord. Chem. (Engl. Transl.)*, 6, 124, **1980**.

[92] E. Weis, *Helv. Chim. Acta*, 46, 2051, **1963**.

[93] H. Nikola, F. Olbrich, U. Behrens, *Z. Anorg. Allg. Chem*., 629, 2067, **2002**.

[94] J. R. Dilworth, J. Hanich, M. Krestel, J. Beck and J. Strahl, *J. Organomet. Chem.*, 315, C9, **1986**.

[95] Z. A. Starikova, E. P. Turevskaya, N. I. Kozlova, N. Ya. Turova, D. V. Berdyev and A. I. Yanovsky, *Polyhedron*, 18, 941, **1999**.

[96] K. Ruhlandt-Senge, R. A. Bartlett, M. M. Olmstead, P. P. Power, *Inorg. Chem*., 32, 1724, **1993**.

[97] J. L. Kerschner, P. E. Fanwick, I. P. Rothwell and J. C. Huffman, *Inorg. Chem.*, 28, 780, **1989**.

[98] N. Y. Turova, E. P. Turevskaya, V. G. Kessler and M. I. Yanovskaya, *The Chemistry of Metal Alkoxides*, Kluwer Academic Publisher, **2002**.

[99] M. Scholz, M. Noltemeyer and H. W. Roesky, *Angew. Chem*., 101, 1419, **1989**.

[100] G. Beck, P. B. Hitchkock, M. F. Lappert and J. A. McKinnon, *J. Chem. Soc., Chem. Commun*., 1312, **1989**.

[101] J. Calabrese, M. A. Cushing Jr. and S. D. Ittel, *Inorg. Chem.*, 27, 867, **1988**.

[102] G. A. Sigel, R. A. Bartlett, D. Decker, M. M. Olmstead and P. P. Power, *Inorg. Chem.*, 26, 1773, **1987**.

[103] S. Brooker, F. T. Edelmann, T. Kottke, H. W. Roesky, G. M. Schledrick, D. Stalke and K. H. Whitmire, *J. Chem. Soc., Chem. Commun*., 144, **1991**.

[104] R. H. Cayton, M. H. Chisholm, E. R. Davidson, V. R. DiStasi, P. Du and J. C. Huffmann, *Inorg. Chem.*, 30, 1020, **1991**.

[105] W. J. Ewans, T. J. Deming, J. M. Olofson and J. W. Ziller, *Inorg. Chem*., 28, 4027, **1989**.

[106] M. P. Murchie, J. W. Bovenkamp, A. Rodrigue, K. A. Watson, S. Fortier, *Can. J. Chem*., 66, 2515, **1988**.

[107] F. Calderazzo, G. Dell'Amico, et. al., *J. Chem. Soc., Dalton Trans.*, 1238, **1979**.

[108] D. M. Barnhart, D. L. Clark, J. C. Gordon, J. C. Huffman, R. L. Vincent, J. G. Watkin and B. D. Zwick, *Inorg. Chem*., 32, 4077, **1993**.

[109] T. J. Boyle, T. M. Alam, E. R. Mechenbier, B. L. Scott and J. W. Ziller, *Inorg. Chem*., 36, 3293, **1997**.

[110] A. A. Pinkerton, D. Schwarzenbach, L. G. Hubert-Pfalzgrag and J. G. Riess, *Inorg. Chem*., 15, 1196, **1976**.

[111] A. I. Yanovsky, E. P. Turevskaya, N. Ya. Turova, F. M. Dolgushin, A. P. Pisarevsky, A. S. Batzanov and Yu. T. Stuchkov, *Russ. J. Inorg. Chem*., 39, 1246, **1994**.

[112] N. Bell, H. M. M. Shearer and J. Twiss, *Acta Crystallogr. C*, 40, 605, **1984**.

[113] M. Veith, S. Mathur, et. al., *Polyhedron*, 17, 1005, **1998**.

[114] M. Veith, S. Mathur, et. al., *Chem. Mater*., 12, 271, **2000**.

[115] A. I. Yanovsky, V. A. Kozunov, N. Ya. Turova, N. G. Furmanova and Yu. T. Stuchkov, *Doklady Chem, Proc. Acad. Sci. USSR*, 26, 244, **1979.**

[116] D. E. Tchebukov, *Disser.*, Moscov University, **1998**.

[117] D. C. Bradley, *Adv. Inorg. Chem. Radiochem.*, 15, 259, **1972**.

[118] N. Y. Turova, V. A. Kozunov, A. I. Yanovsky, N. G. Bokii, Yu. T. Stuchkov and B. L. Tarnopol'skii, *J. Inorg. Nucl. Chem.*, 41, 5, **1979**.

[119] K. Folting, W.E. Streib, K. G. Caulton, O. Poncelet and L. G. Hubert-Pfaltzgraf, *Polyhedron,* 10, 1639, **1991**.

[120] M. Valet and D. M. Hoffman, *Chem. Mater*. 13, 2135, **2001**.

[121] H. Wolfanger, *Dissertation*, University of Saarland, **1991**.

[122] M. Wijk, R. Norrestam, M. Nygren and G. Westin, *Inorg. Chem*., 35, 1077, **1996**.

[123] G. Westin, M. Moustiakimov and M. Kritikos, *Inorg. Chem*., 41, 3249, **2002**.

[124] B. Neumüller, *Chem. Soc. Rev*., 32, 50, **2003**.

[125] D. A. Atwood, J. A. Jegier, S. Liu, D. Rutherford, P. Wie and R. C. Tucker, *Organometallics,* 18, 976, **1999**.

[126] M. D. Healy, M. R. Mason, P. W. Gravelle, S. G. Bott and A. R. Barron, *J. Chem. Soc. Dalton Trans*., 441, **1993**.

[127] M. Veith, N. Köhler, *Proceedings-Electrochemical Society*, 9, 768, **2005**.

[128] C. Jones, G. A. Koutsantonis and C. L. Raston, *Polyhedron*, 12, 1829, **1993.**

[129] G. A. Koutsantonis, F. C. Lee and C. L. Raston, *Mian Group Chemistry*, 1, 21, **1995**.

[130] L. D. Silverman and M. Zeldin, *Inorg. Chim. Acta*., 37, L489, **1979**.

[131] L. D. Silverman and M. Zeldin, *Inorg. Chem*., 19, 270, **1980**.

[132] M. Veith, J. Hans, L. Stahl, P. May, V. Huch and A. Sebald, *Z. Naturforsch, B*, 46, 403, **1991**.

[133] M. Veith et. al., *Chem. Ber*., 125, 1033, **1992**.

[134] M. Veith, S. J. Kneip, A. Jungmann and S. Hüfner, *Z. Anorg. Allg. Chem*, 623, 1507, **1997**.

[135] B. Cetinkaya, I. Gumrukcu, M. F. Lappert, J. L. Atwood, R. D. Rogers, M. J. Zaworotko, *J. Am. Chem. Soc. 102*, 2088, **1980**.

[136] T. Fjeldberg, P. B. Hitchcock, M. F. Lappert, S. J. Smith and A. J. Thorne, *J. Chem. Soc. Chem. Commun*., 939, **1985**.

[137] C. S. Weinert, A. E. Fenwick, P. E. Fanwick, I. P. Rothwell, *Dalton Trans*., 532, **2003**.

[138] M. Veith, S. Mathur, P. König, C. Cavelius, J. biegler, A. Rammo, V. Huch, H. Shen and G. Schmid, *C. R. Chimie*, 7, 509, **2004**.

[139] R. A. Green, C. Moore, A. L. Rheingold and C. S. Weinert, *Inorg. Chem*. 48, 7510, **2009**.

[140] R. Bern and A. Rufiňska, *Angew. Chem.*, 98, 851, **1986**.

[141] R. Benn, A. Rufiňska, H. Lehmkuhl, E. Janssen and C. Krüger, *Angew. Chem. Int. Ed. Engl.*, 22, 779, **1983**.

[142] O. Kriz, B. Casensky, A. Lycka, J. Fusek and S. Hermanek, *J. Magnetic Resonance*, 60, 375, **1984**.

[143] J. Pauls and B. Neumüller, *Z. Anorg. Allg. Chem.*, 626, 270, **2000**.

[144] I. B. Gorrell, P. B. Hitchcock and J. D. Smith, *J. Chem.* Soc., *Chem. Commun.*, 189**, 1993.**

[145] C. L. Raston, *J. Organomet. Chem.*, 15, 475, **1994.**

[146] J. L. Atwood and G. D. Stucky, *J. Organomet. Chem.* 13, 53, **1968**.

[147] G. W. Svetich and A. A. Voge, *Acta Cryst.* 28B, 1760, **1972**.

[148] A. J. Downs, C. R. Pulham, *Chem. Soc. Rev*., 175, **1994**.

[149] G. M. Sheldrick, *Acta Cryst. A*, 64, 112, **2008**.

[150] R. C. Mehrotra, A. K. Rai, *Polyhedron*, 20, 19677, **1991**.

[151] K. W. Terry, P. K. Ganzel, T. D. Tilley, *Chem. Muter.*, 4, 1290, **1992**.

[152] P. Bissinger, P. Mikulcik, J. Riede, A. Schier, H. Schmidbaur, *J. Organornet. Chem.*, 446, 37, **1993**.

[153] M. R. Mason, J. M. Smith, S. G.Bott, A. R.Barron, *J.* Am. *Chem. Soc.*, 115, 4971, **1993**.

[154] M. H. Chisholm, V. F. Distasi and W. E. Streib, *Polyhedron*, 9, 253, **1990**.

[155] Michael Veith, David Kolano, Tatjana Kirs, Volker Huch, *Journal of Organomettalic Chemistry*, 695, 1074, **2010**.

[156] N. Köhler, *Ph. D Dissertation*, University of Saarland, Saarbrücken, **2007**.

[157] R. Benn, A. Rufinska, H. Lehmkuhl, E. Janssen, C. Krüger, *Angew. Chem.*, 95, 808, **1983**.

[158] R. Benn, E. Janssen, H. Lehmkuhl und A. Rufinska, *Journal of Organornetallic Chemistry*, 333, 155, **1987**.

[159] A. Pietrzykowski, T. Skrok, S. Pasynkiewicz, M. Brzoska-Mizgalski, J. Zachara, R. Anulewicz-Ostrowska, K. Suwinska, L. B. Jerzykiewicz, *Inorganica Chimica Acta*, 334, 385, **2002**.

[160] Z. Moravec, R. Sluka, M. Necas, V. Jancik and J. Pinkas, *Inorg. Chem., 48*, 8106, **2009.**

[161] N. Burford, R. G. Hicks, B. W. Royan, B. Borecka and T. S. Cameron, *Acta Cryst.*, C47, 1066, **1991**.

[162] M. J. S. Gynane, D. H. Harris, M. F. Lappert, P. P. Power, P. Riviere and M. Rivieve-Baudet, *J. C. S. Chem. Comm*., 2004, **1977**.

[163] P. J. Davidson, D. H. Harris and M. F. Lappert, *J. Chem. Soc. Dalton Trans*., 2268, **1976**.

[164] R. W. Chorley, P. B. Hitchcock, M. R. Lappert and W. Peung, *Iorganica Chimica Acta*, 198-200, 203, **1992**.

[165] H. Gerung, T. J. Boyle, L. J. Tribby, S. D. Bunge, C. J. Brinker and S. M. Han, *J. Am. Chem. Soc*., 128, 5244, **2006**.

[166] M. Veith and F. Töllner, *J. Organomet. Chem.*, 246, 219, **1983**.

[167] M. Veith, P. Hobein and R. Rösler, *Z. Naturforsch*, 44b, 1067, **1989**.

[168] G. Hendershot, M. Barber, R. Kumar, J. P. Oliver, *Organometallics*, 10, 3302, **1991**.

[169] H. Schumann, M. Frick, B. Heymer, F. Girgsdies, *J. Organomet. Chem*., 512, 117, **1996**.

[170] J. A. Francis, C. N. McMahon, S. G. Bott, A. R. Barron, *Organometallics*, 18, 4399, **1999**.

[171] Chia-Her Lin, Bao-Tsan Ko, Fa-Cherng Wang, Chu-Chieh Lin, Chen-Yuan Kuo, *J. Organomet. Chem*., 575, 67, **1999**.

[172] M. Westerhausen, C. Birg, H. Noth, J. Knizek, T. Seifert, *Eur. J. Inorg. Chem*., 2209, **1999**.

[173] S. Szumacher, I. Madura, J. Zachara, A.R. Kunicki, *J. Organomet. Chem*., 613, 119, **2000**.

[174] M. Grenz, E. Hahn, W. W. Du Mont and J. Pickardt, *Angew. Chem.*, 96, 69, **1984**.

[175] M. Grenz, E. Hahn, W. W. Du Mont and J. Pickardt, *Angew. Chem. Int. Ed. Engl*., 23, 61, **1984**.

[176] B. G. McBurnett and A. H. Cowley, *Chem. Commun.*, 17, **1999**.

[177] A. E. Wetherby Jr., L. R. Goeller, A. G. DiPasquale, A. L. Rheingold, C. S. Weinert, *Inorg. Chem.*, 46, 7579, **2007**.

[178] A. E. Wetherby Jr., L. R. Goeller, A. G. DiPasquale, A. L. Rheingold, C. S. Weinert, *Inorg. Chem.*, 47, 2162, **2008**.

[179] M. Veith, C. Mathur and V. Huch, *J. Chem. Soc., Dalton Trans.*, 995, **1997**.

[180] M. Drager, L. Ross and D. Simon, *Rev. Silicon, Germanium, Tin, Lead Compds.*, **7**, 299, **1983**.

[181] M. Dräger and L. Ross, *Z. Anorg. Allg. Chem.*, 460, 207, **1980**.

[182] M. Dräger and L. Ross, *Z. Anorg. Allg. Chem.*, 476, 94, **1981**.

[183] M. Dräger and D. Simon, *Z. Anorg. Allg. Chem.*, 472, 120, **1981**.

[184] M. Dräger and K. Häberle, *J. Organomet. Chem.*, 280, 183, **1985**.

[185] S. Roller and M. Dräger, *J. Organomet. Chem.*, 316, 57, **1986**.

[186] L. Ross and M. Dräger, *J. Organomet. Chem.*, 199, 195, **1980**.

[187] L. Ross and M. Dräger, *Z. Anorg. Allg. Chem.*, 519, 225, **1984**.

[188] D. Vanoppen, M. Veith and K. Valtchev, *United States Patents*, No. US 7, 026, 269 B2, **2006**.

[189] M. F. Lappert, P. P. Power, A. R. Sanger, S. C. Srivastava, *Metal and Metalloid Amides*, Wiley & Sons, New York, **1980**.

[190] M. Veith, P. Spaniol, *Z. Anorg. Allg. Chem*., 624, 1891, **1998**.

[191] J. A. Francis, S. G. Bott, A. R. Barron, *J. Organomet. Chem*., 597, 29, **2000**.

[192] W. Zheng, N. C. Mosch-Zanetti, H. W. Roesky, M. Noltemeyer, M. Hewitt, H.-G. Schmidt, T. R. Schneider, Angew. *Chem. Int. Ed. Engl*., 39, 4276, **2000**.

[193] H. Nöth, A. Schlegel, S. R. Lima, *Z. anorg. Allg. Chem*., 627, 1793, **2001**.

[194] H. Nöth, A. Schlegel, B. Singaram, J. Knizek, P. Mayer, T. Seifert, *Eur. J. Inorg. Chem*., 173, **2001**.

[195] M. J. Harvey, M. Proffitt, P. Wie, D. A. Atwood, *Chem. Commun*., 2094, **2001**.

[196] W. Zheng, H. W. Roesky, M. Noltemeyer, *Organometallics*, 20, 1033, **2001**.

[197] M. Veith, O. Schütt, J. Blin, J. Frères, S. Becker and V. Huch, *Z. anorg. allg. Chem.*, 628, 138, **2002**.

[198] D. H. Harris and M. F. Lappert, *J. Chem. Soc. Chem. Commun*., 895, **1974**.

[199] W. Wayne and H. Adkins, *Organic Syntheses*, 21, 8, **1941**.

[200] W. Wayne and H. Adkins, *Organic Syntheses*, Coll. Vol. 3, 48, **1955**.

Part 2

Hydrogen Adsorption by Al/Al_2O_3 Composite Nano-Wires (NWs) and Ni/Al_2O_3 Composite Nano-Powders (NPs)

Introduction

1. General Overview

"The ultimate objective of this Convention and any related legal instruments that the Conference of the Parties may adopt is to achieve, in accordance with the relevant provisions of the Convention, stabilization of greenhouse gas concentrations in the atmosphere at a level that would prevent dangerous anthropogenic interference with the climate system. Such a level should be achieved within a time-frame sufficient to allow ecosystems to adapt naturally to climate change, to ensure that food production is not threatened and to enable economic development to proceed in a sustainable manner"[1].

This is the excerpt from the objectives of the Kyoto protocol singed by nearly all the countries of the world in 1997. It emphasized at three main points, reduction of greenhouse gases, giving time to the ecosystem for adaptability, and sustainability of economic growth. The current main sources of energy that is the fossil fuels are the major culprits of the ecosystem. Fossil fuels produce the hazardous gases for environment, which are carbon dioxide (CO_2), methane (CH_4) and nitrous oxide (N_2O). To reduce and/or eliminate these gases in the ecosystem, we need to abandon the use of energy sources responsible for greenhouse gases. Is it possible while keeping sustainable economic development and growth? The answer to this question is yes, but on the expenses of alternative environment friendly energy sources to sustain the economic development. There are many alternatives to fossil fuels that are solar, wind power, geothermal, hydroelectric, biofuel etc. However, all the above sources of energy affect the ecosystem in different ways. If some are unable to be used onboard, the others are not purely eco-friendly. Renewable energy sources producing electricity can provide automobiles with a clean and efficient source of power; however, there are currently no practical methods of storing this electrical energy. Biofuel is used at the moment onboard as an alternative to fossil fuels but this affects the supply of food to the growing masses on one hand and on other hand gives nitrous oxide (N_2O) to the environment during its production which has 310 times more impact on global warming than that per mass unit of carbon dioxide (CO_2).

Apart from all these alternative sources, there is one which is not only perfectly clean and environment friendly but also abundant and endless source of energy, that is the hydrogen. Hydrogen was discovered in 16th century and was recognized by Cavendish as an element in 1766 [2]. It was Jules Verne who for the first time anticipated hydrogen as a future energy carrier [3]. However, it was the oil crisis in the beginning of 1970s which compelled the world to think about an alternative source of energy and hydrogen was chosen as an alternative source of energy. The debate about hydrogen economy started and efforts have been made for the development of new methods of hydrogen production and storage. However, the efforts were revolving around the economic benefits of hydrogen rather than its environmental effects. The universal temperature raise noted in the last few decade as a result of excessive exhaust of the greenhouse gases paved the way for boosting up the efforts for hydrogen fuel.

Hydrogen is the most abundant element in the universe. It constitutes 75% of the universe by mass [4] and the percentage by number of atoms is more than 90% [5]. The earth's atmosphere has negligible amount of hydrogen, which is 1.0 ppm by volume; however it is the third most abundant element on the surface of earth [6]. Hydrogen does not exist free but can be found in chemical compounds in the earth crust. The binding of hydrogen in these compounds is governed by nearly all types of bonds that is covalent, coordinate covalent and ionic [7].

One of the questions is that whether hydrogen is 100% environmentally friendly? The answer is yes. To explain the above answer, let see first the combustion process of hydrogen. Hydrogen gas (dihydrogen) is highly flammable. It burns in air according to the following reaction pathway (Eq. 2.1):

$$2H_2\,(gas) + O_2\,(gas) \rightarrow H_2O\,(liq) + Energy \qquad (2.1)$$

The burning of hydrogen in presence of air gives only pure water as a by-product [8-9] beside energy. There is no other by product produced during the burning of hydrogen in presence of air. From these considerations, it is evident that hydrogen as an energy source is not only environmentally friendly, but will have positive impact upon the ecosystem. It will also support the adaptability of the ecosystem with the natural climate change. If at one side hydrogen fuel will not affect the environment but will contribute positively to the

environment, on the other side it has the highest energy content per unit of mass for any known fuel [8, 10]. Hydrogen gives 120 MJ/kg energy upon burning, which is the highest energy content per kg of the known fuels. Gasoline has three times less energy contents compared to hydrogen (44 MJ/kg). However, the energy content of hydrogen upon volume basis is not so much appreciable. For example 8MJ/L energy could be obtained from liquid hydrogen upon burning which is one fourth of the gasoline (32 MJ/L for gasoline) [11].

As mentioned earlier, hydrogen exists in bonded form and is not readily available for large use. But hydrogen as energy carrier is need of the time to synthesize it using other energy sources and transform further to energy for practical applications. Economical and environmentally friendly methods for hydrogen production are very important and produce a great challenge for the scientific community. Although, the current methods in use are acceptable, up to some extent, both economically and environmentally. However, efforts should be continued for discovering new and environmentally friendly methods for hydrogen production. The amount of energy to provide for the release of hydrogen bonded in different forms depends upon the nature of the chemical bond. Hydrogen can be obtained from natural gas through stream reforming, by the electrolysis of water and by splitting of water molecules at the surface of photovoltaic cells. Biological systems could be termed as the most clean and environmentally friendly methods of hydrogen production. In these methods different organisms produce hydrogen during their metabolisms. Cyanobacteria and green algae are good examples which produce hydrogen during their metabolism but this method is too immature to produce large scale hydrogen.

All the above challenges in production of hydrogen must be addressed. However, the real problem ahead of hydrogen economy is the safe and efficient storage of hydrogen rather than hydrogen production. The transition of fossil fuel economy into the hydrogen economy will come true only when safe and efficient hydrogen storage methods are achieved. The hydrogen is stored in different forms that is gas, liquid and in solid materials. Gaseous hydrogen is stored at very high pressures (300-700 bars). At such a high pressure, the storage tank is always at risk. Therefore, improvement in the tank material must be the first priority to ensure its integrity. Improvement in the compression technology is also necessary which will contribute to quick and efficient filling of the tank on one hand and on the other hand will ensure high pressure fillings. But this method seriously suffers of high cost and pressure,

lower volumetric capacity, very long refilling times, heat management etc. Onboard applications are hindered by the safety concerns.

The volumetric capacity can be improved by storing hydrogen in liquid form where cryogenic hydrogen (23K) is obtained by liquefaction. The energy density of hydrogen in liquid state is 0.070 kg/L compared to 0.030 kg/L at 10,000psi hydrogen gas tanks. Highly insulated tanks are required for hydrogen storage in liquid. Besides this the liquefaction is an energy consuming process. 30% energy contents of the hydrogen fuel is consumed during liquefaction. The input is much more than the out put, therefore, its onboard application is yet a dream to come true.

To reduce the problems related to the gas and liquid (cryogenic) hydrogen, its storage in solid materials is safer and more energy efficient and could substantially reduce these problems. There are three common mechanisms for storing hydrogen in solid materials based upon the mode of interaction of the gas with the solid. These mechanisms are absorption, adsorption and chemical reaction. In absorption, hydrogen absorbs into the bulk of the material. The process started by the adsorption of the H_2 molecules upon the surface of the material followed by the dissociation of molecules into atoms. The atoms diffuse into the appropriate sites where absorption occurs. This process is mostly observed in metals where metal hydrides form. Adsorption could occur either by physisorption or by chemisorption based on the energy of the adsorption mechanism. Physisorption is governed by weak van der Waal forces where the hydrogen molecules make bonds with the surface of material by physical forces. The minimum potential energy is at a distance of one molecular size of hydrogen between the adsorbing surface and hydrogen, therefore, the size of the pores is very important in physisorption. For efficient and maximum hydrogen storage by this mechanism, extremely small pores are necessary [12-13]. Chemisorption, on the other side occurs by the interaction in which the adsorbate is chemically bonded onto the adsorbent. Chemisorption is different from chemical reaction as in chemisorption the hydrogen molecule makes a bond with the surface of material by electron sharing. However, in chemical reaction the hydrogen storage is achieved by a displacive chemical reaction Adsorption processes typically require highly porous materials, which has not only maximum specific surface area (SSA) but also allow easy uptake and release of hydrogen. Of all the modes of hydrogen storage, adsorption has been investigated the most for onboard vehicular applications. The reasons are evident, high

efficiency, easy uptake and release etc. the following section gives a brief account of the materials used for hydrogen adsorption.

Many materials have been considered for the last few decades for hydrogen storage and the last fifteen to twenty years have been devoted to the adsorption of hydrogen (that is physisorption and chemisorption) by porous materials. Most abundantly has been studied the carbon based materials due to their high porosity and pore sizes distributed over a long scale. Fullerene and carbon nano-tubes (CNTs) discovery initiated this field of research in hydrogen storage [14-15]. The first hydrogen storage experiment upon the carbon based material was carried out by Kidnay and Hiza in 1967 [16]. Their experimental work based upon the hydrogen adsorption on high surface area carbon with no aim of hydrogen storage. Carbon based material was used for the first time for hydrogen storage purposes by Carpetis and Peschka in 1970s [17]. They are the actual pioneers of the hydrogen adsorption upon activated carbon, a highly porous carbon obtained by the pyrolysis of carbon containing materials in absence of air followed by chemical activation. Since then carbon based materials have been studied for hydrogen adsorption extensively. This includes high surface area activated carbon materials [16], graphite nano-fibres [18-19], single and multi-walled nano-tubes [20-21]. Various modifications have been brought in to the structure and nature of the carbon based materials to improve the hydrogen adsorption capacity of these materials [22-23]. Beside carbon based materials, many other porous materials have been studied for the last few decades, for example, metal-organic framework compounds [24], Metal hydrides [25], Clatherates [26] etc. but none of them have achieved the target [12, 27-28] defined by the United States department of energy (DOE).

The failures of all these hydrogen storage materials lie in their single storage mechanisms. The hydrogen storage mechanism is either only governed by physisorption [29-30] or by a pure chemical reaction [31 and literature there in]. For example the hydrogen uptake by the carbon based materials is solely due to physical interaction between the adsorbate (hydrogen) and adsorbent (materials) [21, 29-30]. Contrarily the hydrogen uptake by the metal hydrides [many of them are listed in the Hydpark Metal Hydrides Database, 32], complex metal hydrides [33] etc. is due to a complete chemical reaction between hydrogen and the hydrides. One is carried out at cryogenic conditions while the other needs high temperatures. Either is far away from the ambient conditions hydrogen storage.

The challenge for higher amounts of hydrogen storage by using adsorption techniques lies on synthesizing highly porous materials which has a potential for reversible hydrogen storage in such a way that the adsorption mechanism is somewhere in between physical and chemical interaction. Thus the present work is focused on the systematic investigation of the hydrogen adsorption mechanism in different (porous) composite materials, which are Al/Al_2O_3 and Ni/Al_2O_3. The aim is to fill the gap between the two well established mechanisms that is physisorption and chemical reaction and develop a method where the storage could achieve at ambient conditions.

In this part of the thesis is presented preparation of porous material, Al/Al_2O_3 nano-composite for reversible hydrogen storage at ambient condition. The focus is upon construction of reliable hydrogen storage device, Sievert's type apparatus for accurate and precise measurements of hydrogen adsorption isotherms. The results obtained from Sievert's type apparatus are to be compared with those obtained from a commercial state-of-the-art instrument, DSC. This is aimed to establish an exact adsorption mechanism of hydrogen upon the Al/Al_2O_3 nano-composite material. The result obtained using these different experimental approaches on nano-composite materials will contribute to the investigation of a completely novel field.

2. Theoretical Basis and Literature Overview

Hydrogen is the lightest gas of all the gases and has the lowest density. Therefore, it escapes and diffuses easily. Besides this the volumetric energy density of hydrogen at ambient pressure and temperature is too low to use as an energy carrier. To avoid these problems, it is one of the highest challenges to store hydrogen efficiently and safely. In the following sections a brief review of the literature concerning the modes and Methods of hydrogen storage will be presented. Although none of the systems met the target chalked out by the United States department of energy (DOE).

2.1. Compressed Hydrogen

Storing hydrogen in gaseous mode is the simplest of all the storage methods. Hydrogen is stored at high pressure in the compressed hydrogen tanks. Normally hydrogen could be stored

in pressure range of 3000 to 5000-psi. But recent developments in the compression technologies and tank qualities ensured the storage pressure up to 10,000-psi. At this pressure a volumetric energy density of 36 g/L could be achieved at the expense of 15% fuel energy content [34]. Development in the tank material and compression technologies is important to achieve higher pressure storages. Quantum technologies are producing compressed hydrogen tanks with pressure up to 5000-psi and 10000-psi (Figure 2.1). The construction of these tanks has three main parts. The inner thick liner (5mm) formed of high density polyethylene (HDPE) which stops the diffusion of hydrogen gas. It is the barrier for the hydrogen leak off. This layer is covered with a carbon fiber reinforced polymer composite to support the load and the different valves are connected using metal fitting [45]. Carbon fibers and metal fitting increase the cost of the tanks since the materials and processes of production are expensive. To reduce the cost of the tanks, it has been proposed that alternative carbon fiber production methods should be developed and the cost of metal fitting can be reduced by replacing expensive metals with low cost materials which should have good compatibility with hydrogen. A remarkable development has been made during recent research in this direction [35].

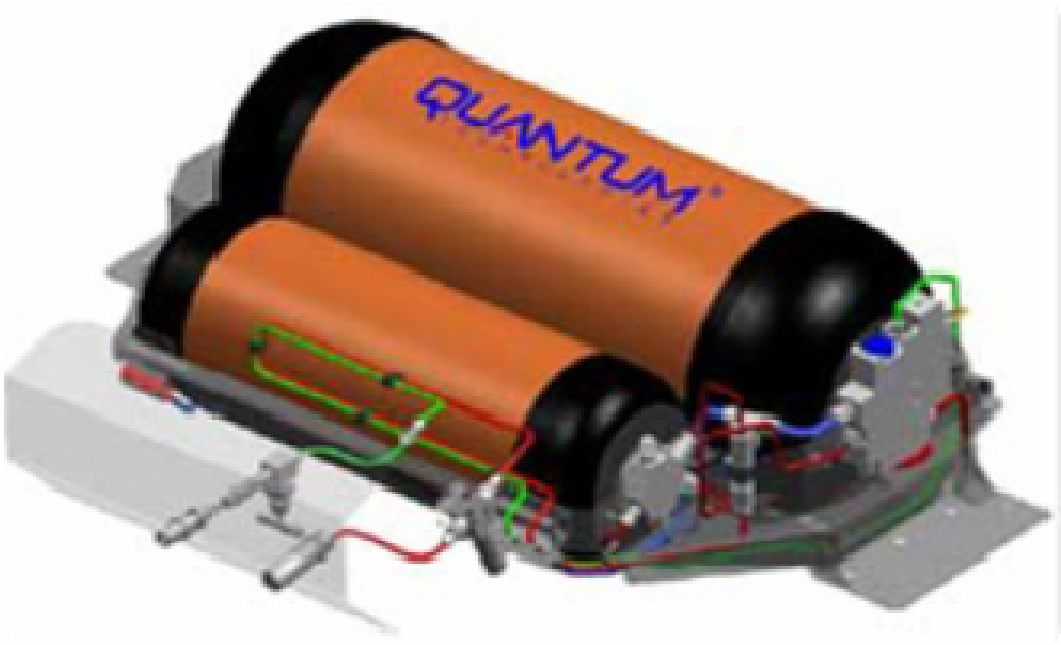

Figure 2.1. Quantum Compressed Hydrogen Storage Tank [Courtesy of Quantum Technologies]

To achieve a longer driving range with the vehicles powered with compressed hydrogen tanks is still a dream. The tank size is quite large compared to the normal gasoline tanks in use. To reduce the size of the tank, the idea of comfortable tank is under investigations. The present gasoline tanks are termed as comfortable as these tanks are well fitted into the available space in the vehicles while the compressed gas tanks are too big to adjust in the available space. Cryo-compressed gas tanks are getting attention due to their greater volumetric energy density. According to this concept the compressed gas tank is cooled to -120 to -196°C using liquid nitrogen. This concept will improve the volumetric capacity of the tank by four fold compared to the normal storage phenomenon [36]. However, the bigger volume of the cooling system will leave little space for the compressed hydrogen tank with in the body of the vehicle. Therefore, the actual volume of tank will be decreased.

It could be concluded that compressed hydrogen storage mode has the advantage of simplicity but high cost, low volumetric energy density, larger tank size etc. are the serious limitations which hinders its practical onboard vehicle applications.

2.2. Liquid Hydrogen

Compressed hydrogen gas has lower volumetric energy density which can be improved by liquefaction since liquid hydrogen has higher volumetric energy density (80 kg/m^3). Hydrogen can be stored in liquid form in different ways; for example in cryogenic temperature liquid hydrogen tanks (Figure 2.2), $NaBH_4$ solution, rechargeable organic liquids etc.

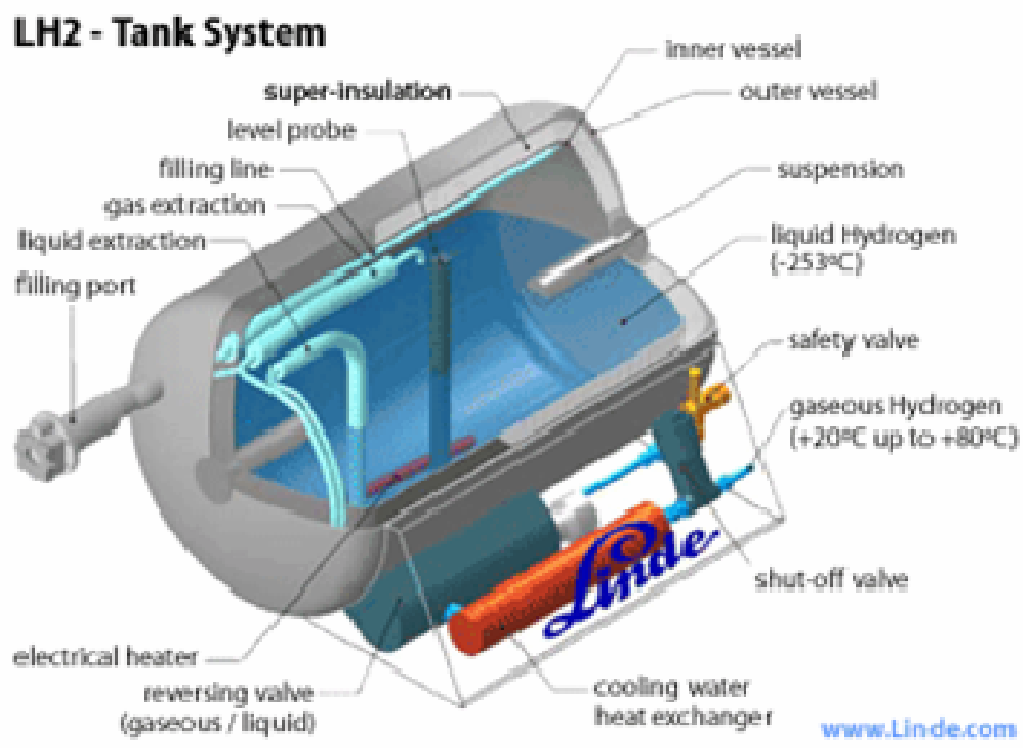

Figure 2.2. Linde tank system for storing cryogenic liquid hydrogen [Courtesy of Linde Gas]

The liquid hydrogen is produced by the Joule-Thompson cycle (Figure 2.3) which is also termed as Linde process. In this process the hydrogen gas is first compressed and then allowed to pass through a throttling valve into an isothermal tank. The gas expands as it enters the tank and cools down to liquefaction. However, the expansion gives liquid gas only when the temperature is well below the inversion temperature of the gas. For most of the gases the inversion temperature is well above room temperature but hydrogen has very low inversion temperature. Therefore, the tank must have the temperature below the inversion temperature of hydrogen (193K), otherwise no liquid hydrogen will form as a result of expansion. The main disadvantage of this mode of hydrogen storage is that the process is highly expensive. The production cost is 8-12 kWh/kg which accounts to 40% of the fuel energy density. Besides, the expansion of the gas is isenthalpic which means that the expansion of H_2 could not bring any beneficial workdone. The process has been improved by modifying it into Reverse-Brayton Joule-Thompson expansion cycle [37]. This new process can reduce the production cost (3.228 kWh/kg) and also gives net energy (work done) since the process is isentropic. This energy can be used for the compression of the gas in recycling process. Turbo-expanders or expansion engines are used in industrial production of liquid hydrogen.

This process is limited for onboard vehicle applications mainly by the cost of production and heat leak, responsible for the “boil off” loss of hydrogen amounting 1% per day.

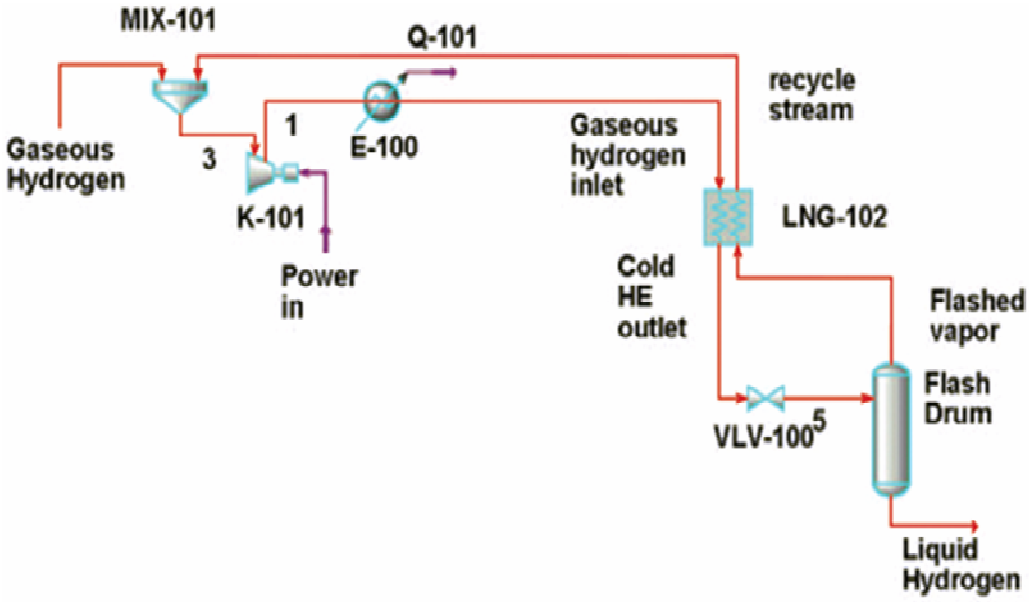

Figure 2.3. Joule-Thompson Expansion Cycle [47]. The gas (H_2) is first compressed and cooled using heat exchangers, then is passed through a throttle valve followed by the isenthalpic expansion which cooled the gas to give a liquid H_2.

NaBH4 solutions are getting attention as liquid hydrogen storage materials [38]. This solution gives 10.9 wt.% of H_2 through a simple reaction (Eq.2.2).

$$NaBH_4\ (l) + 2H_2O\ (l) \rightarrow 4H_2\ (g) + NaBO_2\ \ (S) \qquad (2.2)$$

This process is safe for onboard vehicular applications, but the main problems are the cost of $NaBH_4$ (50 USD/kg) and the recycling of $NaBO_2$. Rechargeable organic liquids can be used as potential hydrogen storage materials. The simplest example is the methylcyclohexane which gives hydrogen through a catalytic reaction. The high reaction temperatures and violent interaction upon exposure to oxidizing agents are the main limitations related to rechargeable liquids.

2.3. Solid Hydrogen (Material-based Hydrogen Storage)

Materials based hydrogen storage can be achieved by three generic mechanisms that are absorption, adsorption and chemical reaction. In the following sections, we will give brief theoretical considerations and literature review of all these three mechanisms.

2.3.1. Absorption

Absorption is the simplest of all the material based hydrogen storage modes. Some metal lattice structures absorb hydrogen by forming nearly all types of bonds that is ionic, covalent and metallic [7]. Hydrogen absorption into the lattice structure is a four-step-process. In first step hydrogen molecules are physisorbed upon the surface of the material. Physisorption is purely governed by the physical interactions, for example van der Waals forces. In the next step the hydrogen interacts in a pure chemical way and is chemisorbed. The chemically adsorbed hydrogen that is the dissociated hydrogen atoms diffuse into appropriate lattice sites and finally absorb into the lattice. The structure of the metal lattice and nature of material is important in absorption process. For example the diffusion is very high in vanadium metal lattice because of two reasons. One V has bcc structure which has higher diffusion rate then the fcc and hcp, second V is more reactive than its bcc counterparts Nb, Ta etc. The higher reactivity of V is responsible for its pre-activation for hydrogen dissociation since an oxide layer is formed at the surface of V lattice upon exposure to oxygen. The activation can be improved by doping V with Zr or Ti. Contrarily Pd dissociates hydrogen without pre-activation. Therefore, the dissociation of hydrogen is either activated or non-activated depending upon the nature of the metals. Hydrogen may dissociate into electrons and protons [39]. Protons diffuse into the lattice interstices and electrons enter into the d orbitals of metals. This approach has been proved by the changing magnetic nature of Pd [39]. Pd is paramagnetic with electrons holes in 4d band. As the hydrogen concentration increases in the Pd lattice, its magnetic strength decreases. At 60 wt.% hydrogen concentration the Pd lattice become completely diamagnetic.

The absorption capacities and conditions are different for different metals. Therefore, the metals can be categorized into two broad groups. Good absorbers are those metals which absorb hydrogen at low temperature. In these metals the increasing temperature has adverse

effect. As the temperature increases the hydrogen absorption decreases. Contrarily, in bad hydrogen absorbers the situation is different. In these metals the absorption occurs at higher temperature and increases with increasing temperature. Silver and gold absorb hydrogen in molten state and give off in solid state. Pd is at the top of all the metals since it absorb even in solid state. Pd can absorb H_2 900 times of its volume during electrolysis.

2.3.2. Adsorption

Adsorption is termed as surface phenomenon. The adsorbate which is dihydrogen, H_2 interacts with the surface of the adsorbent (material). That is why the role of surface area in adsorption processes is very important. Depending upon the nature of interaction between the adsorbate and adsorbent, adsorption is further divided into two generic types, i.e. physisorption and chemisorptions. In the following sections we will briefly overview these two methods of hydrogen storage in light of reported literature.

2.3.2.1. Physisorption

In physisorption mode of H_2 storage the adsorbent adsorbs undissociated hydrogen molecules at its surface. Weak van der Waals forces are responsible for the adsorption of hydrogen over the surface of the materials. The force of attraction originates from the fluctuation of charge at the hydrogen molecule and the surface atoms. The fluctuating charge at hydrogen molecule and the induced dipole produced in the surface atoms contributes to the long range forces of attraction. This force of attraction is experienced when the molecules reach in the periphery of surface at a distance of one hydrogen molecule diameter. Bur at smaller distances the short range repulsive forces originate due to the interaction of the electronic densities of the hydrogen molecules and surface atoms.

The hydrogen adsorption isotherm is calculated by using the grand canonical Monte Carlo simulation [40]. The motion of hydrogen in a given pore is measured using this program at constant temperature and a chemical potential. The energy of interaction between the hydrogen molecules and the surface atom is obtained by Lennard-Jones potential (Eq. 2.3):

$$\mu(s) = 4\varepsilon\left[\left(\frac{\delta}{s}\right)^{12} - \left(\frac{\delta}{s}\right)^{6}\right] \quad (2.3)$$

where,

μ = potential energy

ε = depth of potential well

δ = zero inter-particle potential distance

s = distance between the particles

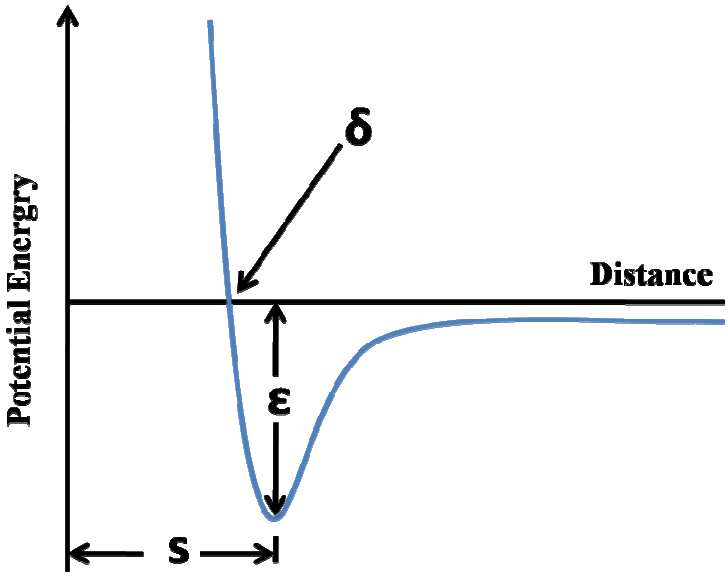

Figure 2.4. Lennard-Jones potential. The minimum potential energy is at distance‘s’ and this is approximately equal to one hydrogen molecular diameter which is the distance at which the van der Waals interaction occurs

Figure 2.4 gives the potential energy curve as a function of distance. The minimum in the potential energy curve reaches at a distance of one molecular diameter from the surface of adsorbent. There is no energy barrier for the hydrogen to pass. If we neglect any diffusion barrier for hydrogen, the adsorption is non-activated.

Since physisorption is a surface phenomenon, therefore, highly porous material is required for maximum adsorption. The pore size is important as very small distance is required for

separation between hydrogen molecules and the solid surface. However, the rule of pore geometry, temperature and pressure is also noteworthy [41].

Among the porous materials carbon based materials are studied the most owing to their versatile structures. The first ever hydrogen adsorption by carbon based materials was reported in early 70s by Kidnay and Hiza [16]. Though the subject of their study was not hydrogen storage at first but later in 1976, they studied systematically the hydrogen adsorption by the activated carbon (coal/charcoal). Carpetis and Peschka in 1976 reported the hydrogen adsorption by activated carbon at liquid nitrogen temperature [42-43]. Since then many researchers have published scientific reports and papers about the hydrogen adsorption by the activated carbon materials. Prof. J. A. Schwarz dedicated nearly one decade (1980s) to the systematic study of hydrogen adsorption by the commercially available activated carbon. According to his findings the highest specific surface area materials are the best candidates for larger amounts of hydrogen storage [44]. He has reported 4.2 wt.% hydrogen adsorption by the activated carbon at 87K and 59 bars [45]. 1.6 wt.% hydrogen adsorption by the activated carbon at room temperature has been also reported [Ströbel et. al., 46]. Recently it has been reported by Hirscher *et. al*. that activated carbon can store hydrogen reversibly up to 4.5 wt.% at cryogenic temperatures and pressures, however the room temperature adsorption capacity of hydrogen has been reported by this group only up to 1 wt.% [30].

The discovery of single walled carbon nanotubes (SWCNTs) in the early 1990s [47] and the first report of hydrogen adsorption over the SWCNTs [Dillon et. el., 20] has changed the course of hydrogen adsorption studies by the carbon based materials. Dillon *et. el.* reported 10 wt.% adsorption by the SWCNTs at 300K and 0.399 atm pressure. Later on, it was reported that Li and/or K doped SWCNTs adsorb hydrogen up to 20 wt.% at 473K/673K and 14 wt.% at room temperature [Chen.et.al., 23]. Liu *et. al*. [48] reported 4.2 wt.% at room temperature and 99 atm pressure. As SWCNTs have been studied very extensively for hydrogen adsorption, the multiple walled carbon nanotubes (MWCNTs) attracted less attention. The MWCNTs are not suitable for hydrogen adsorption due to their small hollow and no space between the concentric walls of the tubes. Work has been done over carbon nanofibers as hydrogen storage materials. It has been reported that the herringbones carbon nanofibers adsorb hydrogen up to 68 wt.% [49]. However, most of the hydrogen released as soon as the hydrogen pressure is decreased to atmospheric level and temperature reaches to that of 25°C.

The mechanism of adsorption is not yet known though several systematic studies have been brought to corroborate it [50-51].

Metal organic frameworks (MOFs) are emerging as potential hydrogen storage materials due to their high porosity and ease of tuning their pores size and volume. MOFs have been discovered at the end of last decade by Yaghi *et. al.* [52]. The $Zn_4O(CO)_6$ supertetrahedra are interlinked using organic linkers such as carboxylate. A family of MOFs has been developed in the following years of this discovery using different organic linkers (mostly carboxylate) as well as metals (Zn, Cu). Figure 2.5 gives a metal organic framework named as MOF-5 [52] with the crystal suggested formula $Zn_4O(BDC)_3.(DMF)_8(C_6H_5Cl)$ (where BDC = 1,4-benzenedicarboxylate and DMF = N,N'-dimethylformamide). The central oxygen is tetrahedral with four tetrahedral Zn atoms in its surroundings making a supertetrahedral cluster. The clusters are interlinked by carboxylate linkers. DMF and chlorobenzene are filled into the cavities. There are two different types of cavities lined with H and C atoms, the larger and smaller cavities with volumes 15.1Å and 11.0 Å, respectively. The atoms of clusters occupy only 20% of the total volume of framework which means 80% volume is unoccupied. Therefore, MOFs are highly porous materials. The specific surface area for MOF-5 is 2900 m^2/g with a pore volume of 0.61-0.54 cm^3/cm^3. Recent development has shown that the specific surface area (SSA) can be increased to 4500 m^2/g [53] and the pore size and volume could be tuned accordingly by changing the linkers. The MOFs show higher thermal stability that is upto 300°C for several hours beside their high SSAs and tunable pore sizes as well as volumes [52].

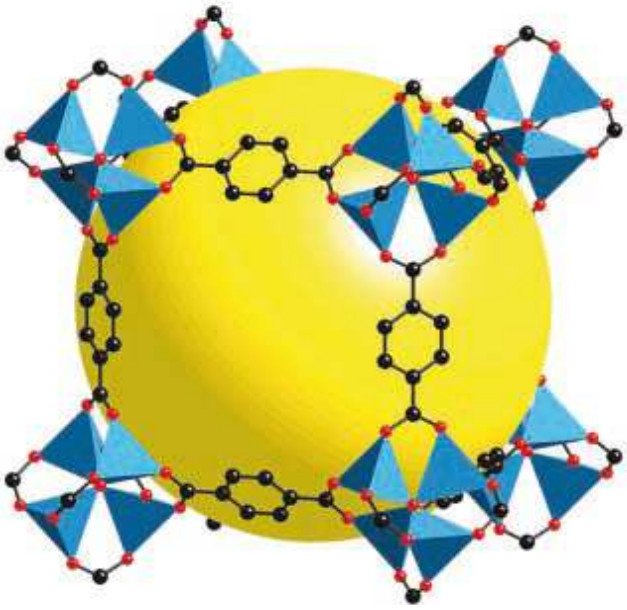

Figure 2.5. Single-crystal x-ray structures of MOF-5 [24].

The first ever hydrogen sorption by MOFs was reported by Yaghi *et. al*. in consecutive papers [24]. 4.5 wt.% hydrogen has been recorded over MOF-5 at 78K and 20 bar pressure which corresponds to 17.2 H_2 per $Zn_4O(BDC)_3$ unit. At room temperature the uptake was measured up to 2 wt.% at 20bar. But the review of very recent literature has shown that the best hydrogen wt.% adsorbed by MOFs is up to 2 wt.% at cryogenic temperature [54]. Contrarily, at room temperature the up take is insignificant (0.2 wt.%) [55].

2.3.2.2. Chemisorption

Contrary to physisorption, chemisorption involves the adsorption of molecules and/or atoms on a surface of adsorbent making a proper bond. Therefore, the wt.% of the hydrogen stored through chemisorption is sufficiently higher compared to physisorption. The bonding is stronger and the binding energy is considerably higher, in excess of 0.5 eV [56]. However, the binding energy in most cases is as high as 3 or 4 eV [56]. The process of chemisorption corresponds to the electrons sharing between the hydrogen atoms/molecules and the atoms in the surface of the adsorbent.

Chemisorption can be divided into two different types, dissociative and non-dissociative. In the first case, the hydrogen molecules dissociate upon reaction with the atoms of the

adsorbent while in the latter case the H-H bonding remains intact. In dissociative mechanism the hydrogen molecules first adsorb at the surface of adsorbent and then dissociates into hydrogen atoms making hydrides (a schematic of the reaction is shown in eq. 2.4) [57].

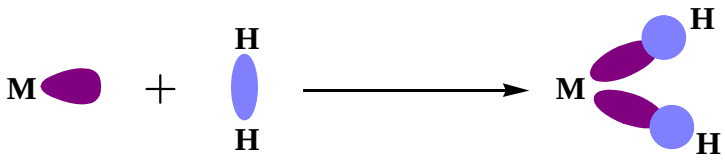

(2.4)

In non-dissociative chemisorption reaction the covalent bond formed between the surface atoms and the hydrogen molecule without the dissociation of H-H bond. An overlapping occurs between the molecular orbitals of H_2 and the atomic orbitals of the atoms in the surface of the storing material. The electrons pair accepting species (specifically the transition metals) enhance the strength of the bond by back donation of their nonbonding electrons into the anti-bonding molecular orbitals of H_2 molecule (eq. 2.5) [56-57].

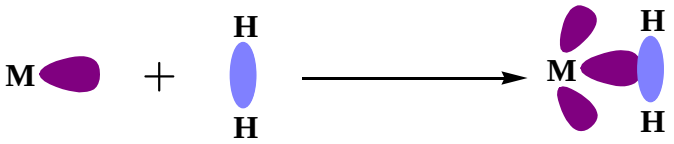

(2.5)

In 2001, it has been proven [Eckert et. al., 58] that molecular H_2 adsorbs on Fe-ZSM5 cluster making a chemical bond without the dissociation of H-H bond. Using inelastic neutron scattering (INS) spectroscopy, it has been studied that the hydrogen molecules adsorb on the extraframework of iron species in a chemical fashion. The Fe-ZSM5 cluster was prepared by the sublimation of $FeCl_3$. From the interpretation of the INS data, they have concluded that there are two adsorbing sites in the cluster where hydrogen molecules form bond with the iron center. An extensive reviews about the M(η^2-H_2) bonds can be found in the references [59-60].

2.4. Materials

The theme of the above discussion is now very clear, that is for higher wt.% hydrogen adsorption, the choice of material is very crucial and important. The material to be used for hydrogen storage must have high specific surface area, which means that high porosity is

important. The interaction between the guest (storage material) and the host (hydrogen) should be somewhere in between physisorption and chemisorption. In the following section we will give a brief review of the materials used in this work for hydrogen storage which meets the above requirements.

2.4.1. Al/Al_2O_3 Composite Nano-Wires (NWs)

The Al/Al_2O_3 composite nano-wires (NWs) were prepared in our research group (M. Veith) [61] by the decomposition of *tert*-butoxyalane of the chemical formula $[H_2Al(OtBu)]_2$ [62] in a cold wall CVD reactor [63]. The highly volatile *tert*-butoxyalane has been decomposed upon a substrate as a thin film. The nature, chemical composition and morphology of the resulting thin films strictly depend upon the substrate temperature. It has been observed that below 300°C substrate temperature, the decomposition of the precursor gives a transparent glass like layer upon the substrate and was termed as HAlO owing to its chemical composition [64]. The chemical composition of HAlO reveals that H, Al and O are present in 1:1:1 ratio. The metastable HAlO converts into Al/Al_2O_3 composite upon heating above 300°C. The direct decomposition of the precursor above 350°C also gives Al/Al_2O_3 composite nano-particles. Electron microscopic investigations revealed that the particles have an aluminum core wrapped up by the amorphous Al_2O_3 layer. The stoichiometric ratio of Al^0/Al^{+3} = 1:2 [65].

After getting two different materials with distinct chemical and structural variations by the same experimental set up but only with different temperatures, the quest for differences in the final product was continued. It was discovered that at temperature above 550° (though the actual process starts at 490°C but 550°C is optimum) core shell nano-wires can be obtained by the decomposition of tert-butoxyalane in the same CVD setup upon a substrate as a thin film [66]. This was a landmark discovery since for the first time nano-wires were prepared in a direct way without the use of catalyst. The core shell NWs have an Al core and Al_2O_3 shell confirmed by HR-TEM. High magnification SEM and TEM images revealed that the NWs can be described as cylinder with a ball like tips. Al is crystalline metal inside the amorphous Al_2O_3. The stoichiometric ratio of Al/ Al_2O_3 = 1:1. SEM images describe the highly porous texture of the NWs.

The decomposition mechanism of the precursor in CVD chamber was studied by in-situ mass spectrometry [65]. From the resulting mass spectrum analysis it was concluded that the byproducts liberated as gases are hydrogen and *iso*-butene and a decomposition mechanism was derived (Scheme 2.1). The size and diameter of the NWs strictly depends upon the decomposition of the precursor and its flow over the substrate. Therefore, optimization of the process for specific dimensions of NWs is important.

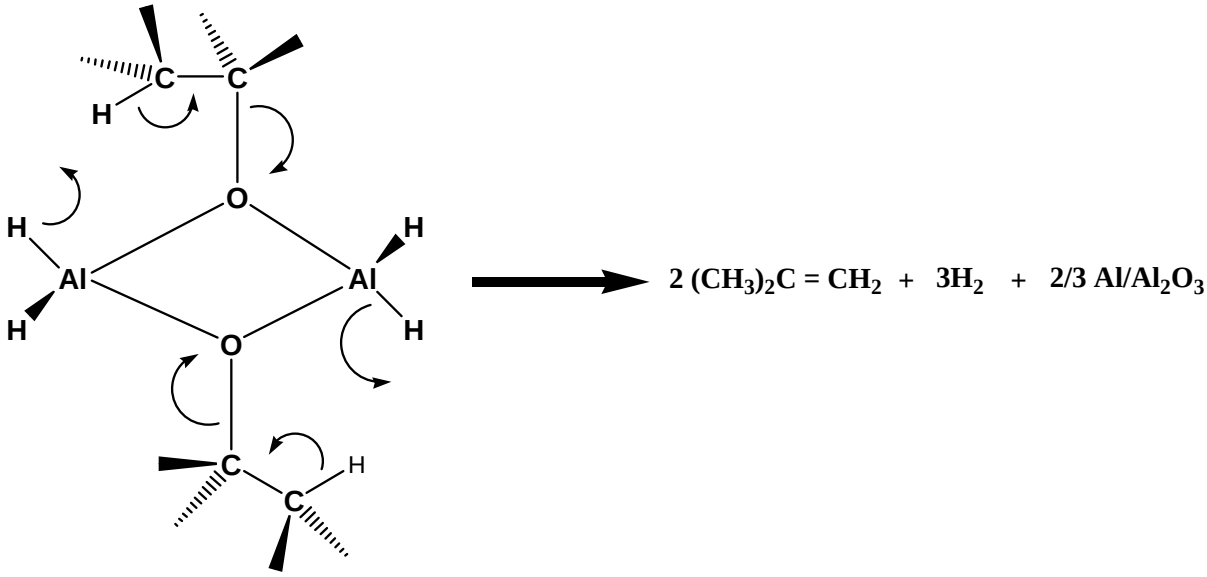

Scheme 2.1. The decomposition mechanism of the single source precursor, $[H_2Al(OtBu)]_2$ in cold wall CVD

2.4.2. Ni/Al_2O_3 Composite Nano-Material

Nickel is frequently used as a catalyst for hydrogenation, especially of carbon double bonds. The most popular of the nickel catalyst is the Raney nickel which is formed by leaching of nickel aluminum alloy using KOH. In this process the Al (catalytically inactive) is leached out leaving behind catalytically active black sponge of Ni. However, this sponge is highly pyrophoric and must be used under inert atmosphere. Also it must be prepared freshly just before use. Once it is oxidized then it is not possible to regenerate. To overcome these problems related with the Ni catalyst, certain modifications have been introduced. The concept of supported Ni catalyst has been investigated and gave very good results in terms of stability and activities. Alumina supported Ni has been produced and studied by various

researchers for their stability in air and reactivity. Juan-Juan *et. al.* [67] reported the alumina supported Ni/Al_2O_3 composite catalyst. It was prepared by excess-solution impregnation. To obtain a 10 wt.% nickel catalyst, a pelletized γ-alumina and $Ni(NO_3)_2$ solution were mixed together. After impregnation the catalyst was dried overnight at 100°C. High energy ball milling technique was used to prepare the Ni/Al_2O_3 composite nano-powder [68]. Al and NiO powders were added in 2:3 ratio and mixed with Al_2O_3 in a composition ratio where the final Ni content was 10 wt.%. The mixture was ball milled for 5 hours and sintered at 1400°C for 1 hour. Yi *et. al.* [69] prepared Ni/Al_2O_3 utilizing sol-gel technique. It was prepared by adding Ni stearate into the Al *sec*-butoxide while using *sec*-butylalcohol as solvent. After addition small amounts of water the reaction mixture was stirred for 48 hours followed by drying at 80°C for 48 hrs. The gel was then sintered at 450°C in air for 3 hrs. However, Veith *et. el.* [80-81] have reported a novel method for the preparation of Ni/Al_2O_3 composite materials with many folds advantages over other processes. For example, the process is simple to perform, high stability of the resulting catalyst in air, low activation temperature needed etc. The catalyst was prepared by the decomposition of $H_2Al(O^tBu)$ over NiO powder in a cold wall CVD reactor [80]. We have prepared Ni/Al_2O_3 nano-composite materials utilizing the same experimental set up but Instead of NiO we have used $Ni(acac)_2$, which is cheap and available commercially. The coating of $Ni(acac)_2$ with the $H_2Al(O^tBu)$ single source precursor gives highly stable Ni/Al_2O_3 nano-composite material.

Objectives

So far the hydrogen storage technologies emerged as a result of popular methods revolve around two common mechanisms. One is physisorption in which the hydrogen storage is solely achieved by weak physical forces. Second is the chemisorption in which the hydrogen storage is controlled by displacive chemical reactions. In both the processes the conditions for hydrogen storage are far away from the ambient due to which the dream of hydrogen economy has not come yet true.

The need of the time is that, to develop a method for hydrogen storage which is governed by the mechanism somewhere in between the two mechanisms that is physisorption and chemisorption. To achieve the desired storage mechanism the choice of material is important. The material should be such which can store hydrogen reversibly at ambient conditions. Therefore, the objectives of this work were to achieve the above defined goals by the synthesis of material:

- Which can reversibly store maximum wt.% hydrogen to meet the target defined by United States department of energy (DOE).
- The hydrogen storage mechanism must be in between the physisorption and chemisorption and/or chemical reaction.
- The storage could achieve at ambient conditions to ensure easy uptake and release of hydrogen.

Reliable measurement of hydrogen adsorption is also important for accurate and precise results, especially when the sample size is very small. Therefore, one of the objectives was to develop a reliable, cheap and portable apparatus for hydrogen adsorption. It was also targeted that the device should be designed in such a way where it could be used for hydrogen adsorption upon thin films. It is also targeted to develop a comparative study of the materials and techniques. This objective has been achieved by synthesizing different materials for hydrogen adsorption as well as using different techniques.

Results

1. Sample Characterization

Al/Al_2O_3 composite Nano-Wires (NWs) have been studied and characterized very well in our research group (research group M. Veith). But the changing parameters (for example temperature, precursor flow, target etc) have a significant effect upon the final product. As we have discussed in the previous section that at temperature below 300°C, the decomposition product of $[H_2Al(O^tBu)]_2$ upon a substrate is the glass like transparent metastable amorphous material HAlO. While at temperature above 300°C, the decomposition of $[H_2Al(O^tBu)]_2$ gives a core shell nano-balls as thin films upon substrate. The deposition of $[H_2Al(O^tBu)]_2$ at temperature above 450°C gives core shell nano-wires upon substrate as thin film. Similarly, the size, thickness, density, surface areas etc. of the wires alter with the changing parameters. Therefore, the process was optimized to get highly porous nano-wires as thin film after repeating the experimental procedure at different deposition temperatures, precursor flows, deposition time etc. The NWs, optimum for the sorption of hydrogen were produced by the decomposition of $[H_2Al(O^tBu)]_2$ upon stainless steel substrate maintained at 580°C temperature. The flow of precursor over the substrate was maintained at 9.0×10^{-2} mbar pressure.

1.1. Al/Al_2O_3 Composite Nano-Wires (NWs)

Al/Al_2O_3 composite Nano-Wires (NWs) have been produced by the decomposition of single source precursor (SSP), $[H_2Al(O^tBu)]_2$, upon a stainless steel substrate in a cold wall CVD reactor at 580°C temperature maintaining the gaseous flow of precursor at 9.0×10^{-2} mbar pressure. For comparison purposes, thin films have been also obtained at other decomposition temperatures and precursor's flow. The decomposition of the molecular precursor occurs according to the following equation (eq. 2.6):

$$\tfrac{1}{2}\,[H_2Al(O^tBu)]_2 \xrightarrow{T=580^\circ C} 1/3\ Al/Al_2O_3 + 3/2\ H_2 + (CH3)_2C{=}CH_2 \qquad (2.6)$$

The detailed synthetic procedure is given in experimental section. The samples were characterized by XRD, SEM, TEM and BET analysis.

1.1.1. XRD Analysis of Al/Al_2O_3 Composite Nano-Wires (NWs)

The Al/Al_2O_3 composite NWs thin film was characterized by powder X-ray diffraction. To avoid interferences from steel, we have deposited the NWs upon a glass substrate at the same temperature and pressure for XRD analysis. Figure 2.6 shows the XRD pattern for the as deposited NWs. The crystalline phase is aluminum (PDF: 85-1327) with five distinct peaks at 38°, 44°, 65°, 78° and 82°. Since the film is very thin, therefore, the intensities of the peaks are comparatively low. However, the quality of the Al crystals is good as the peaks are sharp enough. The wave like background indicates that alumina is amorphous at this deposition temperature. All sorts of depositions above 450°C give similar spectrum which indicates that the material obtained is always biphasic.

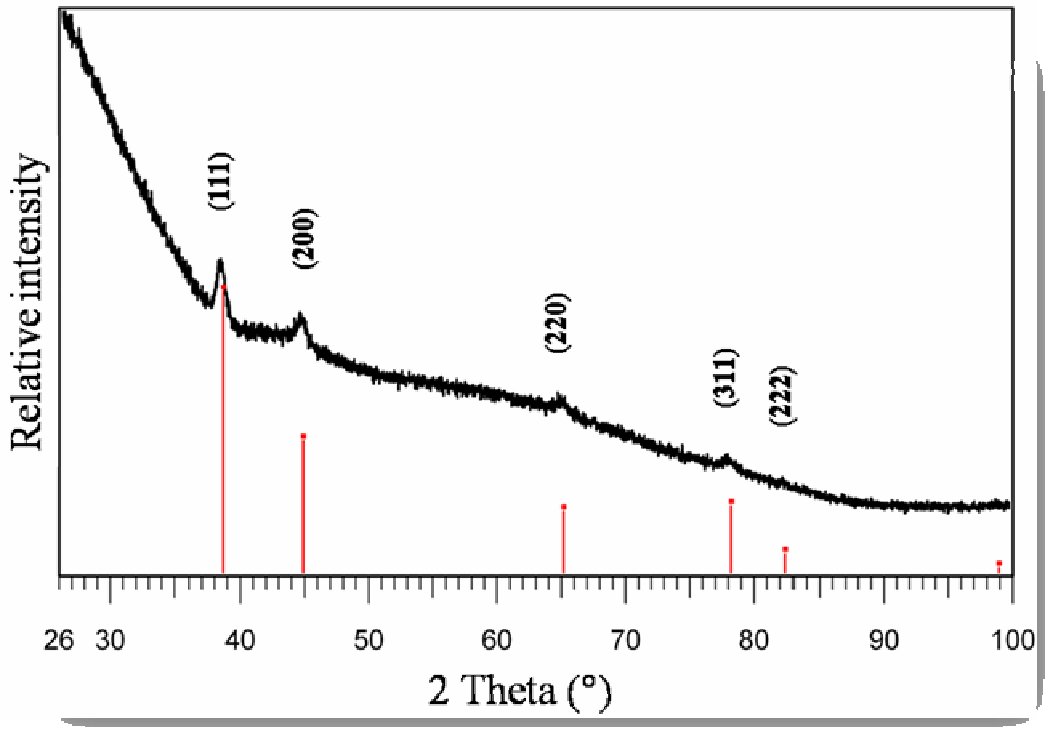

Figure 2.6. X-ray diffractogram of the Al/Al_2O_3 composite NWs deposited on a glass substrate at 580°C temperature.

1.1.2. Morphology of Al/Al_2O_3 Composite Nano-Wires (NWs)

The changing parameters have a certain effect upon the morphology of the NWs. Our quest was to optimize the process to get highly porous material with reasonable diameter of the NWs. Figure 2.7 shows SEM images of Al/Al_2O_3 nano-composite materials obtained at two different temperatures that is 480°C and 580°C. Maintaining the precursor flow at 9.0 x 10^{-2}mbar, the decomposition was carried out at 480°C upon a metallic substrate. SEM analysis of the as prepared film shows that fused balls like structures formed as a thin layer (Figure 2.7**a**). The temperature was raised to 580°C of the same sample without taking out of the CVD reactor and coated once again for a short time to see the effect clearly. The SEM images reveal that the second coating layer comprised of agglomerated NWs upon the first one (Figure 2.7**b**). The diameter of the wires varies considerably between 100 and 400 nm with a length of up to 2 microns.

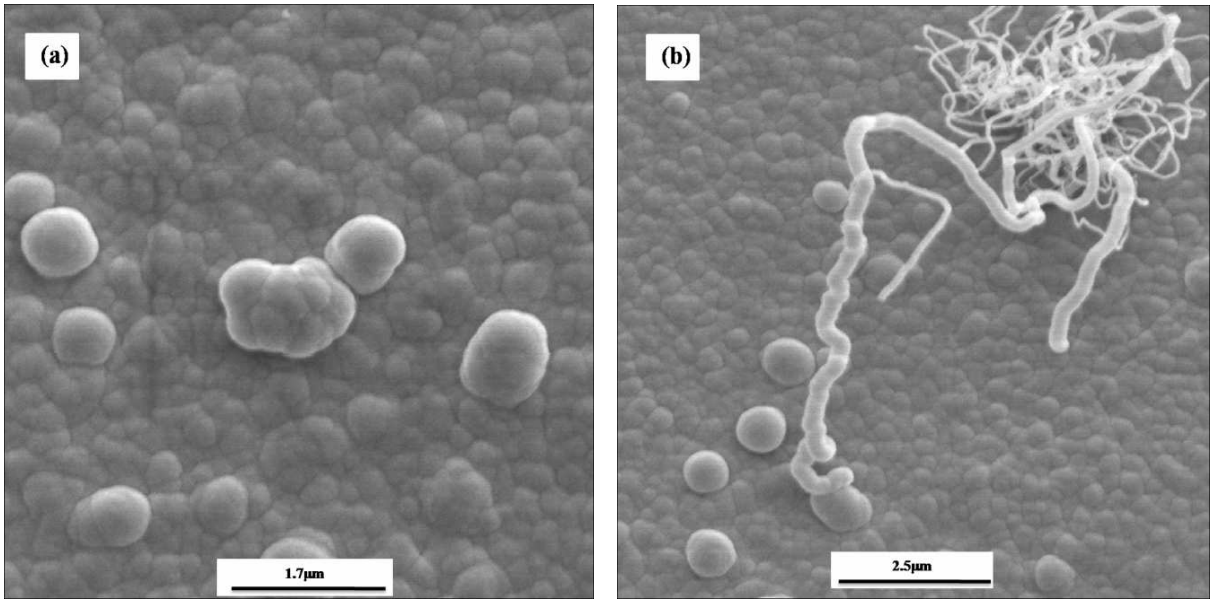

Figure 2.7. SEM images of the as prepared Al/Al_2O_3 composite material at decomposition temperature 480°C (a), and 580°C upon the same material prepared at 480°C (b) maintaining the precursor flow at pressure 9.0 x 10^{-2} mbar.

The same experimental procedure as discussed above was repeated, however, the first layer was deposited at 580°C at a full flow of the precursor at room temperature. The precursor flow was at pressure >10^{-1} mbar. SEM images (Figure 2.8**a**) reveal that the adhesion is very poor of the Al/Al_2O_3 composite material over the substrate at full flow of the precursor and remains over the surface as broken sheets. At such a high flow rate neither the nano-balls nor the NWs are formed (visible from the sheets in Figure 2.8**a**) although the deposition temperature is comparable where normally NWs formed. Then the deposition of the second layer was brought at a controlled flow (9.0 x 10^{-2}mbar pressure) over the already deposited layer. It is observed that agglomerates of NWs formed (Figure 2.8**a** & **b**) over the cracked sheets like birds' nests. The nests are composed of entangled NWs with diameters ranging between 70-140 nm. The intertwined wires have lengths up to few microns. However, it is practically impossible to measure the length of the wires due to their non-linear nature and resulting entanglement (Figure 2.8**b**).

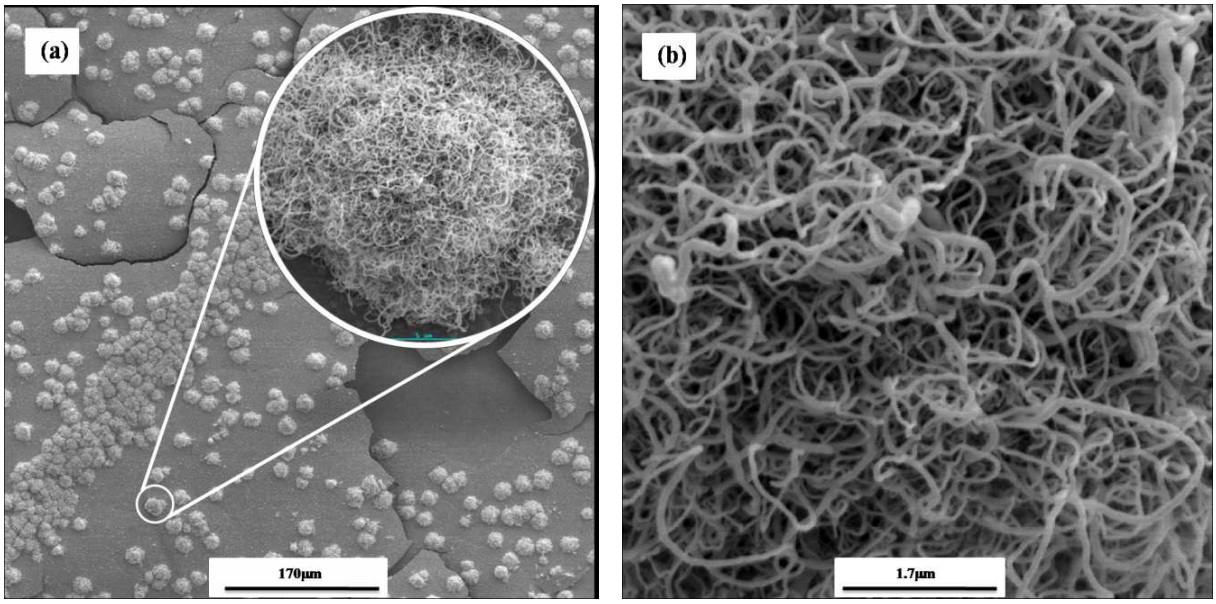

Figure 2.8. SEM images of Al/Al_2O_3. (a) Deposition at 580°C with full flow of precursor followed by deposition at 580°C with controlled flow. The inside circular image shows the magnification of the NWs agglomerate, (b) magnification of the agglomerate.

Figure 2.9 **a** & **b** show the SEM images of the Al/Al_2O_3 composite NWs prepared by depositing directly over metallic substrates at same temperature (580°C) and different precursor flows. It is observed that maintaining the gaseous flow of precursor at 9.0×10^{-2} mbar pressure gives ultra thin NWs (Figure 2.9**a**). The diameter of the NWs is in the range of 20-25 nm. The NWs are uniform in view of their diameters. The NWs are entangled in such a way that it is quite difficult to measure their length, however, roughly speaking it is in microns. The texture of the NWs is highly porous with small pores and holes in between the NWs.

On the other hand the deposition of Al/Al_2O_3 composite upon metallic substrate by the decomposition of $[H_2Al(O^tBu)]_2$ at a flow rate maintained at 5.0×10^{-1} mbar pressure gives also NWs (Figure 2.9**b**). However, the NWs have average diameter of about 110 nm sufficiently higher than those in Figure 2.9**a**. The variation in diameter is sufficiently large, that is, the NWs have diameter in the range of 55-150 nm which indicates that the NWs are not uniform. The NWs grow in entangled fashion with length up to few microns. Though, the texture is highly porous but the pore size is sufficiently larger (Figure 2.9**b**).

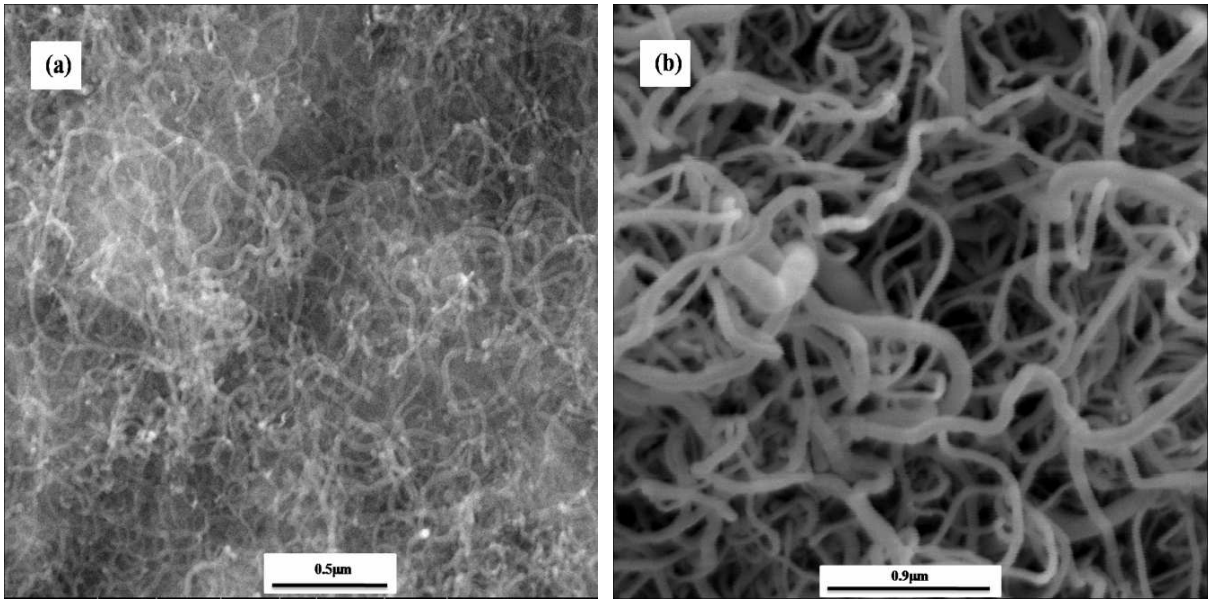

Figure 2.9. SEM images of Al/Al_2O_3 composite NWs produced at 580°C with precursor flow maintained at 8.0 x 10^{-2} mbar (a), and 5.0 x 10^{-1} mbar pressure (b). The magnification is comparable.

The deposition time of the NWs upon the metallic substrate at 580°C has been tested for any possible change. Figure 2.10**a** & 2.10**b** show the SEM images of the NWs produced by the deposition time of 2 minutes and 10 minutes, respectively while maintaining the precursor flow at 9.0 x 10^{-2} mbar pressure. The SEM image (Figure 2.10**a**) of the NWs deposited for 2 minutes gives thinly populated NWs over the substrate where the substrate's surface can be seen very clearly in the image. The NWs have the diameter of about 30 nm and grow in entangled way with a length of few microns. The SEM image for the 10 minutes deposition time of the NWs is given in Figure 2.10**b**. The inter-twisted NWs are grown up to few microns with diameter of <30 nm. In both the cases the NWs have porous texture with smaller pores. It indicates that the 580°C deposition temperature and 9.0 x 10^{-2} mbar pressure are the optimum parameters for NWs production upon metallic substrate suitable for H_2 adsorption.

The as deposited NWs were characterized by transmission electron microscopy (TEM). The TEM image (Figure 2.11**a**) shows the core shell structure of the NWs. The inner core is composed of metallic aluminum which is wrapped up by the amorphous alumina (Al_2O_3). The selected area electron diffraction (SAED) has shown metallic aluminum (Figure 2.11**b**).

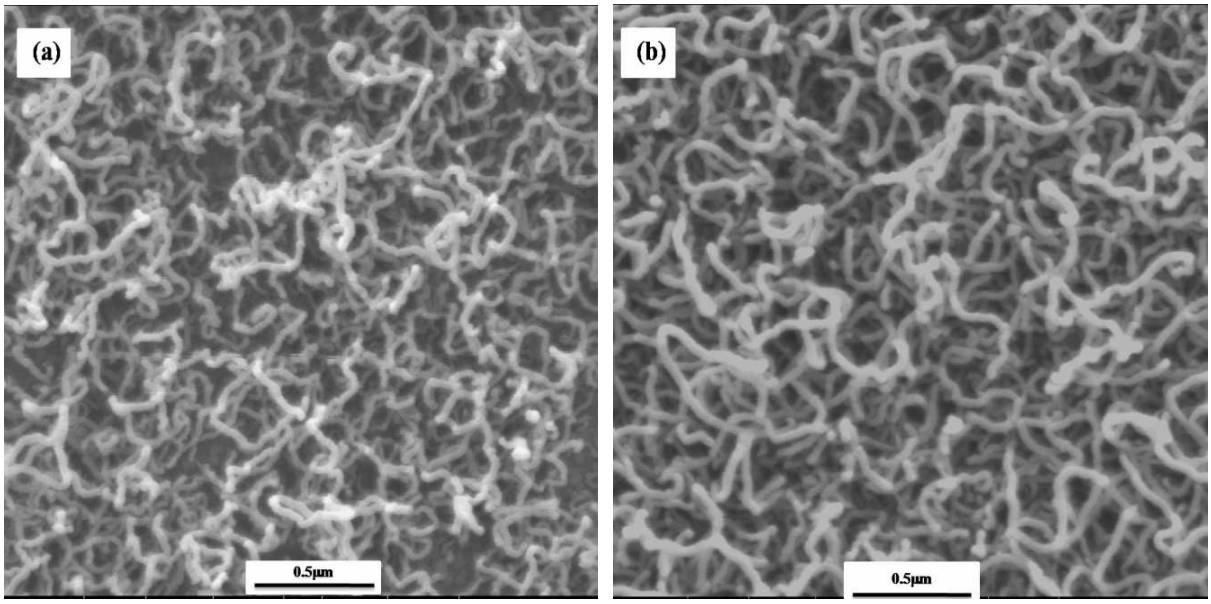

Figure 2.10. Al/Al_2O_3 composite NWs produced at 580°C with precursor flow maintained at 9.0 x 10^{-2} mbar pressure with deposition time of 2 minutes (a), and 10 minutes (b). The magnification of the images is comparable.

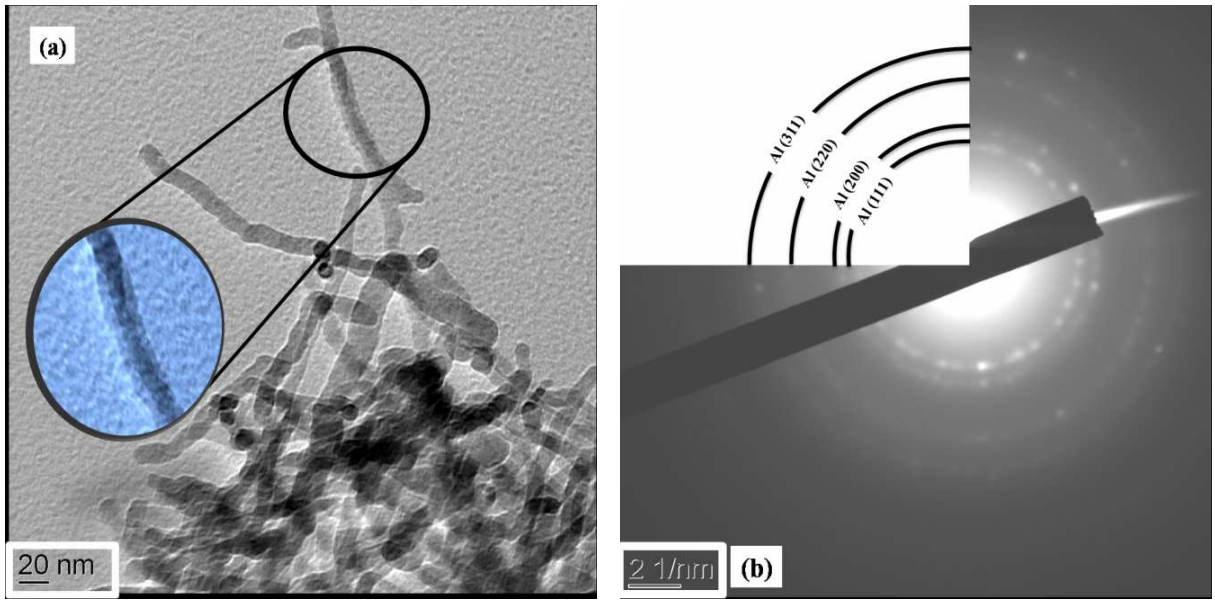

Figure 2.11. TEM image of the Al/Al_2O_3 composite NWs deposited at 580°C showing core-shell structure (a), clear in the circular enlarged pop out. SAED gives fringes for metallic Al (b).

1.1.3. BET Analysis of Al/Al_2O_3 Composite Nano-Wires (NWs)

The specific surface area (SSA), the pores volume and the pore size was determined by an automatic sorption system using N_2 gas at 77K. The sample was outgased at 120°C for 21 hours. The SSA was calculated using multipoint BET method [72] and the pore volume was determined utilizing MP-method. The SSP of Al/Al_2O_3 composite NWs determined is 53.55 m^2/g. However, the actual surface area is thought to be higher than this since the method is limited by the amount of the sample. We could only produce NWs as thin film upon a substrate which carries a very small amount of the sample. In this case, it was hardly managed to get a film weighing about 60 mg. The total pore volume determined is 0.44 cm^3/g for pores having diameter below 355.4 nm, which is well above pore volume of the purified single wall carbon nano-tubes (SWCNTs = 0.39 cm^3/g) [73]. The pore diameter could be determined exactly and precisely irrespective of the quantity of sample. The average pore diameter determined is 32.89 nm which is the ideal pore diameter for physisorption of hydrogen upon Al/Al_2O_3 composite NWs.

1.2. Ni/Al_2O_3 Composite Nano-Powders (NPs)

Ni/Al_2O_3 composite nano-material has been prepared in a cold wall CVD reactor. $Ni(acac)_2$ powder was used as deposition target of the $[H_2Al(O^tBu)]_2$ single source precursor. $Ni(acac)_2$ was placed in a specially designed cuvette (Detail is given in experimental part) which was inserted into a graphite block containing hole of the sized of cuvette. The contact between the walls of the cuvette and graphite block was ensured for efficient heat conduction. A steady stream of the precursor was directed over the $Ni(acac)_2$ powder previously placed in a cuvette inside graphite block. The coating of $Ni(acac)_2$ powder was made at 580°C. The decomposition of the precursor over the $Ni(acac)_2$ powder gives Ni/Al_2O_3 composite nano-powder (eq. 2.7). However, the exact decomposition mechanism is not known.

$$Ni(acac)_2 + [H_2Al(O^tBu)]_2 \xrightarrow{Temp\ =580°C} Ni/Al_2O_3 + H_2 + \text{Organic volatiles} \qquad (2.7)$$

1.2.1. XRD Analysis of Ni/Al_2O_3 Composite Nano-Powders (NPs)

The structure, composition and crystalline phases of the Ni/Al_2O_3 composite material were studied by powder XRD. Figure 2.12 shows the XRD pattern of the as prepared Ni/Al_2O_3 composite powder. There are five distinct peaks at 44.5°, 51.8°, 76.4°, 92.9° and 98.2°, which are typical of face centered cubic Ni entity (PDF: 87-712). There is appeared wave in the background of the diffractogram. These are due to the amorphous alumina. No other peak except that for Ni can be seen which gives that the crystalline phase is only Ni in the powder.

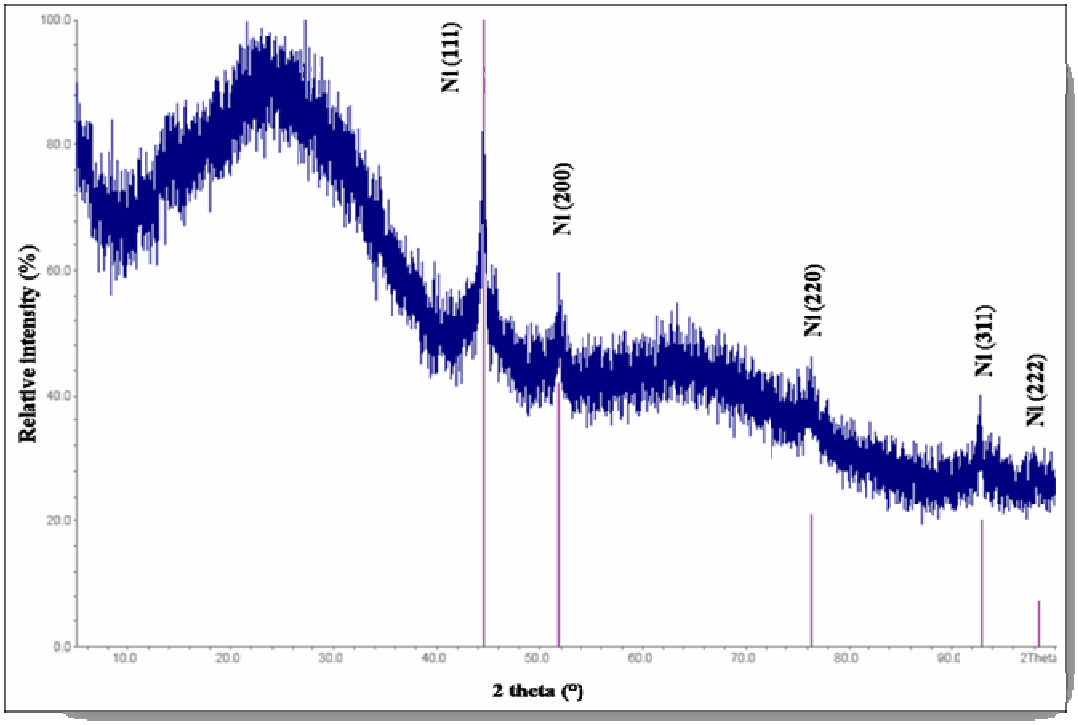

Figure 2.12. X-ray diffractogram of the Ni/Al_2O_3 composite powder prepared by the decomposition of $[H_2Al(O^tBu)]_2$ over the $Ni(acac)_2$ powder at 580°C.

1.2.2. Morphology and Composition of Ni/Al_2O_3 Composite Nano-Powders (NPs)

As mentioned in the case of NWs, the structure of the hydrogen adsorbing material is very important. The more porous the material, the more surface is available and the more hydrogen

uptake could be made possible. The morphology and structure of the Ni/Al_2O_3 composite material was studied by SEM and TEM analysis and the elemental composition (that is Ni, Al and O) by energy dispersive X-ray spectroscopy (EDX). Figure 2.13 gives SEM images of Ni/Al_2O_3 composite material where nano-spheres of the composite can be seen which are squeezed together (Figure 2.13a). The average size of the spheres is about 150nm. Upon magnification (Figure 2.13b), it is observed that each sphere is composed of small particles having sizes in the range 60-100nm. The small particles agglomerate and give spherical shapes like cauliflowers. The EDX spectrum in Figure 2.14 shows that each cauliflower like sphere is composed of Ni, O and Al. The exact ratios of the elements in the powder could not be obtained from the EDX data. However, the elemental composition, qualitatively, can be obtained precisely. The small peaks for carbon and gold appeared due to the specimen preparation process where the material has been sputtered with gold for better resolution and supported over a carbon tape for analysis.

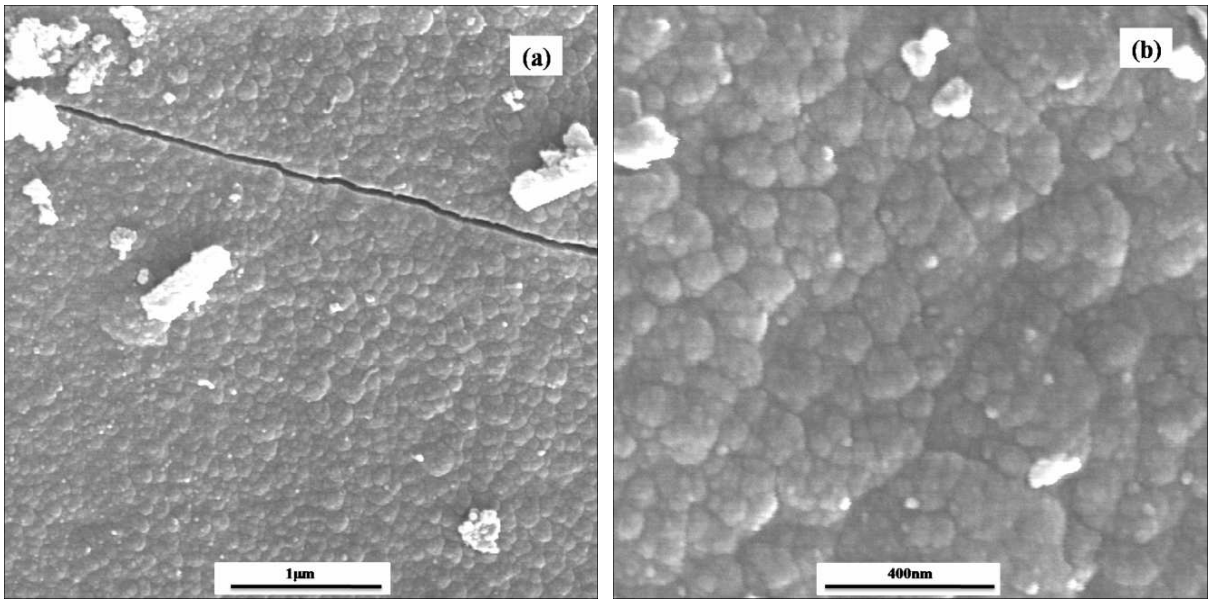

Figure 2.13. SEM images of Ni/Al_2O_3 composite nano-powder prepared at 580°C. Lower magnification (a) and higher magnification (b)

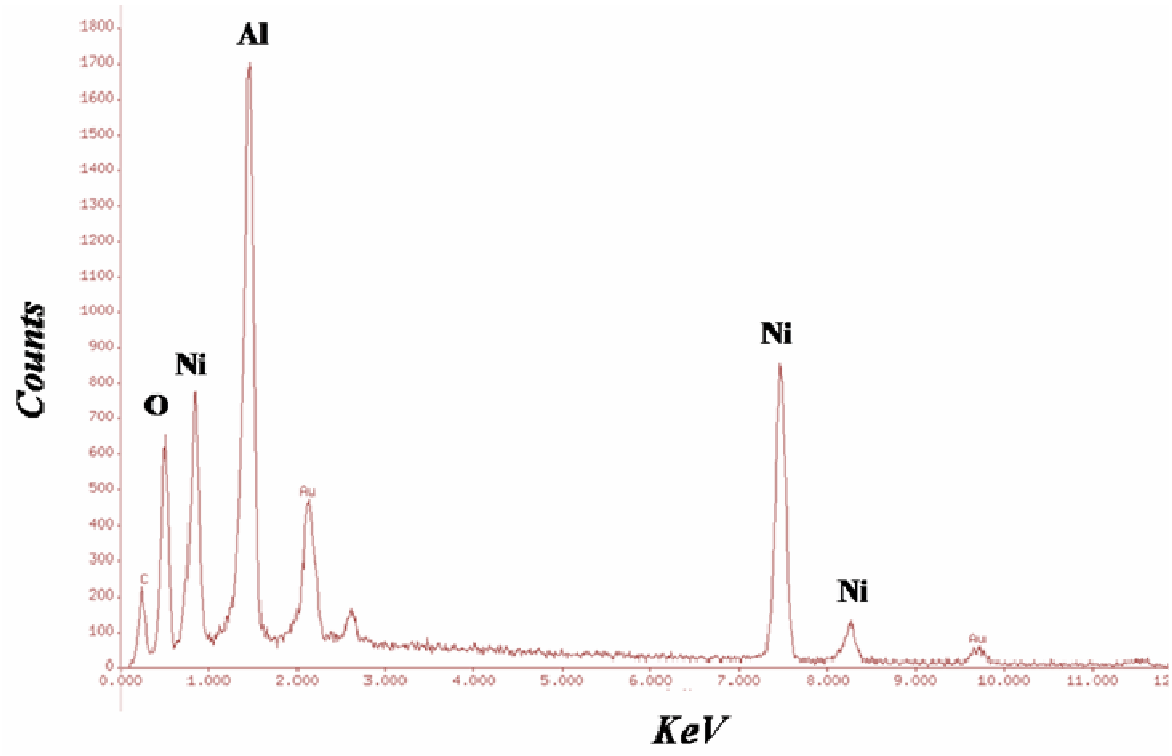

Figure 2.14. EDX spectrum of Ni/Al_2O_3 composite nano-powder. The C peak is due to the carbon tape and Au due to gold sputtering used in specimen preparations

TEM image (2.15 a) shows Ni nano-particles dispersed in an Al_2O_3 matrix. The particles are uniformly distributed in amorphous alumina. The average particle size is approximately 13 nm. Most of the particles have size below 20nm while very few reach 20nm dimension. The selected area electrons diffraction carried out by the TEM instrument shows fringes only for Ni (Figure 2.15 b), which shows that the material is biphasic having crystalline Ni phase and amorphous Al_2O_3.

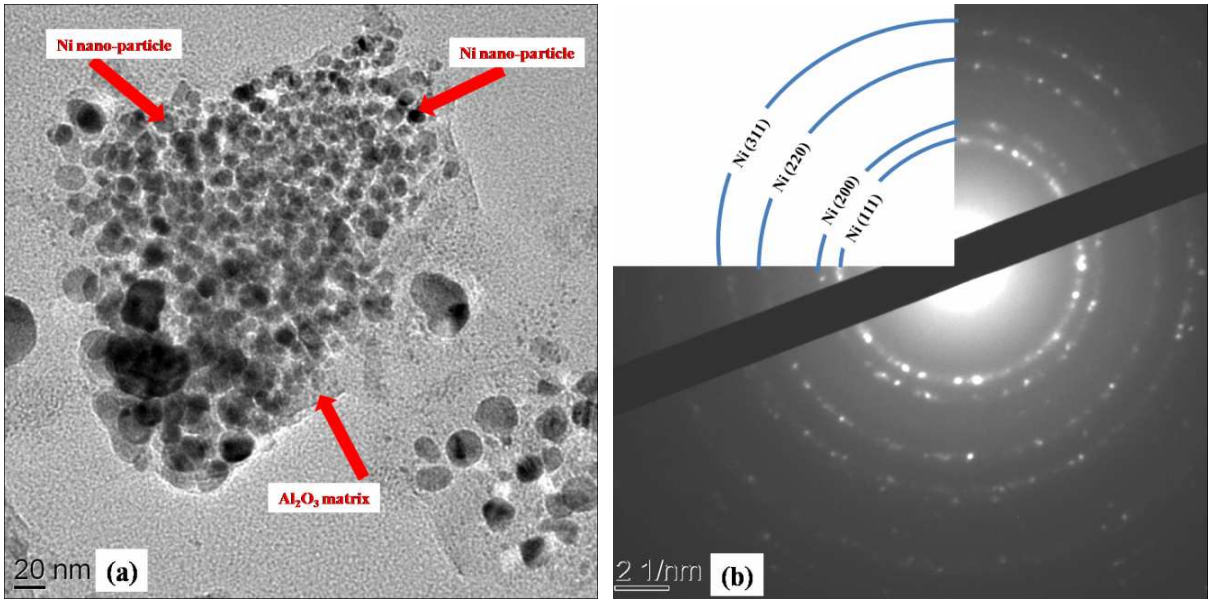

Figure 2.15. TEM image (a) and SAED (b) of the Ni/Al_2O_3 nano-powder prepared by the reaction of $Ni(acac)_2$ and $[H_2Al(O^tBu)]_2$ at 580°C.

2. Hydrogen Adsorption

The hydrogen uptake by the Al/Al_2O_3 composite NWs and Ni/Al_2O_3 composite nano-powder has been determined using Sievert's type hydrogenator at different temperatures and pressures. Additionally the hydrogen adsorption of the NWs was also studied by differential Scanning Calorimetry (DSC). The purpose of using DSC was two fold: one to develop a comparative study of the two instruments and second, to understand the type of the adsorption mechanism. The samples were also analyzed using analytical techniques after hydrogen adsorption to understand the mechanism and mode of the adsorption. The results obtained will be presented in the following sections.

2.1. Hydrogen Sorption Studies Using Sievert's Apparatus

Sievert's type hydrogenator was used for the hydrogen adsorption studies. The hydrogen uptake is reported in wt.%, which was plotted as a function of temperature and pressure. The maximum wt.% obtained are 6.5(±0.2) and 2.9(±0.2) for Al/Al_2O_3 composite NWs and Ni/Al_2O_3 composite NPs, respectively.

2.1.1. Hydrogen Adsorption by Al/Al_2O_3 Composite Nano-Wires (NWs)

Figure 2.16 gives the wt.% of hydrogen adsorbed upon Al/Al_2O_3 Composite Nano-Wires (NWs) plotted as a function of temperature. The adsorption equilibrium was obtained at about 30 minutes. The wt.% of hydrogen adsorbed changes with the temperature. At room temperature it is low but as the temperature increase the wt.% also increases. At temperature ranging between 70 and 100°C, the adsorption reaches its maximum values. Above 100°C a drastic decrease in the amount of adsorbed hydrogen is observed. As the temperature increases above 100°C, the wt.% hydrogen adsorbed decreases and reaches the minimum value at about 300°C. The trend in amount of adsorbed hydrogen is relatively less regular at lower pressures compared to that at higher pressures. This anomalous behaviour of hydrogen adsorption at low pressures may be due to the lack of hydrogen saturation of the NWs. The highest wt.% which is approximately 6.5(±0.2), of hydrogen adsorbed upon Al/Al_2O_3 Composite Nano-Wires (NWs) is obtained at temperature ranging between 70-100°C. It indicates that this range of temperature is the optimum for hydrogen adsorption upon Al/Al_2O_3 composite nano-wires (NWs).

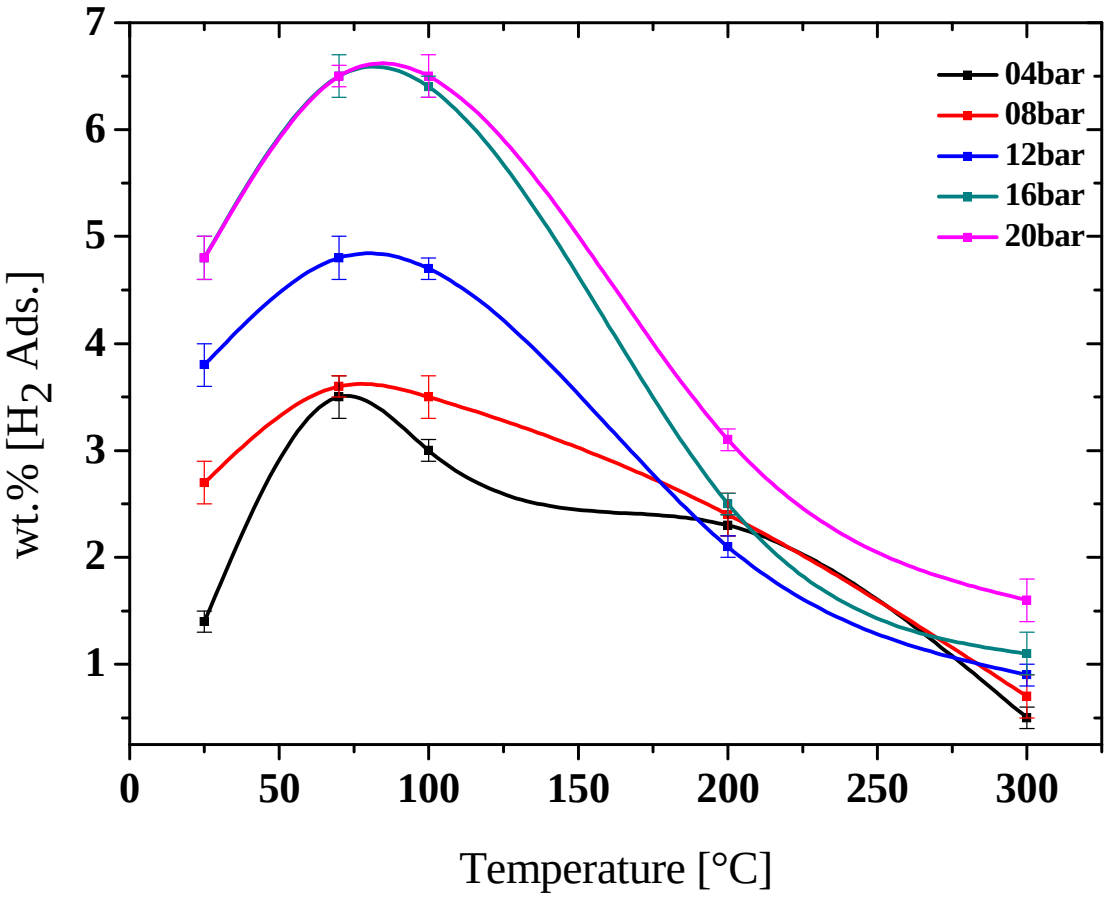

Figure 2.16. Hydrogen adsorption isotherms for Al/Al_2O_3 composite NWs at constant pressures and varying temperatures

The effect of pressure upon the wt.% H_2 adsorption has been studied and is plotted as a function of hydrogen pressure which is given in Figure 2.17. It is observed that at room temperature a constant increase in the amount of hydrogen adsorbed upon Al/Al_2O_3 Composite Nano-Wires (NWs) occurs with increasing pressure. At the temperature ranging between 70-100°C, the wt.% of hydrogen adsorbed increases very slowly as a function of pressure in the beginning and sharp increase is observed at above 8 bars up to 16 bars. However, beyond 16 bars of pressure the amount of hydrogen adsorbed nearly becomes constant. At higher temperatures, that is 200°C and 300°C, the effect of pressure upon the wt.% of hydrogen adsorbed is nearly linear. This effect is very clear at 300°C where a continuous increase in the amount of hydrogen adsorbed upon the NWs is shown. The highest amount of hydrogen adsorbed is observed at moderate temperatures (70 and 100°C) which amounting up to approximately 6.5(±0.2) wt.%. The increase in wt.% as a function of pressure indicates the effect of pressure upon the hydrogen adsorption.

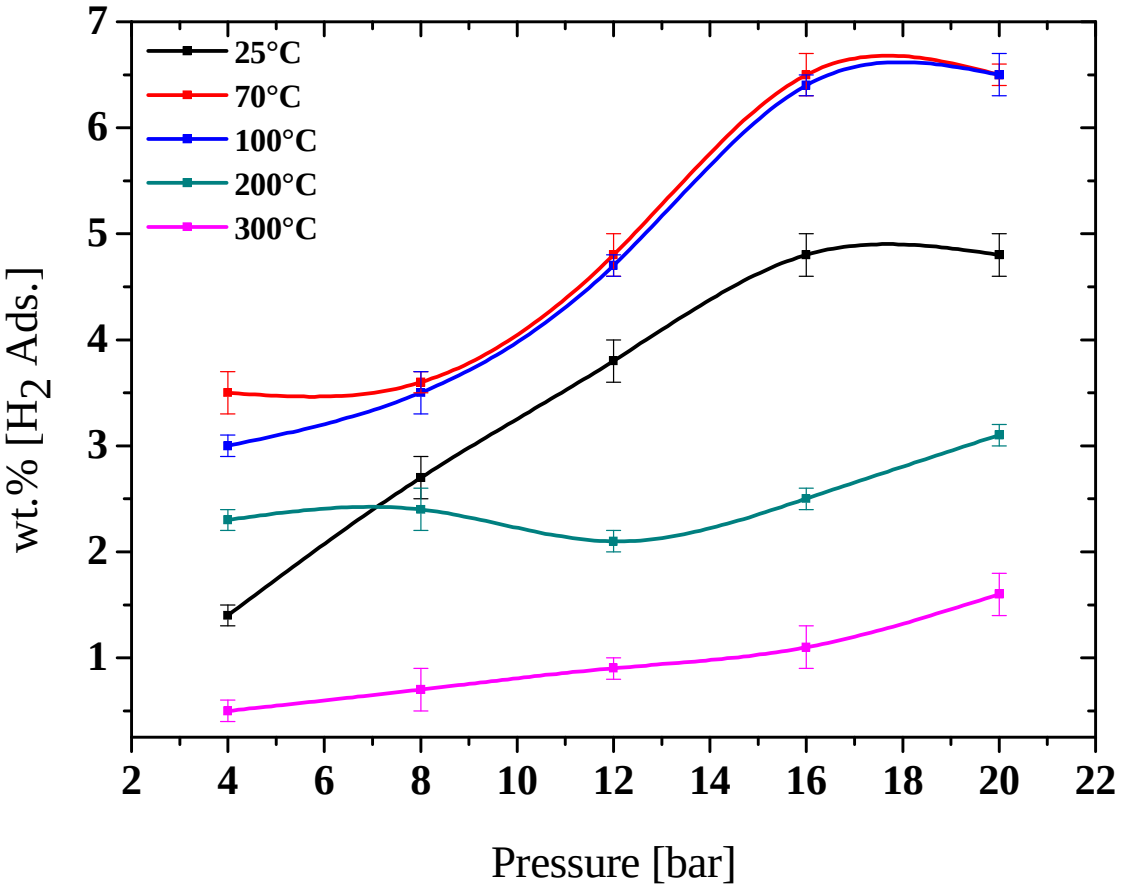

Figure 2.17. Hydrogen adsorption isotherms for Al/Al_2O_3 composite NWs at constant temperatures and varying pressures

2.1.2. Hydrogen Adsorption by Ni/Al_2O_3 Composite Nano-Powders (NPs)

Figure 2.18 gives the hydrogen adsorption isotherm for Ni/Al_2O_3 composite nano-powders (NPs) in which wt.% of hydrogen adsorbed upon Ni/Al_2O_3 composite NPs is plotted as a function of temperature. As is evident from the Figure 2.18, at low pressure (20 bars), the amount of hydrogen adsorbed increases with increasing temperature but the rate is slow. However, at high pressure (40 bars) the increase in amount of hydrogen adsorbed is high and the maximum amount is obtained around 300°C which is approximately 2.9(±0.2) wt.%. The effect of temperature upon the wt.% H_2 adsorbed is linear which means that as the temperature increases the amount of H_2 adsorbed increases too.

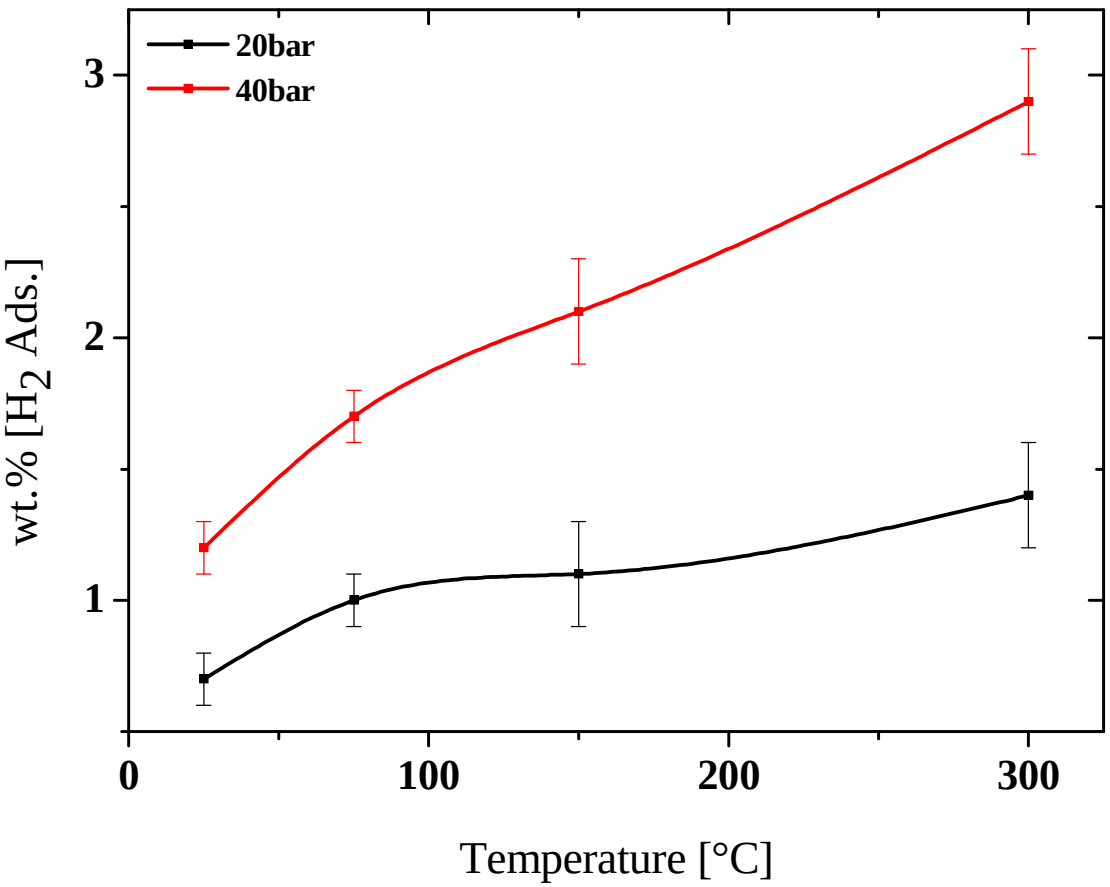

Figure 2.18. Hydrogen adsorption isotherms for Ni/Al_2O_3 composite NPs at constant pressures and varying temperatures

The effect of pressure upon the amount of hydrogen adsorbed by Ni/Al_2O_3 composite NPs is seen to be linear. It is observed that as the pressure increases the amount of hydrogen adsorbed increases too (Figure 2.18). For example at 300°C temperature, the amount of hydrogen adsorbed increases by two fold that is from 1.4(±0.2) wt.% to 2.9(±0.2) wt.% as the pressure increases from 20 bars to 40 bars. The effect is more pronounced at higher temperatures where a fast increase occurred with the changing pressure. The maximum hydrogen adsorption has been achieved at 300°C temperature and 40 bars of pressure amounting 2.9(±0.2) wt.%.

2.2. Infra-Red Spectroscopic Characterization

2.2.1. IR spectroscopic Analysis of Al/Al_2O_3 Composite Nano-Wires (NWs)

The hydrogen adsorption was followed by IR spectroscopy. Figure 2.19**a** presents the IR spectra recorded immediately after hydrogenation of Al/Al_2O_3 composite NWs using Sievert's apparatus. The hydrogenation process was carried out at different temperatures ranging from room temperature up to 300°C. The region above 3000cm^{-1} and up to 4000 cm^{-1} is worthy to consider where the O-H stretching vibration peaks appear. The prominent peak at round about 700 cm^{-1} is due to the Al-O stretching vibration. There is no considerable change in this peak at lower temperatures (25°C and 100°C); however, it narrowed down considerably at higher temperatures (200°C and 300°C). Small C-H stretching vibrations appear at about 2900 cm^{-1} in all the spectra which are not affected by the temperature. These peaks may be due to some organic entities adsorbed upon the nano-wires during the CVD process. The region between 4000 cm^{-1} to 3000 cm^{-1} is magnified out (Figure 219**b**) to see clearly the changes in the O-H stretching vibration region. The effect upon the peak at room temperature is nothing else except the broadening of the peak which is more prominent at 100°C temperature. At 100°C temperature, two distinct changes could be observed. One is the extra-ordinary broadening of the peak with moving of the maximum toward lower value compared to the other counterparts, second is the appearance of new peaks at higher energies. This new peaks become more prominent as the temperature raises to 200°C as well as 300°C but the main peak due to O-H vibration is nearly the same as that of measured at room temperature. These new peaks appear at 3781 cm^{-1} and 3699 cm^{-1} are sharp and well defined. These peaks are due to the free O-H stretching vibrations [74].

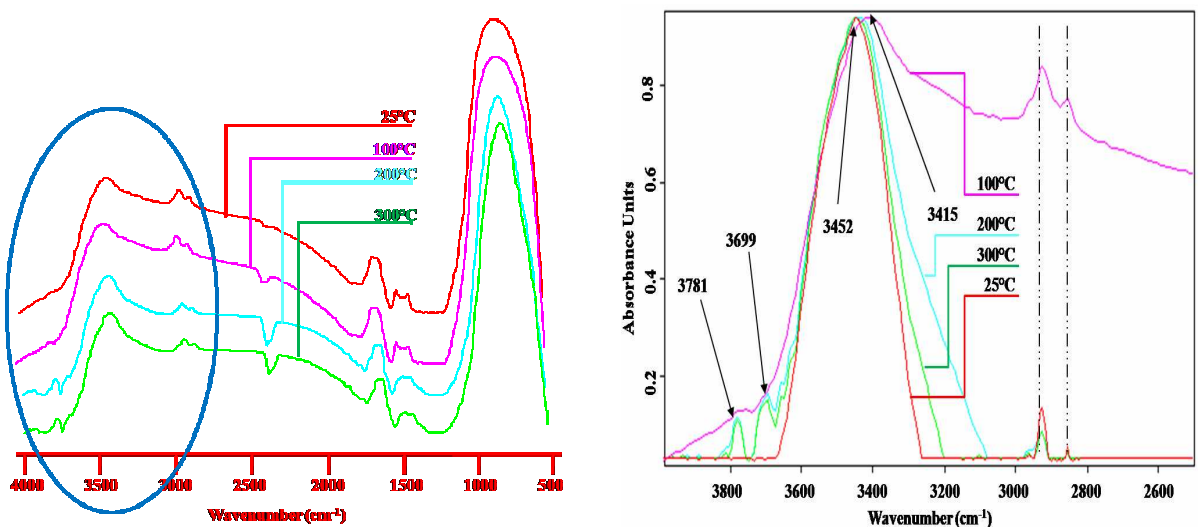

(a) **(b)**

Figure 2.19. IR spectra measured after hydrogen adsorption upon the Al/Al_2O_3 composite NWs using Sievert's type apparatus at different temperatures (a), the encircled area is magnified as (b).

2.2.2. IR spectroscopic Analysis of Ni/Al_2O_3 Composite Nano-Powders (NPs)

The Ni/Al_2O_3 composite nano-powders were analyzed by IR spectroscopy after hydrogen adsorption at different temperatures and pressures. The IR spectra (Figure 2.20) of the as prepared sample give three peaks to be considered that is at 3441cm^{-1}, 2366 cm^{-1} and 786 cm^{-1} which may be assigned to O-H, CO_2 and Al-O stretching vibrations, respectively. However, the peak appears at 2366cm^{-1} is insignificant in the interpretation of the spectra since this peak inherits in the spectra obtained from the IR instrument in our lab facility. The changes in the IR spectra are less significant after hydrogen adsorption at lower temperatures compared to that measured before H_2 adsorption. However, at higher temperatures we not only observe significant changes in the parent peaks but also new peaks appear in the spectra. The spectrum of the Ni/Al_2O_3 composite recorded after hydrogen adsorption at 300°C (both 40 bars and 20 bars of pressure) show changes in the parent peaks and also some new peaks appear. At one hand the peaks appear at 3441 cm^{-1} and 786 cm^{-1} narrowed down. On the other hand more prominent new peaks appears at 2927 cm^{-1}, 1732 cm^{-1} and 1459 cm^{-1} which could be assigned to C-H stretching vibration, C=O stretching vibration and C-H bending vibration, respectively. At lower temperatures also the changes in the parent spectrum are appeared along new peaks. However, these are not as prominent as at higher temperatures. the

observations indicates that the Ni/Al_2O_3 composite NPs facilitates some chemical reactions which give some unknown organic products.

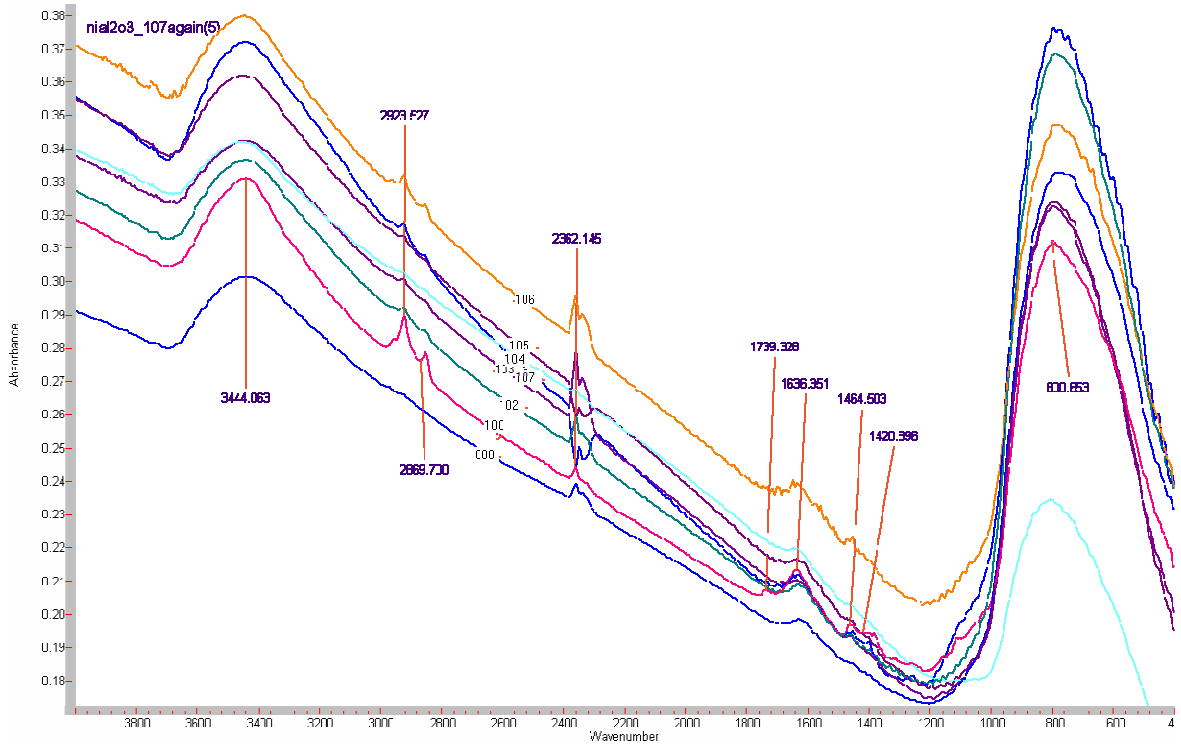

Figure 2.20. IR spectra measured after hydrogen adsorption upon the Ni/Al_2O_3 composite NPs at different temperatures

2.3. Selected Area SEM Analysis of Al/Al_2O_3 Composite Nano-Wires (NWs)

An interesting situation has been appeared when one of the samples was followed by SEM analysis after hydrogen adsorption at 300°C. It has been observed that the longer NWs running across the entire entangled nest are broken apart into shorter bended NWs. It was assumed that the wires broken apart either due to heating or reacting with hydrogen. The interaction of NWs with the H_2 was studied systematically while concentrating over a selected area in the film. The SEM images were taken before and after the hydrogen adsorption and/or heat treatment. Figure 2.21**a** and **b** give the SEM images taken after heating the samples up to 300°C in a close chamber of the Sievert's apparatus; in absence (Figure 2.21**a**) and in presence (Figure 2.21**b**) of the H_2 atmosphere. The inset small images in both the figures are

taken of the same area before heat treatment in absence and/or in presence of the H_2 atmospheres, respectively. It is clear that the heat treatment of the sample at 300°C has not any visible effect upon the nature and structure of the NWs. Figure 2.21**a** (main and inset) shows that the length and the diameter of NWs is the same before and after heat treatment in absence of H_2. However, it is evident from Figure 2.21**b** (main and inset) that there is visible change in the nature and structure of the NWs. Before hydrogen adsorption at 300°C, long entangled wires could be seen (Figure 2.21**b** inset). To see the effect more clear, the density of the wires was kept low and the substrate surface can be seen clearly in the SEM images. The length of the wires was in microns and the average diameter was about 26 nm. After heat treatment in the presence of H_2 atmosphere the longer wires broken apart into small pieces with an average length of 400 nm. The diameter of the NWs increased sufficiently and falls in the range of 40 nm to 50 nm. This indicates that the NWs have been expanded in diameter. Due to breaking down of the NWs into small pieces the surface of the substrate is more visible. Most of the broken NWs have ball like tips at both the sides.

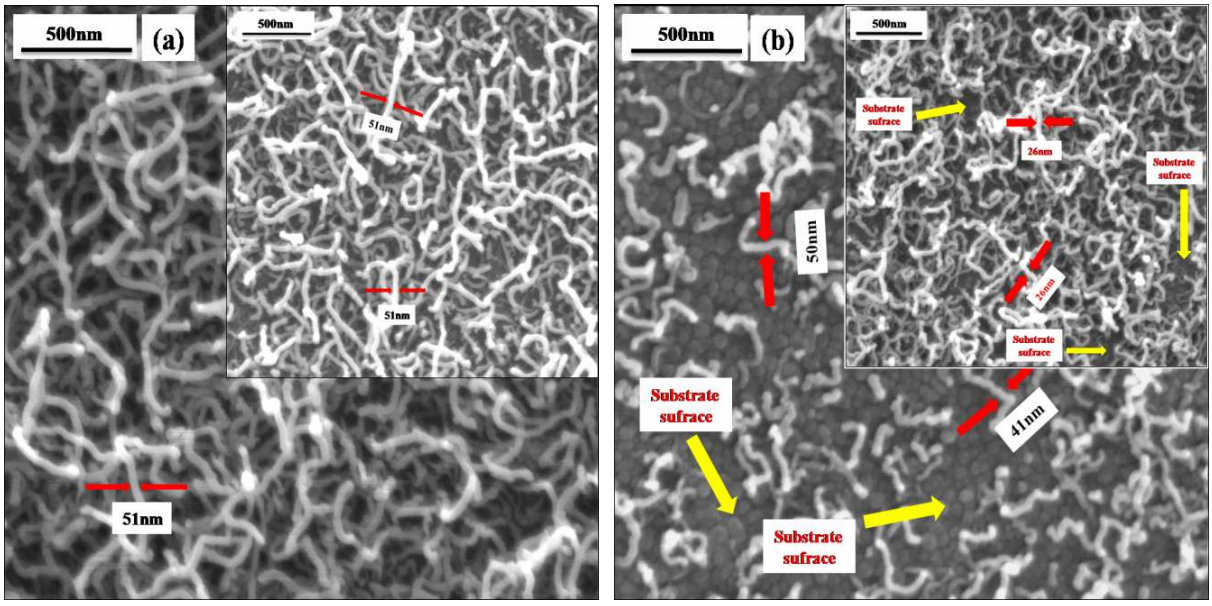

Figure 2.21. Selected area SEM images taken after heating the sample at 300°C without H_2 atmosphere (a), in presence of H_2 atmosphere (b). The inset SEM images are before the heat treatment and/or H_2 introduction into the system

The same procedure was followed at lower temperatures, that is, at 200°C, 100°C and room temperature. The analysis of the SEM images before and after heat treatment at 200°C in presence of H_2 atmosphere did not show any change in the structure and nature of the NWs (Figure 2.22**a**). The wires exist after hydrogen adsorption as were before. At 100°C and room temperature, the situation is the same. The length and diameter of the NWs are intact despite heating in the presence of hydrogen atmosphere at 100°C (Figure 2.22**b** main). At room temperature the NWs were exposed to H_2 at 20 bars for 2 hours, however, the SEM image (Figure 2.22**b** inset) reveals that nothing to be happened to the structure of the wires.

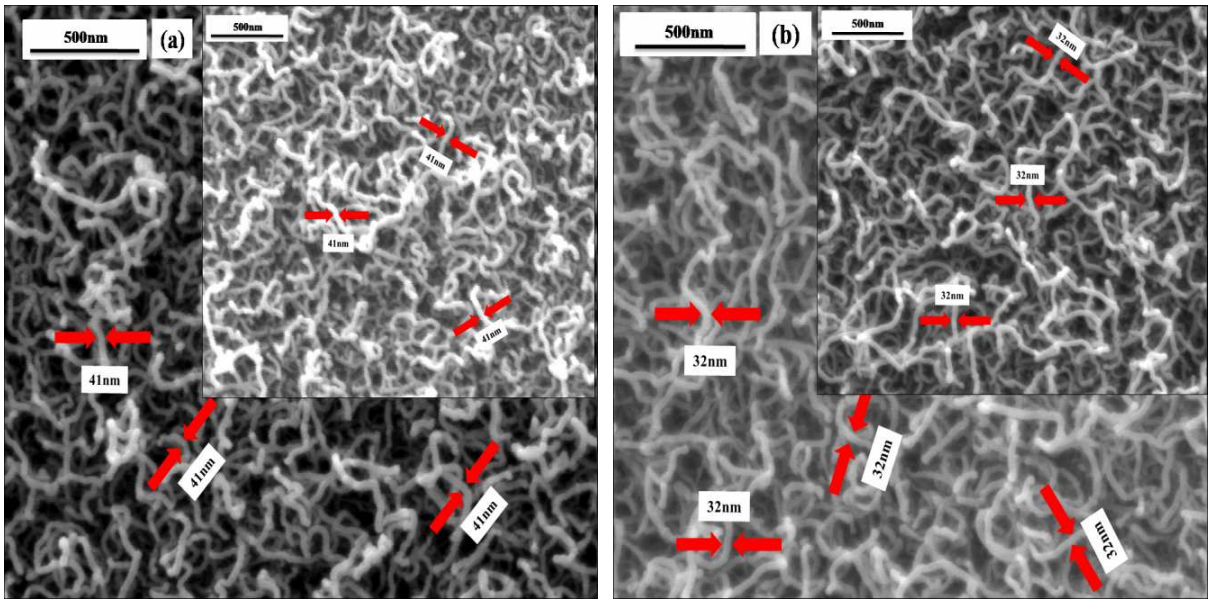

Figure 2.22. SEM images of the heat treated samples in presence of H_2 at 200°C (a) (inset is before heat treatment), and at 100°C (b) (inset is the image of the sample heat treat at 25°C in presence of H_2).

2.4. Differential Scanning Calorimetry (DSC)

2.4.1. DSC measurements of Hydrogen Adsorption by Al/Al_2O_3 Composite Nano-Wires (NWs)

Differential scanning calorimetry (DSC) has been used for the hydrogen adsorption study of Al/Al_2O_3 composite NWs for a two fold purpose. One to generate comparative results to that obtained by the Siever's apparatus and second to get insight into the mechanism of the hydrogen adsorption. The results were obtained upon DSC apparatus of TA instruments which contains two pans, a reference pan and a sample pan. The sample as a thin film deposited upon Al substrate was placed in a sample pan and the reference pan contained an exactly the same amount of the substrate material, that is, Al. the sample was scanned in a temperature range of 40-400°C as well as 40-200°C. The pressure introduced was 20 bars and the chamber was flushed with H_2 before starting the experiment. Each experiment was repeated three times without tanking sample out of the sample chamber. Figure 2.23 gives a typical DSC spectrum obtained by measuring heat flow between the two pans as a function of temperature. The system was heated at a rate of 10°C/min in a temperature range of 40-400°C. The same process was repeated three times while keeping the chamber closed. It is observed that a reversible broad endothermic peak appears in the temperature range of ~55°C to ~100°C with a minimum at ~70°C. At higher temperature, that is, above 200°C a mixture of endothermic and exothermic peaks are appeared without any reversibility. This results are in good agreement with those obtained by using Sievert's apparatus. The reproducibility in the peaks upon repetition of the process at lower temperatures indicates that the adsorption occurs due to non-dissociative adsorption mechanism that is physisorption of H_2 occurs upon the Al/Al_2O_3 composite NWs. At temperatures above 100°C only desorption occurs.

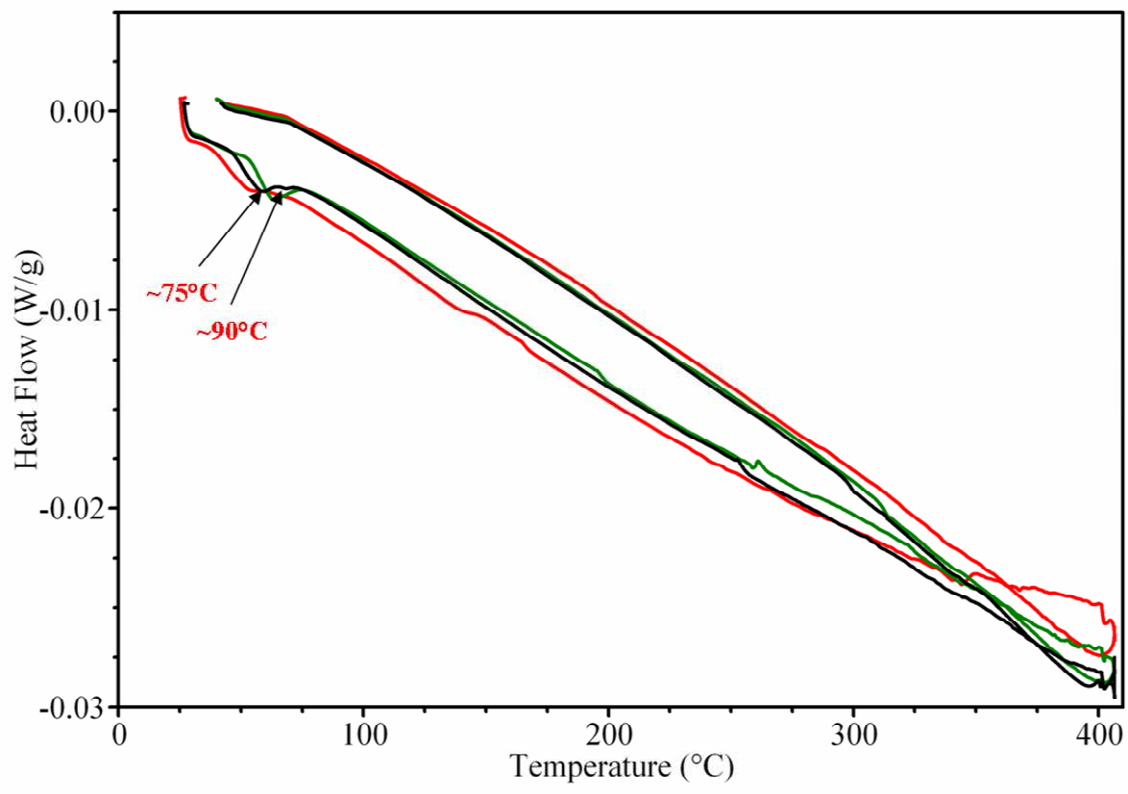

Figure 2.23. DSC curves for Al/Al_2O_3 composite NWs measured at a heating rate of 10 °C/min in the temperature range of 40-400°C and an initial hydrogen pressure of 20 bars. The three different curves represent the successive measurements without opening the sample chamber

To know more about the inside story, the process was repeatedly performed in a temperature range of 40 to 200°C with a relatively lower heating rate, that is, 5°C/min. The endothermic peak appeared in the range of ~50°C to ~100°C resolves into two broad peaks with a minima at ~70°C and ~90°C (Figure 2.24). The peak having minimum at ~70°C is sufficiently broader and intense compared to the one having minimum at ~90°C. The endothermic peaks appeared again and again by repeating the process which indicates that the reaction between the H_2 molecules and the NWs is a reversible one.

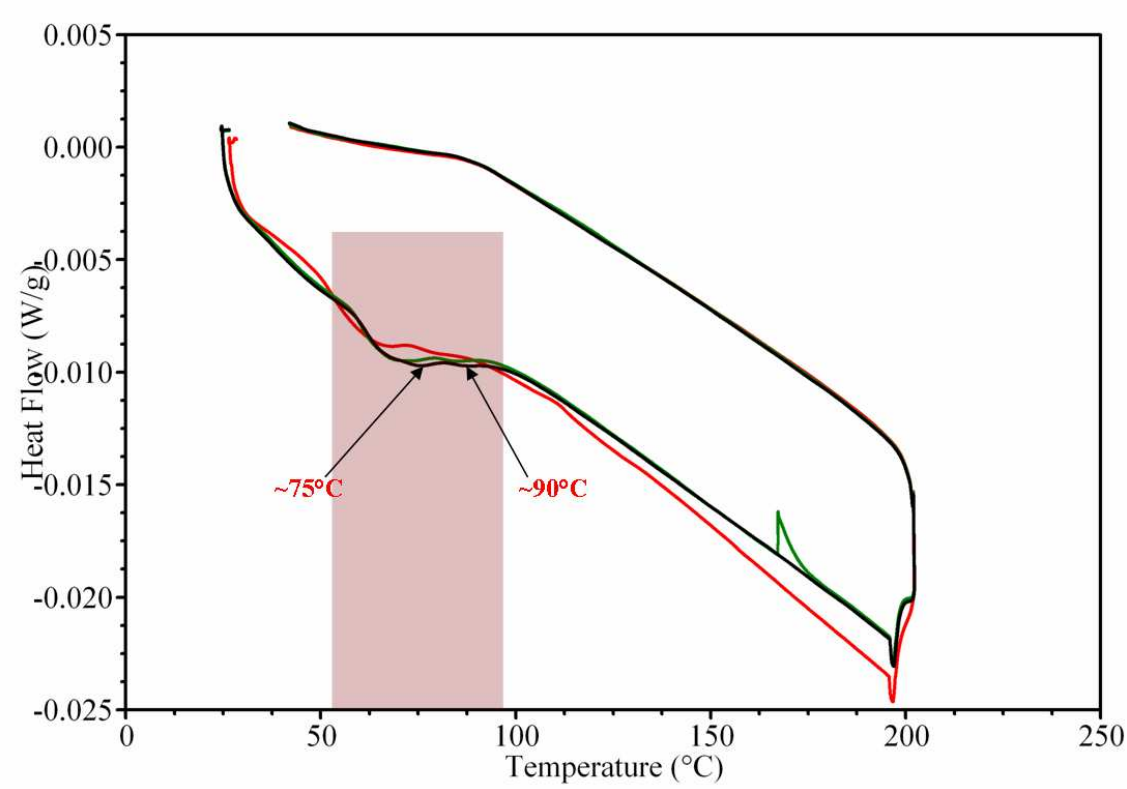

Figure 2.24. DSC curves for Al/Al_2O_3 composite NWs measured at a heating rate of 5 °C/min in the temperature range of 40-200°C and an initial hydrogen pressure of 20 bars. The three different curves represent the successive measurements without opening the sample chamber

To compare the results obtained from DSC analyzer using Al/Al_2O_3 composite NWs as adsorbent, HAlO material was used which has a compact structure like glass. The material was scanned in a temperature range of 40-400°C at a heating rate of 10°C/min. Figure 2.25 shows a DSC curve for HAlO material without having any peak. Since the structure and nature of HAlO is such, where the chance for any sort of reaction is limited. Some nominal endothermic peaks appeared above 300°C which may be due to the elimination of H_2, since HAlO material is highly unstable above 300°C and dissociates upon heating (Eq. 2.8).

$$HAlO \xrightarrow{Temp.\ > 300°C} 1/3\ Al/Al_2O_3 + ½\ H_2 \qquad (2.8)$$

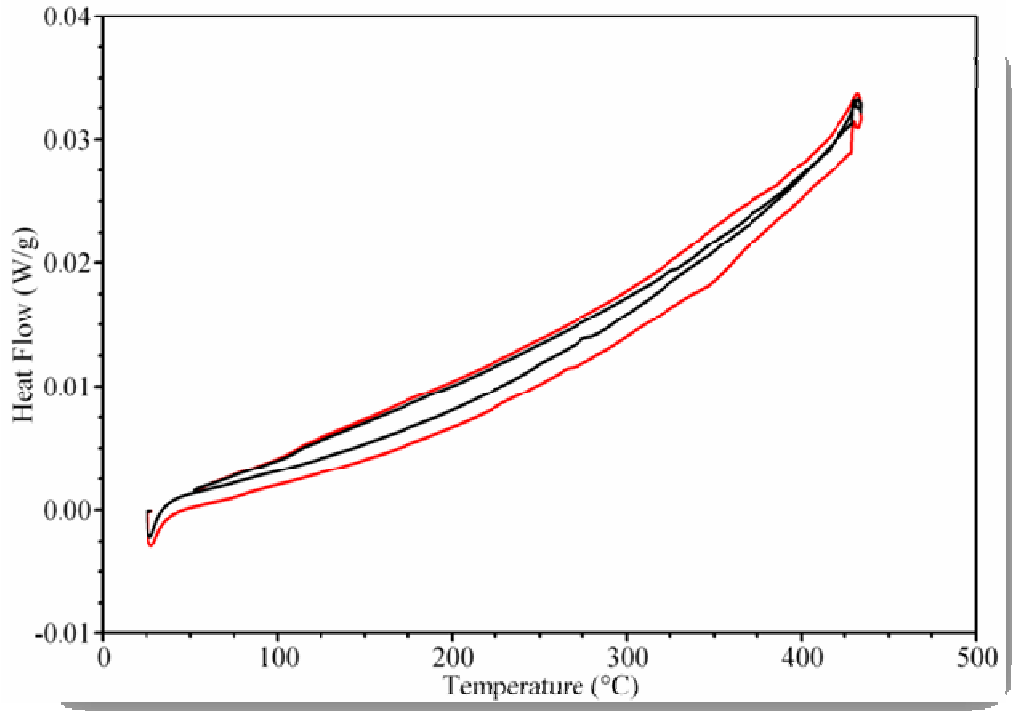

Figure 2.25. DSC curves for HAlO material measured at a heating rate of 10 °C/min in the temperature range of 40-400°C and an initial hydrogen pressure of 20 bars. The three different curves represent the successive measurements of hydrogen interaction with the same sample without opening the sample chamber

Discussion

Detailed results regarding the synthesis of materials and the hydrogen adsorption are presented in the previous section. In the following section will be discussed some key aspects of the experimental work and results obtained in light of highly related literature.

1. Hydrogen Adsorption by Al/Al_2O_3 Composite Nano-Wires (NWs)

Highly porous Al/Al_2O_3 Composite Nano-Wires (NWs) as thin film upon a stainless steel substrate are prepared by the decomposition of the single source precursor, $[H_2Al(OtBu)]_2$ in a CVD chamber and the resulting NWs are used as a potential hydrogen adsorption material at ambient conditions.

1.1. Al/Al_2O_3 Composite Nano-Wires (NWs)

One dimensional Al/Al_2O_3 NWs have been studied extensively by different researcher in our research group. All have concluded that the changing parameters have significant effect upon the structure of the resulting NWs. The NWs have core shell structure where the core is composed of metallic Al and the shell is formed of Al_2O_3 ceramic. The XRD has confirmed the presence of crystalline metallic Al in the NWs. The alumina is amorphous which is given by the wavy background signals in the XRD pattern for the wires. Since the temperature for the production of NWs in this case is low (580°C), therefore, it is difficult to get crystalline alumina. The same reason is also mentioned by O. C. Aktaş in his Ph. D thesis submitted to the faculty of natural sciences of the Saarland University [75]. To get a clear picture of the XRD and avoid the interferences from other metals, we have deposited the NWs upon an amorphous glass substrate. The resulting XRD pattern matches well with the PDF file of Al (PDF: 85-1327). The peak at 38° is assigned to the Al(111) lattice face everywhere [75] but surprisingly E. Sow [61] has mentioned this peak as due to aluminum carbide. However, Aktaş [75] has reported in his Ph. D work for Al (111) lattice face and further confirmations have been obtained from PDF file of Al (PDF: 85-1327).

The final structure of 1D NWs strictly depends upon the deposition temperature and the flow rate of the precursor. The effect of these parameters upon the resulting NWs has been studied extensively by E. Sow [61] and latter by O. C. Aktas [75]. The NWs for the present study has

been obtained at decomposition temperature of 580°C and the precursor flow at 9.0 x 10^{-2} mbar pressure. These parameters were selected for the preparation of the NWs because of two main reasons; one, after repeated experiments at these parameters NWs have been obtained as thin films with the reproducible diameter and porosity. This means that the repeated experiments give identical NWs each time. Second, the thin film obtained has a highly porous structure with strict composition of Al/Al_2O_3. It indicates that highly porous material can be obtained in repeated experiments. The diameter of the NWs falls in the range of 20-30nm which was reproduced in the subsequent experiments while keeping the parameters unchanged. The BET analysis performed for the determination of specific surface area, pore size distribution and pores volume gives 53.55 m^2/g, 32.89 nm and 0.44 cm^3/g, respectively. The SSA can not be measured exactly as the material could be produced only as thin film. For accurate and precise SSA determination the material must weigh above 250 mg which is quite difficult to produce in this way. The Al/Al2O3 composite nano-wires (NWs) obtained as thin films upon steel substrates were hardly 60 mg. However, the pore size determined can portrait the porosity of the material. The larger pore sizes determined for NWs confirms the high porous nature of the NWs. Pore volume determined in this way, limited by the amount of sample, is more than for the purified single wall carbon nano-tubes (SWCNTs ~0.398 m^3/g) [73]. The NWs have core shell structure with Al core and alumina shell. The metallic Al is in the core which is evident from the TEM images and also previously determined by different ways [61, 75]. The core shell nature of the Al/Al_2O_3 composite nano-wires can be visualized as is given in Figure 2.26.

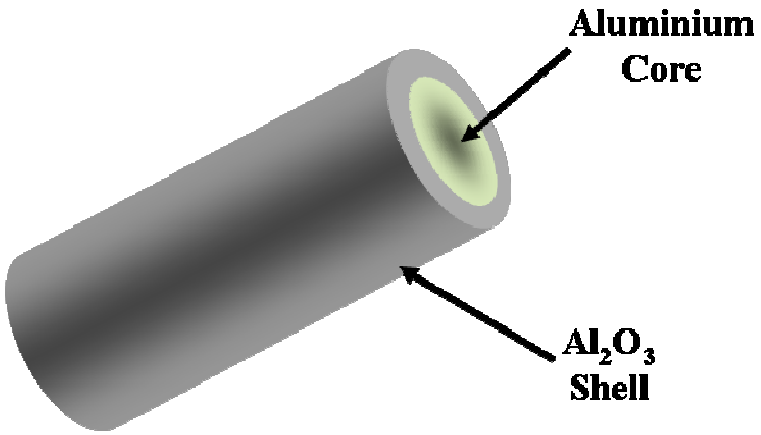

Figure 2.26. Schematic representation of the core-shell Al/Al_2O_3 composite NWs

1.2. Hydrogen Adsorption by Al/Al_2O_3 Composite NWs

As seen in the previous section, the hydrogen adsorption upon the Al/Al_2O_3 composite NWs is significant. A maximum of 6.5(±0.2) wt.% of hydrogen has been taken by the Al/Al_2O_3 composite NWs at ambient conditions. The results correspond well to some of the earlier reported literature. For example, the diameter of the Al/Al_2O_3 composite NWs is in good agreement to that of efficient hydrogen storage materials. Dillon *et. al*. [20] and Chen *et. al*. [23] reported SWCNTs and Li-doped CNTs having diameter in the range of 5-50 nm storing 10 wt% and 20 wt. % hydrogen at ambient conditions, respectively. The Al/Al_2O_3 composite NWs used in this study have diameter in the range of 25-30 nm corresponding to that of SWCNTs and CNTs. Apart from the diameter of the NWs, the pore sizes are also comparable to that of efficient hydrogen storage CNTs [23]. It means that the Al/Al_2O_3 composite NWs are highly suitable material for efficient and reversible hydrogen storage.

The results obtained show sufficiently high amount of hydrogen uptake by the Al/Al_2O_3 composite NWs. The amount of hydrogen uptake by the NWs increases with increasing temperature upto 100°C and then decreases drastically upto 300°C. A relatively similar behaviour of hydrogen uptake by the Li-doped CNTs has been reported by Chen *et. al*. [23]. Contrarily, the hydrogen adsorption by the Al/Al_2O_3 composite NWs is controlled by pure physisorption mechanism which is evident from the higher amount of hydrogen uptake by the NWs at 25°C. Approximately 4.8(±0.2) wt.% hydrogen adsorption occurs on to the NWs at 25°C and 20 bar pressure which indicates that the adsorption occurs by physisorption. The increasing hydrogen adsorption by the NWs with increasing temperature upto 100°C may be due to the activation of the NWs with increasing temperature. It is thought that the opening of NWs occurs with increasing temperature. The opening of the nano-structure makes accessible more surface area to the hydrogen molecules. The effect of temperature upon the hydrogen uptake by the CNTs is previously reported [20]. It has been explained that the increasing temperature ensures access to the interiors of the CNTs and thus increase the amount of hydrogen uptake by the CNTs with increasing temperature [20]. However, the increasing amount of hydrogen uptake by the NWs with increasing temperature has a limit that is 100°C. It is observed that above 100°C, the amount of hydrogen adsorption decreases with increasing temperature. It indicates that above 100°C, desorption of hydrogen occurs. Chen *et. al*. [23] showed that above 773 K, the desorption of hydrogen occurs by the Li-doped CNTs. In the results it is observed that the adsorption studies performed at 200°C and 300°C, the amount of

hydrogen uptake drops drastically that is from maximum 6.5(±0.2) wt.% at 100°C and 20 bars to 1.6(±0.2) wt.% at 300°C and 20 bars. It indicates that desorption of hydrogen starts above 100°C. The smaller amount of hydrogen adsorbed at higher temperature that is at 200°C and 300°C may be due to some chemical reactions occur during the process. However, the wt.% amount determined by Sievert's apparatus and the peaks in the DSC spectra are insignificant.

The physisorption of hydrogen on to the Al/Al_2O_3 composite NWs at temperature below 100°C and desorption above 100°C by the NWs was followed by IR spectroscopy. The IR spectra recorded immediately after hydrogen adsorption experiments performed at temperatures below 100°C does not show any new peaks except for broadening of the existing O-H stretching vibration peak. It is also noteworthy that only the sample hydrogenated at 100°C shows broadening of O-H stretching vibration peak while the same peak for sample hydrogenated at lower temperatures is unaffected. It may be due stronger interaction between the hydrogen molecules and the materials at 100°C.

At temperature above 100°C, the adsorption of H_2 upon the NWs is insignificant which indicates that above 100°C, desorption of hydrogen occurs. Although some sort of chemisorpion could not be ruled out and this is also clear from the IR spectroscopy as well as hydrogen adsorption isotherms. The hydrogen adsorption isotherms show smaller amount of hydrogen adsorbed upon the NWs above 100°C that is at 200°C and 300°C. The IR spectra recorded for the sample hydrogenated at 200°C and 300°C show extra peaks besides the O-H stretching vibration peaks. These new peaks appear in the range of 3500 cm^{-1} to 3800 cm^{-1} are due to the free O-H vibrations. Apart from the appearance of new peaks, the Al-O vibration peaks in the IR spectra of these samples narrowed down. These observations indicate that the alumina network ruptures and Al-O-H bonds form in which the hydrogen bonded oxygen is not shared by two Al centres but instead by only one Al atom (Figure 2.27). This sharpens the Al-O bonding peaks and also the free O-H bonds have vibrational peaks at higher energies [76]. It is evident that the increasing temperature is responsible for splitting of H_2 molecules and making new bonds. One can conclude from these results that at higher temperatures that are at 200°C and 300°C mostly desorption of hydrogen occur except some chemical reaction between the alumina and hydrogen.

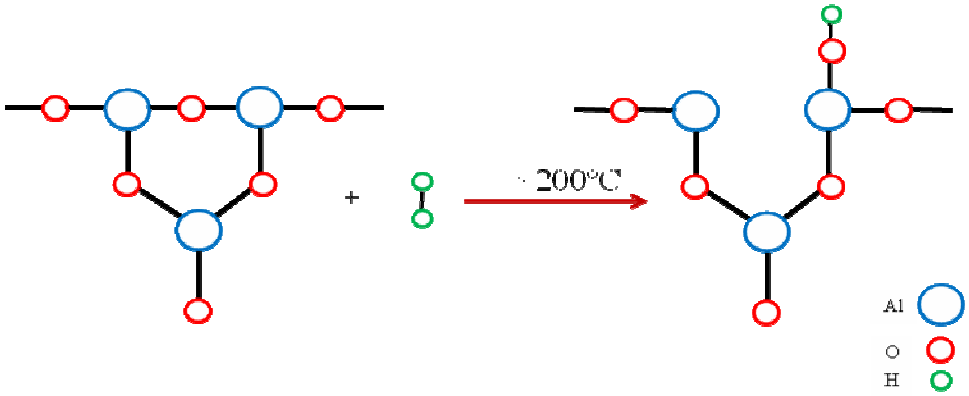

Figure 2.27. Pictorial representation of H_2 interaction with the Al_2O_3 network above 100°C indicated some sort of chemical reaction between the Alumina and hydrogen molecules

The results obtained from the Sievert's apparatus (volumetric process) are in good agreement to that obtained from the differential scanning calorimetry (DSC). The DSC curve in the range of 40-400°C temperature can be divided into two regions. The region below 100°C in which a broad but distinct endothermic peak appears and the post 100°C temperature region. The weak and broad peaks in the range of approximately 60-100°C corresponds to that of volumetric results giving highest amount of hydrogen adsorption at 70°C and 100°C. The peaks are weak and highly reproducible indicating that the hydrogen adsorption is solely controlled by physisorption mechanism. The appearance of the peak in the repeated measurements of the same sample confirms also physisorption as well as that the adsorption is reversible. The hydrogen adsorbed physically upon the Al/Al_2O_3 composite NWs in the range of 60-100°C and then desorbed upon heating above 100°C which is evident from the downward movement of the DSC curve. The same effect occurs in the second run and so on. The energy needed for strong physisorption interactions is sufficient to be detected as heat flow between the two pans in DSC that is sample pan and reference pan. However, it is relatively low, which may be explained while considering some of the following reasons. The first reason is the nature of the reaction. As the adsorption of hydrogen occurs upon the NWs by purely physisorption mechanism which generally involves lower energies. Secondly, the NWs are deposited upon the substrate which comes in between the heat sensitive sample pan and the material. Therefore, some of the heat produced and/or taken in for a chemical process will be dissipated during conduction between the sample and the heat sensitive pan. The third reason may be the NWs itself. The NWs are bad conductor of heat and it is thought that the physisorption occurs at the surface of the NWs. Therefore, the heat is not conducted properly. The fourth reason may be the very small amount of the NWs which are obtained as thin film

upon Al substrate. The deposited sample material is less than 1 mg while the standard sample used in DSC is about 10 mg for better and clearer results. The smaller the amount of the sample the lower the heat produced and/or released during the process.

Above 200°C the sharp peaks, both endothermic and exothermic, indicate dissociative chemisorption where proper reactions take place. The mixture of peaks appeared due to a chain of reactions occurred at different temperatures. This behavior of alumina has been observed by Ehwald and Leibnitz, who have studied the hydrogen adsorption by the Pt/Al_2O_3 system [79]. However, the intensities of the peaks are very smaller which show that the chemical reactions occur above 100°C are insignificant and most of the hydrogen is desorbed as gaseous H_2.

1.3. Hydrogen Adsorption by Ni/Al2O3 Composite NPs

The hydrogen adsorption isotherms obtained for Ni/Al_2O_3 composite nano-powders (NPs) using Sievert's type apparatus show that the amount of hydrogen adsorbed increases with increasing temperature. The adsorption of hydrogen at room temperature is insignificant and higher at higher temperatures. This is contradictory to the hydrogen adsorption isotherms obtained for Al/Al_2O_3 composite nano-wires in which the hydrogen adsorption at higher temperatures is small. It indicates that the hydrogen uptake by the Ni/Al_2O_3 composite NPs occurs by chemisorption. This corresponds to the earlier reported systems in which the hydrogen uptake is a result of pure chemisorption mechanism. H. Ehwald and U. Leibnitz reported Pt/Al_2O_3 composite material which adsorbs hydrogen by pure chemisorption mechanism [77]. They concluded that the amount of hydrogen adsorbed on to the Pt/Al_2O_3 composite increases with increasing temperature. The material used in this study that is Ni/Al_2O_3 is comparable in composition and nature to that Pt/Al_2O_3. The highest amount of hydrogen adsorbed by Ni/Al_2O_3 which is 2.9(±0.2) is comparable in value to that of Pt/Al_2O_3 (~2.50 wt.%). Actually, the Ni nanoparticles dispersed in the alumina matrix facilitate the breaking of H-H bond. The resulting atomic hydrogen reduces the Al-O-Al bond forming a new structure with Al-O-H bonds. To break the H_2 marriage (the term used by Kubas [67]), at first Ni (same is for the transition metals) makes a coordinating complex with H_2 molecule and then Ni dihydride complex (NiH_2). This is followed by the transferring of H into the alumina network where it reacts and reduces the Al-O bond (Figure 2.28). The same mechanism was also concluded for the chemisorption of hydrogen by Pt/Al_2O_3. Also,

Ni/Al_2O_3 is used as catalyst for reduction of unsaturated bonds which involves activation of the catalyst and then reduction of the unsaturated bonds [70].

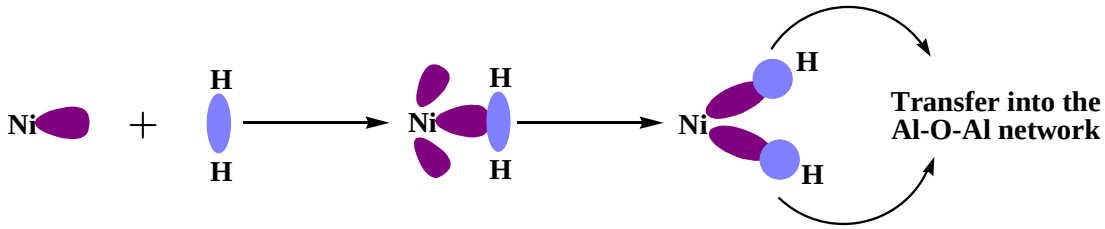

Figure 2.28. H_2 cleavage by the Ni dispersed in alumina matrix

The IR spectra obtained after hydrogen adsorption confirm this sort of reactions between the hydrogen and the alumina. The other interesting things we have observed in the IR spectra are the appearance of new peaks which could be assign to C=O (1732cm^{-1}), C-H (2927 cm^{-1}) stretching vibrations and C-H (1459 cm^{-1}) bending vibration. The C=O vibration peak is characteristic of the aldehydes. These observations show that some organic compounds are formed during the hydrogenation process.

1. Materials

1.1. Al/Al_2O_3 Composite Nano-Wires (NWs)

1.1.1. Synthesis of Precursor, $[H_2Al(O^tBu)]_2$

The single source precursor, $[H_2Al(O^tBu)]_2$ was synthesized according to the procedure reported in literature [62]. 4.554 g (120mmol) of $LiAlH_4$ was dissolved in diethylether in a two neck flask. 5.334 g (40mmol) of $AlCl_3$ dissolved in diethylether under cooling (liquid N_2) was added drop by drop into the above solution. After stirring for one hour, 11.859g (160mmol) of *tert*-butanol was slowly and carefully dropped and evolution of hydrogen was observed. The whole reaction mixture was stirred for another four hours for completion of the reaction. LiCl precipitated out of the mixture and was filtered off. The volatiles (mostly solvent) were removed by applying low pressure and condensed in a cold trap. The precursor was obtained as white powder and purified by sublimation at room temperature and lower pressure. The yield was quite satisfactory (93%). The pure bis(*tert*-butoxy)aluminium dihydride was characterized by ^1H, ^{13}C, IR spectroscopy. Elemental composition was determined by CHN analyzer. The results collected are in good agreement with the reported literature [62].

^{1}HNMR (C_6D_6): δ (ppm) = 1.21(s, 18H, $-CH_3$), 4.44 (s, 4H, AlH_2); ^{13}C (C_6D_6): δ (ppm) = 76.43 (2C, -**C**(CH_3)), 30.36 (6C, $-CH_3$); IR (solid): ν = 1845cm^{-1}; elemental composition ($H_{22}C_8O_2Al_2$) = found (calc.): C 47.02 (47.00), H 10.65 (10.86).

1.1.2. Deposition of Al/Al_2O_3 Composite NWs

Al/Al_2O_3 Composite NWs were prepared in a cold wall CVD reactor (Figure 1) [63]. The home made CVD device is composed of interconnected parts having different functions. The substrate upon which the NWs deposition occurred is placed in a graphite holder. The graphite block works as a support as well as a uniform heating source for the substrate which

is heated by inductive heating coil coupled with high frequency generator. The temperature of the graphite holder is controlled by using an electric temperature controller connected to each other by a thermocouple. The precursor is sublimed by producing vacuum inside the reactor tube connected at one side to the precursor flask and at other with the mechanical vacuum pump. The stream of the sublimed precursor is directed over the heated substrate under dynamic vacuum and the decomposition of precursor takes place. As a result of decomposition of the precursor, Al/Al_2O_3 Composite NWs deposits over the substrate making a thin film and the volatiles byproducts were flushed away with the help of vacuum pump. To save the pump from the corrosive effect of the volatiles organic byproducts and gases produced during the decomposition of the precursor, a cold trap (liquid N_2) was installed in the line before pump which traps all the gases and organic volatiles. The precursor flow control is important for the structure and morphology of the resulting thin films; therefore, it is monitored continuously using a pressure transducer with a reading of base pressure up to 2.0×10^{-2}mbar. The precursor is placed in round bottom flask with a manually controlled on-off valve. Schematic diagram of the cold wall CVD reactor is given in the Figure 2.29.

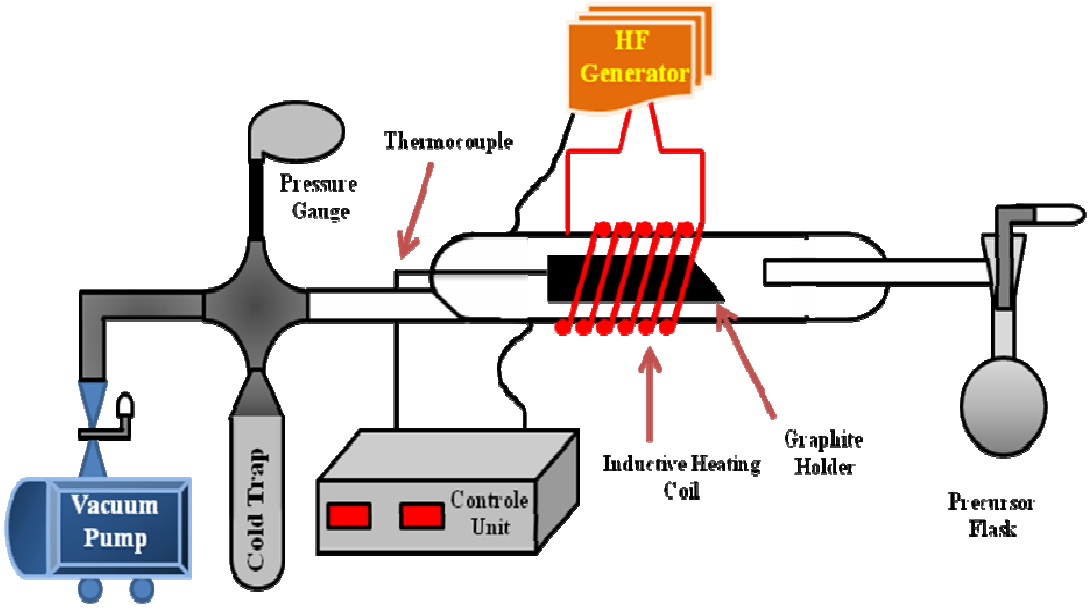

Figure 2.29. Drawing of a typical cold wall CVD reactor used for deposition of Al/Al_2O_3 Composite NWs at 580°C and precursor flow maintained at 9.0×10^{-2}mbar pressure.

Before the deposition of Al/Al_2O_3 Composite NWs upon a heated substrate, the CVD reactor was evacuated with a base pressure of 2.0×10^{-2} mbar and flushed three times with N_2. The process was optimized for highly porous thin films having NWs of diameter not more than 30nm. The decomposition temperature of the precursor upon the substrate was 580°C and the precursor flow was maintained at 9.0×10^{-2} mbar pressure with an average deposition time of 20 minutes. The flow of precursor was maintained manually using an on-off valve keeping an eye on the pressure read out unit. After deposition of the NWs, the heating was terminated and the system was let to cool. The coated substrates were removed and kept in a clean box for further use.

1.2. Synthesis of Ni /Al_2O_3 Composite Nano-Powder

The same CVD reactor discussed above was used except the graphite holder which was modified according to the nature of the coating. The Ni/Al_2O_3 nano-composite powder was prepared by the decomposition of $Ni(acac)_2$ under a steady stream of $[H_2AlO^tBu]_2$ precursor. The exact reaction mechanism and the resulting stoichiometries of the products are not known but the process gives Ni/Al_2O_3 nano-composite powder and the byproducts which are hydrogen and organic gases (Eq. 2.9). The byproducts flush away as the system is connected to a dynamic vacuum.

$$Ni(acac)_2 + [H_2Al(O^tBu)]_2 \longrightarrow Ni/Al_2O_3 + nH_2 + \text{Organic gases} \qquad (2.9)$$

$Ni(acac)_2$ was taken in a specially designed cuvette (Figure 2.30) which was inserted into a graphite block. The graphite block possesses a hole of the same size as that of cuvette which fits well into the hole to ensure efficient heat conduction. The cuvette was filled up with 0.5 g of $Ni(acac)_2$ and was placed inside the graphite block which was inserted into the CVD chamber. The system was initially heated up to 220°C and then was exposed to a steady stream of the precursor, $[H_2Al(O^tBu)]_2$ by applying vacuum. The precursor flow was maintained at 2.0×10^{-1} mbar pressure and was continued for 15 minutes. Then the temperature was increased up to 580°C and the precursor flow was continued for another 10 minutes. After 10 minutes, the precursor flow was discontinued while the heating was continued for another 5 minutes to ensure complete decomposition of the reactants. Then the reactor was allowed to cool to room temperature and finally demounted to remove the sample. The resulting fine powder was analyzed by XRD, SEM, TEM and IR spectroscopy and was

confirmed as biphasic Ni/Al_2O_3 nano-composite material. The material was stable enough at ambient conditions and after keeping for several weeks under open atmosphere, no evidence of the reaction with the atmospheric oxygen or moisture has been found.

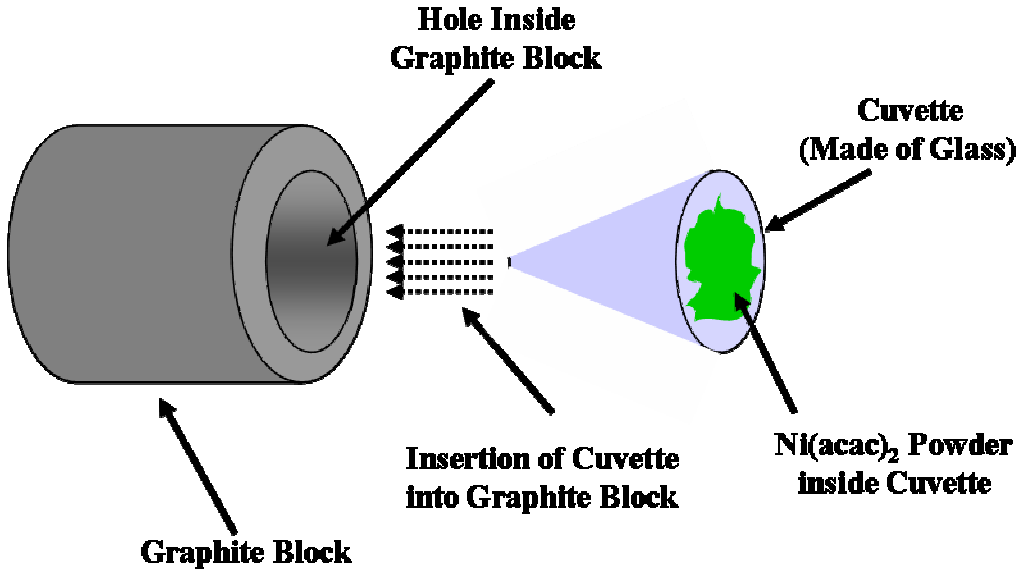

Figure 2.30. Schematic representation of the specially designed cuvette containing $Ni(acac)_2$ powder inserted into a graphite block which was then placed in CVD chamber to expose $Ni(acac)_2$ powder to a steady stream of $[H_2Al(O^tBu)]_2$

2. Methods

The H_2 adsorption by Al/Al_2O_3 and Ni/Al_2O_3 was carried out using Sievert's apparatus. For comparison purposes, differential scanning calorimetry (DSC) was performed upon the NWs. The results obtained at two different techniques were compared. The following sections will cover the essential parts of the experimental procedures of the H_2 adsorption studies.

2.1. Sievert's Apparatus

An efficient hydrogen storage material is important, of course, but the measurements methods, to be simple and reliable, are vital for the hydrogen fuel economy. The most

common techniques in use are volumetric and gravimetric [78] where the former deals with the changing volume inside the system and the latter with the mass of the material. The volumetric technique has the advantage over the gravimetric technique of higher accuracy. Since, the measurement of larger changes in pressure is easy compared to the smaller mass changes. As hydrogen is the lightest of all the gases, therefore, this advantage is more prominent when dealing with it. Sievert's apparatus is also more attractive due to its low cost, portability and simplicity. Besides these it is universally accepted as accurate technique.

A schematic diagram of the apparatus is presented in Figure 2.31. All components of this set up possess VCR connections. It is made of two stainless steel chambers of calibrated volumes, the sample chamber, SC (V_{SC} = 5.2926cm^3), and the reservoir chamber, RC (V_{RC} = 21.1195cm^3), on-off valves(manual), pressure gauge and a heater(inserted so that it heats directly the sample). RC is connected to the gas bottles and the sample chamber through manually controlled on-off valves. The sample is heated directly by a heater inserted into the sample chamber cell and the temperature is monitored by a K-type thermocouple connected to a temperature control display unit. The sample can be heated up to 600K (but actually used only up to 573.15K). The pressure inside the reservoir is measured using a membrane pressure transducer with a sensitivity of 0.1mbar (1.0 x 10^{-4}bar) in the range of 1 bar to 40 bars. The system can be evacuated to a base pressure of 1x10^{-6} mbar with a turbo molecular pump connected to a mechanical pump. During the experimental run, data acquisition is performed by personal computer. The home-made software acquires the sample pressure in RC, $P_{RC,}$ as a function of time. A schematic diagram of SC is presented in Figure 2.32 where the all metal sealing is ensured by a Cu gasket. The sample, typically in the form of a thin film upon a metal substrate, is contained in a sample holder of approximately 10mm diameter excavated in the sample chamber. Heating jacket has been used to maintain the temperature in the RC while the SC chamber was thermally isolated using insulating cover.

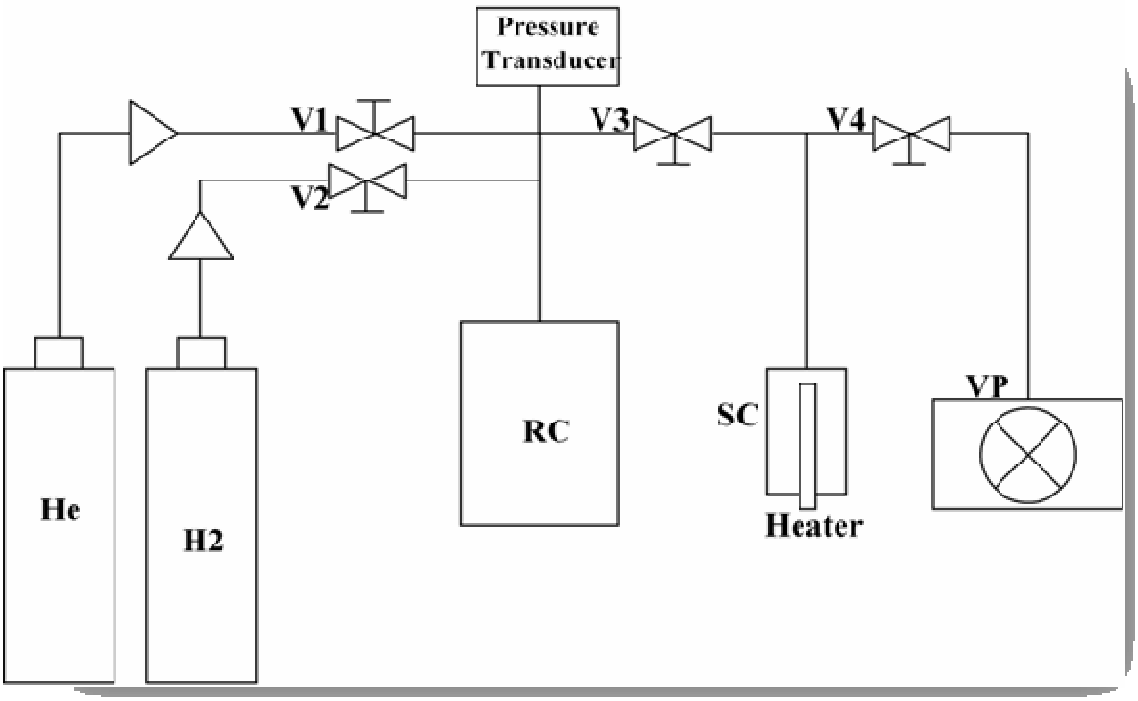

Figure 2.31. Schematic diagram of the Sievert's type apparatus. VP, vacuum pump; SC, sample chamber; RC, reservoir chamber; V_1, V_2, V_3 and V_4, manually operated on-off valves

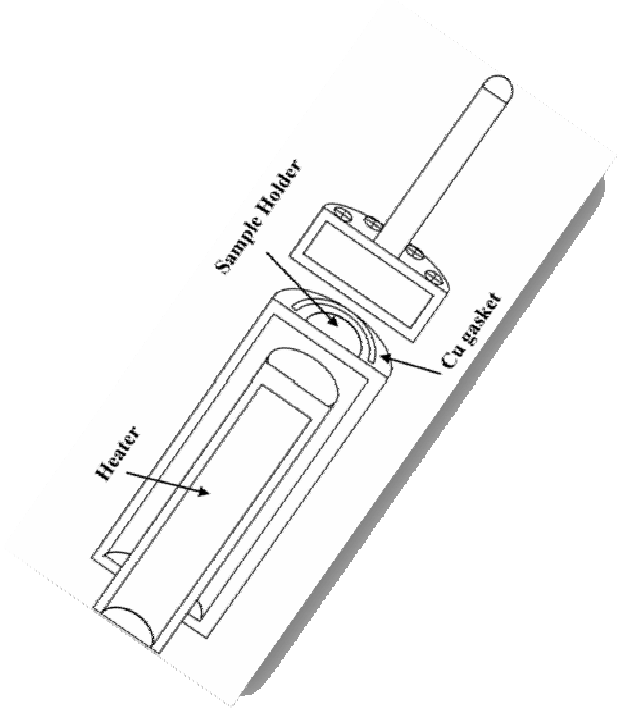

Figure 2.32. Schematic diagram of SC: the Cu gasket is used to ensure sealing of the all metal contacts

Before starting the measurements, the apparatus was tested for any possible leaks. The leak test was carried out using helium leak tester with a base pressure of 1.0 x 10^{-9}mbar. It was proved that there is no leak in the system.

In the next step the apparatus was calibrated, first with a well know alloy and then with sea sand. Misch metal alloy with a general formula, $MmNi_5$ was used where Mm stands for misch metals, which are La, Ce, Nd, and Pr [79]. The composition of the alloy was determined by powder XRD. Prior to hydrogen adsorption and XRD measurements the alloy was grinded into nano-meter level scale particle by high energy ball milling. The X-ray diffractogram of the alloy is given in Figure 2.33.

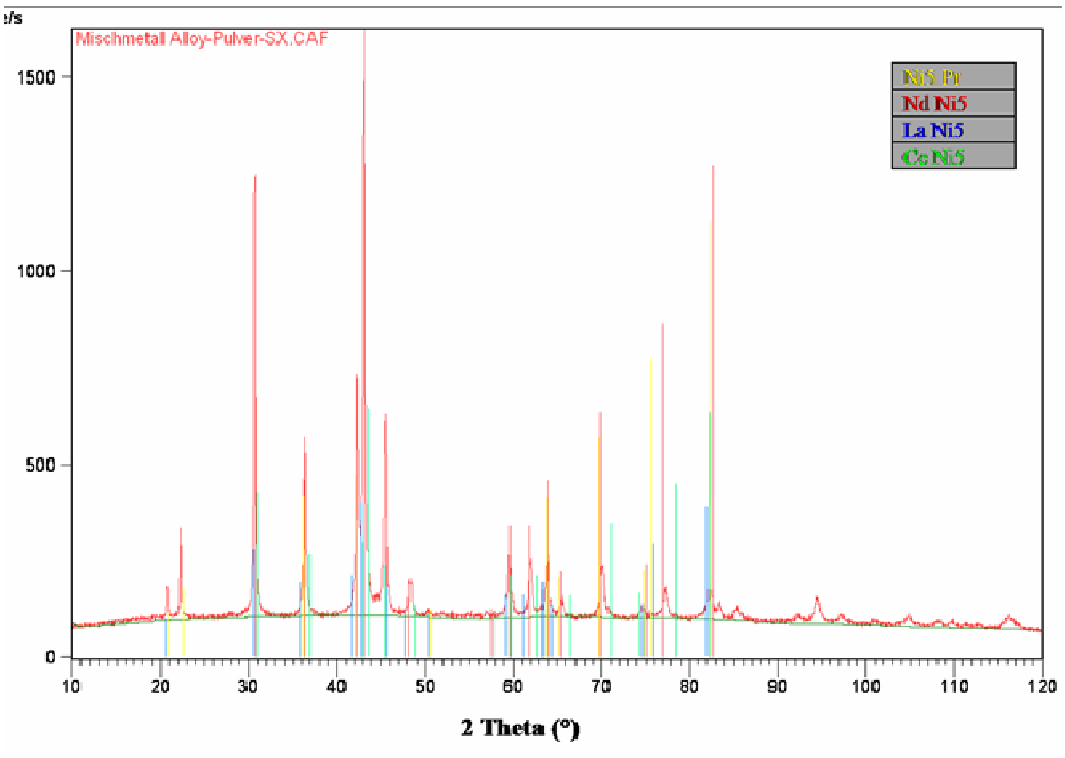

Figure 2.33. Powder X-ray diffractogram of the misch metal alloy $MmNi_5$ ({La, Ce, Nd, Pr}Ni_5)

125.22mg of $MmNi_5$ was loaded into the sample chamber and degassed for 2 hours at 105°C and 1.0 x 10^{-6}mbar pressure. The hydrogen adsorption was carried out at 50°C and 20 bars of hydrogen pressure. The wt.% adsorbed by the alloy is independent of the amount of sample

and a storage capacity of 1.60(±0.20) wt.% was obtained. This amount of hydrogen stored at $MmNi_5$ alloy is comparable to the reported (~1.40 wt.%) [79-80].

Sea sand was used as calibration material following an established literature procedure [84]. Since sea sand is a non-porous material and does not adsorb gases. A measured mass of sample was placed in the sample chamber and the valve between the two chambers was closed. The sample was degassed at 105°C for two hours at a base pressure of 1.0 x 10^{-6}mbar to remove traces of moisture or other adsorb gases, if present. The RC was filled with a desired pressure, P_0, of He gas and allowed to stay for 15 minutes while closing the valve towards the gas bottle. Then the gas was relaxed into the SC by slowly opening the valve. The drop in pressure, P, in the RC was monitored by the pressure transducer connected to PC. The system was allowed to establish equilibrium for 15 minutes. The same procedure was repeated for all the sand samples and the ratios P_0/P were calculated. A linear curve has been obtained by plotting P_0/P against the volume of the samples (Figure 2.34).

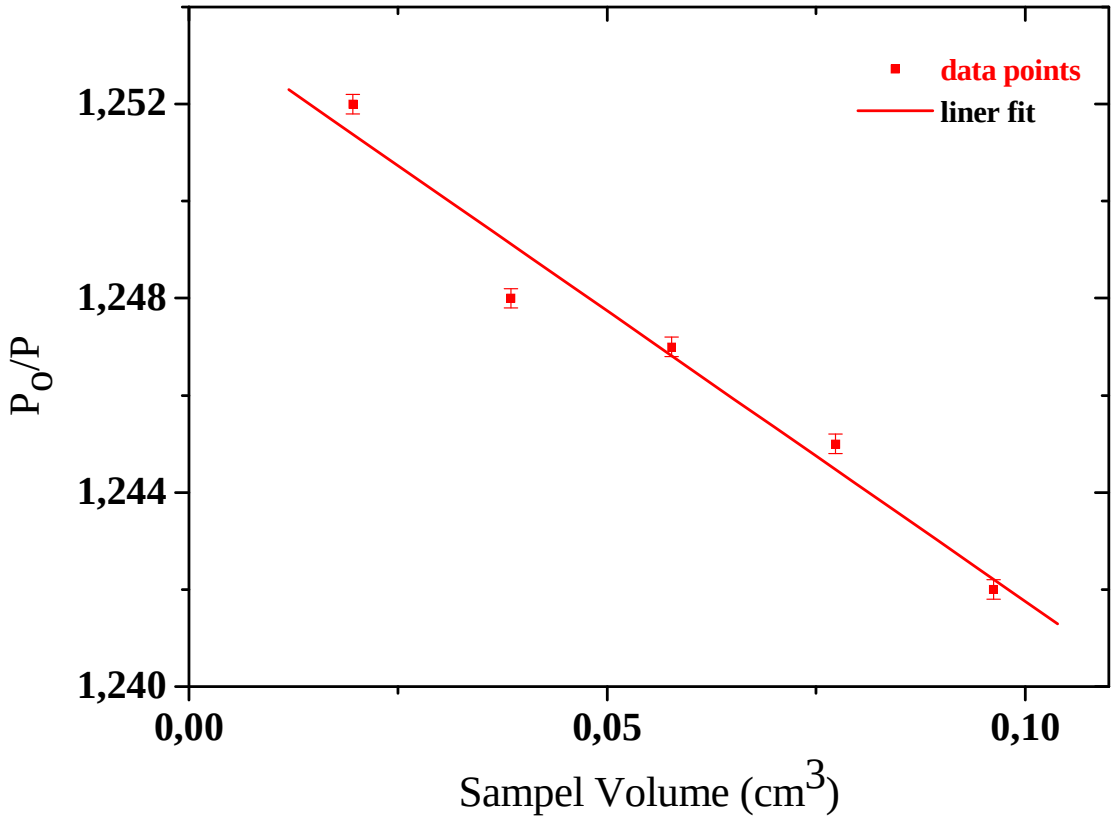

Figure 2.34. Calibration curve of the Sievert's apparatus produced by plotting ratios P_0/P against volumes of different sea sand samples

Once the apparatus has been tested for any possible leaks and calibrated with different standards, then the hydrogen adsorption processes could be carried out with accuracy and reliability.

3. Experimental Procedures

3.1. Sample Preparation and H_2 Adsorption using Sievert's Apparatus

To achieve accurate and reliable results one has to consider some specific problems connected to adsorption analysis. The gases should be as pure as possible since the presence of other gases can compete for adsorption as the adsorption process is not only hydrogen selective. The presence of other gases in hydrogen could introduce serious errors into the final results. Therefore, the gases used in this study, that is Helium and hydrogen were of purity higher than 99.9999%. To avoid moisture the gases were passed through an efficient desiccant.

The samples prepared in the cold wall CVD reactor as thin film upon metallic substrate have been used as such without pre-treatment. The sample was placed in the sample chamber and the chamber was closed. The all metal sealing was made leak proof using a cupper gasket. Prior to the measurements the experimental set up including the sample holder containing the sample was out-gassed for 12 hours at 150°C under ultra-high vacuum(UHV) conditions with a base pressure of 1.0×10^{-6}mbar. This UHV conditions ensures the removal of all adsorbed gases upon the NWs and moisture, if present.

Previously the hydrogen uptake calculations involve the volume as well as the density of the sample. These methods have serious limitations, for example involvement of complex calculations, lack of precise and accurate volume determination techniques etc. But apart from all the above limitations the main drawback is the adsorption of the gas (normally N_2) used for the determination of volume of the porous material. The gas could adsorb into the pores of the sample material which is always considered to be neglected. Infact, the exact volume of the porous material is seriously affected by the adsorption of the gas used in volume measurements. This error at the volume determination process could be reproduced in the final results.

We have developed and tested a new method for the determination of the amount of hydrogen adsorbed by the sample material. First the amount of He transferred from the RC into the SC was calculated. He gas was introduced into the RC by opening V_1 while closing V_3 up to the desired pressure (4-20bar). Closing V_1 and monitoring the pressure in the RC by the pressure transducer, V_3 was opened to relax the gas into the SC and maintained the system for 30 minutes to achieve the equilibrium. The amount of He transferred was determined using the ideal gas equation (eq. 2.10)

$$n = \frac{PV}{Z(P,\ T)\,RT} \tag{2.10}$$

Where n is the number of moles, P is the pressure, V is volume, R is the ideal gas constant, T is the temperature and Z is the compressibility factor which can be expressed by the following equation (eq. 2.11) [73].

$$Z = [1.000547 - (6.07 \times 10^{-7}).T] + [0.000912 - (1.0653 \times 10^{-6}).P] + [(7.373407 - 0.0901.T) \times 10^{-7}].P^2 \tag{2.11}$$

Once the number of moles of He were determined then the same process was repeated for hydrogen too. The numbers of moles of the He in SC were deduced from the number of moles of hydrogen in SC and the numbers of moles adsorbed were calculated. The amount of hydrogen adsorbed was expressed as wt.% and calculated according to the following equation (eq. 2.12).

$$wt.\% = \frac{m_{H_2}}{m_{H_2} + m_S} \times 100 \tag{2.12}$$

Where m_{H_2} is the mass of H_2 adsorbed and m_S is the amount of the sample. The adsorption isotherms were obtained by plotting wt.% against temperature and pressure.

4. Sample Preparation and H_2 Adsorption using Differential Scanning Calorimetry (DSC)

Q1000 differential scanning calorimeter of TA instruments equipped with a gas pressure chamber was used for DSC analysis. A sketch along its out put is given in Figure 2.35. Monitoring the heat flow to the sample as compared to that to the reference allows detecting reactions of the solid sample with gaseous hydrogen [81-82]. The chamber is composed of a heating source which heats the two pans uniformly. The two pans are a reference pan and a sample pan and connected through a low resistance heat flow path which is normally a disc. The sample is placed in the sample pan and the cell is closed tightly. Hydrogen is introduced into the chamber and any sort of reaction between the gas and the sample results into an intake and/or release of heat by the sample. The resulting equilibrium between the two pans is established by the in- and/or out-flow of heat from the sample pan. This heat flow is measured as a function of temperature. The flow of heat into the sample pan as a result of any chemical activity gives a negative peak in the curve of heat flow against temperature and the process is termed as endothermic. The release of heat by the sample pan gives a positive peak and the reaction is exothermic.

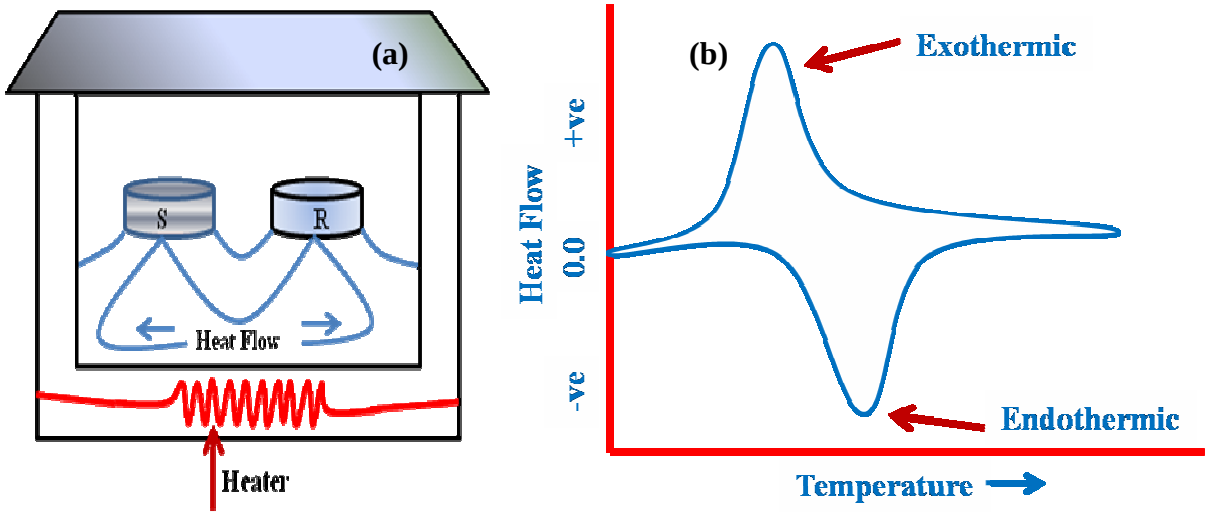

Figure 2.35. A typical DSC chamber with sample pan, s; reference pan, R; single heater and heat flow disc (a); an arbitrary DSC curve of heat flow as a function of temperature showing endothermic and exothermic peaks (b).

The sample was prepared by making a thin film of Al/Al_2O_3 composite NWs upon a 4mm diameter circular metal substrate in a cold wall CVD reactor. The sample was placed in a sample pan made from thin walled aluminum. The reference aluminum pan includes the substrate material, an aluminum discs to eliminate the effect of the substrate. The masses of the sample and reference discs were comparable. The chamber was closed after placing the sample in the sample pan and purged with hydrogen. The heat flow as a function of temperature was measured at different pressures (20bar, 40bar and 65bar) and temperature ranges (40-400°C and 40-200°C). The samples were heated at a heating rate of 10°C/min and 5°C/min as per requirements. In general the same temperature program was rerun three times without opening the sample chamber.

Conclusion

- Highly porous Al/Al_2O_3 composite nano-wires have been synthesized as thin film upon a metallic substrate in cold walled CVD reactor. Highly suitable NWs for hydrogen adsorption have been obtained at 580°C temperature and 9.0 x 10^{-2} mbar pressure.
- The NWs have a highly porous structure which can be viewed in the SEM images. The total pore volume of the NWs is 53.55 m^2/g and average pore size is approximately 32.89 nm.
- The pressure-temperature isotherms were obtained by home made Sievert's type apparatus which was caliberated with well known hydrogen storage materials as well as sea sand (SiO_2).
- The hydrogen adsorption isotherms give a maximum 6.5(±0.2) wt.% hydrogen adsorbed by the Al/Al_2O_3 NWs. It is concluded that the wt.% hydrogen adsorption strongly depends upon the temperature. However, the adsorption mechanisms are different in different temperature ranges. The wt.% hydrogen adsorption increases with the increasing temperature in the range of 25 to 100°C and then decrease up to 300°C. The experimental evidences show that the adsorption is governed by pure physisorption mechanism in the temperature range of 25-100°C. Above 100°C, desorption of hydrogen occurs with an insignificant amount of hydrogen adsorbed by chemisorption. The results obtained from two different instruments, Sievert's apparatus and DSC are in good agreement.
- Ni/Al_2O_3 composite NPs have been prepared by a novel chemical reaction in cold wall CVD reactor. It contains a biphasic nature with Ni nano-particles dispersed in the Al_2O_3 matrix. The average size of the Ni particles is below 20 nm. The hydrogen adsorption studies were performed upon Sievert's type apparatus. The amount of hydrogen adsorbed upon the NPs increases with the increasing temperature and pressure. The highest amount of hydrogen adsorbed upon the NPs is approximately 2.9(±0.2) wt.%. The adsorption at lower temperature is insignificant while at higher temperature it occurs by chemisorption.
- Finally the results show that a novel material for hydrogen adsorption has been developed in the form of Al/Al_2O_3 composite NWs which can store a fair amount of hydrogen at ambient conditions.

References

[1] Wikipedia, Kyoto Protocol, **1997**.

[2] R. C. Weast, *Handbook of Chemistry and Physics*, 83rd Ed., (CRC Press Inc., Florida, **2002**)

[3] J. Verne, *Den Hemlighetsfulla ö*, ISBN 91-71021-011-X (Niloe, Uddevalla, **1986**).

[4] D. Palmer, *hydrogen in the universe*, NASA, **1997**.

[5] G. Steve, *Hydrogen*, Jefferson Labs, **2008**.

[6] M. Dresselhaus, *et. al. Basic Research Needs for the Hydrogen Economy*, **2003**.

[7] Y. Fukai, in *The Metal Hydrogen System, basic bulk properties*, Vol. 21, *Springer Series in Material Sciences*, Edited by U. Gonser (*Springer Verlag. Berlin*, **1993**).

[8] J. Rifkin, *the Hydrogen Economy* (*Tarcher*, New York, **2002**).

[9] DOE Hydrogen Program, FY **2004** Progress Report. <http://www.eere.energy.gov/hydrogenandfuelcells/pdfs/annual04/iii_storage_intro.pdf>. 179-181 (2004).

[10] Hydrogen Economy: Opportunities, Costs, Barriers, and R&D Needs (*National Academies Press*, **2004**).

[11] J. Ogden, Princeton University, *Design and Economics of Hydrogen Energy System, Presentation to the committee*, January 23, **2003**.

[12] A. Zuttel, *Materials Today* 6, 24, **2003**.

[13] L. Schlapbach and A. Zuttel, *Nature*, 414, 353, **2001**.

[14] M. S. Dresselhaus, G. Dresselhaus, and P. C. Eklund, *Science of Fullerenes and Carbon Nanotubes*, (Acdemic Press Ltd., San Diego, 1996).

[15] U. Bünger and W. Zittel, *Applied Physics* A, 72, 147, **2001**.

[16] A. Kidnay and M. Hiza, *Adv. Cryog. Eng.*, 12, 730, **1967**.

[17] C. Carpetis and W. Peschka, *Int. J. Hydr. Energy*, 5, 539, **1980**.

[18] A. Chambers, C. Park, R. T. K. Baker and N. Rodreguez, *J. Phys. Chem., B*, 102, 4253, **1998**.

[19] P. Chen, X. Wu, J. Lin and K. Tan, *Science*, 91, 285, **1995**.

[20] A. Dillon *et. al.*, *Nature*, 386, 377, **1997**.

[21] E. Johansson, B. Hjörvarsson, T. Ekström and M. Jacob, *J. Alloy. Comp.*, 670, 330, **2002**.

[22] S. Orimo, G. Majer, T. Fukunaga, A. Zu¨ttel, L. Schlapbach, H. Fujii, *Appl. Phys. Lett.*, 75, 3093, **1999**.

[23] P. Chen, X. Wu, J. Lin, K.L. Tan, *Science*, 285, 91, **1999**.

[24] N. L. Rosi, J. Eckert, M. Eddaoudi, D. T. Vodak, J. Kim, M. O'Keeffe, and O. Yaghi, *Science*, 300, 1127, **2003**.

[25] J. J. Reilly and G. D. Sandrock, *Scientific American*, 242, 118-119 (1980).

[26] H. Lee, J.-w. Lee, D. Y. Kim, J. Park, Y.-T. Seo, H. Zeng, I. L. Moudrakovski, C. I. Ratcliffe and J. A. Ripmeester, *Nature*, 434, 743, **2005**.

[27] M. Hirscher, and M. Becher, *Journal of Nanoscience and Nanotechnology*, 3, 3, **2003**.

[28] J. A. Ritter, A. D. Ebner, J. Wang and R. Zidan, *Materials Today*, 6, 18, **2003**.

[29] J. Y. Lee, J. Lee and J. Jagiello, *Journal of Solid State Chemistry*, 178, 2527, **2005**.

[30] B. Panella, M. Hirscher and S. Roth, *Carbon*, 43, 2209, **2005**.

[31] Z. X. Guo, C. Shang and K. F. Aguey-Zinsou, Journal of the European Ceramic Society, 28, 1467, **2008**.

[32] G. Sandrock, G. Thomas, IEA/DOE/SNL *Hydride Databases*, *Accessed Online* October 30th, 2006: http://hydpark.ca.sandia.gov.

[33] B. Bogdanovi and M. Schwickardi, *Journal of Alloys and Compounds*, 1, 253, **1997**.

[34] M. Klell, H. Kindermann, and C. Jogl, *Proceedings International Hydrogen Energy Congress and Exhibition IHEC*, Istanbul, **2007**.

[35] Q. Liu, *Low-Cost, High-Efficiency, High-Pressure Hydrogen Storage*, Annual Report, **2009**.

[36] Department of Energy (DOE), www.hydrogen.energy.gov

[37] M. A. Schimko, *US Deapatment of Energy*, Annual Report, **2006**.

[38] T. Riis, E. F. Hagen, P. J. S. Vie and O. Ulleberg, *Hydrogen Production and Storage, R & D Priorities and Gaps*, **2006**.

[39] N. F. Mott and H. Jones, Theory of the Properties of Metals and Alloys (Oxford, London, **1936**), p, 316.

[40] P. N. Aukett, N. Quirke, S. Reddiford, S. R. Tennison, *Carbon*, 30, 913, **1992**.

[41] M. Rzepka, P. Lamp, M. A. de la Casa-Lillo, *J. Phys. Chem. B*, 102, 10894, **1998**.

[42] C. Carpetis, and W. Peschka, *1st World Hydrogen Energy Conference*, 9C-45-9C-54 (*New York, Pergamon Press*, Coral Gables, Fla., University of Miami, **1976**).

[43] C. Carpetis, and W. Peschka, *Second World Hydrogen Energy Conference* 1433-1456 (*Oxford and New York, Pergamon Press*, Zurich, Switzerland, **1978**).

[44] R. K. Agarwal, J. S. Noh, J. A. Schwarz, and P. Davini, *Carbon*, 25, 219, **1987**.

[45] J. S. Noh, R. K. Agarwal, and J. A. Schwarz, *International Journal of Hydrogen Energy*, 12, 693, **1987**.

[46] R. Strobel, L. Jorissen, T. Schliermann, V. Trapp, W. Schutz, K. Bohmhammel, G. Wolf and J. Garche, *Journal of Power Sources*, 84, 221, **1999**.

[47] S. Iijima, *Nature*, 354, 56, **1991**.

[48] C. Liu, Y. Y. Fan, M. Liu, H. T. Cong, H. M. Cheng and M. S. Dresselhaus, *Science*, 286, 1127, **1999**.

[49] A. Chambers, C. Park, T. K. Bakers, N. M. Rodriguez, *J. Phys. Chem* B, 102, 4253, **1998**.

[50] R. T. Yang, *Carbon*, 38, 623. **2000**.

[51] X. B. Wu, P. Chen, J. Lin and K. L. Tan, *Int. J. Hydrogen, Energy*, 25, 26, **2000**.

[52] H. Li, M. Eddaoudi, M. O'Keeffe and O. M. Yaghi, *Nature*, 402, 276, **1999**.

[53] A. G. Wong-Foy, A. J. Matzger, O. M. Yaghi, *J. Am. Chem. Soc.* 128, 3494, **2006**.

[54] B. Chen, N. W. Ockwig, A. R. Millward, D. S. Contreras, and O. M. Yaghi, *Angewandte Chemie International Edition*, 44, 4745, **2005**.

[55] B. Parnella, and M. Hirscher, *Advanced Materials*, 17, 538, **2005**.

[56] R. Gomer, *Critical Reviews in Solid State and Materials Sciences*, 1, 247, **1973**.

[57] G. J. Kubas, *Science*, 314, 1096, **2006**.

[58] B. L. Mojet, J. Eckert, R. A. van Santen, A. Albinati and R. E. Lechner, *J. Am. Chem. Soc.*, 123, 8147, **2001**.

[59] G. J. Kubas, *Metal Dihydrogen and δ-Bond Complexes. Structure, Theory, and Reactivity*; Kluwer: New York, **1999**.

[60] F. Maseras, A. Lledos, E. Clot, O. Eisenstein, *Chem. Rev.*, 100, 601, **2000**.

[61] E. A. Sow, *Dissertation*, University of Saarland (Saarbrücken), **2008**.

[62] M. Veith, S. Faber, H. Wofanger and V. Huch, *Chem. Ber*., 129, 381, **1996**.

[63] M. Veith, S. Kneip, *Jouranl of Material Sciences Letters*, 13, 335, **1994**.

[64] M. Veith, K. Andres, S. Faber, J. Blin, M. Zimmer, Y. Wolf, H. Schnöckel, R. Köppe, R. de Masi and S. Hüfner, *Eur. J. Inorg. Chem.*, 4387, **2003**.

[65] M. Veith, S. Faber, R. Hempelmann, S. Janssen, J. Prewo and H. Eckerlebe, *Journal of Materials Science*, 31, 2009, **1996**.

[66] M. Veith, E. Sow, U. Werner, C. Petersen and O. C. Aktas, *Eur. J. Inorg. Chem*, 5181, **2008**.

[67] J. Juan-Juan, M.C. Román-Martinez, M.J. Illán-Gómez, *Applied Catalysis A: General*, 264, 169, **2004**.

[68] J. Li, F. Li and K. Hu, *Journal of Materials Processing Technology*, 147, 236, **2004**.

[69] Y. Kim, P. Kim, C. Kim and J. Yi, *J. Mater. Chem.*, 13, 2353, **2003**.

[70] D. Vanoppen, M. Veith, K. Valtchev, US Patent, US 7, 026, 269 B2, **2003**.

[71] M. Veith, K. Altherr, N. Lecerf, S. Mathur, M. Valtchev and E. Fritscher, *NanoStructured Materials*, 12, 191, **1999**.

[72] S. Brunauer, P. H. Emmett, E. Teller, *J. Am. Chem. Soc*, 60, 309, **1938**.

[73] B. Panella, *Ph. D thesis*, Stuttgart University, **2005.**

[74] D. B. Mawhinney, J. A. Rossin, K. Gerhart and J. T. Yates Jr., *Langmuir*, 16, 2237, **2000**.

[75] O. C. Aktaş, *Ph. D thesis*, University of Saarland, **2009**.

[76] K. Iyakutti, Y. Kawazoe, M. Rajarajeswari and V. J. Surya, *Int. J. Hydrogen Energy*, 34, 370, **2009**.

[77] H. Ehwald and U. Leibnitz, *Catalysis*, 38, 149, **1996**.

[78] N. Gerard and S. Ono, *Hydrogen in Intermetallic Compounds II, Surface and Dynamic Properties, Applications* (*Springer Topics in Applied Physics* vol 64) ed. L Schlapbach (Berlin: Springer.), **1992**.

[79] L.O. Valøen, A. Zaluska, L. Zaluski, H. Tanaka, N. Kuriyama, J.O. Ström-Olsen, R. Tunold, *Journal of Alloys and Compounds*, 306, 235, **2000**.

[80] hydpark.ca.sandia.gov.

[81] H. Kohlmann, N. Kurtzemann, R. Weihrich, T. Hansen, *Z. Anorg. Allg. Chem., 635*, 2399, **2009**.

[82] H. Kohlmann, *J. Solid State Chem*. **2010**, in press.

Indices

Index I (Crystallographic Data)

Compound 1

Table 1. Atomic coordinates (x 10^4) and equivalent isotropic displacement parameters ($Å^2$x 10^3) for sh2840. U(eq) is defined as one third of the trace of the orthogonalized U^{ij} tensor.

	x	y	z	U(eq)
Al(1)	1356(1)	7500	987(1)	18(1)
Al(2)	3731(1)	6619(1)	1542(1)	17(1)
Al(3)	3639(1)	7500	-109(1)	16(1)
Al(4)	6233(1)	7500	2673(1)	21(1)
O(1)	3451(3)	7500	1248(2)	16(1)
O(2)	1813(2)	6716(1)	1586(1)	20(1)
O(3)	4204(2)	6676(1)	305(1)	19(1)
O(4)	1654(3)	7500	-308(2)	20(1)
O(5)	5083(2)	6810(1)	2703(1)	21(1)
C(1)	807(3)	6262(1)	1847(2)	24(1)
C(2)	435(3)	5744(2)	1057(2)	30(1)
C(3)	-590(4)	5263(2)	1345(2)	40(1)
C(4)	-2(4)	4981(2)	2377(2)	36(1)
C(5)	362(3)	5503(2)	3157(2)	32(1)
C(6)	1410(3)	5981(2)	2873(2)	28(1)
C(7)	4696(3)	6158(1)	-227(2)	20(1)
C(8)	6171(3)	6301(1)	-407(2)	27(1)
C(9)	6682(3)	5744(2)	-961(2)	30(1)
C(10)	5631(3)	5613(1)	-1943(2)	30(1)
C(11)	4149(3)	5475(2)	-1763(2)	31(1)
C(12)	3622(3)	6013(1)	-1186(2)	27(1)
C(13)	665(4)	7500	-1280(3)	23(1)
C(14)	-251(3)	6905(1)	-1414(2)	29(1)
C(15)	-1260(4)	6904(2)	-2456(2)	36(1)
C(16)	-2190(5)	7500	-2617(3)	38(1)
C(17)	5365(3)	6326(1)	3489(2)	22(1)
C(18)	6769(3)	5997(1)	3535(2)	26(1)
C(19)	6987(4)	5470(2)	4323(2)	34(1)
C(20)	6864(4)	5726(2)	5338(2)	42(1)
C(21)	5463(4)	6077(2)	5275(2)	43(1)
C(22)	5257(4)	6605(2)	4489(2)	32(1)

Table 2. Bond lengths [Å] and angles [°] for sh2840.

Al(1)-O(2)#1	1.8452(18)	Al(3)-Al(2)#1	2.9039(11)	C(8)-C(9)	1.529(4)
Al(1)-O(2)	1.8452(18)	Al(4)-O(5)	1.823(2)	C(9)-C(10)	1.516(4)
Al(1)-O(4)	1.855(3)	Al(4)-O(5)#1	1.823(2)	C(10)-C(11)	1.521(4)
Al(1)-O(1)	1.959(3)	O(1)-Al(2)#1	1.8955(9)	C(11)-C(12)	1.525(4)
Al(1)-Al(2)#1	2.8980(12)	O(2)-C(1)	1.454(3)	C(13)-C(14)	1.512(4)
Al(1)-Al(2)	2.8980(12)	O(3)-C(7)	1.443(3)	C(13)-C(14)#1	1.512(4)
Al(1)-Al(3)	2.9110(16)	O(4)-C(13)	1.454(4)	C(14)-C(15)	1.536(4)
Al(2)-O(3)	1.8498(19)	O(5)-C(17)	1.461(3)	C(15)-C(16)	1.521(4)
Al(2)-O(5)	1.859(2)	C(1)-C(6)	1.515(4)	C(16)-C(15)#1	1.521(4)
Al(2)-O(2)	1.863(2)	C(1)-C(2)	1.516(4)	C(17)-C(18)	1.501(4)
Al(2)-O(1)	1.8955(9)	C(2)-C(3)	1.520(4)	C(17)-C(22)	1.513(4)
Al(2)-Al(3)	2.9039(11)	C(3)-C(4)	1.520(4)	C(18)-C(19)	1.524(4)
Al(3)-O(4)	1.861(3)	C(4)-C(5)	1.515(5)	C(19)-C(20)	1.517(5)
Al(3)-O(3)#1	1.8612(18)	C(5)-C(6)	1.527(4)	C(20)-C(21)	1.516(5)
Al(3)-O(3)	1.8612(18)	C(7)-C(12)	1.510(4)	C(21)-C(22)	1.525(4)
Al(3)-O(1)	1.905(3)	C(7)-C(8)	1.517(4)		

O(2)#1-Al(1)-O(2)	125.77(1)	O(4)-Al(3)-O(3)#1	105.29(7)	Al(1)-O(4)-Al(3)	103.14(1)
O(2)#1-Al(1)-O(4)	110.71(7)	O(4)-Al(3)-O(3)	105.29(7)	C(17)-O(5)-Al(4)	123.58(16)
O(2)-Al(1)-O(4)	110.71(7)	O(3)#1-Al(3)-O(3)	136.33(1)	C(17)-O(5)-Al(2)	117.47(16)
O(2)#1-Al(1)-O(1)	77.62(7)	O(4)-Al(3)-O(1)	80.19(11)	Al(4)-O(5)-Al(2)	117.49(1)
O(2)-Al(1)-O(1)	77.62(7)	O(3)#1-Al(3)-O(1)	77.68(7)	O(2)-C(1)-C(6)	110.1(2)
O(4)-Al(1)-O(1)	78.92(1)	O(3)-Al(3)-O(1)	77.68(7)	O(2)-C(1)-C(2)	111.0(2)
O(2)#1-Al(1)-Al(2)#1	38.81(6)	O(4)-Al(3)-Al(2)#1	88.21(7)	C(6)-C(1)-C(2)	111.5(2)
O(2)-Al(1)-Al(2)# 1	110.77(7)	O(3)#1-Al(3)-Al(2)#1	38.37(6)	C(1)-C(2)-C(3)	110.7(3)
O(4)-Al(1)-Al(2)#1	88.49(7)	O(3)-Al(3)-Al(2)#1	113.32(7)	C(2)-C(3)-C(4)	111.8(3)
O(1)-Al(1)-Al(2)#1	40.43(2)	O(1)-Al(3)-Al(2)# 1	40.05(2)	C(5)-C(4)-C(3)	110.7(3)
O(2)#1-Al(1)-Al(2)	110.77(7)	O(4)-Al(3)-Al(2)	88.21(7)	C(4)-C(5)-C(6)	110.9(2)
O(2)-Al(1)-Al(2)	38.81(6)	O(3)#1-Al(3)-Al(2)	113.32(7)	C(1)-C(6)-C(5)	110.6(2)
O(4)-Al(1)-Al(2)	88.49(7)	O(3)-Al(3)-Al(2)	38.37(6)	O(3)-C(7)-C(12)	110.8(2)
O(1)-Al(1)-Al(2)	40.43(2)	O(1)-Al(3)-Al(2)	40.05(2)	O(3)-C(7)-C(8)	110.7(2)
Al(2)#1-Al(1)-Al(2)	79.12(4)	Al(2)#1-Al(3)-Al(2)	78.93(4)	C(12)-C(7)-C(8)	112.3(2)
O(2)#1-Al(1)-Al(3)	95.61(7)	O(4)-Al(3)-Al(1)	38.37(8)	C(7)-C(8)-C(9)	110.0(2)
O(2)-Al(1)-Al(3)	95.61(7)	O(3)#1-Al(3)-Al(1)	92.52(7)	C(10)-C(9)-C(8)	110.9(2)
O(4)-Al(1)-Al(3)	38.50(8)	O(3)-Al(3)-Al(1)	92.52(7)	C(9)-C(10)-C(11)	110.6(2)
O(1)-Al(1)-Al(3)	40.42(7)	O(1)-Al(3)-Al(1)	41.82(8)	C(10)-C(11)-C(12)	111.8(2)
Al(2)#1-Al(1)-Al(3)	59.99(3)	Al(2)#1-Al(3)-Al(1)	59.78(3)	C(7)-C(12)-C(11)	111.1(2)
Al(2)-Al(1)-Al(3)	59.99(3)	Al(2)-Al(3)-Al(1)	59.78(3)	O(4)-C(13)-C(14)	110.8(2)
O(3)-Al(2)-O(5)	120.27(9)	O(5)-Al(4)-O(5)# 1	104.89(13)	O(4)-C(13)-C(14)#1	110.8(2)
O(3)-Al(2)-O(2)	117.70(9)	Al(2)#1-O(1)-Al(2)	153.66(15)	C(14)-C(13)-C(14)#1	111.0(3)
O(5)-Al(2)-O(2)	117.04(9)	Al(2)#1-O(1)-Al(3)	99.65(8)	C(13)-C(14)-C(15)	110.1(3)
O(3)-Al(2)-O(1)	78.19(9)	Al(2)-O(1)-Al(3)	99.65(8)	C(16)-C(15)-C(14)	111.3(3)
O(5)-Al(2)-O(1)	90.66(1)	Al(2)#1-O(1)-Al(1)	97.48(8)	C(15)#1-C(16)-C(15)	110.3(4)
O(2)-Al(2)-O(1)	78.82(1)	Al(2)-O(1)-Al(1)	97.48(8)	O(5)-C(17)-C(18)	111.6(2)
O(3)-Al(2)-Al(1)	93.18(6)	Al(3)-O(1)-Al(1)	97.76(12)	O(5)-C(17)-C(22)	111.0(2)
O(5)-Al(2)-Al(1)	116.47(7)	C(1)-O(2)-Al(1)	125.98(17)	C(18)-C(17)-C(22)	112.2(2)
O(2)-Al(2)-Al(1)	38.38(6)	C(1)-O(2)-Al(2)	130.38(16)	C(17)-C(18)-C(19)	110.1(2)
O(1)-Al(2)-Al(1)	42.09(8)	Al(1)-O(2)-Al(2)	102.81(9)	C(20)-C(19)-C(18)	111.5(3)
O(3)-Al(2)-Al(3)	38.65(6)	C(7)-O(3)-Al(2)	125.92(15)	C(21)-C(20)-C(19)	111.5(3)
O(5)-Al(2)-Al(3)	115.14(7)	C(7)-O(3)-Al(3)	130.54(16)	C(20)-C(21)-C(22)	111.5(3)
O(2)-Al(2)-Al(3)	95.44(7)	Al(2)-O(3)-Al(3)	102.99(9)	C(17)-C(22)-C(21)	109.5(3)
O(1)-Al(2)-Al(3)	40.29(7)	C(13)-O(4)-Al(1)	131.9(2)		
Al(1)-Al(2)-Al(3)	60.23(3)	C(13)-O(4)-Al(3)	124.9(2)		

Symmetry transformations used to generate equivalent atoms: #1 x,-y+3/2,z

Table 3. Anisotropic displacement parameters ($Å^2$x 10^3) for sh2840. The anisotropic displacement factor exponent takes the form: $-2\pi^2[h^2 a^{*2} U^{11} + ... + 2 h k a^* b^* U^{12}]$

	U^{11}	U^{22}	U^{33}	U^{23}	U^{13}	U^{12}
Al(1)	19(1)	15(1)	20(1)	0	4(1)	0
Al(2)	19(1)	14(1)	17(1)	1(1)	4(1)	0(1)
Al(3)	21(1)	12(1)	16(1)	0	4(1)	0
Al(4)	19(1)	19(1)	25(1)	0	3(1)	0
O(1)	18(1)	14(1)	15(1)	0	2(1)	0
O(2)	21(1)	16(1)	26(1)	3(1)	7(1)	-2(1)
O(3)	26(1)	13(1)	19(1)	-1(1)	6(1)	3(1)
O(4)	20(1)	20(1)	16(1)	0	-1(1)	0
O(5)	22(1)	18(1)	20(1)	4(1)	0(1)	0(1)
C(1)	23(1)	18(1)	31(2)	6(1)	8(1)	-4(1)
C(2)	35(2)	28(2)	24(2)	6(1)	-1(1)	-11(1)
C(3)	41(2)	37(2)	38(2)	3(2)	-3(2)	-21(2)
C(4)	35(2)	28(2)	46(2)	11(2)	8(2)	-10(1)
C(5)	29(2)	37(2)	32(2)	13(1)	13(1)	-1(1)
C(6)	30(2)	31(2)	24(1)	3(1)	8(1)	-7(1)
C(7)	29(2)	13(1)	20(1)	-1(1)	8(1)	3(1)
C(8)	22(1)	26(2)	30(2)	-6(1)	3(1)	3(1)

C(9)	27(2)	30(2)	35(2)	-3(1)	12(1)	6(1)
C(10)	45(2)	21(2)	26(2)	-4(1)	13(1)	7(1)
C(11)	38(2)	22(2)	30(2)	-8(1)	1(1)	1(1)
C(12)	28(2)	21(2)	32(2)	-8(1)	3(1)	-1(1)
C(13)	20(2)	26(2)	18(2)	0	-4(2)	0
C(14)	33(2)	23(2)	25(2)	-2(1)	-4(1)	-3(1)
C(15)	38(2)	35(2)	29(2)	-5(1)	-4(1)	-7(2)
C(16)	29(2)	51(3)	28(2)	0	-9(2)	0
C(17)	24(1)	20(1)	19(1)	8(1)	0(1)	1(1)
C(18)	28(2)	23(2)	25(1)	2(1)	3(1)	4(1)
C(19)	37(2)	29(2)	35(2)	12(1)	3(1)	8(1)
C(20)	53(2)	40(2)	28(2)	13(2)	-1(2)	10(2)
C(21)	62(2)	44(2)	24(2)	12(2)	15(2)	11(2)
C(22)	42(2)	31(2)	25(2)	6(1)	10(1)	10(1)

Table 4. Hydrogen coordinates (x 10^4) and isotropic displacement parameters (Å^{2}x 10^3) for sh2840.

	x	y	z	U(eq)
H(1)	-260(50)	7500	860(30)	35(13)
H(2)	3920(30)	5906(16)	1670(20)	32(9)
H(3)	3980(40)	7500	-1150(30)	23(11)
H(5)	7410(50)	7500	3610(30)	37(13)
H(4)	6660(50)	7500	1650(30)	37(13)
H(1A)	-92	6496	1875	28
H(2A)	1320	5524	983	37
H(2B)	-11	5940	405	37
H(3A)	-767	4915	844	48
H(3B)	-1516	5474	1340	48
H(4A)	-722	4691	2557	44
H(4B)	867	4728	2365	44
H(5A)	792	5311	3815	38
H(5B)	-524	5728	3216	38
H(6A)	1599	6328	3376	33
H(6B)	2329	5765	2873	33
H(7)	4778	5770	208	24
H(8A)	6853	6369	242	32
H(8B)	6136	6695	-809	32
H(9A)	7632	5847	-1095	36
H(9B)	6786	5358	-536	36
H(10A)	5965	5242	-2278	36
H(10B)	5585	5987	-2390	36
H(11A)	4176	5072	-1381	37
H(11B)	3468	5418	-2415	37
H(12A)	3459	6401	-1608	33
H(12B)	2699	5889	-1028	33
H(13)	1241	7500	-1807	27
H(14A)	-820	6890	-892	34
H(14B)	369	6523	-1339	34
H(15A)	-688	6883	-2975	43
H(15B)	-1880	6522	-2525	43
H(16A)	-2786	7500	-3307	46
H(16B)	-2836	7500	-2144	46
H(17)	4598	5995	3312	26
H(18A)	7559	6310	3705	31
H(18B)	6785	5811	2873	31
H(19A)	6260	5133	4110	41
H(19B)	7944	5277	4379	41
H(20A)	6928	5367	5816	50
H(20B)	7672	6020	5593	50
H(21A)	5450	6265	5937	51

H(21B)	4660	5771	5105	51
H(22A)	4308	6806	4433	39
H(22B)	6000	6937	4692	39

Compound 2

Table 1. Atomic coordinates (x 10^4) and equivalent isotropic displacement parameters ($Å^2$x 10^3) for sh2860. U(eq) is defined as one third of the trace of the orthogonalized U^{ij} tensor.

	x	y	z	U(eq)
Al(1)	4229(1)	6091(1)	5043(1)	10(1)
Al(2)	5584(1)	8853(1)	5194(1)	13(1)
Al(3)	1464(1)	6113(1)	5402(1)	12(1)
O(1)	4024(1)	4172(1)	4188(1)	11(1)
O(2)	4785(1)	9369(1)	4036(1)	15(1)
O(3)	-475(1)	5606(1)	4439(1)	13(1)
C(1)	3149(1)	3219(1)	3064(1)	13(1)
C(2)	1455(1)	2792(1)	2982(1)	20(1)
C(3)	566(1)	1716(2)	1804(1)	30(1)
C(4)	916(2)	2363(2)	920(1)	33(1)
C(5)	2627(2)	2837(2)	1029(1)	31(1)
C(6)	3511(1)	3911(1)	2210(1)	24(1)
C(7)	4510(1)	8562(1)	2850(1)	15(1)
C(8)	2811(1)	7883(1)	2315(1)	23(1)
C(9)	2487(2)	7021(2)	1065(1)	29(1)
C(10)	3215(2)	7981(2)	466(1)	30(1)
C(11)	4925(2)	8647(2)	1013(1)	27(1)
C(12)	5237(1)	9541(1)	2260(1)	21(1)
C(13)	-1173(1)	6336(1)	3765(1)	14(1)
C(14)	-1504(1)	5424(1)	2534(1)	22(1)
C(15)	-2306(2)	6150(1)	1813(1)	26(1)
C(16)	-1345(1)	7729(1)	2066(1)	22(1)
C(17)	-954(1)	8639(1)	3310(1)	21(1)
C(18)	-190(1)	7905(1)	4042(1)	18(1)

Table 2. Bond lengths [Å] and angles [°] for sh2860.

Al(1)-O(1)	1.8394(7)	O(1)-Al(1)#1	1.8676(7)	C(7)-C(12)	1.5239(15)
Al(1)-O(1)#1	1.8676(7)	O(2)-C(7)	1.4507(12)	C(8)-C(9)	1.5272(16)
Al(1)-Al(2)	2.6797(4)	O(2)-Al(2)#2	1.8870(8)	C(9)-C(10)	1.520(2)
Al(1)-Al(3)	2.7020(4)	O(3)-C(13)	1.4493(11)	C(10)-C(11)	1.5263(19)
Al(1)-Al(1)#1	2.8381(5)	O(3)-Al(3)#3	1.8373(7)	C(11)-C(12)	1.5316(16)
Al(2)-O(2)	1.8191(7)	C(1)-C(6)	1.5143(15)	C(13)-C(14)	1.5158(15)
Al(2)-O(2)#2	1.8870(8)	C(1)-C(2)	1.5165(13)	C(13)-C(18)	1.5166(14)
Al(2)-Al(2)#2	2.8659(6)	C(2)-C(3)	1.5306(15)	C(14)-C(15)	1.5336(16)
Al(3)-O(3)#3	1.8373(7)	C(3)-C(4)	1.521(2)	C(15)-C(16)	1.5237(17)
Al(3)-O(3)	1.8711(7)	C(4)-C(5)	1.527(2)	C(16)-C(17)	1.5243(16)
Al(3)-Al(3)#3	2.8864(6)	C(5)-C(6)	1.5313(17)	C(17)-C(18)	1.5325(15)
O(1)-C(1)	1.4469(11)	C(7)-C(8)	1.5163(14)		

O(1)-Al(1)-O(1)#1	80.08(3)	O(2)-Al(2)-O(2)#2	78.71(4)	O(3)-Al(3)-Al(3)#3	38.47(2)
O(1)-Al(1)-Al(2)	139.36(3)	O(2)-Al(2)-Al(1)	114.77(3)	Al(1)-Al(3)-Al(3)#3	32.872(1)
O(1)#1-Al(1)-Al(2)	95.38(2)	O(2)#2-Al(2)-Al(1)	128.84(3)	C(1)-O(1)-Al(1)	133.45(6)
O(1)-Al(1)-Al(3)	106.06(2)	O(2)-Al(2)-Al(2)#2	40.22(2)	C(1)-O(1)-Al(1)#1	123.94(5)
O(1)#1-Al(1)-Al(3)	134.62(3)	O(2)#2-Al(2)-Al(2)#2	38.50(2)	Al(1)-O(1)-Al(1)#1	99.92(3)
Al(2)-Al(1)-Al(3)	105.441(1)	Al(1)-Al(2)-Al(2)#2	132.755(1)	C(7)-O(2)-Al(2)	127.18(6)
O(1)-Al(1)-Al(1)#1	40.40(2)	O(3)#3-Al(3)-O(3)	77.79(3)	C(7)-O(2)-Al(2)#2	131.53(6)
O(1)#1-Al(1)-Al(1)#1	39.67(2)	O(3)#3-Al(3)-Al(1)	112.04(2)	Al(2)-O(2)-Al(2)#2	101.29(4)
Al(2)-Al(1)-Al(1)#1	23.608(1)	O(3)-Al(3)-Al(1)	132.92(3)	C(13)-O(3)-Al(3)#3	124.93(6)
Al(3)-Al(1)-Al(1)#1	129.906(1)	O(3)#3-Al(3)-Al(3)#3	39.31(2)	C(13)-O(3)-Al(3)	132.74(6)

Al(3)#3-O(3)-Al(3)	102.21(3)	O(2)-C(7)-C(8)	109.98(8)	O(3)-C(13)-C(18)	111.50(8)
O(1)-C(1)-C(6)	111.43(8)	O(2)-C(7)-C(12)	111.70(8)	C(14)-C(13)-C(18)	111.77(9)
O(1)-C(1)-C(2)	111.23(8)	C(8)-C(7)-C(12)	111.15(9)	C(13)-C(14)-C(15)	110.16(9)
C(6)-C(1)-C(2)	111.78(9)	C(7)-C(8)-C(9)	111.14(9)	C(16)-C(15)-C(14)	110.76(9)
C(1)-C(2)-C(3)	110.10(9)	C(10)-C(9)-C(8)	111.54(1)	C(15)-C(16)-C(17)	111.16(9)
C(4)-C(3)-C(2)	111.20(1)	C(9)-C(10)-C(11)	110.25(1)	C(16)-C(17)-C(18)	112.21(9)
C(3)-C(4)-C(5)	111.36(1)	C(10)-C(11)-C(12)	111.05(1)	C(13)-C(18)-C(17)	110.12(8)
C(4)-C(5)-C(6)	111.37(1)	C(7)-C(12)-C(11)	109.99(9)		
C(1)-C(6)-C(5)	109.84(1)	O(3)-C(13)-C(14)	109.65(8)		

Symmetry transformations used to generate equivalent atoms: #1 -x+1,-y+1,-z+1 #2 -x+1,-y+2,-z+1 #3 -x,-y+1,-z+1

Table 3. Anisotropic displacement parameters ($Å^2 x\ 10^3$) for sh2860. The anisotropic displacement factor exponent takes the form: $-2\pi^2[\ h^2\ a^{*2}U^{11} + ... + 2\ h\ k\ a^*\ b^*\ U^{12}\ ]$

	U^{11}	U^{22}	U^{33}	U^{23}	U^{13}	U^{12}
Al(1)	10(1)	9(1)	13(1)	5(1)	3(1)	3(1)
Al(2)	14(1)	11(1)	14(1)	6(1)	3(1)	3(1)
Al(3)	10(1)	12(1)	13(1)	4(1)	3(1)	2(1)
O(1)	11(1)	10(1)	11(1)	3(1)	0(1)	3(1)
O(2)	22(1)	12(1)	11(1)	4(1)	3(1)	6(1)
O(3)	12(1)	14(1)	15(1)	8(1)	2(1)	3(1)
C(1)	14(1)	12(1)	12(1)	3(1)	1(1)	4(1)
C(2)	14(1)	22(1)	17(1)	3(1)	1(1)	1(1)
C(3)	21(1)	29(1)	23(1)	-1(1)	-4(1)	0(1)
C(4)	37(1)	36(1)	16(1)	1(1)	-7(1)	13(1)
C(5)	42(1)	36(1)	13(1)	7(1)	5(1)	10(1)
C(6)	28(1)	27(1)	15(1)	10(1)	5(1)	3(1)
C(7)	19(1)	14(1)	11(1)	3(1)	3(1)	5(1)
C(8)	20(1)	25(1)	18(1)	4(1)	3(1)	3(1)
C(9)	29(1)	30(1)	18(1)	2(1)	-2(1)	4(1)
C(10)	41(1)	32(1)	15(1)	7(1)	1(1)	15(1)
C(11)	37(1)	31(1)	18(1)	11(1)	12(1)	12(1)
C(12)	26(1)	20(1)	17(1)	8(1)	7(1)	5(1)
C(13)	15(1)	14(1)	15(1)	7(1)	2(1)	5(1)
C(14)	32(1)	16(1)	15(1)	5(1)	1(1)	7(1)
C(15)	34(1)	22(1)	17(1)	8(1)	-4(1)	5(1)
C(16)	25(1)	24(1)	20(1)	12(1)	5(1)	8(1)
C(17)	28(1)	16(1)	20(1)	9(1)	3(1)	7(1)
C(18)	20(1)	15(1)	18(1)	7(1)	2(1)	3(1)

Table 4. Hydrogen coordinates ($x\ 10^4$) and isotropic displacement parameters ($Å^2 x\ 10^3$) for sh2860.

	x	y	z	U(eq)
H(1)	5085(16)	6980(16)	4295(12)	22(3)
H(2)	4645(16)	7952(16)	5870(12)	20(3)
H(3)	7288(17)	9126(17)	5576(13)	28(4)
H(4)	2429(16)	6231(16)	4439(12)	20(3)
H(5)	3198(15)	5797(15)	5918(11)	18(3)
H(6)	1686(17)	7561(18)	6309(13)	29(4)
H(7)	3467(15)	2289(15)	2891(11)	17(3)
H(8)	1267(17)	2382(17)	3542(13)	27(4)
H(9)	1107(17)	3686(17)	3141(12)	25(4)
H(10)	887(19)	840(19)	1666(14)	36(4)
H(11)	-500(20)	1510(20)	1773(16)	46(5)
H(12)	530(20)	3210(20)	1017(15)	44(5)
H(13)	420(20)	1640(20)	200(15)	42(5)
H(14)	2984(19)	1911(19)	854(14)	36(4)
H(15)	2840(20)	3290(20)	489(16)	44(5)

H(16)	3232(18)	4818(18)	2359(13)	27(4)
H(17)	4601(19)	4227(19)	2312(14)	35(4)
H(18)	5008(15)	7741(15)	2790(11)	17(3)
H(19)	2339(18)	8718(18)	2424(13)	31(4)
H(20)	2371(18)	7257(18)	2717(13)	31(4)
H(21)	1360(20)	6590(20)	725(16)	48(5)
H(22)	2922(19)	6170(19)	959(14)	37(4)
H(23)	3050(20)	7440(20)	-280(16)	42(5)
H(24)	2760(20)	8820(20)	529(15)	39(4)
H(25)	5449(19)	7832(19)	919(14)	38(4)
H(26)	5395(19)	9340(20)	715(14)	37(4)
H(27)	6370(19)	10003(18)	2621(14)	34(4)
H(28)	4763(17)	10356(17)	2321(13)	27(4)
H(29)	-2163(16)	6370(15)	3949(11)	18(3)
H(30)	-2131(18)	4426(18)	2387(13)	31(4)
H(31)	-569(17)	5350(16)	2380(12)	24(4)
H(32)	-3340(20)	6190(20)	1992(15)	41(5)
H(33)	-2550(20)	5578(19)	1016(15)	39(4)
H(34)	-396(18)	7695(18)	1838(13)	30(4)
H(35)	-1888(18)	8197(17)	1652(13)	29(4)
H(36)	-1902(16)	8692(15)	3497(11)	16(3)
H(37)	-298(19)	9628(19)	3465(14)	34(4)
H(38)	799(18)	7910(17)	3935(13)	27(4)
H(39)	12(16)	8462(16)	4817(13)	21(3)

Compound 4

Table 2. Atomic coordinates (x 10^4) and equivalent isotropic displacement parameters ($Å^2$x 10^3) for sh3055. U(eq) is defined as one third of the trace of the orthogonalized U^{ij} tensor.

	x	y	z	U(eq)
Al(1)	6667	3333	833	42(1)
Al(2)	8082(1)	3333	833	49(1)
O(1)	6107(1)	2400(1)	591(1)	45(1)
O(2)	8202(2)	2705(2)	595(1)	64(1)
C(1)	6303(2)	2065(2)	315(1)	52(1)
C(2)	5932(3)	2106(3)	1(1)	70(1)
C(3)	6145(3)	1759(3)	-288(1)	87(2)
C(4)	5938(3)	954(3)	-212(1)	83(2)
C(5)	6306(3)	915(3)	103(1)	76(1)
C(6)	6085(3)	1256(2)	394(1)	60(1)
C(7)	8729(3)	2479(2)	551(1)	67(1)
C(8)	9227(4)	2851(3)	262(2)	137(3)
C(9)	9794(5)	2587(4)	197(2)	186(4)
C(10)	9421(4)	1746(3)	157(2)	119(2)
C(11)	8928(3)	1359(3)	461(1)	95(2)
C(12)	8364(3)	1626(3)	528(1)	93(2)

Table 3. Bond lengths [Å] and angles [°] for sh3055.

Al(1)-O(1)	1.919(2)	Al(2)-O(2)	1.711(3)	C(2)-C(3)	1.535(6)
Al(1)-O(1)#1	1.919(2)	Al(2)-O(2)#1	1.711(3)	C(3)-C(4)	1.503(7)
Al(1)-O(1)#2	1.919(2)	Al(2)-O(1)#5	1.797(3)	C(4)-C(5)	1.499(6)
Al(1)-O(1)#3	1.919(2)	Al(2)-O(1)#3	1.798(3)	C(5)-C(6)	1.540(5)
Al(1)-O(1)#4	1.919(2)	O(1)-C(1)	1.464(4)	C(7)-C(8)	1.480(6)
Al(1)-O(1)#5	1.919(2)	O(1)-Al(2)#4	1.798(3)	C(7)-C(12)	1.509(6)
Al(1)-Al(2)#4	2.8728(16)	O(2)-C(7)	1.369(5)	C(8)-C(9)	1.517(8)
Al(1)-Al(2)	2.8728(16)	C(1)-C(2)	1.498(5)	C(9)-C(10)	1.491(8)
Al(1)-Al(2)#3	2.8728(16)	C(1)-C(6)	1.506(5)	C(10)-C(11)	1.529(7)

C(11)-C(12) 1.516(7)

O(1)-Al(1)-O(1)#1	168.71(14)	O(1)#1-Al(1)-Al(2)	95.64(7)	O(1)#5-Al(2)-Al(1)	40.95(8)
O(1)-Al(1)-O(1)#2	75.73(13)	O(1)#2-Al(1)-Al(2)	133.71(7)	O(1)#3-Al(2)-Al(1)	40.95(8)
O(1)#1-Al(1)-O(1)#2	96.35(9)	O(1)#3-Al(1)-Al(2)	37.87(7)	C(1)-O(1)-Al(2)#4	125.1(2)
O(1)-Al(1)-O(1)#3	96.34(9)	O(1)#4-Al(1)-Al(2)	133.71(7)	C(1)-O(1)-Al(1)	133.2(2)
O(1)#1-Al(1)-O(1)#3	92.57(14)	O(1)#5-Al(1)-Al(2)	37.87(7)	Al(2)#4-O(1)-Al(1)	101.18(11)
O(1)#2-Al(1)-O(1)#3	168.71(14)	Al(2)#4-Al(1)-Al(2)	120.0	C(7)-O(2)-Al(2)	138.5(3)
O(1)-Al(1)-O(1)#4	96.34(9)	O(1)-Al(1)-Al(2)#3	133.72(7)	O(1)-C(1)-C(2)	111.1(3)
O(1)#1-Al(1)-O(1)#4	75.74(13)	O(1)#1-Al(1)-Al(2)#3	37.87(7)	O(1)-C(1)-C(6)	110.2(3)
O(1)#2-Al(1)-O(1)#4	92.58(14)	O(1)#2-Al(1)-Al(2)#3	95.65(7)	C(2)-C(1)-C(6)	111.0(3)
O(1)#3-Al(1)-O(1)#4	96.34(9)	O(1)#3-Al(1)-Al(2)#3	95.65(7)	C(1)-C(2)-C(3)	110.8(4)
O(1)-Al(1)-O(1)#5	92.57(14)	O(1)#4-Al(1)-Al(2)#3	37.87(7)	C(4)-C(3)-C(2)	110.7(4)
O(1)#1-Al(1)-O(1)#5	96.34(9)	O(1)#5-Al(1)-Al(2)#3	133.71(7)	C(5)-C(4)-C(3)	110.8(4)
O(1)#2-Al(1)-O(1)#5	96.34(9)	Al(2)#4-Al(1)-Al(2)#3	120.0	C(4)-C(5)-C(6)	111.1(4)
O(1)#3-Al(1)-O(1)#5	75.73(13)	Al(2)-Al(1)-Al(2)#3	120.0	C(1)-C(6)-C(5)	109.7(4)
O(1)#4-Al(1)-O(1)#5	168.71(14)	O(2)-Al(2)-O(2)#1	117.9(2)	O(2)-C(7)-C(8)	112.3(4)
O(1)-Al(1)-Al(2)#4	37.87(7)	O(2)-Al(2)-O(1)#5	117.37(12)	O(2)-C(7)-C(12)	112.1(4)
O(1)#1-Al(1)-Al(2)#4	133.71(7)	O(2)#1-Al(2)-O(1)#5	108.59(12)	C(8)-C(7)-C(12)	110.8(4)
O(1)#2-Al(1)-Al(2)#4	37.86(7)	O(2)-Al(2)-O(1)#3	108.59(12)	C(7)-C(8)-C(9)	113.7(5)
O(1)#3-Al(1)-Al(2)#4	133.72(7)	O(2)#1-Al(2)-O(1)#3	117.37(12)	C(10)-C(9)-C(8)	112.6(6)
O(1)#4-Al(1)-Al(2)#4	95.65(7)	O(1)#5-Al(2)-O(1)#3	81.90(16)	C(9)-C(10)-C(11)	109.2(5)
O(1)#5-Al(1)-Al(2)#4	95.65(7)	O(2)-Al(2)-Al(1)	121.02(11)	C(12)-C(11)-C(10)	112.1(5)
O(1)-Al(1)-Al(2)	95.65(7)	O(2)#1-Al(2)-Al(1)	121.03(11)	C(7)-C(12)-C(11)	113.4(4)

Symmetry transformations used to generate equivalent atoms: #1 x-y+1/3,-y+2/3,-z+1/6 #2 y+1/3,x-1/3,-z+1/6 #3 -y+1,x-y,z #4 -x+y+1,-x+1,z #5 -x+4/3,-x+y+2/3,-z+1/6 #6 y-2/3,x+2/3,-z+1/6 #7 -x,-y,-z

Table 4. Anisotropic displacement parameters ($Å^2 x\ 10^3$) for sh3055. The anisotropic displacement factor exponent takes the form: $-2\pi^2[\ h^2\ a^{*2}U^{11} + ... + 2\ h\ k\ a^*\ b^*\ U^{12}\ ]$

	U^{11}	U^{22}	U^{33}	U^{23}	U^{13}	U^{12}
Al(1)	48(1)	48(1)	32(1)	0	0	24(1)
Al(2)	50(1)	54(1)	45(1)	11(1)	5(1)	27(1)
O(1)	51(2)	51(2)	36(1)	-4(1)	3(1)	27(1)
O(2)	72(2)	67(2)	65(2)	4(2)	12(2)	44(2)
C(1)	56(2)	58(3)	42(2)	-11(2)	7(2)	29(2)
C(2)	100(4)	77(3)	41(2)	-7(2)	-5(2)	51(3)
C(3)	132(5)	92(4)	45(3)	-13(3)	4(3)	62(4)
C(4)	112(4)	87(4)	57(3)	-27(3)	2(3)	54(3)
C(5)	93(4)	84(3)	66(3)	-19(3)	-3(3)	56(3)
C(6)	77(3)	66(3)	49(2)	-12(2)	-5(2)	45(3)
C(7)	74(3)	67(3)	63(3)	-1(2)	4(2)	38(3)
C(8)	158(6)	85(4)	192(7)	61(4)	118(5)	79(4)
C(9)	175(7)	89(5)	317(11)	75(6)	171(7)	85(5)
C(10)	173(6)	113(5)	119(5)	30(4)	61(5)	108(5)
C(11)	116(5)	77(4)	111(4)	8(3)	21(4)	63(4)
C(12)	95(4)	68(4)	120(5)	8(3)	19(3)	43(3)

Compound 5

Table 1. Atomic coordinates ($x\ 10^4$) and equivalent isotropic displacement parameters ($Å^2 x\ 10^3$) for sh2888. U(eq) is defined as one third of the trace of the orthogonalized U^{ij} tensor.

	x	y	z	U(eq)

Al(1)	344(1)	1020(1)	4377(1)	27(1)
O(1)	119(1)	1021(1)	5513(1)	22(1)
C(1)	-60(1)	2391(1)	6060(1)	25(1)
C(2)	746(1)	3644(1)	5823(1)	32(1)
C(3)	1864(1)	3162(1)	6020(1)	35(1)
C(4)	1982(1)	2714(2)	6941(1)	37(1)
C(5)	1219(1)	1402(1)	7173(1)	32(1)
C(6)	98(1)	1857(1)	6966(1)	29(1)
C(7)	-1172(1)	2961(2)	5913(1)	42(1)

Table 2. Bond lengths [Å] and angles [°] for sh2888.

Al(1)-O(1)#1	1.8314(7)	O(1)-Al(1)#1	1.8314(7)	C(2)-C(3)	1.5192(17)
Al(1)-O(1)	1.8348(6)	C(1)-C(7)	1.5207(15)	C(3)-C(4)	1.5260(14)
Al(1)-Al(1)#1	2.7742(5)	C(1)-C(2)	1.5252(15)	C(4)-C(5)	1.5226(16)
O(1)-C(1)	1.4685(10)	C(1)-C(6)	1.5279(12)	C(5)-C(6)	1.5208(15)

O(1)#1-Al(1)-O(1)	81.65(3)	O(1)-C(1)-C(7)	107.66(8)	C(3)-C(2)-C(1)	113.49(8)
O(1)#1-Al(1)-Al(1)#1	40.87(2)	O(1)-C(1)-C(2)	107.17(8)	C(2)-C(3)-C(4)	110.98(9)
O(1)-Al(1)-Al(1)#1	40.78(2)	C(7)-C(1)-C(2)	111.99(9)	C(5)-C(4)-C(3)	110.59(8)
C(1)-O(1)-Al(1)#1	129.42(6)	O(1)-C(1)-C(6)	108.01(7)	C(6)-C(5)-C(4)	111.58(9)
C(1)-O(1)-Al(1)	127.74(5)	C(7)-C(1)-C(6)	111.26(9)	C(5)-C(6)-C(1)	113.84(8)
Al(1)#1-O(1)-Al(1)	98.35(3)	C(2)-C(1)-C(6)	110.53(8)		

Symmetry transformations used to generate equivalent atoms: #1 -x,-y,-z+1

Table 3. Anisotropic displacement parameters ($Å^2 x\ 10^3$) for sh2888. The anisotropic displacement factor exponent takes the form: $-2\pi^2[\ h^2\ a^{*2}U^{11} + ...\ + 2\ h\ k\ a^*\ b^*\ U^{12}\ ]$

	U^{11}	U^{22}	U^{33}	U^{23}	U^{13}	U^{12}
Al(1)	38(1)	24(1)	19(1)	0(1)	4(1)	-9(1)
O(1)	29(1)	19(1)	18(1)	-3(1)	2(1)	-2(1)
C(1)	30(1)	22(1)	23(1)	-7(1)	-2(1)	4(1)
C(2)	48(1)	20(1)	29(1)	-1(1)	-8(1)	-3(1)
C(3)	37(1)	37(1)	31(1)	0(1)	-3(1)	-13(1)
C(4)	36(1)	42(1)	32(1)	-2(1)	-9(1)	-4(1)
C(5)	41(1)	33(1)	23(1)	2(1)	-6(1)	2(1)
C(6)	35(1)	32(1)	20(1)	-6(1)	3(1)	-1(1)
C(7)	36(1)	45(1)	45(1)	-15(1)	-8(1)	15(1)

Table 4. Hydrogen coordinates (x 10^4) and isotropic displacement parameters ($Å^2 x\ 10^{\ 3}$) for sh2888.

	x	y	z	U(eq)
H(1)	1501(11)	1063(16)	4072(8)	37(3)
H(2)	-391(11)	2068(18)	3939(9)	43(4)
H(3)	573(12)	4610(20)	6121(9)	48(4)
H(4)	646(11)	3905(15)	5237(9)	36(3)
H(5)	2323(13)	4023(17)	5883(9)	46(4)
H(6)	2076(10)	2268(17)	5688(8)	37(3)
H(7)	2680(12)	2393(17)	7054(9)	47(4)
H(8)	1827(11)	3668(17)	7282(9)	42(4)
H(9)	1257(11)	1158(16)	7777(9)	41(4)
H(10)	1416(10)	450(15)	6868(8)	34(3)
H(11)	-397(9)	996(15)	7089(8)	28(3)
H(12)	-135(11)	2754(17)	7327(9)	40(4)
H(13)	-1279(14)	3890(20)	6263(12)	68(5)
H(14)	-1647(13)	2079(19)	6079(9)	52(4)
H(15)	-1252(12)	3243(18)	5335(10)	50(4)

Compound 7

Table 1. Atomic coordinates (x 10^4) and equivalent isotropic displacement parameters ($Å^2$x 10^3) for sh2887. U(eq) is defined as one third of the trace of the orthogonalized U^{ij} tensor.

	x	y	z	U(eq)
Al(1)	5987(1)	5813(1)	3679(1)	15(1)
O(1)	5633(1)	4061(1)	4768(1)	16(1)
O(2)	7492(1)	6585(1)	3344(1)	21(1)
O(3)	5626(1)	6099(1)	2272(1)	23(1)
C(1)	6436(1)	2909(1)	4526(1)	17(1)
C(2)	7177(2)	2504(2)	5500(2)	22(1)
C(3)	8197(2)	1431(2)	5170(2)	28(1)
C(4)	9281(2)	1854(2)	3594(2)	32(1)
C(5)	8555(2)	2252(2)	2610(2)	31(1)
C(6)	7531(2)	3318(2)	2952(2)	24(1)
C(7)	8393(2)	6788(1)	3925(1)	20(1)
C(8)	9763(2)	6119(2)	3311(2)	24(1)
C(9)	10578(2)	6694(2)	1682(2)	29(1)
C(10)	10930(2)	8174(2)	1221(2)	33(1)
C(11)	9590(2)	8882(2)	1803(2)	29(1)
C(12)	8759(2)	8280(2)	3430(2)	24(1)
C(13)	6020(2)	6723(1)	791(1)	18(1)
C(14)	4704(2)	6580(1)	582(2)	20(1)
C(15)	4872(2)	7340(2)	-931(2)	27(1)
C(16)	5292(2)	8790(2)	-1341(2)	31(1)
C(17)	6604(2)	8978(2)	-1164(2)	32(1)
C(18)	6420(2)	8196(2)	358(2)	27(1)
C(19)	5378(2)	1810(2)	4882(2)	29(1)
C(20)	7673(2)	6226(2)	5564(2)	28(1)
C(21)	7251(2)	6043(2)	-66(2)	30(1)

Table 2. Bond lengths [Å] and angles [°] for sh2887.

Al(1)-O(3)	1.6760(10)	C(1)-C(6)	1.5228(19)	C(9)-C(10)	1.524(2)
Al(1)-O(2)	1.6838(10)	C(1)-C(2)	1.523(2)	C(10)-C(11)	1.522(2)
Al(1)-O(1)	1.8305(10)	C(2)-C(3)	1.527(2)	C(11)-C(12)	1.522(2)
Al(1)-O(1)#1	1.8323(10)	C(3)-C(4)	1.520(2)	C(13)-C(21)	1.519(2)
Al(1)-Al(1)#1	2.7740(8)	C(4)-C(5)	1.520(2)	C(13)-C(14)	1.528(2)
O(1)-C(1)	1.4684(16)	C(5)-C(6)	1.527(2)	C(13)-C(18)	1.5309(19)
O(1)-Al(1)#1	1.8323(10)	C(7)-C(20)	1.523(2)	C(14)-C(15)	1.525(2)
O(2)-C(7)	1.4195(16)	C(7)-C(8)	1.527(2)	C(15)-C(16)	1.517(2)
O(3)-C(13)	1.4104(15)	C(7)-C(12)	1.534(2)	C(16)-C(17)	1.516(2)
C(1)-C(19)	1.5219(19)	C(8)-C(9)	1.519(2)	C(17)-C(18)	1.532(2)
O(3)-Al(1)-O(2)	116.21(5)	O(1)-C(1)-C(19)	107.35(1)	C(20)-C(7)-C(12)	110.45(1)
O(3)-Al(1)-O(1)	111.16(5)	O(1)-C(1)-C(6)	107.57(1)	C(8)-C(7)-C(12)	108.64(1)
O(2)-Al(1)-O(1)	117.16(5)	C(19)-C(1)-C(6)	111.66(1)	C(9)-C(8)-C(7)	112.84(1)
O(3)-Al(1)-O(1)#1	108.88(5)	O(1)-C(1)-C(2)	108.88(1)	C(8)-C(9)-C(10)	110.64(1)
O(2)-Al(1)-O(1)#1	116.92(5)	C(19)-C(1)-C(2)	111.13(1)	C(11)-C(10)-C(9)	110.93(1)
O(1)-Al(1)-O(1)#1	81.54(5)	C(6)-C(1)-C(2)	110.11(1)	C(12)-C(11)-C(10)	111.32(1)
O(3)-Al(1)-Al(1)#1	116.87(4)	C(1)-C(2)-C(3)	112.15(1)	C(11)-C(12)-C(7)	113.01(1)
O(2)-Al(1)-Al(1)#1	126.89(4)	C(4)-C(3)-C(2)	111.40(1)	O(3)-C(13)-C(21)	108.83(1)
O(1)-Al(1)-Al(1)#1	40.79(3)	C(5)-C(4)-C(3)	111.12(1)	O(3)-C(13)-C(14)	106.14(1)
O(1)#1-Al(1)-Al(1)#1	40.75(3)	C(4)-C(5)-C(6)	111.24(1)	C(21)-C(13)-C(14)	111.64(1)
C(1)-O(1)-Al(1)	131.29(7)	C(1)-C(6)-C(5)	112.48(1)	O(3)-C(13)-C(18)	110.32(1)
C(1)-O(1)-Al(1)#1	130.16(7)	O(2)-C(7)-C(20)	110.98(1)	C(21)-C(13)-C(18)	111.13(1)
Al(1)-O(1)-Al(1)#1	98.46(5)	O(2)-C(7)-C(8)	108.36(1)	C(14)-C(13)-C(18)	108.66(1)
C(7)-O(2)-Al(1)	146.16(8)	C(20)-C(7)-C(8)	110.26(1)	C(15)-C(14)-C(13)	113.78(1)
C(13)-O(3)-Al(1)	149.08(9)	O(2)-C(7)-C(12)	108.08(1)	C(16)-C(15)-C(14)	110.79(1)

C(17)-C(16)-C(15) 111.79(1) C(16)-C(17)-C(18) 111.51(1) C(13)-C(18)-C(17) 112.86(1)

Symmetry transformations used to generate equivalent atoms: #1 -x+1,-y+1,-z+1

Table 3. Anisotropic displacement parameters ($Å^2$x 10^3) for sh2887. The anisotropic displacement factor exponent takes the form: $-2\pi^2[h^2 a^{*2}U^{11} + ... + 2 h k a^* b^* U^{12}]$

	U^{11}	U^{22}	U^{33}	U^{23}	U^{13}	U^{12}
Al(1)	15(1)	16(1)	13(1)	-4(1)	-6(1)	1(1)
O(1)	17(1)	14(1)	16(1)	-5(1)	-6(1)	3(1)
O(2)	18(1)	25(1)	21(1)	-6(1)	-9(1)	-3(1)
O(3)	26(1)	28(1)	15(1)	-2(1)	-11(1)	-2(1)
C(1)	18(1)	13(1)	19(1)	-6(1)	-7(1)	4(1)
C(2)	23(1)	24(1)	20(1)	-7(1)	-12(1)	6(1)
C(3)	26(1)	28(1)	31(1)	-8(1)	-16(1)	9(1)
C(4)	21(1)	28(1)	38(1)	-12(1)	-6(1)	7(1)
C(5)	35(1)	27(1)	23(1)	-11(1)	-4(1)	9(1)
C(6)	29(1)	22(1)	17(1)	-6(1)	-8(1)	7(1)
C(7)	19(1)	22(1)	21(1)	-8(1)	-10(1)	1(1)
C(8)	21(1)	23(1)	32(1)	-10(1)	-14(1)	4(1)
C(9)	21(1)	32(1)	31(1)	-15(1)	-6(1)	2(1)
C(10)	22(1)	33(1)	33(1)	-7(1)	-4(1)	-5(1)
C(11)	27(1)	21(1)	35(1)	-5(1)	-11(1)	-2(1)
C(12)	22(1)	22(1)	31(1)	-12(1)	-12(1)	3(1)
C(13)	21(1)	19(1)	13(1)	-3(1)	-8(1)	0(1)
C(14)	25(1)	19(1)	18(1)	-5(1)	-12(1)	0(1)
C(15)	35(1)	28(1)	22(1)	-6(1)	-17(1)	3(1)
C(16)	40(1)	25(1)	24(1)	1(1)	-17(1)	3(1)
C(17)	39(1)	22(1)	25(1)	1(1)	-11(1)	-7(1)
C(18)	31(1)	23(1)	26(1)	-4(1)	-14(1)	-6(1)
C(19)	24(1)	20(1)	45(1)	-12(1)	-14(1)	2(1)
C(20)	28(1)	33(1)	24(1)	-10(1)	-13(1)	4(1)
C(21)	27(1)	33(1)	22(1)	-6(1)	-8(1)	7(1)

Table 4. Hydrogen coordinates (x 10^4) and isotropic displacement parameters ($Å^2$x 10^3) for sh2887.

	x	y	z	U(eq)
H(1)	7710(17)	3274(16)	5348(16)	26(4)
H(2)	6464(17)	2242(15)	6516(18)	31(4)
H(3)	8657(19)	1238(16)	5796(18)	36(5)
H(4)	7650(17)	584(16)	5445(16)	28(4)
H(5)	9880(20)	1139(19)	3402(19)	47(5)
H(6)	9906(18)	2603(17)	3388(17)	35(5)
H(7)	8020(18)	1481(17)	2716(17)	34(5)
H(8)	9250(20)	2604(18)	1590(20)	48(5)
H(9)	7048(17)	3520(16)	2363(17)	29(4)
H(10)	8085(16)	4105(15)	2730(16)	25(4)
H(11)	9535(17)	5117(16)	3661(17)	31(4)
H(12)	10358(18)	6214(15)	3735(17)	30(4)
H(13)	10028(18)	6546(16)	1228(17)	31(5)
H(14)	11450(20)	6250(17)	1343(18)	39(5)
H(15)	11442(18)	8533(16)	186(19)	37(5)
H(16)	11572(19)	8308(16)	1607(18)	35(5)
H(17)	9866(17)	9825(16)	1544(17)	32(4)
H(18)	8999(19)	8794(17)	1329(18)	40(5)
H(19)	7871(17)	8733(14)	3783(16)	22(4)
H(20)	9322(18)	8420(16)	3905(18)	34(5)
H(21)	4456(17)	5603(16)	854(16)	27(4)
H(22)	3908(17)	6939(15)	1269(17)	27(4)
H(23)	5639(18)	6967(15)	-1633(17)	28(4)
H(24)	3970(19)	7261(16)	-999(17)	33(5)

H(25)	5440(19)	9235(17)	-2310(20)	42(5)
H(26)	4484(19)	9188(16)	-727(18)	34(5)
H(27)	7437(19)	8676(16)	-1867(18)	37(5)
H(28)	6791(17)	9920(17)	-1343(17)	32(4)
H(29)	5602(19)	8540(16)	1079(18)	36(5)
H(30)	7266(18)	8300(16)	429(17)	32(5)
H(31)	4640(20)	1587(17)	5910(20)	45(5)
H(32)	5851(18)	987(17)	4819(17)	34(5)
H(33)	4920(19)	2049(17)	4192(19)	40(5)
H(34)	6851(19)	6700(16)	5946(17)	34(5)
H(35)	7368(18)	5255(18)	5927(18)	39(5)
H(36)	8300(20)	6334(17)	5982(19)	43(5)
H(37)	7580(20)	6425(18)	-1130(20)	47(5)
H(38)	6993(17)	5100(17)	215(17)	32(4)
H(39)	8060(20)	6151(17)	101(18)	38(5)

Compound 8

Table 1. Atomic coordinates (x 10^4) and equivalent isotropic displacement parameters ($Å^2$x 10^3) for sh2943. U(eq) is defined as one third of the trace of the orthogonalized U^{ij} tensor.

	x	y	z	U(eq)
Cl	2346(1)	1300(1)	840(1)	38(1)
Al	3949(1)	1266(1)	-106(1)	24(1)
O	5889(2)	733(2)	678(1)	22(1)
C(1)	6883(3)	1516(3)	1640(2)	22(1)
C(2)	6509(3)	708(4)	2598(2)	30(1)
C(3)	7642(4)	1215(4)	3652(2)	36(1)
C(4)	9307(3)	889(4)	3634(2)	36(1)
C(5)	9684(3)	1715(4)	2683(2)	34(1)
C(6)	8560(3)	1196(3)	1640(2)	26(1)
C(7)	6486(3)	3313(3)	1550(2)	31(1)

Table 2. Bond lengths [Å] and angles [°] for sh2943.

Cl-Al	2.1197(9)	O-Al#1	1.8231(17)	C(3)-C(4)	1.517(4)
Al-O	1.8224(17)	C(1)-C(7)	1.514(4)	C(4)-C(5)	1.527(4)
Al-O#1	1.8231(17)	C(1)-C(6)	1.522(3)	C(5)-C(6)	1.527(4)
Al-Al#1	2.7660(14)	C(1)-C(2)	1.527(3)		
O-C(1)	1.483(3)	C(2)-C(3)	1.539(4)		
O-Al-O#1	81.30(8)	C(1)-O-Al#1	129.99(14)	C(6)-C(1)-C(2)	110.5(2)
O-Al-Cl	111.35(6)	Al-O-Al#1	98.70(8)	C(1)-C(2)-C(3)	112.4(2)
O#1-Al-Cl	112.81(6)	O-C(1)-C(7)	106.27(19)	C(4)-C(3)-C(2)	111.0(2)
O-Al-Al#1	40.66(5)	O-C(1)-C(6)	107.35(18)	C(3)-C(4)-C(5)	111.0(2)
O#1-Al-Al#1	40.64(5)	C(7)-C(1)-C(6)	112.3(2)	C(4)-C(5)-C(6)	111.6(2)
Cl-Al-Al#1	119.70(5)	O-C(1)-C(2)	107.14(19)	C(1)-C(6)-C(5)	111.8(2)
C(1)-O-Al	130.12(14)	C(7)-C(1)-C(2)	112.9(2)		

Symmetry transformations used to generate equivalent atoms: #1 -x+1,-y,-z

Table 3. Anisotropic displacement parameters ($Å^2$x 10^3) for sh2943. The anisotropic displacement factor exponent takes the form: $-2\pi^2[h^2 a^{*2}U^{11} + ... + 2 h k a^* b^* U^{12}]$

	U^{11}	U^{22}	U^{33}	U^{23}	U^{13}	U^{12}
Cl	33(1)	50(1)	36(1)	-7(1)	15(1)	6(1)
Al	23(1)	27(1)	22(1)	-5(1)	5(1)	4(1)
O	21(1)	28(1)	18(1)	-6(1)	4(1)	0(1)
C(1)	24(1)	26(1)	16(1)	-6(1)	5(1)	-3(1)

C(2)	33(1)	38(2)	22(1)	-3(1)	11(1)	-8(1)
C(3)	49(2)	42(2)	17(1)	-3(1)	11(1)	-9(1)
C(4)	43(2)	44(2)	16(1)	-2(1)	-2(1)	-5(1)
C(5)	28(1)	44(2)	27(1)	-2(1)	3(1)	-6(1)
C(6)	26(1)	33(1)	19(1)	-1(1)	7(1)	-2(1)
C(7)	36(2)	28(1)	28(1)	-6(1)	6(1)	2(1)

Table 4. Hydrogen coordinates (x 10^4) and isotropic displacement parameters ($Å^2$x 10^{-3}) for sh2943.

	x	y	z	U(eq)
H(1)	3713(12)	2894(13)	-858(9)	-44(2)
H(3)	6550(30)	-440(40)	2530(20)	33(8)
H(4)	7480(30)	2330(40)	3760(20)	31(8)
H(11)	8660(30)	60(30)	1527(19)	18(6)
H(10)	8760(30)	1690(30)	1050(20)	25(7)
H(9)	10650(40)	1530(40)	2630(30)	45(9)
H(2)	5490(40)	900(40)	2580(20)	40(8)
H(6)	9510(30)	-270(40)	3620(20)	41(8)
H(8)	9580(30)	2830(40)	2720(20)	32(8)
H(7)	9950(40)	1290(30)	4240(30)	36(8)
H(5)	7440(40)	670(40)	4230(30)	47(9)
H(14)	7080(30)	3910(30)	2140(20)	35(8)
H(13)	6670(30)	3770(30)	890(20)	38(8)
H(12)	5380(40)	3480(40)	1520(20)	43(9)

Compound 9

Table 1. Atomic coordinates (x 10^4) and equivalent isotropic displacement parameters ($Å^2$x 10^3) for sh2966. U(eq) is defined as one third of the trace of the orthogonalized U^{ij} tensor.

	x	y	z	U(eq)
Cl(1)	4798(1)	5807(1)	2260(1)	32(1)
Al(1)	4517(1)	4647(1)	849(1)	18(1)
O(1)	5825(1)	4419(1)	389(1)	18(1)
O(2)	3731(1)	3353(1)	825(1)	25(1)
C(1)	6906(1)	3839(2)	933(1)	18(1)
C(2)	7526(2)	4781(2)	1765(2)	26(1)
C(3)	8734(2)	4351(2)	2270(2)	32(1)
C(4)	9394(2)	4112(2)	1391(2)	34(1)
C(5)	8791(2)	3164(2)	556(2)	32(1)
C(6)	7577(2)	3573(2)	65(2)	25(1)
C(7)	6608(2)	2639(2)	1466(2)	28(1)
C(8)	3022(2)	2642(2)	1370(2)	24(1)
C(9)	1880(2)	2465(2)	589(2)	30(1)
C(10)	1945(2)	1665(2)	-398(2)	34(1)
C(11)	2475(2)	386(2)	-51(2)	39(1)
C(12)	3635(2)	553(2)	694(2)	40(1)
C(13)	3571(2)	1361(2)	1671(2)	32(1)
C(14)	2865(2)	3332(2)	2392(2)	40(1)

Table 2. Bond lengths [Å] and angles [°] for sh2966.

Cl(1)-Al(1)	2.1230(6)	O(1)-Al(1)#1	1.8132(12)	C(3)-C(4)	1.517(3)
Al(1)-O(2)	1.6685(13)	O(2)-C(8)	1.424(2)	C(4)-C(5)	1.520(3)
Al(1)-O(1)#1	1.8132(12)	C(1)-C(7)	1.517(2)	C(5)-C(6)	1.532(2)
Al(1)-O(1)	1.8157(12)	C(1)-C(6)	1.520(2)	C(8)-C(14)	1.524(3)
Al(1)-Al(1)#1	2.7456(10)	C(1)-C(2)	1.522(2)	C(8)-C(13)	1.524(3)
O(1)-C(1)	1.4759(18)	C(2)-C(3)	1.534(3)	C(8)-C(9)	1.526(3)

C(9)-C(10)	1.517(3)	C(11)-C(12)	1.523(3)		
C(10)-C(11)	1.524(3)	C(12)-C(13)	1.512(3)		
O(2)-Al(1)-O(1)#1	114.22(6)	Al(1)#1-O(1)-Al(1)	98.33(5)	C(1)-C(6)-C(5)	112.33(1)
O(2)-Al(1)-O(1)	114.75(6)	C(8)-O(2)-Al(1)	146.01(1)	O(2)-C(8)-C(14)	110.29(1)
O(1)#1-Al(1)-O(1)	81.67(5)	O(1)-C(1)-C(7)	106.41(1)	O(2)-C(8)-C(13)	108.38(1)
O(2)-Al(1)-Cl(1)	118.71(5)	O(1)-C(1)-C(6)	107.71(1)	C(14)-C(8)-C(13)	110.31(1)
O(1)#1-Al(1)-Cl(1)	111.33(5)	C(7)-C(1)-C(6)	112.01(1)	O(2)-C(8)-C(9)	108.32(1)
O(1)-Al(1)-Cl(1)	110.39(5)	O(1)-C(1)-C(2)	107.51(1)	C(14)-C(8)-C(9)	109.81(1)
O(2)-Al(1)-Al(1)#1	123.22(5)	C(7)-C(1)-C(2)	112.25(1)	C(13)-C(8)-C(9)	109.69(1)
O(1)#1-Al(1)-Al(1)#1	40.87(4)	C(6)-C(1)-C(2)	110.64(1)	C(10)-C(9)-C(8)	113.20(1)
O(1)-Al(1)-Al(1)#1	40.80(4)	C(1)-C(2)-C(3)	111.94(1)	C(9)-C(10)-C(11)	110.97(1)
Cl(1)-Al(1)-Al(1)#1	118.07(3)	C(4)-C(3)-C(2)	110.82(1)	C(12)-C(11)-C(10)	110.40(1)
C(1)-O(1)-Al(1)#1	129.88(1)	C(3)-C(4)-C(5)	111.18(1)	C(13)-C(12)-C(11)	111.20(1)
C(1)-O(1)-Al(1)	131.10(1)	C(4)-C(5)-C(6)	111.54(1)	C(12)-C(13)-C(8)	113.63(1)

Symmetry transformations used to generate equivalent atoms: #1 -x+1,-y+1,-z

Table 3. Anisotropic displacement parameters ($Å^2x\ 10^3$) for sh2966. The anisotropic displacement factor exponent takes the form: $-2\pi^2[\ h^2\ a^{*2}U^{11} + ...\ + 2\ h\ k\ a^*\ b^*\ U^{12}\ ]$

	U^{11}	U^{22}	U^{33}	U^{23}	U^{13}	U^{12}
Cl(1)	30(1)	37(1)	28(1)	-12(1)	6(1)	0(1)
Al(1)	17(1)	19(1)	20(1)	0(1)	5(1)	1(1)
O(1)	12(1)	20(1)	20(1)	3(1)	2(1)	2(1)
O(2)	26(1)	22(1)	29(1)	0(1)	13(1)	-3(1)
C(1)	13(1)	19(1)	22(1)	1(1)	1(1)	3(1)
C(2)	17(1)	29(1)	29(1)	-7(1)	2(1)	1(1)
C(3)	18(1)	38(1)	35(1)	-8(1)	-3(1)	1(1)
C(4)	15(1)	42(1)	43(1)	-1(1)	4(1)	2(1)
C(5)	20(1)	43(1)	34(1)	-4(1)	7(1)	11(1)
C(6)	20(1)	31(1)	24(1)	-1(1)	5(1)	6(1)
C(7)	22(1)	25(1)	35(1)	8(1)	2(1)	1(1)
C(8)	24(1)	24(1)	28(1)	4(1)	11(1)	-2(1)
C(9)	21(1)	31(1)	40(1)	6(1)	10(1)	1(1)
C(10)	33(1)	37(1)	30(1)	3(1)	1(1)	-5(1)
C(11)	49(1)	28(1)	39(1)	-7(1)	7(1)	-6(1)
C(12)	38(1)	26(1)	56(1)	-2(1)	8(1)	6(1)
C(13)	31(1)	25(1)	36(1)	8(1)	1(1)	-2(1)
C(14)	51(1)	40(1)	35(1)	-4(1)	25(1)	-6(1)

Compound 10

Table 1. Atomic coordinates ($x\ 10^4$) and equivalent isotropic displacement parameters ($Å^2x\ 10^3$) for sh2947. U(eq) is defined as one third of the trace of the orthogonalized U^{ij} tensor.

	x	y	z	U(eq)
Al(1)	-1055(1)	8887(1)	16(1)	16(1)
Cl(1)	-1244(1)	6873(1)	-882(1)	28(1)
Cl(2)	-2634(1)	9005(1)	939(1)	31(1)
O(1)	881(1)	9396(1)	718(1)	15(1)
C(1)	1907(1)	8716(1)	1684(1)	17(1)
C(2)	1580(1)	9530(1)	2630(1)	24(1)
C(3)	2718(1)	9061(2)	3662(1)	30(1)
C(4)	4362(1)	9343(2)	3614(1)	33(1)
C(5)	4695(1)	8547(2)	2666(1)	35(1)
C(6)	3548(1)	9020(1)	1637(1)	25(1)
C(7)	1534(2)	7015(1)	1648(1)	35(1)

Table 2. Bond lengths [Å] and angles [°] for sh2947.

Al(1)-O(1)#1	1.8043(7)	O(1)-C(1)	1.4892(11)	C(2)-C(3)	1.5321(15)
Al(1)-O(1)	1.8083(7)	O(1)-Al(1)#1	1.8043(7)	C(3)-C(4)	1.5201(17)
Al(1)-Cl(1)	2.0919(4)	C(1)-C(7)	1.5119(14)	C(4)-C(5)	1.5211(17)
Al(1)-Cl(2)	2.0968(4)	C(1)-C(6)	1.5207(14)	C(5)-C(6)	1.5339(15)
Al(1)-Al(1)#1	2.7194(5)	C(1)-C(2)	1.5236(13)		

O(1)#1-Al(1)-O(1)	82.34(3)	Cl(1)-Al(1)-Al(1)#1	122.789(1)	O(1)-C(1)-C(2)	107.76(7)
O(1)#1-Al(1)-Cl(1)	113.21(2)	Cl(2)-Al(1)-Al(1)#1	123.737(1)	C(7)-C(1)-C(2)	113.01(9)
O(1)-Al(1)-Cl(1)	114.90(3)	C(1)-O(1)-Al(1)#1	131.62(5)	C(6)-C(1)-C(2)	110.23(8)
O(1)#1-Al(1)-Cl(2)	115.71(3)	C(1)-O(1)-Al(1)	130.27(5)	C(1)-C(2)-C(3)	111.99(8)
O(1)-Al(1)-Cl(2)	113.72(3)	Al(1)#1-O(1)-Al(1)	97.66(3)	C(4)-C(3)-C(2)	111.06(9)
Cl(1)-Al(1)-Cl(2)	113.473(1)	O(1)-C(1)-C(7)	106.02(8)	C(3)-C(4)-C(5)	111.13(10)
O(1)#1-Al(1)-Al(1)#1	41.23(2)	O(1)-C(1)-C(6)	107.15(7)	C(4)-C(5)-C(6)	111.78(10)
O(1)-Al(1)-Al(1)#1	41.11(2)	C(7)-C(1)-C(6)	112.31(9)	C(1)-C(6)-C(5)	111.19(9)

Symmetry transformations used to generate equivalent atoms: #1 -x,-y+2,-z

Table 3. Anisotropic displacement parameters ($Å^2 x\ 10^3$) for sh2947. The anisotropic displacement factor exponent takes the form: $-2\pi^2[\ h^2\ a^{*2}U^{11} + ... + 2\ h\ k\ a^*\ b^*\ U^{12}\ ]$

	U^{11}	U^{22}	U^{33}	U^{23}	U^{13}	U^{12}
Al(1)	14(1)	14(1)	18(1)	0(1)	4(1)	-3(1)
Cl(1)	30(1)	18(1)	31(1)	-7(1)	2(1)	-4(1)
Cl(2)	25(1)	43(1)	30(1)	2(1)	15(1)	-3(1)
O(1)	14(1)	15(1)	16(1)	2(1)	2(1)	-1(1)
C(1)	17(1)	17(1)	16(1)	2(1)	2(1)	1(1)
C(2)	23(1)	31(1)	18(1)	0(1)	8(1)	5(1)
C(3)	31(1)	41(1)	16(1)	1(1)	6(1)	5(1)
C(4)	28(1)	48(1)	19(1)	-1(1)	-2(1)	-1(1)
C(5)	19(1)	62(1)	22(1)	2(1)	1(1)	11(1)
C(6)	16(1)	42(1)	17(1)	1(1)	3(1)	4(1)
C(7)	46(1)	18(1)	31(1)	7(1)	-6(1)	-3(1)

Table 4. Hydrogen coordinates ($x\ 10^4$) and isotropic displacement parameters ($Å^2 x\ 10^3$) for sh2947.

	x	y	z	U(eq)
H(1)	1674(16)	10589(17)	2544(10)	27(3)
H(2)	520(20)	9357(19)	2648(13)	50(5)
H(3)	2540(20)	9650(20)	4248(13)	48(4)
H(4)	2557(17)	7949(17)	3774(11)	27(3)
H(5)	4506(18)	10454(19)	3591(12)	39(4)
H(6)	5065(18)	9011(15)	4249(12)	31(4)
H(7)	5700(20)	8750(20)	2613(15)	56(5)
H(8)	4609(17)	7460(20)	2725(11)	33(4)
H(9)	3645(16)	10158(16)	1554(10)	22(3)
H(10)	3750(20)	8445(19)	1049(14)	47(4)
H(11)	510(20)	6921(19)	1661(13)	46(5)
H(12)	2120(20)	6513(19)	2187(14)	46(4)
H(13)	1770(20)	6580(20)	1013(15)	55(5)

Compound 11

Table 1. Atomic coordinates ($x\ 10^4$) and equivalent isotropic displacement parameters ($Å^2 x\ 10^3$) for sh2848. U(eq) is defined as one third of the trace of the orthogonalized U^{ij} tensor.

	x	y	z	U(eq)
Ge(1)	3739(1)	5114(1)	6318(1)	17(1)
O(1)	4024(1)	6021(1)	4610(1)	18(1)

O(2)	6131(1)	5983(1)	6746(1)	22(1)
C(1)	2023(1)	6740(1)	4099(1)	18(1)
C(2)	922(2)	7705(1)	4940(1)	21(1)
C(3)	-1172(2)	8498(1)	4402(1)	26(1)
C(4)	-404(2)	9185(1)	3111(1)	27(1)
C(5)	764(2)	8222(1)	2280(1)	31(1)
C(6)	2868(2)	7449(1)	2826(1)	26(1)
C(7)	5700(2)	6451(1)	7901(1)	18(1)
C(8)	5178(2)	7914(1)	7718(1)	34(1)
C(9)	4879(3)	8467(1)	8927(1)	44(1)
C(10)	7012(2)	8115(1)	9622(1)	32(1)
C(11)	7539(2)	6653(1)	9804(1)	35(1)
C(12)	7849(2)	6109(1)	8588(1)	31(1)

Table 2. Bond lengths [Å] and angles [°] for sh2848.

Ge(1)-O(2)	1.8148(6)	C(1)-C(6)	1.5195(13)	C(7)-C(8)	1.5137(12)
Ge(1)-O(1)#1	1.9676(6)	C(1)-C(2)	1.5203(11)	C(7)-C(12)	1.5139(13)
Ge(1)-O(1)	1.9771(6)	C(2)-C(3)	1.5336(13)	C(8)-C(9)	1.5239(15)
O(1)-C(1)	1.4475(10)	C(3)-C(4)	1.5198(15)	C(9)-C(10)	1.5128(17)
O(1)-Ge(1)#1	1.9676(6)	C(4)-C(5)	1.5229(15)	C(10)-C(11)	1.5139(15)
O(2)-C(7)	1.4260(10)	C(5)-C(6)	1.5328(14)	C(11)-C(12)	1.5280(14)

O(2)-Ge(1)-O(1)#1	93.47(3)	O(1)-C(1)-C(2)	109.68(6)	O(2)-C(7)-C(12)	109.75(7)
O(2)-Ge(1)-O(1)	94.72(3)	C(6)-C(1)-C(2)	110.69(7)	C(8)-C(7)-C(12)	110.76(8)
O(1)#1-Ge(1)-O(1)	75.72(3)	C(1)-C(2)-C(3)	110.53(7)	C(7)-C(8)-C(9)	111.93(9)
C(1)-O(1)-Ge(1)#1	122.48(5)	C(4)-C(3)-C(2)	111.59(8)	C(10)-C(9)-C(8)	112.11(1)
C(1)-O(1)-Ge(1)	122.25(5)	C(3)-C(4)-C(5)	111.27(8)	C(9)-C(10)-C(11)	111.19(9)
Ge(1)#1-O(1)-Ge(1)	104.28(3)	C(4)-C(5)-C(6)	111.11(8)	C(10)-C(11)-C(12)	111.53(9)
C(7)-O(2)-Ge(1)	117.11(5)	C(1)-C(6)-C(5)	110.21(8)	C(7)-C(12)-C(11)	111.96(8)
O(1)-C(1)-C(6)	109.78(7)	O(2)-C(7)-C(8)	110.38(7)		

Symmetry transformations used to generate equivalent atoms: #1 -x+1,-y+1,-z+1

Table 3. Anisotropic displacement parameters ($Å^2 x\ 10^3$) for sh2848. The anisotropic displacement factor exponent takes the form: $-2\pi^2[\ h^2\ a^{*2}U^{11} + ...\ + 2\ h\ k\ a^*\ b^*\ U^{12}\ ]$

	U^{11}	U^{22}	U^{33}	U^{23}	U^{13}	U^{12}
Ge(1)	18(1)	17(1)	16(1)	-5(1)	-3(1)	1(1)
O(1)	21(1)	18(1)	17(1)	-5(1)	-7(1)	6(1)
O(2)	23(1)	28(1)	18(1)	-11(1)	-3(1)	-3(1)
C(1)	20(1)	16(1)	19(1)	-4(1)	-8(1)	2(1)
C(2)	24(1)	22(1)	18(1)	-3(1)	-4(1)	6(1)
C(3)	24(1)	24(1)	28(1)	-1(1)	-4(1)	8(1)
C(4)	33(1)	22(1)	27(1)	-1(1)	-10(1)	7(1)
C(5)	43(1)	31(1)	20(1)	-3(1)	-13(1)	11(1)
C(6)	32(1)	29(1)	16(1)	-3(1)	-4(1)	10(1)
C(7)	22(1)	19(1)	15(1)	-6(1)	-3(1)	0(1)
C(8)	54(1)	22(1)	30(1)	-10(1)	-24(1)	12(1)
C(9)	59(1)	37(1)	44(1)	-28(1)	-29(1)	25(1)
C(10)	46(1)	27(1)	26(1)	-12(1)	-15(1)	2(1)
C(11)	55(1)	31(1)	23(1)	-8(1)	-20(1)	8(1)
C(12)	38(1)	31(1)	29(1)	-14(1)	-18(1)	14(1)

Table 4. Hydrogen coordinates ($x\ 10^4$) and isotropic displacement parameters ($Å^2 x\ 10^3$) for sh2848.

	x	y	z	U(eq)
H(1)	830(20)	6160(12)	4050(12)	25(3)
H(2)	2170(20)	8262(13)	5033(13)	27(3)
H(3)	380(30)	7217(14)	5685(14)	35(4)
H(4)	-1770(30)	9157(14)	4931(14)	33(4)

H(5)	-2380(30)	7937(14)	4402(14)	34(4)
H(6)	780(20)	9856(13)	3111(13)	32(3)
H(7)	-1770(30)	9629(16)	2810(16)	54(5)
H(8)	1230(30)	8629(15)	1497(16)	43(4)
H(9)	-450(30)	7594(15)	2171(15)	41(4)
H(10)	4120(30)	8027(14)	2895(13)	30(3)
H(11)	3460(30)	6809(14)	2314(15)	37(4)
H(12)	4240(20)	6048(11)	8406(11)	20(3)
H(13)	6440(30)	8288(17)	7212(18)	55(5)
H(14)	3730(30)	8086(15)	7346(15)	42(4)
H(15)	4640(30)	9419(17)	8784(17)	60(5)
H(16)	3550(30)	8098(16)	9417(16)	43(5)
H(17)	6800(30)	8450(15)	10410(15)	43(4)
H(18)	8460(30)	8535(14)	9121(14)	38(4)
H(19)	6130(30)	6230(14)	10355(14)	33(4)
H(20)	8900(30)	6448(15)	10212(15)	41(4)
H(21)	8110(30)	5143(16)	8744(15)	48(4)
H(22)	9210(30)	6523(14)	8089(14)	39(4)

Compound 12

Table 1. Atomic coordinates (x 10^4) and equivalent isotropic displacement parameters ($Å^2$x 10^3) for sh2891. U(eq) is defined as one third of the trace of the orthogonalized U^{ij} tensor.

	x	y	z	U(eq)
Ge(1)	526(1)	4870(1)	1145(1)	12(1)
O(1)	1646(1)	6272(1)	1208(1)	16(1)
O(2)	-772(1)	5811(1)	165(1)	13(1)
C(1)	2532(1)	6656(1)	2086(1)	14(1)
C(2)	1886(1)	6996(1)	2952(1)	18(1)
C(3)	2804(1)	7312(1)	3920(1)	20(1)
C(4)	3738(1)	6143(1)	4206(1)	22(1)
C(5)	4399(1)	5784(1)	3362(1)	24(1)
C(6)	3463(1)	5474(1)	2406(1)	20(1)
C(7)	3194(1)	7918(1)	1774(1)	27(1)
C(8)	-1345(1)	7146(1)	284(1)	15(1)
C(9)	-1393(1)	7345(1)	1383(1)	20(1)
C(10)	-2251(1)	6326(1)	1769(1)	23(1)
C(11)	-3565(1)	6376(1)	1138(1)	24(1)
C(12)	-3533(1)	6109(1)	48(1)	18(1)
C(13)	-2676(1)	7132(1)	-335(1)	16(1)
C(14)	-572(1)	8285(1)	-67(1)	25(1)

Table 2. Bond lengths [Å] and angles [°] for sh2891.

Ge(1)-O(1)	1.8204(5)	C(1)-C(2)	1.5338(10)	C(8)-C(9)	1.5321(11)
Ge(1)-O(2)	1.9760(5)	C(1)-C(6)	1.5382(11)	C(8)-C(13)	1.5338(10)
Ge(1)-O(2)#1	1.9819(5)	C(2)-C(3)	1.5316(11)	C(9)-C(10)	1.5264(13)
O(1)-C(1)	1.4390(8)	C(3)-C(4)	1.5242(12)	C(10)-C(11)	1.5258(13)
O(2)-C(8)	1.4615(8)	C(4)-C(5)	1.5220(12)	C(11)-C(12)	1.5266(12)
O(2)-Ge(1)#1	1.9819(5)	C(5)-C(6)	1.5272(11)	C(12)-C(13)	1.5259(11)
C(1)-C(7)	1.5245(11)	C(8)-C(14)	1.5247(11)		

O(1)-Ge(1)-O(2)	94.24(2)	Ge(1)-O(2)-Ge(1)#1	104.89(2)	C(2)-C(1)-C(6)	108.53(6)
O(1)-Ge(1)-O(2)#1	94.70(2)	O(1)-C(1)-C(7)	104.57(6)	C(3)-C(2)-C(1)	113.14(6)
O(2)-Ge(1)-O(2)#1	75.11(2)	O(1)-C(1)-C(2)	111.58(6)	C(4)-C(3)-C(2)	111.50(7)
C(1)-O(1)-Ge(1)	124.70(4)	C(7)-C(1)-C(2)	111.15(7)	C(5)-C(4)-C(3)	111.59(7)
C(8)-O(2)-Ge(1)	126.80(4)	O(1)-C(1)-C(6)	110.23(6)	C(4)-C(5)-C(6)	111.15(7)
C(8)-O(2)-Ge(1)#1	122.27(4)	C(7)-C(1)-C(6)	110.77(7)	C(5)-C(6)-C(1)	113.14(7)

O(2)-C(8)-C(14)	109.23(6)	C(14)-C(8)-C(13)	110.85(7)	C(10)-C(11)-C(12)	110.49(7)
O(2)-C(8)-C(9)	108.69(6)	C(9)-C(8)-C(13)	109.53(6)	C(13)-C(12)-C(11)	111.20(7)
C(14)-C(8)-C(9)	110.38(7)	C(10)-C(9)-C(8)	113.70(6)	C(12)-C(13)-C(8)	113.26(6)
O(2)-C(8)-C(13)	108.12(5)	C(11)-C(10)-C(9)	110.90(8)		

Symmetry transformations used to generate equivalent atoms: #1 -x,-y+1,-z

Table 3. Anisotropic displacement parameters ($Å^2 x\ 10^3$) for sh2891. The anisotropic displacement factor exponent takes the form: $-2\pi^2[\ h^2\ a^{*2}U^{11} + ...\ + 2\ h\ k\ a^*\ b^*\ U^{12}\ ]$

	U^{11}	U^{22}	U^{33}	U^{23}	U^{13}	U^{12}
Ge(1)	11(1)	14(1)	11(1)	1(1)	1(1)	-1(1)
O(1)	15(1)	20(1)	11(1)	-1(1)	-1(1)	-6(1)
O(2)	12(1)	12(1)	13(1)	-2(1)	1(1)	2(1)
C(1)	14(1)	18(1)	11(1)	-1(1)	1(1)	-4(1)
C(2)	14(1)	24(1)	14(1)	-4(1)	1(1)	2(1)
C(3)	19(1)	26(1)	14(1)	-6(1)	1(1)	2(1)
C(4)	25(1)	26(1)	13(1)	-1(1)	-2(1)	3(1)
C(5)	18(1)	32(1)	19(1)	-7(1)	-3(1)	7(1)
C(6)	16(1)	26(1)	16(1)	-6(1)	1(1)	3(1)
C(7)	32(1)	30(1)	18(1)	3(1)	-2(1)	-17(1)
C(8)	12(1)	11(1)	20(1)	-3(1)	1(1)	0(1)
C(9)	16(1)	22(1)	21(1)	-10(1)	-1(1)	2(1)
C(10)	21(1)	33(1)	16(1)	-4(1)	4(1)	4(1)
C(11)	17(1)	32(1)	24(1)	-5(1)	8(1)	1(1)
C(12)	12(1)	21(1)	21(1)	-3(1)	1(1)	-1(1)
C(13)	14(1)	15(1)	19(1)	-1(1)	0(1)	2(1)
C(14)	20(1)	14(1)	40(1)	3(1)	5(1)	-4(1)

Table 4. Hydrogen coordinates ($x\ 10^4$) and isotropic displacement parameters ($Å^2 x\ 10^3$) for sh2891.

	x	y	z	U(eq)
H(1)	1386(11)	6197(12)	3079(9)	21(3)
H(2)	1335(12)	7750(14)	2760(10)	29(3)
H(3)	3248(11)	8172(13)	3831(9)	25(3)
H(4)	2372(12)	7488(14)	4445(11)	32(3)
H(5)	3275(14)	5320(15)	4374(11)	32(4)
H(6)	4333(12)	6366(14)	4810(10)	32(3)
H(7)	4974(17)	4988(13)	3544(14)	39(4)
H(8)	4881(11)	6546(13)	3227(9)	24(3)
H(9)	3917(14)	5278(14)	1852(12)	34(4)
H(10)	2999(13)	4661(13)	2527(10)	25(3)
H(11)	3815(13)	8295(15)	2313(11)	38(4)
H(12)	2604(12)	8613(14)	1583(10)	29(3)
H(13)	3570(13)	7674(14)	1245(11)	35(4)
H(14)	-1666(11)	8260(12)	1464(9)	23(3)
H(15)	-562(10)	7317(12)	1769(9)	19(3)
H(16)	-1888(11)	5354(13)	1761(9)	19(3)
H(17)	-2247(12)	6572(13)	2474(11)	34(3)
H(18)	-3915(13)	7282(15)	1205(10)	34(3)
H(19)	-4125(13)	5697(16)	1356(10)	34(3)
H(20)	-4381(12)	6161(14)	-349(10)	30(3)
H(21)	-3252(13)	5176(11)	-36(11)	20(3)
H(22)	-2986(11)	8061(13)	-316(9)	22(3)
H(23)	-2680(11)	6946(12)	-1046(9)	21(3)
H(24)	309(12)	8277(13)	307(10)	25(3)
H(25)	-554(12)	8171(14)	-756(11)	32(3)
H(26)	-943(13)	9201(16)	21(10)	37(4)

Compound 14

Table 1. Atomic coordinates (x 10^4) and equivalent isotropic displacement parameters ($Å^2$x 10^3) for sh2919. U(eq) is defined as one third of the trace of the orthogonalized U^{ij} tensor.

	x	y	z	U(eq)
Al(1)	5963(1)	445(1)	5828(1)	18(1)
Si(1)	8360(1)	809(1)	7574(1)	22(1)
Si(2)	7890(1)	-1167(1)	6607(1)	21(1)
N(1)	7440(1)	-9(1)	6607(1)	19(1)
O(1)	5432(1)	213(1)	4054(1)	19(1)
C(1)	7752(2)	1056(1)	9135(2)	37(1)
C(2)	8474(1)	1927(1)	6673(2)	31(1)
C(3)	9988(1)	436(1)	8073(2)	35(1)
C(4)	8299(2)	-1650(1)	8329(2)	38(1)
C(5)	9222(1)	-1328(1)	5742(2)	31(1)
C(6)	6660(1)	-1946(1)	5740(2)	29(1)
C(7)	6023(1)	371(1)	2890(1)	24(1)
C(8)	6488(2)	-560(1)	2473(2)	46(1)
C(9)	5094(2)	776(2)	1784(2)	43(1)
C(10)	7066(2)	1036(2)	3299(2)	50(1)

Table 2. Bond lengths [Å] and angles [°] for sh2919.

Al(1)-N(1)	1.8244(11)	Si(1)-C(1)	1.8752(17)	O(1)-C(7)	1.4770(16)
Al(1)-O(1)	1.8415(10)	Si(1)-C(3)	1.8801(16)	O(1)-Al(1)#1	1.8433(10)
Al(1)-O(1)#1	1.8433(10)	Si(2)-N(1)	1.7359(12)	C(7)-C(10)	1.508(2)
Al(1)-Al(1)#1	2.8062(8)	Si(2)-C(6)	1.8719(15)	C(7)-C(9)	1.514(2)
Si(1)-N(1)	1.7491(12)	Si(2)-C(5)	1.8726(16)	C(7)-C(8)	1.521(2)
Si(1)-C(2)	1.8669(17)	Si(2)-C(4)	1.8766(16)		

N(1)-Al(1)-O(1)	118.63(5)	C(2)-Si(1)-C(3)	103.48(8)	Si(1)-N(1)-Al(1)	113.95(6)
N(1)-Al(1)-O(1)#1	119.94(5)	C(1)-Si(1)-C(3)	107.33(8)	C(7)-O(1)-Al(1)	131.01(8)
O(1)-Al(1)-O(1)#1	80.80(4)	N(1)-Si(2)-C(6)	112.56(6)	C(7)-O(1)-Al(1)#1	129.20(8)
N(1)-Al(1)-Al(1)#1	129.96(4)	N(1)-Si(2)-C(5)	111.85(7)	Al(1)-O(1)-Al(1)#1	99.20(4)
O(1)-Al(1)-Al(1)#1	40.42(3)	C(6)-Si(2)-C(5)	106.23(7)	O(1)-C(7)-C(10)	107.72(1)
O(1)#1-Al(1)-Al(1)#1	40.37(3)	N(1)-Si(2)-C(4)	112.13(7)	O(1)-C(7)-C(9)	108.60(1)
N(1)-Si(1)-C(2)	112.40(6)	C(6)-Si(2)-C(4)	105.34(8)	C(10)-C(7)-C(9)	111.20(1)
N(1)-Si(1)-C(1)	110.21(7)	C(5)-Si(2)-C(4)	108.31(8)	O(1)-C(7)-C(8)	108.24(1)
C(2)-Si(1)-C(1)	108.92(8)	Si(2)-N(1)-Si(1)	120.05(6)	C(10)-C(7)-C(8)	110.45(1)
N(1)-Si(1)-C(3)	114.14(7)	Si(2)-N(1)-Al(1)	125.56(6)	C(9)-C(7)-C(8)	110.52(1)

Symmetry transformations used to generate equivalent atoms: #1 -x+1,-y,-z+1

Table 3. Anisotropic displacement parameters ($Å^2$x 10^3) for sh2919. The anisotropic displacement factor exponent takes the form: $-2\pi^2[h^2 a^{*2}U^{11} + ... + 2 h k a^* b^* U^{12}]$

	U^{11}	U^{22}	U^{33}	U^{23}	U^{13}	U^{12}
Al(1)	16(1)	19(1)	18(1)	0(1)	2(1)	0(1)
Si(1)	20(1)	26(1)	20(1)	-3(1)	0(1)	-2(1)
Si(2)	21(1)	21(1)	22(1)	2(1)	3(1)	3(1)
N(1)	17(1)	21(1)	19(1)	0(1)	1(1)	0(1)
O(1)	18(1)	24(1)	16(1)	1(1)	5(1)	-2(1)
C(1)	40(1)	46(1)	25(1)	-11(1)	7(1)	-5(1)
C(2)	28(1)	28(1)	37(1)	-3(1)	2(1)	-7(1)
C(3)	23(1)	43(1)	36(1)	-4(1)	-6(1)	-2(1)
C(4)	43(1)	37(1)	32(1)	12(1)	2(1)	6(1)
C(5)	24(1)	35(1)	35(1)	-5(1)	6(1)	6(1)
C(6)	28(1)	22(1)	38(1)	0(1)	5(1)	1(1)
C(7)	22(1)	32(1)	19(1)	4(1)	8(1)	-1(1)

C(8)	56(1)	45(1)	47(1)	4(1)	33(1)	11(1)
C(9)	35(1)	70(1)	25(1)	16(1)	8(1)	10(1)
C(10)	51(1)	69(1)	34(1)	-1(1)	16(1)	-34(1)

Table 4. Hydrogen coordinates (x 10^4) and isotropic displacement parameters ($Å^2$x 10^3) for sh2919.

	x	y	z	U(eq)
H(1)	5801(15)	1449(12)	6240(17)	31(4)
H(1A)	6940	1334	8910	55
H(1B)	8296	1490	9688	55
H(1C)	7701	473	9621	55
H(2A)	8842	1811	5886	47
H(2B)	8981	2367	7258	47
H(2C)	7660	2192	6402	47
H(3A)	10023	-141	8588	53
H(3B)	10444	925	8613	53
H(3C)	10347	331	7277	53
H(4A)	9044	-1350	8784	57
H(4B)	8431	-2323	8283	57
H(4C)	7636	-1528	8820	57
H(5A)	9041	-1049	4857	47
H(5B)	9383	-1995	5661	47
H(5C)	9939	-1026	6256	47
H(6A)	5951	-1910	6185	44
H(6B)	6956	-2590	5766	44
H(6C)	6428	-1747	4816	44
H(8A)	7061	-825	3213	70
H(8B)	6900	-467	1712	70
H(8C)	5802	-987	2226	70
H(9A)	4402	349	1579	65
H(9B)	5466	862	992	65
H(9C)	4813	1379	2063	65
H(10A)	6754	1630	3572	75
H(10B)	7489	1141	2549	75
H(10C)	7634	769	4041	75

Compound 15

Table 1. Atomic coordinates (x 10^4) and equivalent isotropic displacement parameters ($Å^2$x 10^3) for sh2925. U(eq) is defined as one third of the trace of the orthogonalized U^{ij} tensor.

	x	y	z	U(eq)
Al(1)	10562(1)	9266(1)	4375(1)	18(1)
Si(1)	7982(1)	8010(1)	4533(1)	22(1)
Si(2)	10980(1)	7396(1)	3326(1)	23(1)
N(1)	9814(2)	8176(1)	4128(1)	18(1)
O(1)	9208(2)	10734(1)	4608(1)	17(1)
C(1)	8414(2)	11707(2)	4088(1)	19(1)
C(2)	6965(3)	12503(2)	4588(1)	24(1)
C(3)	6188(3)	13662(2)	4145(2)	29(1)
C(4)	7383(3)	14287(2)	3798(2)	33(1)
C(5)	8805(3)	13510(2)	3274(2)	33(1)
C(6)	9573(3)	12360(2)	3726(1)	26(1)
C(7)	7948(3)	11184(2)	3480(2)	30(1)
C(8)	6868(3)	9057(2)	5302(1)	25(1)
C(9)	6690(3)	8301(3)	3776(2)	34(1)
C(10)	8161(4)	6527(2)	5028(2)	35(1)
C(11)	10956(4)	8385(2)	2414(1)	33(1)

C(12)	13075(3)	6644(2)	3463(2)	33(1)
C(13)	10335(4)	6161(2)	3145(2)	39(1)
Al(2)	4362(1)	4300(1)	592(1)	16(1)
Si(3)	3761(1)	2249(1)	1603(1)	23(1)
Si(4)	6942(1)	1774(1)	528(1)	21(1)
N(2)	5074(2)	2727(1)	860(1)	19(1)
O(2)	5694(2)	5187(1)	441(1)	16(1)
C(14)	6367(2)	5524(2)	1024(1)	17(1)
C(15)	5352(3)	6760(2)	1235(1)	24(1)
C(16)	6071(3)	7273(2)	1752(2)	29(1)
C(17)	7750(3)	7236(2)	1369(2)	36(1)
C(18)	8774(3)	5992(3)	1193(2)	33(1)
C(19)	8055(3)	5483(2)	669(1)	28(1)
C(20)	6327(3)	4649(2)	1727(1)	28(1)
C(21)	3587(3)	2860(2)	2548(1)	30(1)
C(22)	1747(3)	2655(3)	1351(2)	35(1)
C(23)	4357(4)	623(2)	1803(2)	42(1)
C(24)	6899(4)	553(2)	1(2)	35(1)
C(25)	8095(4)	1116(3)	1336(2)	36(1)
C(26)	8179(3)	2544(2)	-172(1)	27(1)

Table 2. Bond lengths [Å] and angles [°] for sh2925.

Al(1)-N(1)	1.8236(18)	C(1)-C(7)	1.516(3)	Si(3)-C(23)	1.871(3)
Al(1)-O(1)	1.8359(14)	C(1)-C(6)	1.519(3)	Si(4)-N(2)	1.7334(18)
Al(1)-O(1)#1	1.8451(14)	C(1)-C(2)	1.525(3)	Si(4)-C(26)	1.867(2)
Al(1)-Al(1)#1	2.8197(12)	C(2)-C(3)	1.533(3)	Si(4)-C(24)	1.873(3)
Si(1)-N(1)	1.7401(18)	C(3)-C(4)	1.517(4)	Si(4)-C(25)	1.876(3)
Si(1)-C(10)	1.865(3)	C(4)-C(5)	1.524(4)	O(2)-C(14)	1.470(2)
Si(1)-C(8)	1.869(2)	C(5)-C(6)	1.532(3)	O(2)-Al(2)#2	1.8429(14)
Si(1)-C(9)	1.883(3)	Al(2)-N(2)	1.8295(18)	C(14)-C(20)	1.519(3)
Si(2)-N(1)	1.7491(17)	Al(2)-O(2)#2	1.8429(14)	C(14)-C(19)	1.520(3)
Si(2)-C(11)	1.868(3)	Al(2)-O(2)	1.8443(14)	C(14)-C(15)	1.522(3)
Si(2)-C(12)	1.870(3)	Al(2)-Al(2)#2	2.8193(12)	C(15)-C(16)	1.530(3)
Si(2)-C(13)	1.879(3)	Si(3)-N(2)	1.7564(18)	C(16)-C(17)	1.525(4)
O(1)-C(1)	1.471(2)	Si(3)-C(21)	1.868(2)	C(17)-C(18)	1.519(4)
O(1)-Al(1)#1	1.8451(14)	Si(3)-C(22)	1.868(3)	C(18)-C(19)	1.536(3)

N(1)-Al(1)-O(1)	120.34(7)	O(1)-C(1)-C(7)	107.47(1)	N(2)-Si(4)-C(24)	113.28(1)
N(1)-Al(1)-O(1)#1	118.87(7)	O(1)-C(1)-C(6)	107.63(1)	C(26)-Si(4)-C(24)	106.11(1)
O(1)-Al(1)-O(1)#1	80.00(6)	C(7)-C(1)-C(6)	112.22(1)	N(2)-Si(4)-C(25)	112.41(1)
N(1)-Al(1)-Al(1)#1	130.15(7)	O(1)-C(1)-C(2)	107.51(1)	C(26)-Si(4)-C(25)	104.81(1)
O(1)-Al(1)-Al(1)#1	40.12(4)	C(7)-C(1)-C(2)	111.40(1)	C(24)-Si(4)-C(25)	108.18(1)
O(1)#1-Al(1)-Al(1)#1	39.88(4)	C(6)-C(1)-C(2)	110.38(1)	Si(4)-N(2)-Si(3)	120.19(1)
N(1)-Si(1)-C(10)	112.56(1)	C(1)-C(2)-C(3)	112.78(1)	Si(4)-N(2)-Al(2)	125.78(1)
N(1)-Si(1)-C(8)	111.59(9)	C(4)-C(3)-C(2)	110.9(2)	Si(3)-N(2)-Al(2)	113.58(9)
C(10)-Si(1)-C(8)	105.30(1)	C(3)-C(4)-C(5)	111.3(2)	C(14)-O(2)-Al(2)#2	131.05(1)
N(1)-Si(1)-C(9)	111.58(1)	C(4)-C(5)-C(6)	110.4(2)	C(14)-O(2)-Al(2)	128.51(1)
C(10)-Si(1)-C(9)	108.90(14)	C(1)-C(6)-C(5)	112.72(1)	Al(2)#2-O(2)-Al(2)	99.75(6)
C(8)-Si(1)-C(9)	106.55(12)	N(2)-Al(2)-O(2)#2	119.29(7)	O(2)-C(14)-C(20)	106.91(1)
N(1)-Si(2)-C(11)	110.69(1)	N(2)-Al(2)-O(2)	120.99(7)	O(2)-C(14)-C(19)	108.41(1)
N(1)-Si(2)-C(12)	112.24(1)	O(2)#2-Al(2)-O(2)	80.25(6)	C(20)-C(14)-C(19)	111.34(1)
C(11)-Si(2)-C(12)	109.27(1)	N(2)-Al(2)-Al(2)#2	131.04(7)	O(2)-C(14)-C(15)	108.05(1)
N(1)-Si(2)-C(13)	113.94(1)	O(2)#2-Al(2)-Al(2)#2	40.14(4)	C(20)-C(14)-C(15)	111.38(1)
C(11)-Si(2)-C(13)	107.21(1)	O(2)-Al(2)-Al(2)#2	40.11(4)	C(19)-C(14)-C(15)	110.59(1)
C(12)-Si(2)-C(13)	103.10(14)	N(2)-Si(3)-C(21)	111.15(1)	C(14)-C(15)-C(16)	112.71(1)
Si(1)-N(1)-Si(2)	119.72(10)	N(2)-Si(3)-C(22)	111.95(1)	C(17)-C(16)-C(15)	110.7(2)
Si(1)-N(1)-Al(1)	125.52(10)	C(21)-Si(3)-C(22)	109.10(1)	C(18)-C(17)-C(16)	110.4(2)
Si(2)-N(1)-Al(1)	114.18(10)	N(2)-Si(3)-C(23)	114.11(1)	C(17)-C(18)-C(19)	110.9(2)
C(1)-O(1)-Al(1)	129.57(12)	C(21)-Si(3)-C(23)	106.12(1)	C(14)-C(19)-C(18)	112.08(1)
C(1)-O(1)-Al(1)#1	129.49(12)	C(22)-Si(3)-C(23)	103.99(1)		
Al(1)-O(1)-Al(1)#1	100.00(7)	N(2)-Si(4)-C(26)	111.51(1)		

Symmetry transformations used to generate equivalent atoms: #1 -x+2,-y+2,-z+1 #2 -x+1,-y+1,-z

Table 3. Anisotropic displacement parameters ($Å^2 x\ 10^3$) for sh2925. The anisotropic displacement factor exponent takes the form: $-2\pi^2[\ h^2\ a^{*2}U^{11} + ...\ + 2\ h\ k\ a^*\ b^*\ U^{12}\ ]$

	U^{11}	U^{22}	U^{33}	U^{23}	U^{13}	U^{12}
Al(1)	17(1)	19(1)	16(1)	-2(1)	-4(1)	-4(1)
Si(1)	20(1)	24(1)	24(1)	-6(1)	-4(1)	-8(1)
Si(2)	24(1)	23(1)	21(1)	-7(1)	-4(1)	-1(1)
N(1)	16(1)	18(1)	18(1)	-5(1)	-4(1)	-3(1)
O(1)	18(1)	16(1)	15(1)	0(1)	-7(1)	-2(1)
C(1)	20(1)	16(1)	18(1)	1(1)	-9(1)	-1(1)
C(2)	23(1)	22(1)	23(1)	-2(1)	-6(1)	-1(1)
C(3)	27(1)	23(1)	31(1)	-5(1)	-11(1)	3(1)
C(4)	44(2)	18(1)	37(1)	2(1)	-22(1)	-4(1)
C(5)	33(1)	29(1)	34(1)	12(1)	-11(1)	-9(1)
C(6)	23(1)	25(1)	27(1)	7(1)	-7(1)	-4(1)
C(7)	34(1)	26(1)	28(1)	-5(1)	-18(1)	1(1)
C(8)	20(1)	28(1)	25(1)	-5(1)	-1(1)	-6(1)
C(9)	26(1)	44(2)	37(1)	-13(1)	-11(1)	-9(1)
C(10)	41(2)	30(1)	37(1)	-7(1)	-2(1)	-17(1)
C(11)	41(2)	31(1)	20(1)	-5(1)	-6(1)	0(1)
C(12)	24(1)	37(1)	29(1)	-13(1)	-4(1)	5(1)
C(13)	45(2)	30(1)	44(2)	-16(1)	-8(1)	-10(1)
Al(2)	15(1)	18(1)	15(1)	-1(1)	-3(1)	-5(1)
Si(3)	25(1)	24(1)	21(1)	1(1)	-3(1)	-11(1)
Si(4)	21(1)	19(1)	21(1)	-2(1)	-6(1)	-3(1)
N(2)	20(1)	18(1)	17(1)	-1(1)	-3(1)	-5(1)
O(2)	16(1)	20(1)	14(1)	-1(1)	-6(1)	-7(1)
C(14)	17(1)	19(1)	16(1)	-3(1)	-7(1)	-5(1)
C(15)	22(1)	21(1)	28(1)	-6(1)	-10(1)	-2(1)
C(16)	34(1)	21(1)	33(1)	-8(1)	-14(1)	-4(1)
C(17)	47(2)	40(1)	34(1)	-2(1)	-14(1)	-29(1)
C(18)	22(1)	53(2)	32(1)	-13(1)	-4(1)	-19(1)
C(19)	19(1)	44(1)	24(1)	-11(1)	-4(1)	-12(1)
C(20)	42(2)	26(1)	23(1)	2(1)	-16(1)	-15(1)
C(21)	35(1)	38(1)	20(1)	0(1)	-1(1)	-19(1)
C(22)	30(1)	49(2)	34(1)	5(1)	-8(1)	-24(1)
C(23)	50(2)	28(1)	46(2)	4(1)	-1(1)	-18(1)
C(24)	40(2)	23(1)	41(2)	-10(1)	-7(1)	-4(1)
C(25)	34(1)	36(1)	32(1)	2(1)	-14(1)	-2(1)
C(26)	21(1)	27(1)	29(1)	-5(1)	-1(1)	-4(1)

Table 4. Hydrogen coordinates ($x\ 10^4$) and isotropic displacement parameters ($Å^2 x\ 10^3$) for sh2925.

	x	y	z	U(eq)
H(1)	12120(30)	9330(20)	3706(15)	29(7)
H(2)	2820(30)	4900(20)	1145(16)	37(7)
H(1)	6250(30)	12120(20)	4784(15)	30(7)
H(2)	7260(30)	12690(20)	5020(16)	32(7)
H(3)	5770(30)	13500(20)	3720(15)	24(6)
H(4)	5350(30)	14140(30)	4493(17)	41(8)
H(5)	6890(30)	15000(30)	3527(17)	41(8)
H(6)	7790(30)	14460(30)	4207(18)	42(8)
H(7)	9610(30)	13880(20)	3061(17)	39(8)
H(8)	8480(30)	13340(20)	2799(14)	21(6)
H(9)	10460(30)	11850(20)	3384(15)	27(6)
H(10)	9920(30)	12550(20)	4148(15)	25(6)
H(11)	7250(40)	10680(30)	3722(19)	52(9)
H(12)	8830(40)	10770(30)	3193(17)	36(8)

H(13)	7420(30)	11790(20)	3116(14)	24(6)
H(14)	6620(30)	9860(20)	5096(15)	30(7)
H(15)	5880(40)	8860(20)	5546(17)	40(8)
H(16)	7460(40)	8970(30)	5720(20)	59(10)
H(17)	6880(50)	8800(30)	3400(20)	67(12)
H(18)	5710(60)	8630(40)	3950(30)	98(16)
H(19)	6700(60)	7670(50)	3590(30)	109(17)
H(20)	7160(60)	6520(40)	5290(20)	86(13)
H(21)	8590(50)	6010(30)	4760(20)	68(12)
H(22)	9930(40)	8800(30)	2338(18)	49(9)
H(22)	8670(60)	6350(40)	5400(30)	93(16)
H(23)	11400(40)	8940(30)	2430(18)	47(9)
H(24)	11440(40)	7980(30)	2020(20)	50(9)
H(25)	13540(40)	7180(30)	3483(19)	49(9)
H(26)	13580(40)	6220(30)	3048(18)	43(8)
H(27)	13050(40)	6130(30)	3950(20)	57(10)
H(28)	9170(40)	6380(30)	3151(18)	46(8)
H(29)	10430(40)	5560(30)	3560(20)	53(9)
H(30)	11050(50)	5880(30)	2630(20)	81(12)
H(31)	5300(30)	7210(20)	749(16)	27(6)
H(32)	4320(30)	6740(20)	1509(16)	35(7)
H(33)	5460(30)	8000(30)	1818(16)	34(7)
H(34)	6120(30)	6840(20)	2240(15)	22(6)
H(35)	7760(40)	7720(30)	895(19)	49(9)
H(36)	8210(40)	7560(30)	1689(19)	50(9)
H(37)	9700(40)	5980(30)	959(19)	51(9)
H(38)	8860(30)	5520(20)	1688(16)	27(6)
H(39)	8030(30)	5920(20)	200(15)	22(6)
H(40)	8710(30)	4660(20)	563(15)	32(7)
H(41)	5350(40)	4650(30)	1911(18)	42(8)
H(42)	6810(30)	4800(20)	2107(16)	34(7)
H(43)	6870(30)	3910(30)	1571(16)	36(7)
H(44)	3170(30)	3650(30)	2514(17)	39(8)
H(45)	4600(40)	2680(30)	2672(17)	42(8)
H(46)	2960(40)	2570(30)	2930(19)	47(9)
H(47)	1270(40)	3450(30)	1278(18)	46(9)
H(48)	1810(40)	2350(30)	860(19)	45(8)
H(49)	1050(40)	2390(30)	1751(19)	48(8)
H(50)	3590(40)	450(30)	2240(20)	58(10)
H(51)	5410(40)	250(30)	1990(20)	57(10)
H(52)	4350(50)	260(40)	1430(20)	77(13)
H(53)	6600(50)	820(30)	-420(20)	71(12)
H(54)	7890(60)	110(40)	-140(30)	87(14)
H(55)	6510(50)	50(40)	300(30)	84(13)
H(56)	8390(40)	1680(30)	1513(19)	54(9)
H(57)	7620(40)	690(30)	1710(20)	67(11)
H(58)	9050(40)	610(30)	1140(20)	58(10)
H(59)	8410(30)	3130(30)	83(17)	37(7)
H(60)	9130(40)	1980(30)	-381(19)	51(9)
H(61)	7770(40)	2970(30)	-646(18)	43(8)

Index II (List of Schemes)

Scheme 1.1.	Different reactions routes for the synthesis of metal alkoxides	7
Scheme 1.2.	Synthetic reactions for the preparation of compounds **1**-**4**	22
Scheme 1.3.	Tetramer-Trimer interconversion equilibrium of $[Al(O^cHex)_3]_n$	37
Scheme 1.4.	Reaction scheme for the synthesis of **5**, **6** and **7**	41
Scheme 1.5.	Synthetic strategy for the preparation of compounds **8**, **9** and **10**	53
Scheme 1.6.	Synthetic reactions for the preparation of **11**, **12** and **13**	66
Scheme 1.7.	Schematic representation of reactions between $Ge\{N(SiMe_3)_2\}_2$ and $[H_2Al(OR)]_2$	79
Scheme 1.8.	Reduction of $Ge\{N(SiMe_3)_2\}_2$ by $[H_2Al(OR)]_2$	91
Scheme 1.9.	Reduction of $Ge\{N(SiMe_3)_2\}_2$ by $[HAl(OR)_2]_2$	92
Scheme 1.10.	Schematic representation of the reaction between $LiAlH_2(O^tBu)_2$ and $NiCl_2$	96
Scheme 2.1.	The decomposition mechanism of the single source precursor in cold wall CVD	147

Index III (List of Figures)

Figure 1.1.	Coordination modes of oxygen in metal alkoxides	11
Figure 1.2.	Virtually drawn cubane structure of metal alkoxides	12
Figure 1.3.	Sketches of observed structures of dimeric alkoxides	14
Figure 1.4.	Structural possibilities in trimeric metal alkoxides	15
Figure 1.5.	Mitsubishi motif like structure of tetrameric alkoxides	15
Figure 1.6.	Dimeric structure of $[H_2Al(O^tBu)]$	16
Figure 1.7.	Hydride-modified heterometal alkoxide of Al with Mg	17
Figure 1.8.	Dimeric structural motif of Ge(II) alkoxides	18
Figure 1.9.	Solid state ^{27}Al-NMR spectrum of $[H_2Al(O^cHex)]_n$ **2**	24
Figure 1.10.	Solution ^{27}Al-NMR spectrum of $[HAl(O^cHex)_2]_n$ **3**	25
Figure 1.11.	Solution ^{27}Al-NMR of compound $[Al(O^cHex)_3]_4$ **4**.	26
Figure 1.12.	Molecular structure of **1**	28
Figure 1.13.	Molecular structure of compound **2**	31
Figure 1.14.	Molecular structure of compound **2**	31
Figure 1.15.	Al centres having octahedral and trigonal bipyramidal…	33
Figure 1.16.	Molecular structure of $[Al(O^cHex)_3]_4$ **4**	36
Figure 1.17.	Projection of $[Al(O^cHex)_3]_4$ **4** on metal atoms plane	37
Figure 1.18.	The $Al\{(\mu\text{-}O)_2Al\}_3$ core of compound **4** having Mitsubishi motif like structure	39
Figure 1.19.	^{27}Al-NMR spectrum of compound $[H_2Al(O^cHex$*Me*$\text{-}1)]$ **5**	42
Figure 1.20.	^{1}H-NMR spectrum of **6**	43
Figure 1.21.	IR spectra of compounds **5** (red) and **6** (blue)	44
Figure 1.22.	Proposed structures for *trans*- and *cis*-isomer of compound **6**	45
Figure 1.23.	^{1}H and ^{13}C-NMR spectra of the compound $[Al(O^cHex$*Me*$\text{-}1)_3]_2$ **7**	46
Figure 1.24.	Proposed molecular structure of $[Al(O^cHex$*Me*$\text{-}1)_3]_2$ **7** in solution	46
Figure 1.25.	Molecular structure of compound $[H_2Al(O^cHex$*Me*$\text{-}1)]_2$ **5**	48
Figure 1.26.	Molecular structure of compound $[Al(O^cHex$*Me*$\text{-}1)_3]_2$ **7**	50
Figure 1.27.	^{1}H-NMR spectra of compounds **8**, **9** and **10**	55
Figure 1.28.	^{13}C NMR spectrum for α-carbon of compound **9**	56
Figure 1.29.	Al_2O_2 planar ring forming central unit of compounds **8**, **9** and **10**	57
Figure 1.30.	Molecular structure of $[ClAl(H)(O^cHex$*Me*$\text{-}1)]_2$ **8**	59
Figure 1.31.	Molecular structure of compound $[ClAl(O^cHex$*Me*$\text{-}1)_2]_2$ **9**	61

Figure 1.32.	Molecular structure of $[Cl_2Al(O^cHexMe\text{-}1)]_2$ **10**	64
Figure 1.33.	^{13}C-NMR spectrum of $Ge(O^cHex)_2$ **11**	68
Figure 1.34.	^{1}H and 1^3C (inset) NMR spectra of $Ge(O^cHexMe\text{-}1)$ **12**	69
Figure 1.35.	^{1}H-NMR spectrum of compound $[Ge(O^iPr)_2]_2$ **13**	70
Figure 1.36.	Proposed molecular structure of compound $[Ge(O^iPr)_2]_2$ **13**	70
Figure 1.37.	Central Ge_2O_2 ring of $[Ge(OR)_2]_2$ (R = ^{c}Hex **11**, or ^{c}Hex*Me*-1 **12**)	71
Figure 1.38.	Molecular structure of $[Ge(O^cHex)_2]_2$ **11**	72
Figure 1.39.	Molecular structure of $[Ge(O^cHexMe\text{-}1)_2]_2$ **12**	76
Figure 1.40.	^{1}H-NMR spectra of compounds **14** (blue) and **15** (red)	81
Figure 1.41.	IR spectra of compounds **14** (red) and **15** (blue)	82
Figure 1.42.	Molecular structure of compound $[HAl(O^tBu)\{N(SiMe_3)_2\}]_2$ **14**	84
Figure 1.43.	Molecular structure of compound $[HAl(O^cHexMe\text{-}1)\{N(SiMe_3)_2\}]_2$ **15**	87
Figure 1.44.	^{1}H-NMR spectrum of the reaction mixture	94
Figure 1.45.	^{1}H and ^{13}C NMR spectra of the sublimed product	96
Figure 2.1.	Quantum Compressed Hydrogen Storage Tank	135
Figure 2.2.	Tank system for storing cryogenic liquid hydrogen	137
Figure 2.3.	Joule-Thompson Expansion Cycle	138
Figure 2.4.	Lennard-Jones Potential……..	141
Figure 2.5.	Single-crystal x-ray structures of MOF-5	144
Figure 2.6.	X-ray diffractogram of the Al/Al_2O_3 composite NWs…	153
Figure 2.7.	SEM images of the as prepared Al/Al_2O_3 composite NWs….	154
Figure 2.8.	SEM images of Al/Al_2O_3 composite NWs….	155
Figure 2.9.	SEM images of Al/Al_2O_3 composite NWs…	156
Figure 2.10.	Al/Al_2O_3 composite NWs produced at 580°C….	157
Figure 2.11.	TEM image of the Al/Al_2O_3 composite NWs….	157
Figure 2.12.	X-ray diffractogram of the Ni/Al_2O_3 composite NPs….	159
Figure 2.13.	SEM images of Ni/Al_2O_3 composite NPs…..	160
Figure 2.14.	EDX spectrum of Ni/Al_2O_3 composite NPs…	161
Figure 2.15.	TEM image (a) and SAED (b) of the Ni/Al_2O_3 NPs…	162
Figure 2.16.	Hydrogen adsorption isotherms of Al/Al_2O_3 composite NWs…	164
Figure 2.17.	Hydrogen adsorption isotherms of Al/Al_2O_3 composite NWs…	165
Figure 2.18.	Hydrogen adsorption isotherms of Ni/Al_2O_3 composite NPs….	166
Figure 2.19.	IR spectra recorded for Al/Al_2O_3 composite NWs…	168

Figure 2.20. IR spectra recorded for Ni/Al_2O_3 composite NPs…. 169
Figure 2.21. Selected area SEM images……. 170
Figure 2.22. SEM images of the heat treated…….. 171
Figure 2.23. DSC curves for Al/Al_2O_3 composite NWs….. 173
Figure 2.24. DSC curves for Al/Al_2O_3 composite NWs…… 174
Figure 2.25. DSC curves for HAlO material measured…… 175
Figure 2.26. Schematic representation of the core-shell……. 177
Figure 2.27. Pictorial representation of H_2 interaction…… 180
Figure 2.28. H_2 cleavage by the Ni dispersed in alumina matrix 182
Figure 2.29. Drawing of a typical cold wall CVD reactor…….. 184
Figure 2.30. Schematic representation of the……. 186
Figure 2.31. Schematic diagram of the Sievert's type apparatus….. 188
Figure 2.32. Schematic diagram of SC:…… 188
Figure 2.33. Powder X-ray diffractogram of the misch….. 189
Figure 2.34. Calibration curve of the Sievert's apparatus…….. 190
Figure 2.35. A typical DSC chamber……. 193

Index IV (List of Tables)

Table 1.	Crystal Data of Compound **1**	29
Table 2.	Bond Angles and Lengths of Compound **1**	30
Table 3.	Crystal Data of Compound $[H_2Al(O^cHex)]_n$ **2**	34
Table 4.	Bond Angles and Lengths for Compound $[H_2Al(O^cHex)]_n$ **2**	35
Table 5.	Crystal Data of Compound **4**	39
Table 6.	Bond Angles and Lengths for Compound **4**	40
Table 7.	Crystal data of compound **5**	48
Table 8.	Selected bond lengths and angles of compound **5**	49
Table 9.	Crystal data of the compound **7**	50
Table 10.	Selected bond lengths and angles of the compound **7**	51
Table 11.	Crystal data of compound **8**	59
Table 12.	Pertinent bond lengths (Å) and angles (°) of **8**	60
Table 13.	Crystal data of compound **9**	62
Table 14.	Pertinent bond lengths (Å) and angles (°) of the compound **9**	63
Table 15.	Crystal data of compound **10**	64
Table 16.	Pertinent bond lengths (Å) and angles (°) for the compound **10**	65
Table 17.	Crystal data of compound **11**	73
Table 18.	Selected bond lengths (Å) and angles (°) of compound **11**	74
Table 19.	Crystal data of compound **12**	76
Table 20.	Selected bond lengths (Å) and angles (°) of **12**	77
Table 21.	Relevant crystal data of $[HAl(O^tBu)\{N(SiMe_3)_2\}]_2$ **14**	84
Table 22.	Selected bond lengths (Å) and bond angles (°) of compound **14**	85
Table 23.	Relevant crystal data of the compound **15**	87
Table 24.	Selected bond lengths (Å) and bond angles (°) of compound **15**	88